University of Alberta
Department of Civil Engineering

Structural Engineering Report 206

SHRINKAGE AND FLEXURAL TESTS OF A FULL-SCALE COMPOSITE TRUSS

by

Michael B. Maurer

and

D.J. Laurie Kennedy

December 1994

Structural Engineering Report 206

SHRINKAGE AND FLEXURAL TESTS OF A FULL-SCALE COMPOSITE TRUSS

by

Michael B. Maurer
and
D.J. Laurie Kennedy

Department of Civil Engineering
University of Alberta
Edmonton, Alberta, Canada
T6G 2G7

December 1994

ABSTRACT

The shrinkage and flexural behaviour of a composite truss consisting of WT chords with double angle web members was studied. In the triangulation system used the web members intersect at the mid-depth of the concrete cover slab and at the centroid of the bottom chord. The flexural capacity was based on the bottom chord reaching 90% of its upper specified factored tensile resistance, with the remaining elements of the truss designed to resist concomitant forces.

Shrinkage measurements to determine the effects of slab shrinkage on truss deflection and chord stresses were recorded over a period of 68 days. An apparent modulus of elasticity of concrete in tension was defined, for use in Shaker's general method (Shaker 1991), to account for the increased flexibility due to interfacial slip and the open web system. The equilibrium method of determining shrinkage deflection was confirmed. The method given in CSA Standard S16.1 - 94 to calculate shrinkage deflections overestimates the deflection of a composite truss. This method can be modified, by using the apparent modulus, to give a better estimate of the shrinkage deflection. However, the apparent modulus is difficult to estimate, because it depends upon many factors.

The failure of the truss in flexure, under the action of a four point load, was very ductile. The maximum applied moment exceeded the values calculated using CSA Standard S16.1 - M89 to determine the moment resistance. To ensure that a composite truss fails in a ductile manner, it would appear sufficient to have the components designed for forces concomitant with a force in the bottom chord that ensures it does yield (even if the yield strength is greater than the minimum specified) before any other component fails. Also, it may be unsafe to neglect the contribution of the top chord to the horizontal shear carried by the shear connectors, which is an assumption inherent in the design model of S16.1.

Many other aspects of the shrinkage and flexural behaviour of the composite truss and its elements are discussed, including, but not limited to, the adequacy of the Canadian Standard S16.1 design criteria.

ACKNOWLEDGEMENTS

It is in awe and with praise that I look upon the creation of the almighty God. I thank Him (and my Lord, Jesus), that I was allowed to uncover a small piece of the workings of His universe.

This research was conducted under the supervision of Dr. D. J. Laurie Kennedy. His sincere guidance, unlimited patience and freely given time throughout the project were invaluable and are greatly appreciated.

Financial support for this research was provided by funds granted to Dr. Kennedy by the Natural Sciences and Engineering Research Council of Canada. For the steel deck, the crimping tool and the labour to crimp the individual sheets together were supplied by Vic-West Steel, at no cost. Personal funding of the author from the Province of Alberta and the Canadian Institute of Steel Construction Alberta Regional Committee is gratefully acknowledged.

I would also like to express my appreciation to the staff of the I. F. Morrison Structural Laboratory and my fellow graduate students for their technical assistance and cooperation during the experimental part of this study. As well, the assistance of Jo Ann and Eleanor in handling the university bureaucracy was greatly appreciated.

Special thanks are extended to Dr. David Murray for his interest and helpful comments, Anita Brattland for her cooperation in providing elements of her research completed in 1986 and to Berhanu Woldegiorgis for providing discussion and insights of his work before its completion in 1994.

Finally, sincere thanks to my parents, without whose inspiration to endeavour farther and higher, this project would never have been undertaken.

TABLE OF CONTENTS

Chapter Page

Chapter Page

Chapter Page

Chapter Page

Chapter Page

LIST OF TABLES

LIST OF FIGURES

LIST OF SYMBOLS

a = effective depth of rectangular stress block in concrete slab, mm; distance between the shrinkage forces T_s and C_{tc}, mm

A = area, mm^2

A_{bc} = area of steel bottom chord, mm^2

A_c = effective area of the concrete slab, mm^2

A_g = net area of steel section, mm^2

A_n = net area of steel section, mm^2

A_{tc} = area of steel top chord, mm^2

b = WT flange width, mm; angle leg size, mm; slab width, mm; distance between the shrinkage forces C_{tc} and T_{bc}, mm

c = depth of concrete in compression, mm

C_r = factored resistance of a compression member, N

C_{tc} = shrinkage induced compression in the top chord, N

d = WT depth, mm

d_1 = distance from the centroid of the bottom chord to the line of action of the compressive force in the concrete, mm

d_2 = distance from the centroid of the top chord to the line of action of the compressive force in the concrete, mm

E = modulus of elasticity, MPa

e' = distance between compressive force in concrete and tensile force in bottom chord, mm

E_a = apparent modulus of elasticity of concrete in tension, MPa

E_{bc} = modulus of elasticity of steel bottom chord, MPa

E_c = nominal modulus of elasticity from concrete in compression, MPa

E_c^* = measured tangent modulus of elasticity of concrete in compression, MPa

E'_c = effective modulus of elasticity of concrete in tension under restrained shrinkage conditions as the concrete dries and creeps and may eventually crack while being gradually loaded from the green state over the time interval during which the shrinkage deflection is determined, MPa

E_{ct} = effective modulus of elasticity of concrete in tension, MPa

E_{tc} = modulus of elasticity of steel top chord, MPa

f'_c = nominal compressive strength of concrete, MPa

F_u = nominal tensile strength of steel, MPa

F_{us} = measured static tensile strength of steel, MPa

F_y = nominal yield strength of steel, MPa

F_{ys} = measured static yield strength of steel, MPa

H = out-to-out depth of steel truss, mm

h_d = height of steel deck, mm

I_e = effective moment of inertia of the composite truss, mm^4

I_{et} = effective moment of inertia as given in Clauses 17.3.1(a) be based on the modular ratio n_t, mm^4

I_s = moment of inertia of the steel truss, mm^4

I'_s = moment of inertia of the steel truss with the flexibility of the open web taken into account - i.e., $I'_s = I_s / 1.10$, mm^4

I_t = transformed moment of inertia of the composite truss, mm^4

I_{tEa} = transformed moment of inertia of the composite truss based on the apparent modulus of elasticity of concrete in tension, mm^4

$I_{tE'c}$ = transformed moment of inertia of the composite truss based on the effective modulus of elasticity of concrete in tension, mm^4

I'_t = transformed moment of inertia of the composite truss with the flexibility of the open web taken into account - i.e., $I'_t = I_t / 1.10$, mm^4

I_x = moment of inertia about an axis perpendicular to the plane of the truss, mm^4

I_y = moment of inertia about the weak axis of the truss, mm^4

L = span of beam or truss, mm

M_r = moment resistance of the composite section based on S16.1 and nominal section and material properties, N·mm

M_{rc} = factored moment resistance of the composite section, N·mm

M_u = ultimate moment resistance of the composite section based on measured section and material properties neglecting contribution to moment resistance from the top chord, N·mm

M_y = yield moment resistance of the composite section based on measured section and material properties neglecting contribution to moment resistance from the top chord, N·mm

n = number of measurements or regression points

n_t = modular ratio E / E_{ct}

p = fraction of partial shear connection

P = applied load at one of four load points, N

R = correlation coefficient from regression analysis

R^2 = coefficient of determination from regression analysis

t = flange thickness, mm; leg thickness, mm; time, days

T_{bc} = shrinkage induced tension in the bottom chord, N

t_c = thickness of concrete cover slab, mm

T_r = factored resistance of a tension member, N

T_s = shrinkage induced tension in the concrete, N

V = Coefficient of variation

V_r = factored shear resistance of stud shear connectors, N

w = WT web thickness, mm

y = centroidal distance, mm; distance from elastic neutral axis to centroid of effective area of concrete slab, mm

α = equation parameter that depends on the concrete mix, $\mu\varepsilon$

β = equation parameter which depends on the concrete mix, 1/days

γ = residual strain linear correction factor

Δ_c = calculated shrinkage deflection, mm

Δ_m = measured shrinkage deflection at midspan, mm

Δq = measured shrinkage deflection at a quarter point, mm

Δ_s = shrinkage deflection, mm

Δ_{sh} = shrinkage deflection, mm

ε_{bc} = induced shrinkage strain of the steel bottom chord, $\mu\varepsilon$

ε_c = strain of the concrete, $\mu\varepsilon$

ε_f = free or unrestrained shrinkage strain of the concrete, $\mu\varepsilon$

ε_r = restrained shrinkage strain of the concrete, $\mu\varepsilon$

ε_s = tensile shrinkage strain of the concrete, $\mu\varepsilon$

ε_{st} = strain of the steel, $\mu\varepsilon$

ε_{tc} = induced shrinkage strain of the steel top chord, $\mu\varepsilon$

ϕ = resistance factor for steel = 0.90

Φ = equation parameter

ϕ_c = resistance factor for concrete = 0.65

Λ = equation parameter

ρ = radius of curvature, mm

σ_s = tensile shrinkage stress of the concrete, MPa

Ω = equation parameter

1 INTRODUCTION

1.1 General

The term "composite truss" means a steel truss that physically is connected to and acts compositely with a concrete slab and is designed on an individual basis for a specific job (Brattland and Kennedy 1986). By providing interconnection between the concrete slab and the steel supporting members of a floor system to take advantage of the performance of concrete in compression and steel in tension, an economical composite system with increased strength and stiffness is achieved. The development of composite flexural members has progressed from solid concrete slabs acting compositely with rolled steel beams to concrete slabs supported on ribbed deck acting compositely with rolled steel beams, open-web steel joists or trusses. Limit states design has resulted in substantial weight savings for these members.

Composite trusses with deck-slab systems that incorporate wide rib profile steel decks enable longer spans and larger spacings to be used for design. This provides flexibility in office layout and use. Although more labour is required per tonne of steel for fabrication, total erected steel costs (as compared to the use of composite beams) are reduced due to the saving in the weight of steel when the number of trusses in a project is sufficiently great so that standardized fabrication techniques can be developed. Unshored construction, with the steel deck supporting the wet concrete and the steel trusses supporting themselves and the wet concrete, is fast and permits other trades to follow closely behind. The open web system provides great flexibility for placement of mechanical and electrical services and reduces the ceiling to floor distance. Composite trusses are very stiff, hence deflections under service conditions are typically small.

The design of composite trusses is currently based on the requirements in CSA Standard S16.1 - M89, Limit States Design of Steel Structures (CSA 1989) for composite beams and in particular for open-web steel joists. These requirements are based on a considerable amount of test data on composite open-web steel joists. However, only limited data are available from tests on long span composite trusses. Additional testing of a practical array of composite trusses is required to ensure that a proven set of design procedures is available to designers. The overall behaviour of one such composite truss is examined in this thesis.

1.2 Objectives

The objectives of this experimental study of composite trusses are:

1. to determine the effects of slab shrinkage on truss deflection and strains in the concrete slab and steel chords,

2. to determine truss stiffness prior to and after composite action is achieved based on measured deflections under dead and applied loads,
3. to examine the load deflection response, load-carrying capacity and failure mode of a composite truss loaded to failure, including observations of the distribution of strains across the width of the slab, the effect of interfacial slip on shear transfer at the steel-concrete interface and indications of longitudinal shear failure in the concrete slab, and
4. to assess the adequacy of the current design provisions in CSA Standard S16.1 for establishing the strength and stiffness of these members.

1.3 Scope

One 11 500 mm span composite truss was designed, constructed, instrumented and tested. The steel truss configuration chosen was simple to fabricate, consisting of WT top and bottom chords and double angle web members with square-cut ends welded to the stems of the WT chords. The concrete slab was cast on wide rib profile steel deck, with the ribs oriented perpendicular to the axis of the truss. Welded stud shear connectors provided composite action. The test specimen was monitored for over 60 days to study the effects of slab shrinkage and then tested in flexure to failure under four concentrated loads. Shrinkage and flexural test data were analyzed and conclusions were drawn regarding composite truss behaviour under these conditions. The adequacy of current design requirements was assessed.

2 LITERATURE REVIEW

2.1 Shrinkage behaviour of composite trusses

Appendix L of CSA Standard S16.1 - 94 (1994) states that shrinkage induced deflections result in composite construction from the decrease in volume of the concrete as it cures, at first rapidly, and then at a decreasing rate. When restrained, by the steel shape to which it is attached, tensile strains, and therefore tensile stresses, are developed in the concrete. (It may even crack if the tensile strength is reached.) Shoring reduces the shrinkage deflection considerably, especially in the early stages, when the rate of shrinkage is the greatest.

Generally, the out-to-out depth to span ratio for composite trusses is large, with typical values ranging from 1 / 17 to 1 / 11. Chien and Ritchie (1984) suggest that with such member depths, shrinkage and creep deflections of composite trusses tend to be insignificant compared with the values one would find with a similar deck-slab on a shallower solid web steel beam.

When no other data is available, a value of 800 με may be used for the free (unrestrained) shrinkage strain (ACI 1982). For small plain concrete specimens at relative humidity of 50% the free shrinkage strain is typically 600 με to 800 με (Chien and Ritchie 1984). Also, typically one third of the ultimate free shrinkage will occur in the first month and 90% of the ultimate free shrinkage will occur in the first 11 months. Free shrinkage is affected by curing conditions, surface area to volume ratio, average relative humidity, average temperature, slump (water content), size and type of aggregate, time and restraint from steel.

Shrinkage tests on two full-scale composite trusses by Brattland (Brattland and Kennedy 1986, Kennedy and Brattland 1992) revealed the free shrinkage strains ranged from 600 με to 900 με. Shrinkage deflections before the polyethylene sheets used during curing were removed were small, but, after removal of the polyethylene, the deflections increased rapidly and then at a decreasing rate. However, even at the end of 65 and 85 day test periods, the shrinkage deflection was still increasing. About 70% of the shrinkage deflection measured had occurred in the first month.

The tests by Brattland also showed that the overall longitudinal strains in the concrete slab were about 45% of the free shrinkage strain at 65 days because of the restraint provided by the steel truss to the concrete slab. Local longitudinal shrinkage measurements at mid-span were larger than the overall measured strains. Measured strains at mid-span showed that the variation of shrinkage induced strain through the depth of the truss could be considered to be linear.

Shaker and Kennedy (1991) showed that both the free and restrained shrinkage strains increased at a gradually decreasing rate over the test period. An exponential equation was

found to fit the test data better than the hyperbolic equations used in the ACI and the CEB / FIP standards. The maximum free shrinkage recorded was 844 με at 169 days for concrete mix 1 and 742 με at 141 days for concrete mix 2.

A numerical parametric study performed (Dezi and Tarartino 1993), based on a model they also proposed, indicated that, in time, creep reduces the stresses induced by the shrinkage by about 35%, without being appreciably affected by the stiffness of the shear connectors.

Bradford and Gilbert (1992) state that the slip strains are relatively small, at service loads, compared to the concrete and steel strains at the interface over the practical ranges of shear connector stiffness.

Chien and Ritchie (1993) give a history of composite construction in Canada, the evolution of deck-slab systems and a summary of shear stud connector design requirements.

2.1.1 Modulus of elasticity of concrete in tension

Shaker and Kennedy (1991), in investigating the restrained concrete shrinkage, showed that the effective modulus of elasticity of concrete in tension is maximum at the beginning of drying and decreases exponentially as drying continues. The value of the effective modulus at a given time decreases with the increase in the percentage of steel because of the increase in the creep due to the increased shrinkage induced tensile stresses. At 150 days, the effective modulus ranged from 0.10 to 0.20 of the modulus of elasticity of concrete in compression. The modular ratios relative to the elastic modulus of steel were in the range of 45 to 200. As well, within the scope of the investigation, neither the free shrinkage of the concrete nor its effective modulus of elasticity in tension is significantly affected by its compressive strength of the concrete.

From Kennedy and Brattland (1992), the effective modulus of elasticity in tension (herein redefined as the apparent modulus), deduced from the equilibrium method, was found to range from 645 MPa to 1190 MPa, which corresponds to about 0.04 to 0.07 of the 28 day secant modulus of concrete in compression.

2.1.2 Shrinkage deflection calculation methods

Bradford and Gilbert (1991) determined that the shrinkage deflections and strains of four full-scale composite beams were not greatly sensitive to the number of shear connectors, although, there was definite correlation between the density of connectors and deflection.

2.1.2.1 Equilibrium method

From the shrinkage tests performed by Brattland and Kennedy in 1985 (Brattland and Kennedy 1986, Kennedy and Brattland 1992), it was found that the restraint to shrinkage of the slab was developed within a short distance from each end. The constant tensile force in the concrete cover slab over the remainder of the truss length is in equilibrium with a compressive force developed in the top chord and a much smaller tensile force developed in the bottom chord. Most of the shrinkage force is transferred to the bottom chord by the web members closest to each end of the truss. Therefore, the assumption that the truss has uniform curvature creates little error in shrinkage deflection calculations.

An equilibrium method was proposed for calculating shrinkage deflections, based on the equilibrium of the shrinkage induced forces at midspan, a linear strain distribution thorough the depth, the free shrinkage strain of the concrete, the stress-strain characteristics of the concrete in tension over the period that shrinkage occurs and the stress-strain characteristics of the steel. For a given truss geometry, only one set of ratios of strains $\varepsilon_r:\varepsilon_{tc}:\varepsilon_{bc}$ will satisfy equilibrium conditions.

2.1.2.2 Shaker's methods

By using the time dependent effective modulus of elasticity of concrete in tension and the free shrinkage strain, Shaker and Kennedy (1991) developed a general procedure for the calculation of shrinkage deflections of composite flexural members, based on the equilibrium method, proposed initially by Brattland and Kennedy (1986). They showed that the development of shrinkage deflections of composite flexural members with time could be established using the equilibrium method. This method is described in detail in Section 8.1.1.2.

Another procedure, called the approximate procedure, was developed, again based on the equilibrium method, but using a tensile stress-strain curve and a fixed value for the free shrinkage strain. This allowed the shrinkage deflection to be estimated with reasonable accuracy and its application was somewhat less complicated than the general method.

2.1.2.3 Branson's method

In Branson's method (Branson 1964), the shrinkage deflection is calculated as

$$[2.1] \quad \Delta_s = \frac{\varepsilon_f A_c L^2 y}{8 n_t I_{et}} .$$

This method, based on strain compatibility and equilibrium, as are both the equilibrium and Shaker's general method, may give the same result, provided only that the correct value of the modulus of elasticity of concrete is used. It is simpler to use because the modulus of elasticity of concrete is simply assumed and not based on a specific relationship with the tensile stress in the concrete. However, the tensile stress-strain relationship of the concrete is not necessarily satisfied.

2.1.2.4 Unrestrained shrinkage method

This method, reported by Montgomery et al. (1983), uses an age adjusted modulus of elasticity of the concrete to take creep effects into account. It is suggested that this modulus, based on the 28 day modulus of elasticity of concrete in compression, may bear little resemblance to the effective modulus of the green concrete loaded in tension as it dries, shrinks and creeps.

2.1.2.5 CSA Standard S16.1 - 94 design provisions

Clause 17.3.1 states that for shrinkage of concrete, calculate deflection using a selected free shrinkage strain, strain compatibility between the steel and concrete and a time-dependent modulus of elasticity of the concrete in tension, as it dries, shrinks and creeps from [2.1].

Appendix L, which is not a mandatory part of the Standard, suggests that the relationship between the modulus of elasticity of concrete in tension and the tensile stress in the concrete is

[2.2] $E_{ct} = 8300 - 4800\sigma_{ct}$ where $0.3 \leq \sigma_{ct} \leq 1.2$

based on the work by Shaker and Kennedy (1991).

2.1.2.6 Other proposed time-dependent methods

A theoretical model for the short-term and time-dependent response of simply supported composite beams was developed by Bradford and Gilbert (1992) using an age adjusted effective modulus for concrete in compression. This analysis leads to an iterative solution for curvatures, strains and deflections. Agreement between theory and tests reported elsewhere was good.

Lawther and Gilbert (1992) present a time-dependent analysis of a general, monosymmetric composite cross section. The method is illustrated by example and the effects of both creep and shrinkage on the behaviour of the cross-section are determined

and discussed. This method is based on the rate-of-creep method proposed by Gilbert (1989). This method, as presented, uses Dischinger's differential constitutive relationship

$$[2.3] \quad \dot{\varepsilon} = \frac{\dot{\sigma}}{E_c} + \dot{\phi}\left[\frac{\sigma}{E_c} + \frac{\varepsilon^*_{sh}}{\phi^*}\right]$$

(where a dot above a variable indicates rate of change with respect to time for that variable) to model the inelastic creep and shrinkage strains that develop with time in the concrete. The procedure involves a stiffness formulation of the coupled differential equations that describe cross-sectional behaviour and a simple mathematical solution. Compatibility of strains is enforced over the entire cross-section; specifically, slip is assumed to contribute negligibly to the deflection, and hence, a linear strain distribution is used. This assumption is based on the work of Bradford and Gilbert (1992). The predicted deflections agree well with measured values of several composite beams tested under sustained loads.

2.2 Effective stiffness of steel trusses

To estimate the elastic deflection of a steel truss, an effective moment of inertia equal to the gross moment of inertia of the chords about the truss centroid, divided by a factor of 1.10 to account for the decreased stiffness of the open web system, can be used (Brattland and Kennedy 1992). This is consistent with the design recommendation in Clause 16.6.14.2 of S16.1 - M89. For trusses with cold formed HSS bottom chords, the non-linear stress-strain curve may result in deflections at the specified load level of up to 25% greater than the value predicted from the above procedure.

2.3 Flexural behaviour composite trusses

Brattland and Kennedy (1986) report the results of tests by Iyengar and Zils (1973) on a pair of full-scale composite trusses spanning 22 900 mm spaced at 4570 mm, with a 65 mm cover slab cast on the 76 mm steel deck, revealed that the load-deflection response was only slightly non-linear and agreed well with a theoretical prediction. No slab cracks formed or truss deformations were observed. The test was not taken to failure.

A 12 000 mm span composite truss was tested by Bjorhovde (1981). This truss consisted of HSS top and bottom steel chords, with double angle diagonals in a Warren configuration and HSS verticals. The out-to-out depth of the steel truss was 850 mm. The steel truss supported a 2300 mm wide normal weight concrete slab with a cover depth of 63 mm over 76 mm wide rib profile steel deck. Shear stud connectors with a diameter of 19 mm and length of 114 mm were uniformly distributed along the truss length. The test specimen was loaded with three point loads located over the top chord at the quarter

points. The response at service level loads was essentially elastic. Failure was precipitated by buckling of the first compression diagonal prematurely at a load reported to be 95% of the design load.

Full-scale flexural tests to failure of two composite trusses by Brattland and Kennedy (1986, 1992) reveal that:

1. at low loads, the moment deflection response of the composite trusses is essentially linearly elastic. The maximum moments attained were about 1.2 times the unfactored ultimate moments predicted by S16.1. Deflections at maximum moment of 5 to 7 times the yield value demonstrate the ductility of the trusses,
2. neglecting the discontinuity at the concrete-steel interface due to interfacial slip, a linear regression of the measured strain data at mid-span fit the data well. The position of the neutral axis rises for higher loads, indicative of yielding in the bottom chord,
3. compressive strains across the width of the concrete slabs were essentially uniform. Significant shear lag was observed only in close proximity to the ends of the truss, and
4. strains on the web members were converted to axial forces and bending moments about their principal axes. Eccentricities about the in-plane and out-of-plane axes (of the truss) were calculated. For members subjected to axial loads and end moments, the eccentricities will not vary linearly due to the deformation of the member between its ends.

Further analysis by Woldegiorgis and Kennedy (1994) on the web members of the trusses tested by Brattland and Kennedy, was performed. The results are summarized below.

1. Three plane-frame analyses were carried out. A comparison of a pin-jointed truss analysis with that considering the member ends to be fixed shows that the truss carries load primarily as axial forces in the members and that frame action contributes little to the overall strength.
2. Many different models were examined for the detailed plane-frame analysis. The model considered to be most valid, on the basis of the comparisons with the results of the strain analysis, considered all members including shear connectors to be prismatic extending from node to node, considered all joint eccentricities, considered connection eccentricities by introducing connection eccentricity moments at appropriate nodes and considered the concrete cover slab to extend over its full width and thickness.
3. Multiple regression analyses were performed on the strain data obtained for eight web members at five load steps on two trusses. In the first of these, independent analyses of the strain data at the three levels served to check the accuracy of the strain data. The ratio of the maximum calculated axial load in a member to the minimum had a mean value of 1.037 and a coefficient of variation of 0.029. The strain analyses are also compared to a plane-frame analysis where applicable.

4. The second set of multiple regression analyses was performed on all the strain data for particular load steps on given members. From these data, the axial load and moments about the principal axes at the three locations were determined. These data were subsequently analyzed to establish the end moments and hence eccentricities about the principal axes. In turn, these moments and eccentricities were resolved to establish the out-of-plane and in-plane eccentricities.

2.3.1 Effective stiffness of composite trusses

Two methods are described by Chien and Ritchie (1984) to calculate the deflection of a composite truss under occupancy loads. The manual computational procedure is as follows:

1. Compute the effective slab area of the concrete top flange and transform into equivalent steel area.
2. Compute the gross moment of inertia of the composite member, I_t, using only the steel bottom chord and the transformed concrete top chord.
3. Estimate the reduction in the moment of inertia of the steel member, I_r, using the moment of inertia computed from the steel chord members and multiply the result by 0.15. (This is an estimated reduction of moment of inertia to account for the contribution of the web to the deflection.)
4. Subtract the value obtained from Step 3 from the value obtained in Step 2. The resulting value is then divided by (1.00 + 0.15 + 0.15) to allow for the effect of increased flexibility due to interfacial slip and creep.
5. Compute composite truss deflection using the moment of inertia value obtained in Step 4.

The second method described is implemented using a computer plane frame analysis program with a suggested model to calculate deflections. The effective concrete top flange is transformed to an equivalent area of steel. The interconnection of concrete slab and steel top chord is modeled by short bar members having large moments of inertia and area. The resulting deflection should account for interfacial slip and flexibility of the concrete ribs formed by the steel deck. The truss deflection computed in this manner also includes the web contribution.

The forthcoming Canadian Standard, S16.1 - 94, unchanged from the current S16.1 - M89, requires that the calculation of deflections take into account the effects of creep of concrete, shrinkage of concrete and the increased flexibility resulting from partial shear connection and from interfacial slip. Consideration is also be given to the effects of full or partial continuity in the steel beams and concrete slabs in reducing calculated deflections. In lieu of analysis, the effects of partial shear connection and interfacial slip, creep and shrinkage may be assessed as follows:

1. For increased flexibility resulting from partial shear connection and interfacial slip, calculate the deflections using an effective moment of inertia given by

[2.4] $$I_e = I_s + 0.85(p)^{0.25}(I_t - I_s)\,,$$

2. For creep, increase the elastic deflections caused by dead loads and long-term live loads, as calculated from the above equation by 15%; and
3. For shrinkage of concrete, this calculation was summarized previously, in Section 2.1.2.5.

To estimate the elastic deflection of a composite truss, the effective moment of inertia, calculated in Clause 17.3.1.1 of S16.1 - 94, should be divided by 1.10, the same factor suggested by Brattland and Kennedy (1992) to account for the decreased stiffness of the open web system . Also, based on their two tests, Brattland and Kennedy suggested that the factor of 0.85 in [2.4] be changed to 0.77.

2.3.2 Flexural capacity of composite trusses

The maximum moments attained, by Brattland and Kennedy (1986) were 99% and 101% of the predicted ultimate moment based on rupture of the bottom chord. The prediction did not take into account that the top chord was strained appreciably in tension and therefore was contributing significantly to the flexural strength of the composite truss. A comparison with previous test results (Bjorhovde 1981) in which failure was precipitated by buckling of a compression diagonal shows that increased strength and ductility are obtained when the various components are designed for forces consistent with the ultimate strength of the bottom chord.

2.3.3 Design considerations

A rational design proposal for longitudinal shear was proposed by Chien and Ritchie (1984), based on the longitudinal shear capacity being sufficient to develop the capacity of the shear connectors, neglecting any transverse forces that might be created by membrane action of the slab. As well, they suggest that with less than 75% shear connection, buckling of the steel top chord may be critical.

The failure of any component of a composite truss (diagonals, shear connection, top chord or bottom chord) or connection results in failure of the truss as a whole. Brattland and Kennedy (1986, 1992) suggest that to ensure that the desired flexural mode of failure is obtained, the flexural capacity could be based on the ultimate tensile strength of the bottom chord, with the other components designed for the concomitant forces. Alternately, if the capacity of the bottom chord is assumed to be its yield load, that other components should be designed for forces corresponding to the yield load of the bottom

chord times the ratio F_u / F_y of the bottom chord. Another alternative would be to assign reduced resistance factors to components with brittle failure modes to provide an acceptable level of ductility. The serviceability criterion of a limited deflection may be critical when the chord design is based on its ultimate strength.

Two trusses tested by Brattland and Kennedy (1986, 1992) were composed of HSS top and bottom chords and double angle web members. Premature failure of an improperly welded shear connector caused failure in one of the two trusses tested. To guard against this type of failure, they recommended that either the end diagonal should be positioned so that its line of action intersects the centroid of the steel top chord directly over the reaction, or the reaction shear reinforcement should be extended to the first interior panel point and the reinforced chord designed to the local bending moments, or extra studs should be provided locally to prevent separation of the top chord and slab.

2.3.3.1 Web members

CSA Standard S16.1 - M84 (1984) requires that web members be proportioned to carry the total vertical shear. Local moments occurring at the web to chord junction may be neglected for the design of tension diagonals, however, the maximum slenderness requirement for tension members should be met to facilitate handling and erection (Chien and Ritchie 1984). Because induced moments may adversely affect compression diagonals they should be considered in the design of these members. Specifically, moments arising from floor loading on equal or unequal top chord panels, web to chord joint eccentricities, connection eccentricities and localized overturning due to steel-to-concrete shear connection should be taken into account.

In the tests by Brattland and Kennedy (1986), failure of the web members did not occur. Hence it was suggested that an adequate design procedure for double angle web members, based on test observations, appears to be to design them for the axial loads consistent with the bottom chord reaching its ultimate strength together with their portion of the in-plane joint eccentricity moment plus one-third of the out-of-plane connection eccentricity moment as based on their analysis.

Further analyses by Woldegiorgis and Kennedy (1994), showed that the out-of-plane end eccentricities were found to range from about one-fifth to two-fifths of the centroidal distance of the angle. The out-of-plane eccentricity was reduced because of moments developed in the connections. The reduction was a function of the out-of-plane stiffness of the chord member and was found to be less (i.e., the eccentricity was larger) for the bottom chord having a more flexible side wall. Overall, a mean end eccentricity of about one-third was considered appropriate for the design of web members.

When the angles are not connected to each other, between their ends, whether the angles are connected to the truss on one side or both, they resist loads as single angle elements

(Chien and Ritchie 1993). Research by Temple and Sakla (1994), reveals that the distribution of weldment affects the tested strength of angles loaded in compression (the strength of angles loaded in tension is not affected by the distribution of weldment). The strength of intermediate length (inelastic buckling mode) angle compression members is adversely affected when the centroid of the weldment does not coincide with the centroid of the angle (unbalanced welded connections). Conversely, slender members with unbalanced welded connections displayed higher strengths than slender members with balanced welded connections.

2.3.3.2 Welded connections of web members

Brattland and Kennedy (1986, 1992) suggest that the welds may be designed to transmit the axial force plus the in-plane moment than can coexist in the members at its ultimate limit state, neglecting the out-of-plane eccentricity of the connected angle. As well, the distribution of the weldment affects the strength of the compression members, as noted previously, in Section 2.3.3.1.

2.3.3.3 Shear connection

CSA Standard S16.1 - M84 required compositely designed trusses to have full shear connection between the concrete and steel top chord, as reported by Chien and Ritchie (1984). The total horizontal shear between the point of maximum bending and each adjacent point of zero moment can be represented as the factored yield resistance of the bottom chord if it is assumed that the top chord does not contribute to the shear. Stud shear connectors may be distributed uniformly along the top chord member.

Brattland and Kennedy (1986) suggested, due to premature failure of the shear studs in one of their trusses, that the equations of Grant, Fisher and Slutter (1977), to calculate the reduced strength of stud shear connectors in deck-slabs, be used to calculate minimum stud length. The requirements of CSA Standard S16.1 - M84 were modified in S16.1 - M89, based on the work of Jayas and Hosain (1988, 1989).

2.3.3.4 Bottom chord

The function of the steel bottom chord is to provide the tensile component of moment resistance to a composite truss (Chien and Ritchie 1984). The depth of the bottom chord should also be large enough to develop connection forces for the web members. Because the plastic neutral axis of a composite truss is required by S16.1 - M89 to be in the slab, the factored yield force of the bottom chord, $\phi A_s F_y$, must be less than the maximum force that could be developed in the in the concrete, i.e., $0.85\phi_c f'_c t_c b$.

2.3.3.5 Top chord

Chien and Ritchie (1984) suggest that each panel of the composite truss steel top chord must be designed for the axial forces and bending moments induced during construction. During construction, the top chord must be restrained to prevent lateral buckling, until the deck is properly welded to the top chord to provide lateral support. CSA Standard S16.1 - M89 Clause 17.9.2 states that the area of the steel top chord shall be neglected in determining the properties of the composite section.

2.3.3.6 Triangulation

Three types of web-framing configurations are common in composite floor truss designs (Chien and Ritchie 1984). These are: Pratt, Warren and modified Warren. This selection will affect the efficiency of web members in the resisting of vertical shear, the unsupported panel length of the top chord, web to chord connection details, adequate web openings for mechanical and electrical services and the number of web components handled during fabrication. Two design examples are presented, using a modified Warren configuration. In both, the triangulation system minimized joint eccentricities in the steel truss.

In designing their test trusses, Brattland and Kennedy (1986) chose to minimize the joint eccentricities of the composite truss, by having the centroidal axes of the double angle web members intersect at the mid-depth of the concrete cover slab. It was hoped that improved ultimate flexural performance would be achieved by using this triangulation system. In the tests, no distress of the top chord was noted due to the web member configuration. This triangulation system was therefore recommended, because of the more efficient shear resisting capacity provided by the webs being steeper than the configuration in which the web members meet at the centroids of the steel chords.

3 COMPOSITE TRUSS DESIGN

3.1 General design procedures

Currently, the design of composite trusses is based on CSA Standard S16.1 - M89 (CSA 1989), Clauses 16 and 17 for open-web steel joists and composite beams, respectively. Few rules are given specifically for the design of composite trusses.

The truss system must be designed to resist factored loads during deck placement, concrete placement and occupancy. When unshored construction techniques are used, as is typical, the steel top chord must be designed to resist construction loads. The steel top chord is neglected in determining the properties of the composite section. Also, full shear connection between the concrete slab and the steel top chord is required. There must also be sufficient concrete cross sectional area to place the plastic neutral axis in the slab.

3.1.1 Moment resistance of a composite truss

Because full shear connection with the plastic neutral axis in the slab is required, the moment resistance is that of the couple formed by the tensile force in the steel and the compressive force in the concrete shown in Figure 3.1. The factored yield strength of the bottom chord is

[3.1] $T_r = \phi A_g F_y$.

CSA Standard S16.1 also gives a factored tensile resistance based on fracture of the net section of

[3.2] $T_r = 0.85\phi A_n F_u$.

When welded connections are used, as is the case here, the net area, A_n, is equal to the gross area, A_g. The factored yield resistance of [3.1] is the lesser when

[3.3] $F_y < 0.85F_u$.

For structural quality steels given in CSA Standard G40.21 - M92 (CSA 1992b) only the quenched and tempered low alloy steels with a yield strength of 700 MPa and a tensile strength of 800 MPa do not meet the restriction of [3.3].

The factored compressive strength of a depth, a, of the concrete slab is

[3.4] $C_r = 0.85\phi_c f_c' ab$.

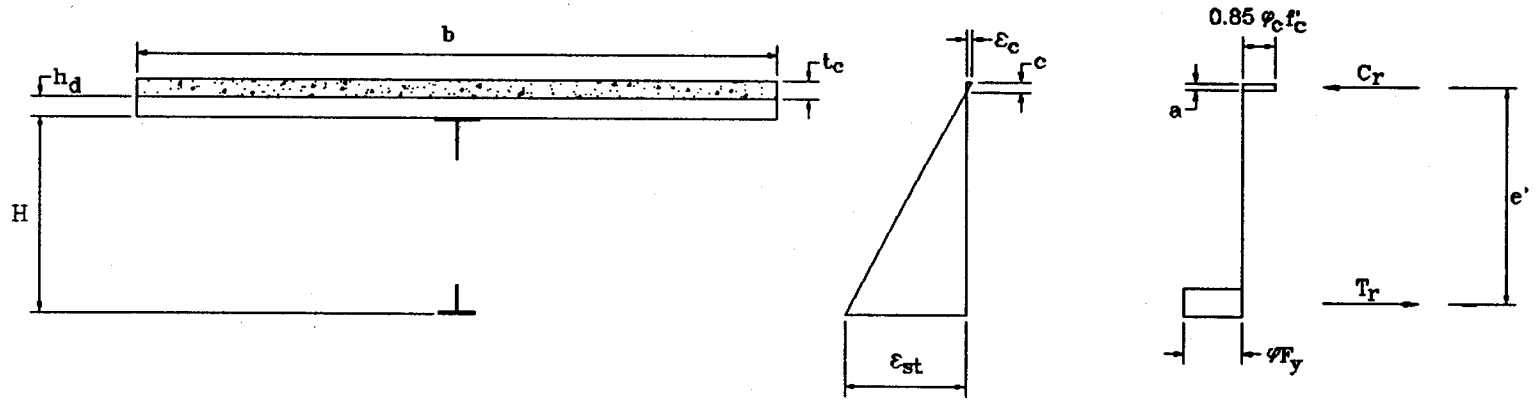

Fig. 3.1 Composite cross-section moment resistance

For horizontal equilibrium, $T_r = C_r$ and therefore

$$[3.5] \quad a = \frac{\phi A_g F_y}{0.85\phi_c f_c' b} \not> t_c ,$$

where t_c is the thickness of the cover slab. The moment resistance is then

$$[3.6] \quad M_{rc} = \phi T_r e' = \phi A_g F_y e' ,$$

where e' is the distance between the compressive and tensile forces.

3.1.2 Steel top chord

Because composite trusses are typically constructed unshored, the steel top chord acts as the compressive chord of the truss before the concrete hardens. During deck placement, the top chord may be laterally unsupported. During concrete placement, the top chord is laterally supported by the deck welded to it. Loads to be carried include dead loads and construction live loads.

3.1.3 Web members and connections

Clause 17.3.2 in S16.1 states that the web members shall be proportioned to carry the total vertical shear. The effects of joint and connection eccentricities are normally considered for the design of compression web members, but are typically neglected for the design of tension web members. Primary in-plane joint eccentricities can be avoided by aligning the centroidal axis of the members being connected to meet at a point.

3.1.4 Shear interconnection between the truss and slab

To prevent pull-out type failures in the part to which the shear stud is connected, S16.1 requires that the diameter of the stud be less than 2.5 times the thickness of this part. The height to diameter ratio of the stud shall not be less than four. The projection of a stud in a ribbed slab, based on its length prior to welding, shall be at least two stud diameters above the top surface of the steel deck. Furthermore, in the 1989 edition of S16.1, for the first time, a reduced capacity of studs in ribbed slabs with the ribs perpendicular to the beam based on a pyramidal concrete pull out area is given. Chien and Ritchie (1984) suggest that studs placed in pairs be a minimum of four stud diameters center to center.

For full shear connection with the plastic neutral axis in the concrete slab, the shear force to be transferred between the point of maximum moment and zero moment is

[3.7] $V_r = T_r = \phi A_g F_y$.

3.1.5 Serviceability

The camber of a given composite truss may account for the elastic deflection of the steel truss due to the dead load of the deck and wet concrete, the deflection of the composite truss due to additional dead loads, shrinkage, creep, interfacial slip, and perhaps some portion of the live load.

If the elastic deflection of the steel truss is not calculated using a computer frame analysis program, the approximate method, suggested in S16, Clause 16.6.14.2, of assuming the truss to have a moment of inertia, I_S, equal to the gross moment of inertia of the chords about the centroidal axis, and increasing the deflection calculated on this basis by 10% to account for the flexibility of the open web system, may be used.

To calculate the increase in the deflection due to partial shear connection and interfacial slip, S16.1 suggests the use of an effective moment of inertia of

[2.4] $I_e = I_s + 0.85p^{0.25}(I_t - I_s)$,

where p = 1.00 for full shear connection. An approximate method to allow for creep, is to increase the deflection calculated for dead load and long term live load using the above procedure by 15%. Because composite trusses are relatively stiff, live load deflections rarely exceed the maximum recommended values given in Appendix I of S16.1 (Chien and Ritchie 1984).

Brattland and Kennedy (1986) suggest that for composite trusses the effective moment of inertia, I_e, as calculated from [2.4], should be divided by a factor of 1.10 to account for the flexibility of the open web system. A better fit to their test results was achieved when the coefficient 0.85 in [2.4] was replaced by 0.77.

In CSA Standard S16.1 - 94 (CSA 1994), based on the work of Kennedy and Brattland (1992), the shrinkage deflection is computed as

[2.1] $\Delta_s = \dfrac{\varepsilon_f A_c L^2 y}{8 n_t I_{et}}$.

Chien and Ritchie (1984) suggest that composite trusses provide strong and stiff floors in most instances. When such a system is used to support a large open area, free of partitions and other natural damping features, special consideration should be given to susceptibility to walking vibration to ensure that vibration characteristics are acceptable for the intended use and occupancy. Analyses of dynamic experimental data of two full-scale composite trusses by Woldegiorgis and Kennedy (1994), where the only damping was attributable to the composite truss itself (and the friction in the knife edges and rollers, which is considered to be very small), showed that this structural system exceeded CSA Standard S16.1 - M89 Appendix G annoyance threshold guidelines. In a building, considerably more damping would exist, attributable to partitions and other furnishings, actual structural connections and building continuity.

3.2 Test specimen design

3.2.1 Description

The configuration chosen for testing is based on Design Example 5.8 of Chien and Ritchie (1984). The uniformly loaded composite trusses span 11 500 mm and are spaced at 3000 mm on center. The steel deck is 76 mm deep wide rib (HB 30V, manufactured by Vic-West Steel) with the ribs oriented perpendicular to the truss. A 65 mm thick cover slab of 20 MPa normal density concrete was specified. The slab width is 2350 mm, consistent with the trusses tested by Brattland (1986). Slab reinforcement consists of 152 x 152 - MW9.1 x MW9.1 welded wire mesh. The steel truss has WT top and bottom chords and double angle web members in a Warren configuration with 8 top chord panels and an out-to-out depth of 730 mm. All steel is CSA G40.21M Grade 300W (CSA 1992b). The specified dead and live loads are 14.2 kN/m and 6.0 kN/m, respectively, resulting in a factored moment of 443 kN·m and a factored shear of 153.9 kN, using the load factors of 1.25 for dead load and 1.50 for live load as given in the National Building Code of Canada (1990).

The design of the test specimen followed the requirements given in CSA Standard S16.1 - M89 for composite beams and joists, with the incorporation of some unique design features as discussed in Section 3.2.2. The concrete slab was specified to be the same as that in Design Example 5.8, even though the truss was designed for a test loading consisting of four concentrated loads. The selection of members is discussed subsequently. A half elevation of the steel truss is shown in Figure 3.2. The factored moment resistance of the composite truss, based on S16.1 and using specified material and geometric properties, was 453 kN·m, 1.02 times the factored moment.

The truss was not cambered. The elastic deflection of the steel truss under the weight of the wet concrete was estimated to be 16.7 mm. The deflection of the composite truss due to the specified superimposed dead and live loads plus shrinkage and creep (assuming 50% of the live load was sustained) was estimated to be 16.1 mm or L / 714, considerably less

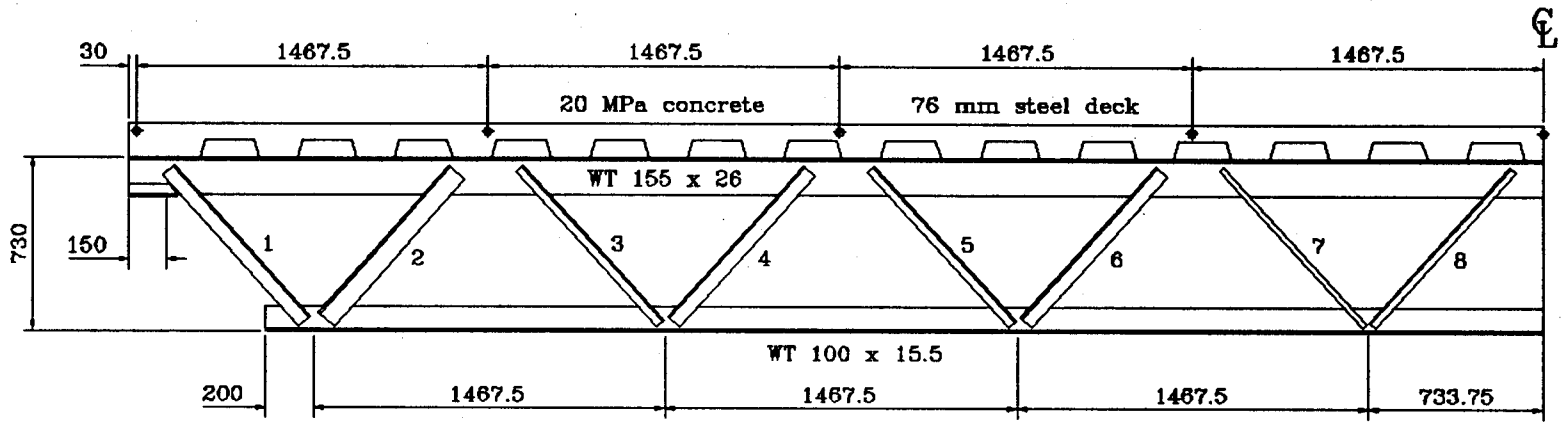

Web members (imperial sizes)

1	2 L 2 1/2 x 2 1/2 x 5/16
2	2 L 3 1/2 x 3 1/2 x 3/8
3	2 L 1 1/2 x 1 1/2 x 1/4
4	2 L 2 1/2 x 2 1/2 x 5/16
5	2 L 2 1/2 x 2 1/2 x 1/4
6	2 L 2 1/2 x 2 1/2 x 5/16
7	2 L 1 x 1 x 1/8
8	2 L 1 1/4 x 1 1/4 x 3/16

Fig. 3.2 Half elevation of truss

than the recommended maximum value for live load deflection acting alone of L / 360, or 31.9 mm, as given in S16.1 - M89.

3.2.2 Special design considerations

3.2.2.1 Bottom chord

Although S16.1 defines the tensile resistance, T_r, as the lesser of the values given by [3.1] and [3.2], yielding of the bottom chord does not precipitate collapse, rather, the truss deflects inelastically as the most heavily loaded bottom chord segments yield. In several previous full scale tests by others to failure of composite trusses (Cran 1972; Bjorhovde 1981), failure was initiated by the buckling of a compression diagonal. To ensure against this and other such failure modes, the web members and their connections, shear connectors and the bearing details, were designed for loads corresponding to a moment of 821 kN·m, obtained when the bottom chord reaches 90% of the upper limit of its factored tensile strength. At this load level, the concrete slab is more than adequate with a rectangular stress block of only 0.35 of the cover slab thickness.

In retrospect, this approach, in which it was envisaged that the bottom chord would reach a load corresponding to a stress of 90% of the upper limit of the tensile strength ($0.90 \times 620 = 558$ MPa), may have been somewhat conservative. To guard against premature failure of more brittle components, it would appear sufficient to have these components designed for a force that ensures that the bottom chord, with a yield strength greater than the minimum specified, does in fact yield. One approach, when [3.1] governs, would be to design for the mean yield strength plus a number of standard deviations determined from a statistical analysis. Kennedy and Baker (1984) give, for rolled sections, a mean value of the yield strength of 1.06 times the specified minimum and a coefficient of variation of 0.051. The yield strength corresponding to three standard deviations above the mean would be 1.22 times the specified minimum value, or $1.22 \times 300 = 366$ MPa, considerably less than 558 MPa. For a normal distribution, this corresponds to a probability of only 0.0013 of the yield strength exceeding the value used for design. When [3.2] controls the design of a truss, as is the case for trusses using 700Q steels or having bolted connections with $0.85A_nF_u$ less than A_gF_u, a similar approach based on the statistical variation of the tensile strength could be used.

3.2.2.2 Triangulation

Joint eccentricities are avoided by positioning web members so that the centroidal axes of the members meeting at a joint intersect at a common point. With the relatively deep stem of the WT bottom chord, it was possible to align the web members to avoid any joint eccentricities.

In positioning the ends of the diagonals on the top chord, Brattland (1986) minimized the joint eccentricities of the composite truss by placing the diagonals so that the centroidal axis of a joint pair intersected at the mid-depth of the cover slab. This procedure should provide better ultimate performance, but requires larger moments to be taken into account in the design of the top chord during the unshored construction stage.

This triangulation system caused the construction load case to govern the design of the top chord. A relatively large top chord was required not only because the WT's in the size range needed were, at best, Class 3 sections, but also because WT's are inefficient in bending, especially when their stems are in compression. Nevertheless, this system was used to give improved performance for ultimate load conditions. The extra weight of steel required was 13%.

3.2.2.3 Web members

The web members were selected to resist axial forces, as determined in Section 3.2.2.1, consistent with 90% of the factored upper limit of the tensile strength of the bottom chord. These force levels equal $0.90\,\phi\,620\,/\,(\phi\,300) = 1.86$ times those based on the specified yield force of the bottom chord.

The tension members were designed for axial forces only, because no bending moments can exist in a cross section at full yield.

Compression diagonals were designed as beam-columns, using an effective length equal to the distance between the centroids of the connecting welds. This length could be considered to be the actual unbraced length that is required to be used by Clause 9.3.4 of S16.1 - 94 for members that fail by bending, which is the case here, with end moments applied about two principal axes, as discussed subsequently. The effective length between the centroids of the weldments is slightly more conservative than the approach used by Chien and Ritchie (1984) who used an effective length equal to the clear distance between the ends of the weldments. Because the compression members were aligned to have their centroidal axis intersect at a common point with the centroidal axis of the steel bottom chord and the concrete cover slab, no in-plane joint eccentricities exist. However, out-of-plane connection eccentricity moments exist, because the angles are connected on one leg only. Based on Brattland and Kennedy (1992), as confirmed by Woldegiorgis (1994), an end eccentricity equal to one-third of the centroidal distance of the angle was used. The resulting moment was resolved about the principal axes of the angle, and the angles were designed as columns subjected to biaxial bending. The angles were also checked for torsional-flexural buckling in accordance with the procedures given by the Structural Stability Research Council (Galambos 1986) and now incorporated in S16.1 - 94. Only the end compression diagonal was governed by torsional-flexural buckling.

3.2.2.4 Welded connections

The out-of-plane moments due to connection eccentricity were neglected in the design of the welds, as proposed by Blodgett (1976) and as used by Brattland (1986). The welds were designed to transfer the axial load plus the maximum in-plane moment that could coexist when the interaction value for the member subjected to biaxial bending was set equal to 1.0.

3.2.2.5 Shear connectors

Paralleling the design of the web members, the shear connectors were designed to transmit 0.9 times the factored upper limit of the tensile strength of the bottom chord (i.e., 1.86 times its minimum specified yield strength). Nineteen mm diameter studs, with an after weld length of 115 mm, were selected. The factored shear resistance of a single stud in a ribbed slab, with the ribs perpendicular to the beam, by Clause 17.7.2.3 of S16.1 - M89 is 65.4 kN, and for a pair of studs, spaced at 87 mm on center, the shear resistance is 87.7 kN. The studs were placed at the center of the flutes. Using ten pairs and four single studs, the total factored shear resistance was 1139 kN as compared to a factored tensile force of 1004 kN in the bottom chord, determined as above. The extra shear capacity more than compensates for the three single studs placed in a region of zero shear, each side of the centerline, and, also, guarded against premature stud failure, as had occurred in Brattland's tests.

3.2.2.6 Bearing detail

Figure 3.3 shows the bearing details. By welding the shoe angles to the stem of the WT and by positioning the end tension diagonals to overlap the bearing length of 80 mm, shear resistance in excess of the factored reaction of 286 kN was obtained. The end tension diagonal was positioned so that the extension of its centroidal axis intersected that of the cover slab outside the reaction to reduce bending of the steel top chord. The small negative moment that resulted combined with the axial force in the steel top chord near the bearing was well within the resistance of the top chord.

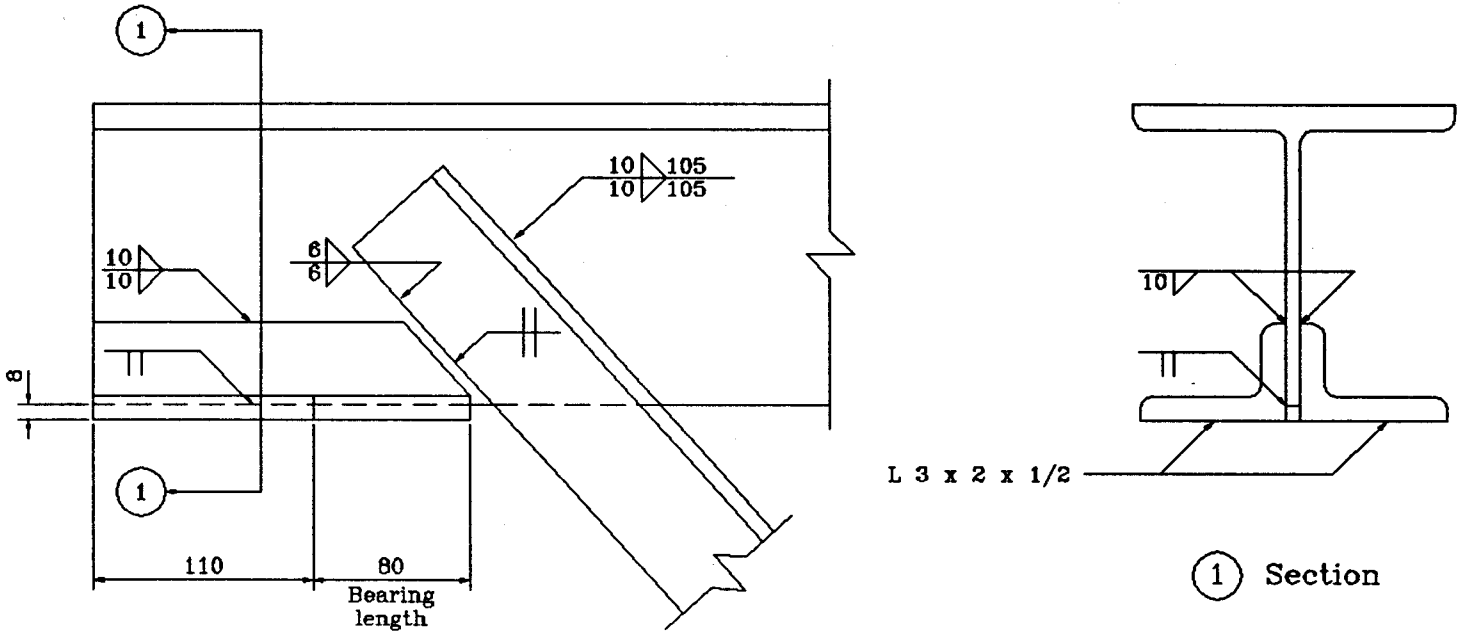

Elevation

Fig. 3.3 Bearing details

4 EXPERIMENTAL PROGRAM

4.1 General

Shrinkage and flexural tests were conducted on the steel and composite truss to investigate:

1. the deflection of the steel truss under the weight of the wet concrete to verify camber requirements for unshored construction,
2. the deflection of the composite truss and development of top and bottom chord and slab strains due to shrinkage of the concrete over a period of 60 days,
3. the load deflection response, the test-to-predicted failure load ratio and the failure mode,
4. the effective moment of inertia of the composite truss,
5. the distribution of concrete strains over the width of the slab,
6. interfacial slip and shear transfer between the concrete and steel,
7. the forces in the chords, slab and web members and the behaviour of these components,
8. the longitudinal cracking of the concrete slab and
9. the yielding at the connections.

Ancillary tests conducted to determine the properties of the components of the composite truss included:

1. concrete compression cylinders tests,
2. concrete split cylinder tests,
3. stud push-out tests,
4. shrinkage control tests,
5. steel tension coupon tests and
6. residual strain tests on the steel chords and one web member.

4.2 Test specimen

4.2.1 Fabrication

Design drawings for the steel truss and a list of the materials required for ancillary testing were given to two local fabricators for bidding. At the request of the low bidder, the studs were welded to the truss in their shop. On delivery, the truss was measured to verify conformance to the design drawings. A summary of the measurements is given in Chapter 5. The studs originally provided were too short and were replaced by longer ones. Two short lengths of weld that were missing on delivery were added by laboratory personnel.

4.2.2 Assembly of composite truss

Prior to assembly of the composite truss, 105 electrical resistance strain gauges were applied to the steel truss, as discussed subsequently. The steel truss was then simply supported on pedestals about 1 m high. This was done so that after placing the concrete shrinkage measurements could be made readily. Hemispherical rockers with matching female parts or "pucks", which allow rotation in any direction, were provided at both supports, and a roller allowing horizontal movement was provided at the north end.

The steel deck was supplied in sheets 813 mm wide by 2350 mm long. (The specified width of the slab was 2350 mm.) The deck was installed over the studs by cutting holes through which the studs projected. After placing the deck on the truss, the sheets were crimped at four locations per joint using a crimping tool supplied by the deck supplier. The deck was spot welded to the truss at two locations per flute.

Twenty gauge cold formed 142 mm high edge angles were installed on all four sides of the truss. Wooden shoring was built to support the outer edges of the deck, as shown in Figure 4.1, to prevent the deck from buckling under the weight of the wet concrete. This shoring was braced against the bottom chord, so that vertical deflections during the shrinkage test would not be impeded. Lifting plates were welded to the ends of the steel top chord to allow repositioning of the truss for the flexural test.

The welded wire mesh, supplied in a roll 1.524 m wide, was installed in two rows along the length of the truss, giving an overlap of about 700 mm at the center. Plastic chairs were used to support the mesh 25 mm below the surface of the concrete slab. The mesh was tied down with wire ties through the steel deck to prevent the mesh from lifting.

A frame was constructed around the truss to provide scaffolding for placing the concrete and for taking shrinkage measurements. Six pedestals, one at each corner and one at mid-length of each side, with screw devices to allow vertical adjustment, were placed to provide stability and support. As the concrete was cast, the screws were lowered to accommodate the deflection of the steel truss. Three rod-dial gauge assemblies, as discussed subsequently, were installed to measure the overall change in length of the top and bottom steel chords. Dial gauges were installed at the mid-span and the quarter points to measure vertical deflections.

The concrete was placed on July 22, 1993. It was shoveled into place, vibrated, screeded and then wood trowelled. Eighteen 150 mm diameter concrete cylinders were cast. The four concrete sections of two push-out test specimens and two concrete shrinkage control specimens were also cast. The time that elapsed during casting was about two hours. When the concrete was finished, it was covered with polyethylene to reduce moisture loss and improve the curing conditions. When first tested, the slump of the 3.5 m^3 batch of concrete was 70 mm, as compared to the specified slump of 80 mm. With the addition of about 20 L of water, the measured slump increased to 75 mm.

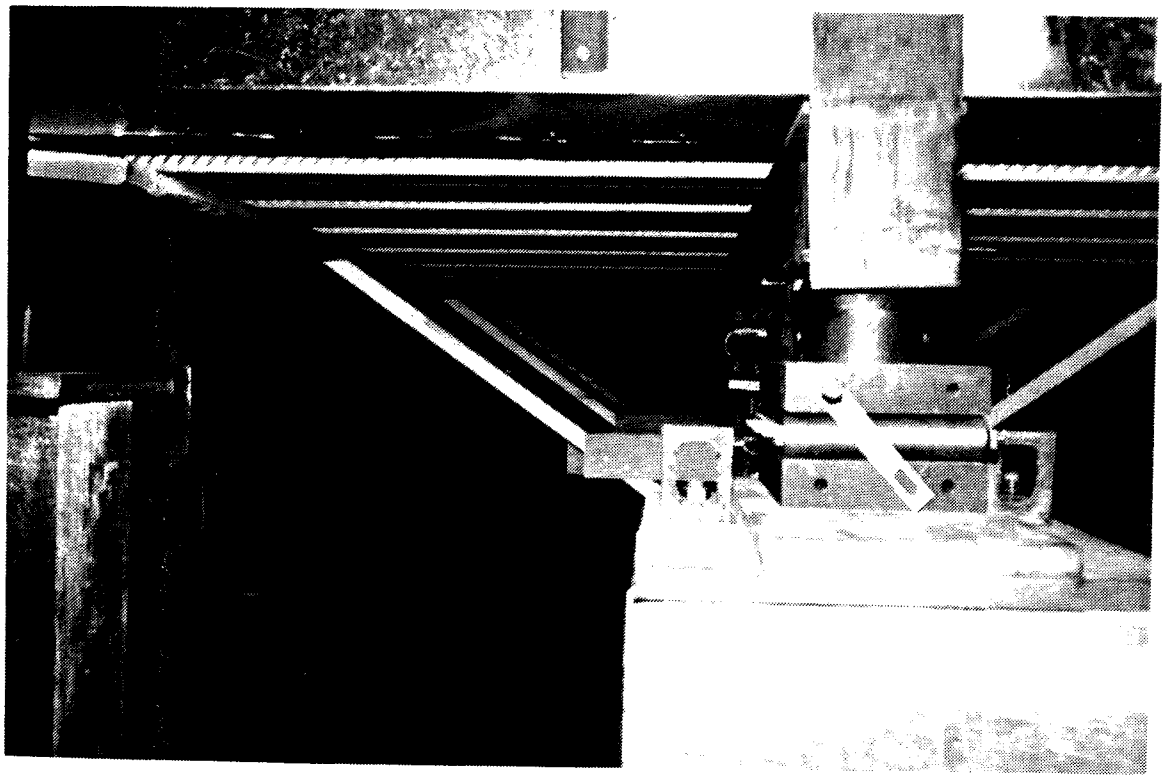

Fig. 4.1 Wooden bracing

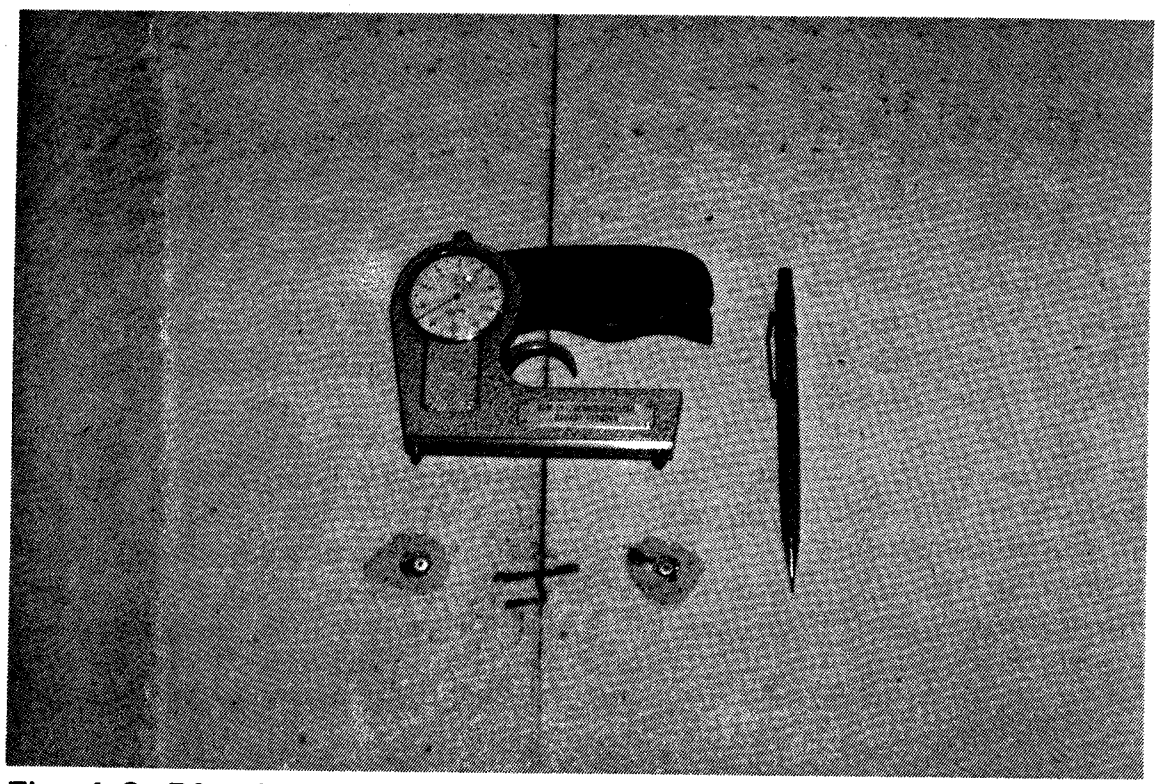

Fig. 4.2 Pfender gauge and points

One day after casting, the concrete cylinders were stripped and placed in a standard saturated lime bath.

4.3 Shrinkage test

4.3.1 Test set up

One day after casting, the 100 mm square by 1000 mm long shrinkage control specimens were stripped, coated with tar on all sides except the top and supported on rollers on the floor near the quarter points of the truss. The specimens and the concrete slab were instrumented for the shrinkage test. During the shrinkage test, the screw supports, used to ensure stability, were adjusted to maintain a small clearance with the underside of the deck.

4.3.2 Instrumentation

Instrumentation for the shrinkage test included:

1. rod-dial gauge assemblies to measure overall changes in dimensions of both the steel chords and the concrete slab,
2. electrical resistance strain gauges to measure local strains on the steel chords,
3. Pfender type gauge points for use with a Pfender type demountable mechanical extensometer to measure local concrete strains (shown in Figure 4.2),
4. dial gauges to measure vertical deflections,
5. a thermometer to measure air temperature,
6. a hygrometer to measure the relative humidity and
7. a load cell to measure the weights of the truss.

The rod-dial gauge assemblies consisted of dial gauges, reading to 0.01 inches, fixed to the specimen with the spindles reacting against light steel rods that extended over the length to be measured and fixed at the far end to the specimen. The light steel rods were supported at intervals along their length. Figure 4.3 shows the location of the four rod-dial gauge assemblies used to measure the change in length and width of the concrete slab. The location of the rod-dial gauge assemblies measuring deformation of the top and bottom chords is shown in Figure 4.4a. As well, rod-dial gauge assemblies were used to measure the overall shrinkage of the shrinkage control specimens.

Five electrical resistance strain gauges were placed on each of the top and bottom steel chords to measure local steel strains during concrete shrinkage. The gauges on the top chord were about 734 mm north of the truss mid-span, and those on the bottom chord about 100 mm south of the mid-span. The location of the strain gauges on the chord cross sections are shown on Figures 4.4b and 4.4c.

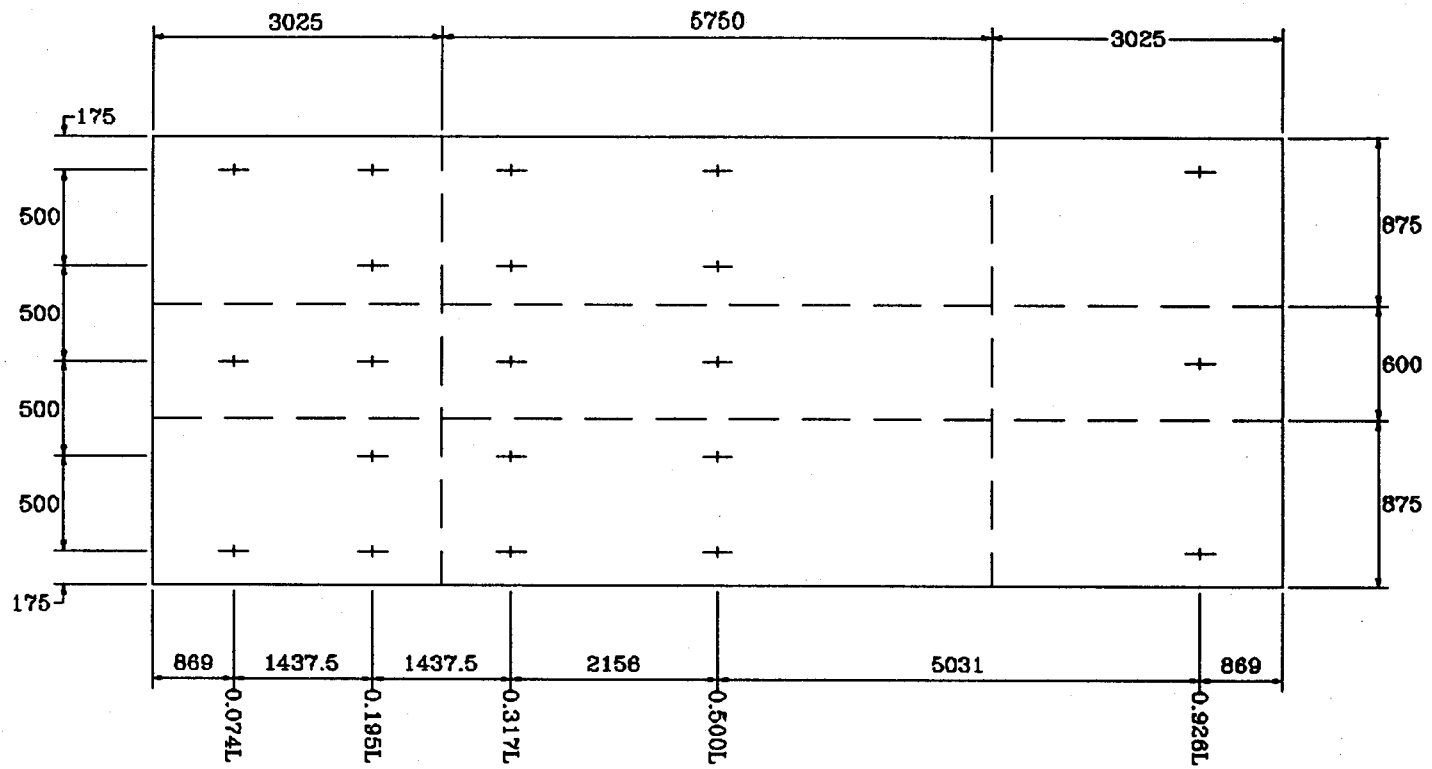

Fig. 4.3 Shrinkage test concrete strain measurement locations

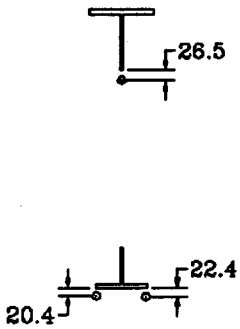

Fig. 4.4a Location of rod-dial gauge assemblies for shrinkage test

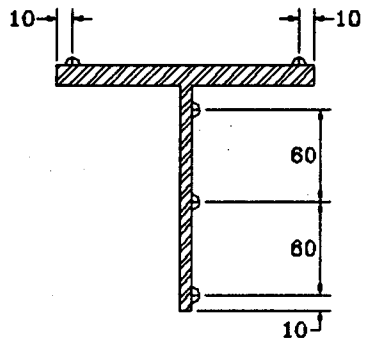

Fig. 4.4b Location of strain gauges on top chord for shrinkage test

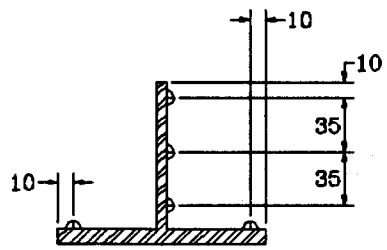

Fig. 4.4c Location of strain gauges on bottom chord for shrinkage test

The locations of the 21 pairs of Pfender gauge points are shown in Figure 4.3. Each point consists of a 1/16 inch diameter steel ball, which is pressed into a Demec point, for convenience, which was then fixed to the concrete surface. The procedure for fixing the points to the concrete was to grind to remove laitance, to dry the surface using a propane torch and then affix the point with five minute epoxy. The gauge length of the Pfender gauge is 100 mm.

The dial gauges used to measure the vertical deflection at the mid-span and the quarter points measured to 0.01 mm.

All readings were recorded manually, essentially on a daily basis.

4.3.3 Testing procedure

The weight of the truss at various stages of construction was measured.

Before casting the concrete, initial readings were taken of the strain gauges mounted on the steel chords, the rod-dial gauge assemblies and the deflections of the truss. These readings were repeated immediately after the concrete was cast and about two hours later when the concrete was judged to have set. Polyethylene sheets were placed over the slab, push-out test specimens and shrinkage test specimens within five hours of completion of casting. The polyethylene was removed briefly one day after casting to install the concrete instrumentation. The polyethylene was permanently removed after an initial curing period of seven days. Shrinkage measurements were taken for a period of 68 days, until September 28, 1993.

At this time, the wooden shoring was removed from the truss. The edge angles were also removed so that Pfender gauge points could be applied to the edge of the concrete slab.

4.4 Flexural test

4.4.1 Test set up

Load cells, knife edges and rollers were installed at both reaction points and reaction frames for the loading jacks were erected. The reaction assembly details are shown in Figure 4.5 and the loading jack assembly details are shown in Figure 4.6.

Figure 4.7 shows that, with the selected four point loading, the bending moment diagram approximates that of a uniformly distributed load closely.

A pneumatically activated hydraulic system with a reservoir, control console, control valve and control manifold was used to supply pressure to the jacks. The four jacks could be subjected to the same hydraulic pressure and thereby provide essentially the same load. By

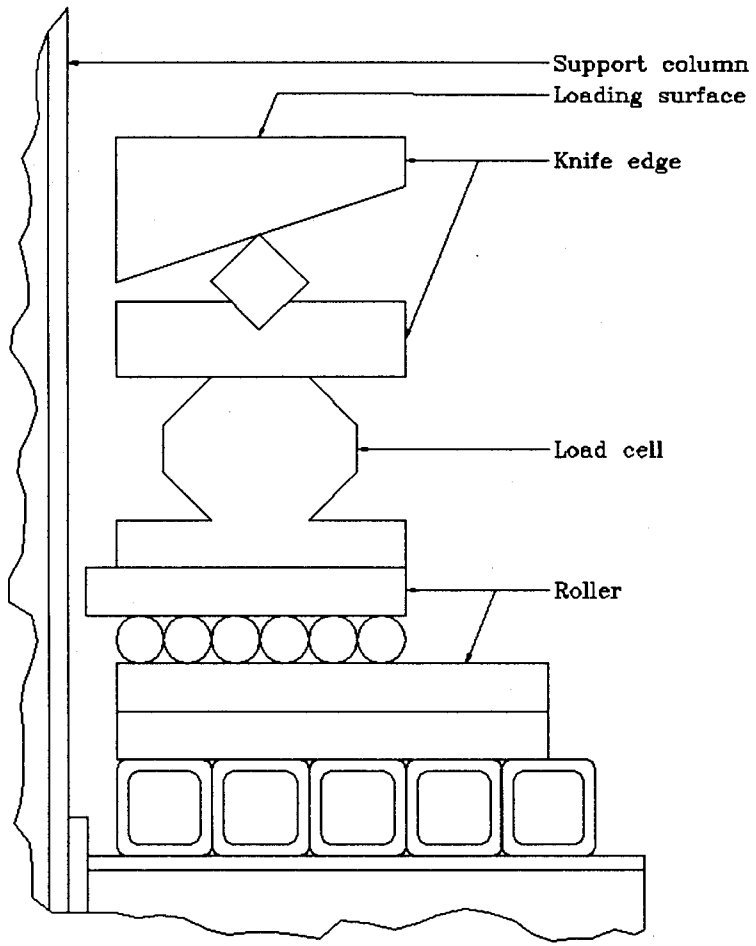

Fig. 4.5a Reaction assembly detail

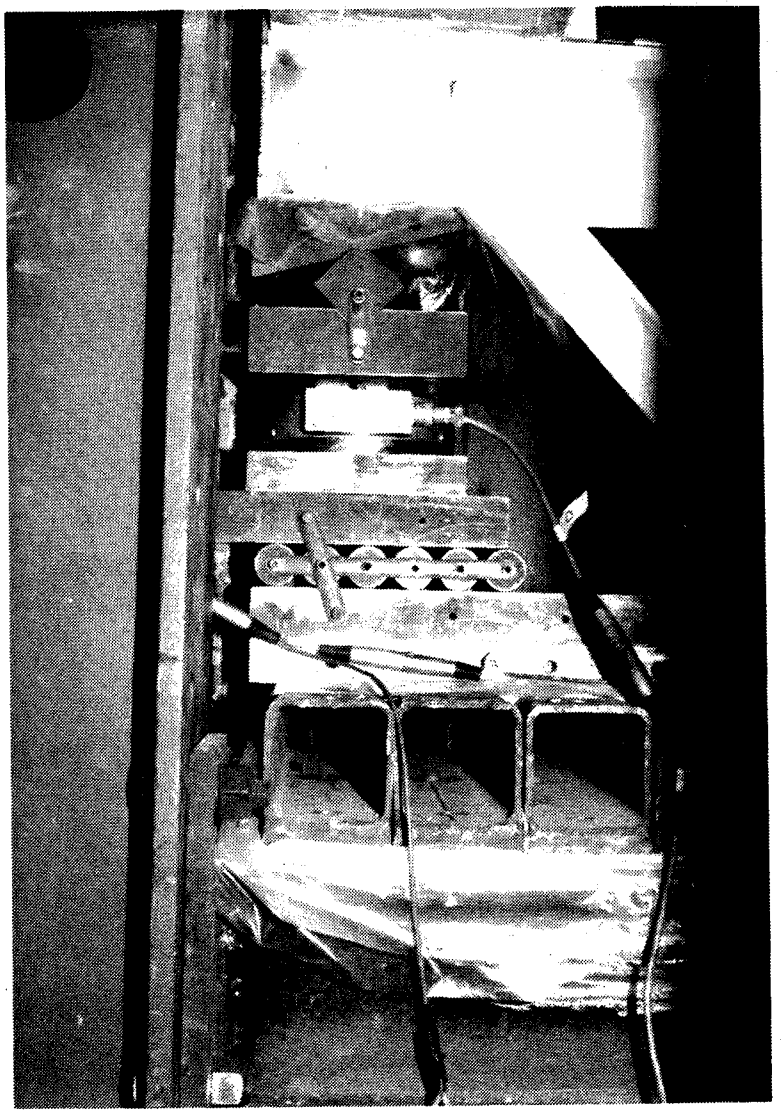

Fig. 4.5b Reaction assembly detail

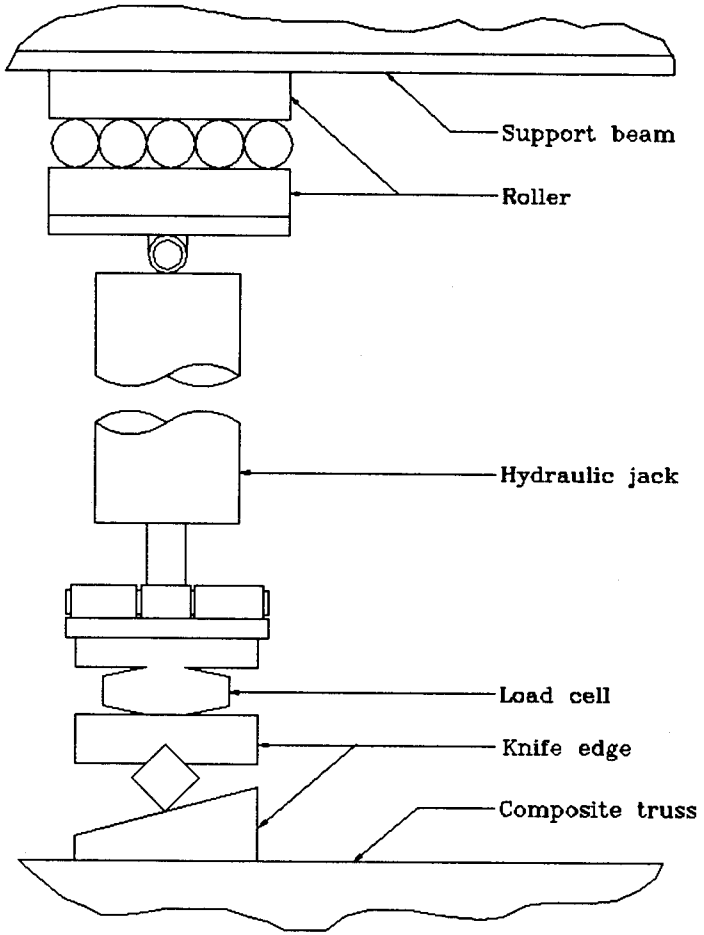

Fig. 4.6a Jack assembly detail

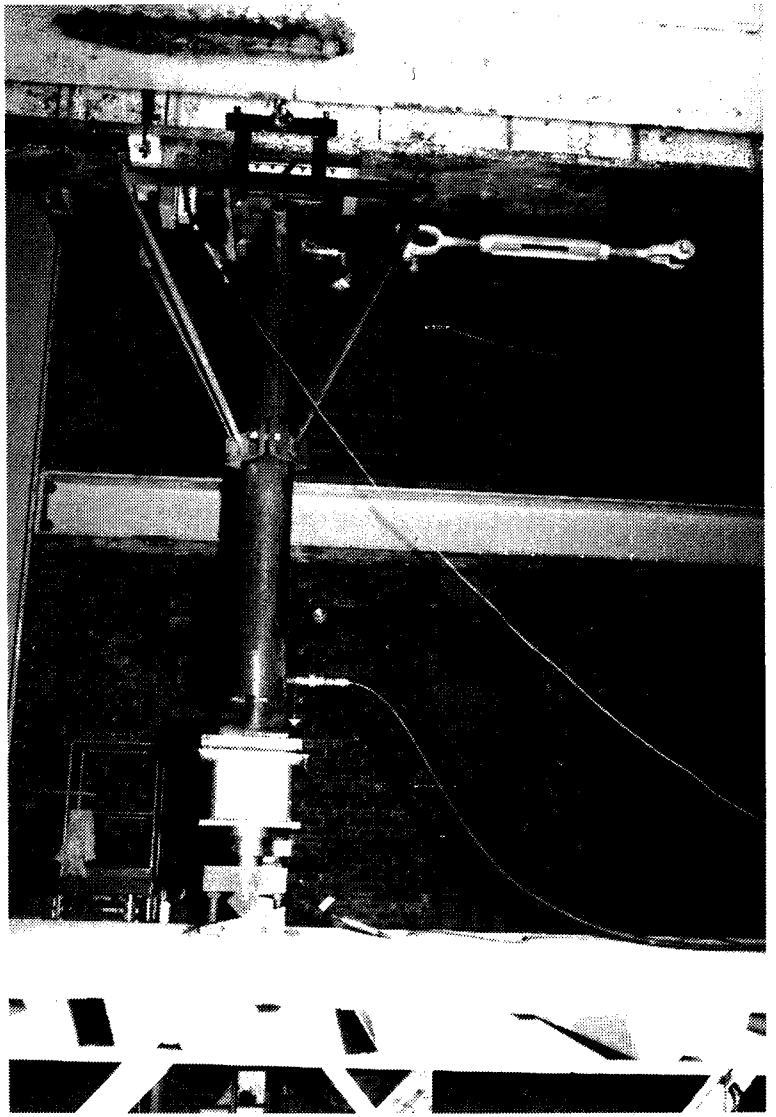

Fig. 4.6b Jack assembly detail

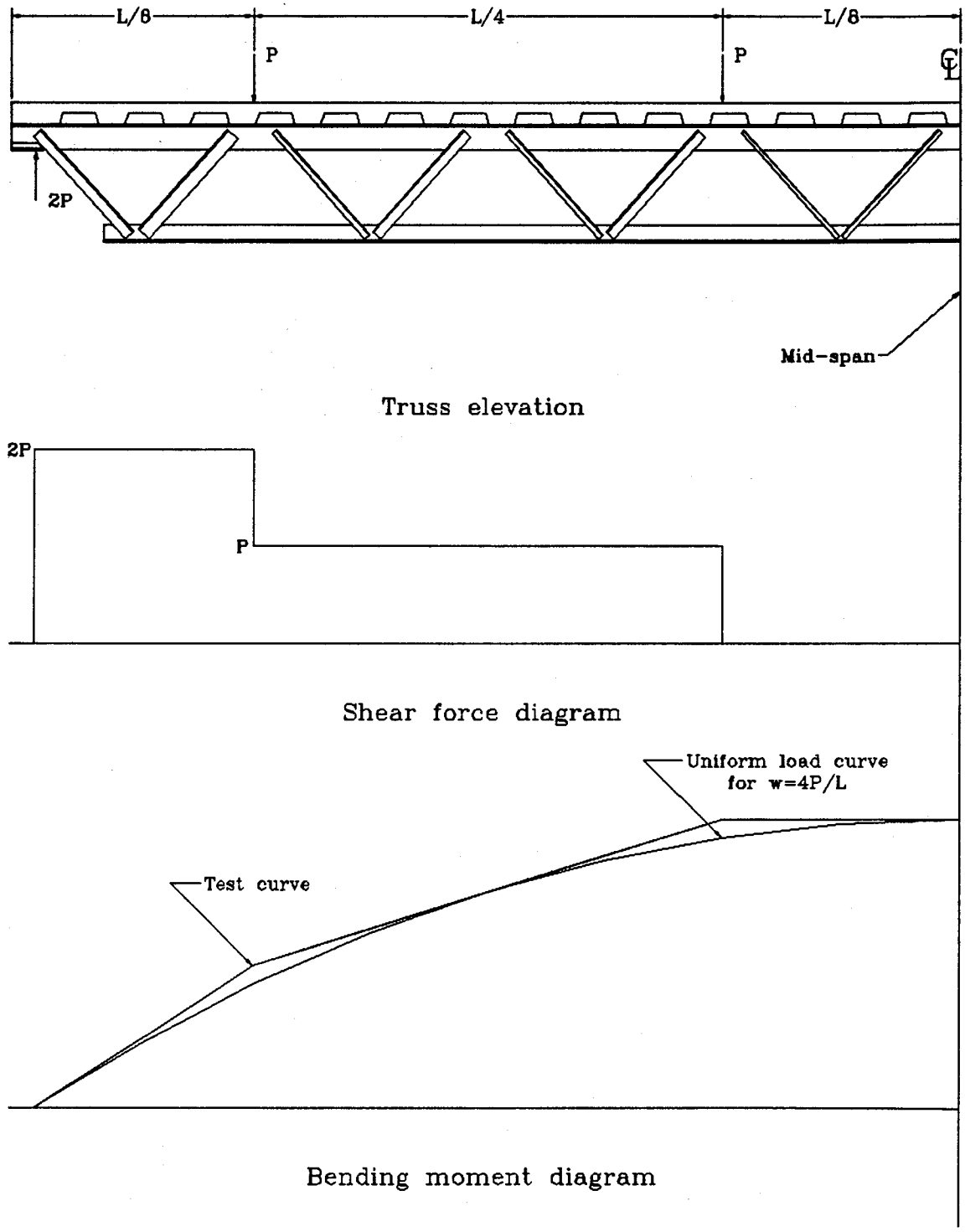

Fig. 4.7 Composite truss elevation, shear force and bending moment diagrams

closing selected valves, loads could be maintained on some jacks while the pressure could be adjusted on others. The load cell on the north interior jack was used to monitor load increments.

Because of the severe straining that was anticipated for the bottom chord, special consideration had to be given to the design of the loading and reaction assemblies to accommodate the large distortions. Jacks, with a stroke of 1200 mm, were available. Without resetting, this stroke (on the interior jacks) would accommodate a strain in the most heavily loaded bottom chord panels of about 9%. This, in turn, meant that the bottom chord could be loaded to within about 2% of its ultimate tensile strength. The corresponding inward movement of the reaction was 177 mm and the rotation at the reaction was 17°. The roller and knife edge assemblies for the reaction provided a movement of 250 mm and a rotation of 30°. The 30° rotation was made possible by using a 15° beveled plate placed initially in the reverse position, as shown in Figure 4.5, so that the final slope was only 15°. The lateral movements and rotations for the exterior jacks were less than those of the reactions, and the stroke was less than for the interior jacks.

In the test set up, the test specimen was partially constrained, with no restraint in the horizontal direction. Large steel columns were erected at each end of the specimen to restrict outward longitudinal movement to about 50 mm in either direction. Also, at each end, the base plate of the knife edge was connected to the columns using a threaded rod so that the position of the mid-span of the truss could be maintained. To ensure that the truss did not tip by rotating about its longitudinal axis, adjustable screw devices were installed beneath the four corners of the slab and kept a few millimetres clear during the test. Horizontal screw devices were installed on each jack so that the verticality of each jack could be maintained. The truss was white washed the day before testing so that yielding, as manifested by flaking of the whitewash, could be observed.

4.4.2 Instrumentation

Instrumentation for the flexural test included:

1. load cells at each reaction and load point,
2. electronic resistance strain gauges to measure steel strains,
3. Pfender type gauge points to measure concrete strains. In addition to the 21 used for the shrinkage test, a pair were placed on each side of the slab at the mid-depth of the cover slab, and
4. linear variable differential transformers (LVDTs) and cable transducers to measure various displacements.

All load cells were calibrated before use. The supply voltage for the load cells described in Table 4.1 was 15 V.

Table 4.1 Load cell information

Location	Type	Capacity, kN	Serial number
Reaction	Strainsert	446	08409-1 / 03691-1
Exterior load point	Sensotec	223	104697 / 104698
Interior load point	Kyowa	178	26395 / 26396

The positions of the 105 electrical resistance strain gauges are shown in Figure 4.8a. Of the ten gauges placed to measure shrinkage strains on the two steel chords, only nine were used in the flexural test. The five on the bottom chord and four of the five on the top chord were connected to the data acquisition system. The remaining 96 were placed in equal numbers on the four web members shown in Figure 4.8a to monitor web member behaviour. The 24 strain gauges per web member were placed in sets of six at four different locations along the length of the member, with the first sets at a distance of 1.5 times the leg size from the end of the weldment at either end, and the remaining two sets equally spaced. The use of four sets, an increase from three sets used by Brattland (1986), was an attempt to determine better the behaviour of the web members. Figure 4.8b shows the location of the six gauges at a given location for the two sizes of angles gauged. Woldegiorgis' (1994) analysis showed that six gauges defined well the planar strain distribution across the angle.

All ten LVDTs, calibrated before use, were supplied with 6 V from a controlled power source. Four, with a stroke of ±25 mm, were used to measure the interfacial slip between the steel truss and the deck at each end and the quarter points. The separation of the web angles that were strain gauged was measured at mid-length using LVDTs with a ±12 mm stroke. To obtain large bottom chord strains and to confirm, at least in part, the readings from the electrical resistance strain gauges, two LVDTs with a stroke of ±76 mm were mounted at the mid-span of the truss. These acted on a gauge length of 368 mm.

Nine calibrated cable transducers, supplied with 15 V from a controlled power source, were used. Three of these measured deflections at the mid-span and quarter points of the truss. The six remaining were used to measure the lateral movement of the reaction and load rollers so that the distance between loads could be determined at each load step.

4.4.3 Testing procedure

The composite truss flexural test was carried out on November 18 and 19, 1993, 119 and 120 days after casting the concrete. The truss was expected to behave in a linearly elastic manner up to a load of 70 kN per jack. Load steps of 10 kN were used in this range and 5 kN thereafter unless events, such as cracking noises or large deflections, dictated otherwise. General observations included measurements of mid-span deflection and reaction roller movements using a tape. As well, the extent of the cracking of the concrete was marked and yielding of the steel, made evident by flaking of the whitewash, was noted. At most load steps, all electronic readings were recorded twice, using a Fluke 2400

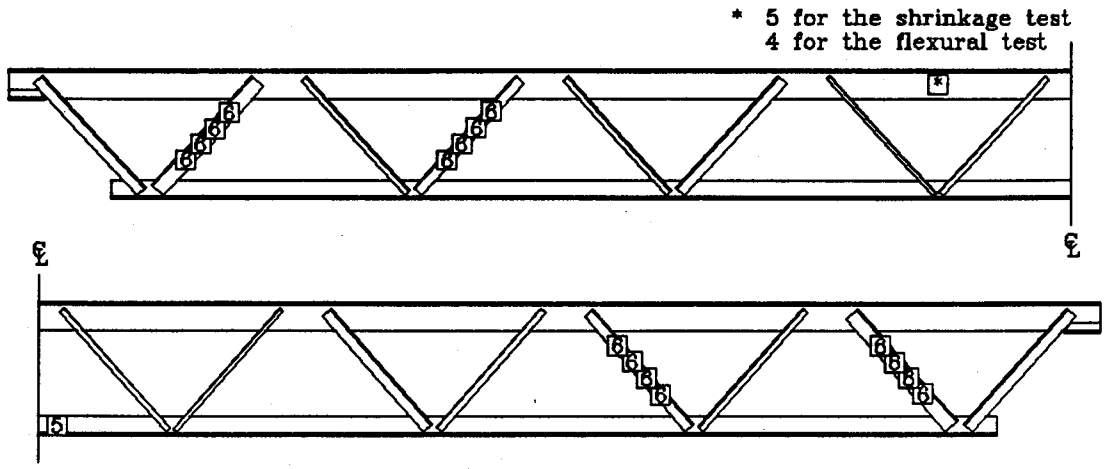

Fig. 4.8a Location of strain gauges on steel truss members

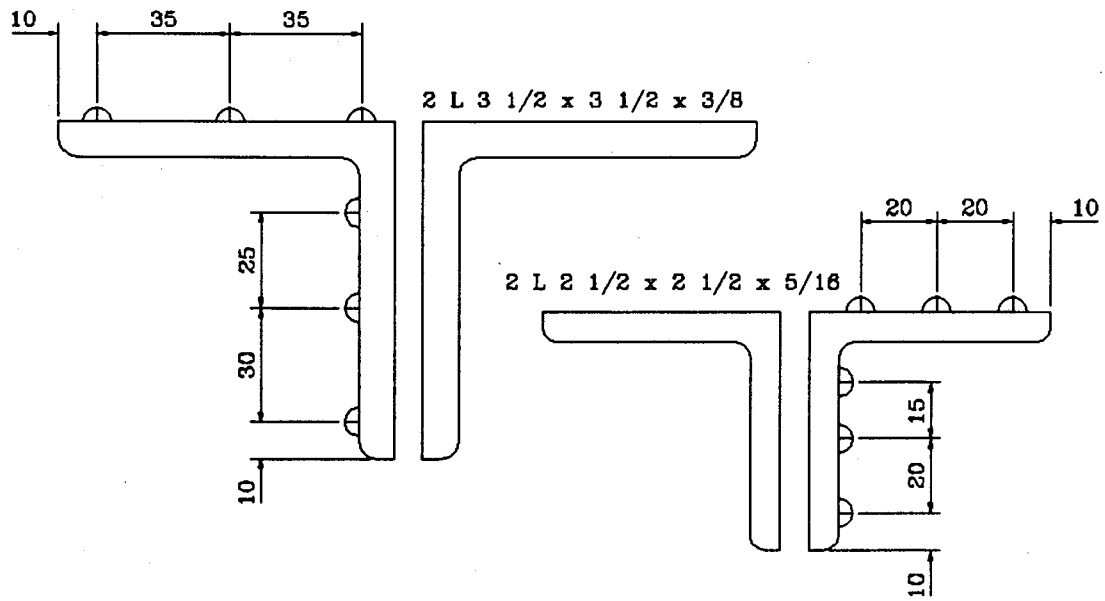

Fig. 4.8b Location of strain gauges on web member cross-sections

data acquisition system. Before taking the first readings, the sum of the vertical forces was checked to see that static equilibrium was satisfied. If the jack loads were not equal, within a tolerance of a few percent, they were adjusted. The second set of readings followed recording of manual measurements, just before the next load step. At each load step, the truss was centered using the threaded rod on the knife edge plates to bring the plumb bob at mid-span to its mark on the floor. The four loading jacks were plumbed, as required, using the screw devices. All devices, such as LVDTs and rollers, were checked to ensure there was sufficient travel.

At about every other load step, concrete strains were measured manually using the Pfender gauge. All data were transferred to a computer for processing.

5 GEOMETRIC AND OTHER MEASURED PROPERTIES

5.1 Steel sections

5.1.1 Dimensions

The cross sectional dimensions of the steel components were measured with micrometers or calipers, as appropriate. These dimensions, as listed in Table 5.1, are within the rolling tolerances prescribed by CAN / CSA G40.20 - M92 (CSA 1992a). No tolerance limits were specified for the WT section flange or web thickness, or for the leg thickness of structural size angles, which are angles with at least one leg of 75 mm or longer.

Table 5.1 Steel section properties

Element	Section	Dimension	n	Mean, mm	V	Mean / Specified	Tolerance, mm
Top chord	WT 155 x 26	b	28	166.60	0.0023	0.998	162-173
		t	30	12.963	0.0425	0.982	-
		w	52	7.484	0.0048	0.985	-
		d	30	157.46	0.0109	0.997	155-162
Bottom chord	WT 100 x 15.5	b	53	134.71	0.0052	1.005	129-140
		t	68	10.043	0.0274	0.985	-
		w	64	6.469	0.0099	1.011	-
		d	28	103.46	0.0086	0.985	102-109
Web 2	L 3 1/2 x 3 1/2 x 3/8	b	48	89.78	0.0136	1.009	86-92
		t	48	9.543	0.0116	1.005	-
Webs 1, 4 & 6	L 2 1/2 x 2 1/2 x 5/16	b	96	63.63	0.0064	0.994	62-66
		t	99	7.907	0.0127	1.001	7.5-8.3
Webs 3 & 5	L 1 1/2 x 1 1/2 x 1/4	b	48	38.22	0.0026	1.006	37-39
		t	50	6.273	0.0086	0.980	6.1-6.7
Web 7	L 1 1/4 x 1 1/4 x 3/16	b	47	31.65	0.0048	0.989	31-33
		t	47	4.648	0.0238	0.968	4.6-5.0
Web 8	L 1 x 1 x 1/8	b	48	25.52	0.0038	1.021	24-26
		t	47	3.050	0.0251	0.953	3.0-3.4

5.1.2 Section properties

For each cross section, the sectional properties were calculated from the mean measured values given in Table 5.1. The fillets and rounds were assumed to be circular arcs, with the radii of the fillets assumed to be the thickness of the flange or leg of the WT or angle. The radii of the rounds were assumed to be one half of the radii of the corresponding fillets. The results are listed in Table 5.2. Also given in the table is the mean measurement divided by the specified value. CSA Standard G40.20 - M92 (CSA 1992a) specifies a mass or area tolerance of ±2.5% from the specified value. All the sections, except the smallest angles, used for the central web members, number 7 and 8, where the shear force for a symmetric loading would be zero, meet the specified tolerances.

Table 5.2 Section properties

Element	Property	Calculated value		Calculated / specified
Top chord	A	3259	mm^2	0.979
	y	32.7	mm	0.992
	I_x	6.385	x 10^6 mm^4	0.967
	I_y	5.001	x 10^6 mm^4	0.975
Bottom chord	A	1968	mm^2	0.984
	y	20.9	mm	0.993
	I_x	1.570	x 10^6 mm^4	0.963
	I_y	2.048	x 10^6 mm^4	0.999
Web 2	A	1607	mm^2	1.005
	y	25.7	mm	0.998
	I_x	1.19	x 10^6 mm^4	1.000
Webs 1, 4 & 6	A	934	mm^2	0.984
	y	18.6	mm	0.982
	I_x	0.340	x 10^6 mm^4	0.942
Webs 3 & 5	A	434	mm^2	0.975
	y	11.6	mm	0.987
	I_x	0.055	x 10^6 mm^4	0.941
Web 7	A	269	mm^2	0.948
	y	9.47	mm	0.971
	I_x	0.024	x 10^6 mm^4	0.910
Web 8	A	145	mm^2	0.966
	y	7.40	mm	0.998
	I_x	0.009	x 10^6 mm^4	0.948

5.2 Steel truss

5.2.1 Dimensions

Table 5.3 gives the mean value of measured dimensions, with associated coefficients of variation, of the steel truss divided by those specified on the shop drawings. The average overall geometry agrees well with that specified. The welds, in general, are slightly longer than specified and, based on measurements made with a weld gauge, considerably larger, having a relatively large coefficient of variation, 0.16, associated with the latter. This is attributed to two factors: the welds are relatively small, for the most part ranging between five and seven mm, and the error in measurement using the weld gauge is considered to be appreciable.

Table 5.3 Steel truss measured dimensions

Dimension	Specified value, mm	n	Mean / specified	Coefficient of variation
Web length	varies	32	0.999	0.0012
Weld length	varies	136	1.061	0.0985
Weld fillet size	varies	142	1.136	0.1634
Nelson stud length	119	61	0.995	0.0042
Out to out truss depth	730	16	0.999	0.0019
Top chord length	10675	2	1.000	-
Bottom chord length	10800	2	1.000	-

No camber was specified. That measured varied from 1 mm upward at the north quarter point to 2 mm downward at the mid-span.

5.2.2 Truss properties

As discussed in Chapter 6, the modulus of elasticity of the top chord was 1.022 times the value of 203 100 MPa, of the bottom chord. Therefore, to calculate the moment of inertia, based on the areas of the chords, as is commonly done, the area and moment of inertia about the centroidal axis of the top chord were multiplied by this ratio. The elastic neutral axis was located 446 mm above the lower surface of the bottom chord and the moment of inertia, I_S, based on the steel chords, was 573.0×10^6 mm^4. When modified, as given in Section 3.1.5, to allow for the flexibility of the open web system, the moment of inertia, I'_S, was 520.9×10^6 mm^4.

5.2.3 Out-of-straightness of web members

The out-of-straightness of both angles of web members 2, 4, 13, 14 and 15 in both the plane of the truss (in-plane) and perpendicular to the plane of the truss (out-of-plane) was measured using the specially fabricated device shown in Figure 5.1. The gauge length is 599 mm and the dial gauge reads to 0.001 inches. The in-plane out-of-straightness was measured by placing the device on the upper side of the outstanding leg of the angle and for the out-of-plane out-of-straightness the device was attached to the outer surface of the attached leg. The out-of-straightness in millimetres and the reciprocal of the gauge length divided by the out-of-straightness are given in Table 5.4a for in-plane and 5.4b for out-of-plane measurements.

Table 5.4a In-plane web member out-of-straightness

Web	Angle	Measured mean, mm	Standard deviation, mm	Δ / L	Tolerance
2	East	-0.01	0.054	1 / 49900	1 / 500
	West	-0.50	0.049	1 / 1190	1 / 500
4	East	-0.18	0.012	1 / 3340	1 / 250
	West	-0.37	0.022	1 / 1640	1 / 250
13	East	-0.21	0.070	1 / 2920	1 / 250
	West	-0.24	0.043	1 / 2500	1 / 250
14	East	-0.32	0.246	1 / 1880	1 / 250
	West	-0.53	0.092	1 / 1110	1 / 250
15	East	-0.27	0.028	1 / 2250	1 / 500
	West	-0.24	0.035	1 / 2510	1 / 500

Table 5.4b Out-of-plane web member out-of-straightness

Web	Angle	Measured, mm	Standard deviation, mm	Δ / L	Tolerance
2	East	-0.24	0.057	1 / 2530	1 / 500
	West	0.03	0.034	1 / 17600	1 / 500
4	East	-0.04	0.052	1 / 14600	1 / 250
	West	-0.12	0.010	1 / 4950	1 / 250
13	East	-0.08	0.017	1 / 7310	1 / 250
	West	-0.14	0.019	1 / 4310	1 / 250
14	East	-0.59	0.081	1 / 1010	1 / 250
	West	0.03	0.015	1 / 18200	1 / 250
15	East	-0.11	0.094	1 / 5350	1 / 500
	West	-0.22	0.030	1 / 2770	1 / 500

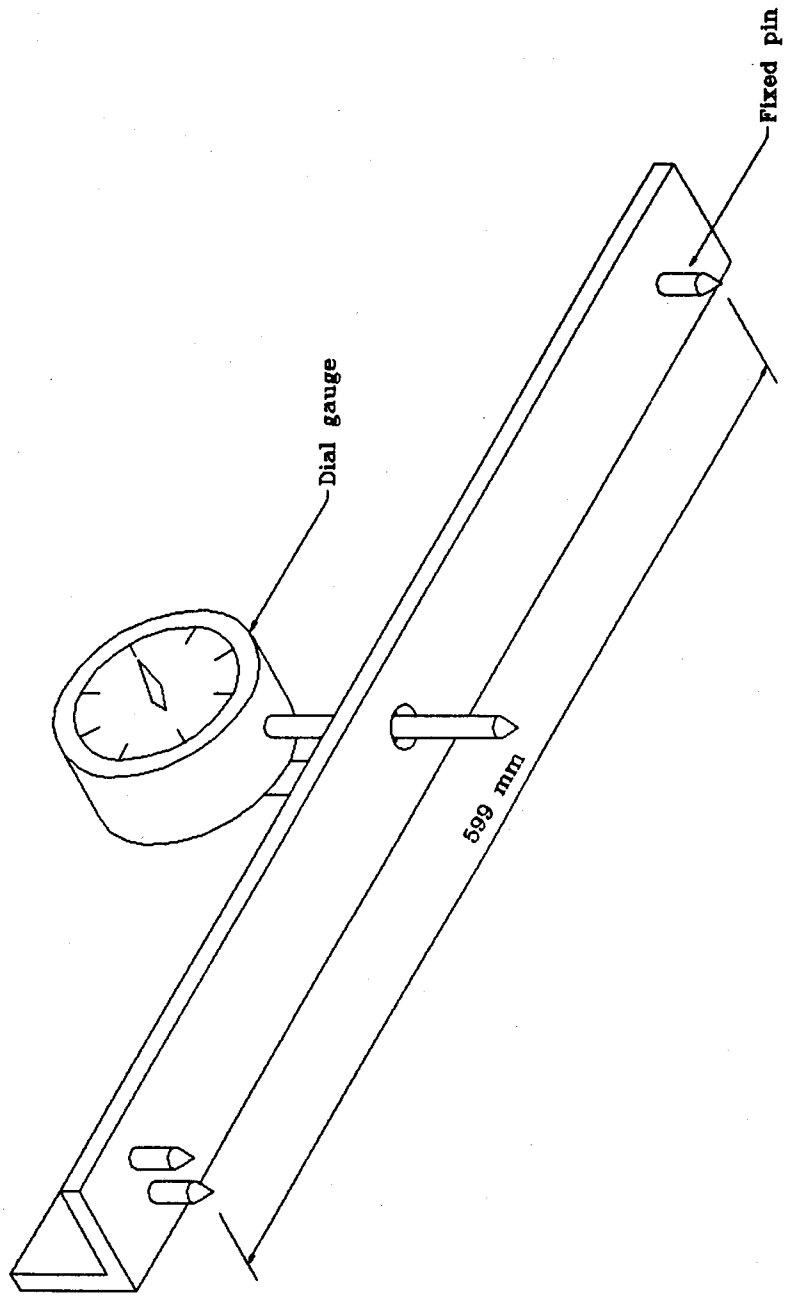

Fig. 5.1 Out-of-straightness measuring device

Negative values for the in-plane out-of-straightness indicate an upward bow, and for out-of-plane out-of-straightness an outward bow. The values recorded are the mean of five measurements. The tolerances given in the tables are one of two figures: 1 / 250 for bar size shapes, that is, angles with a leg size of less than 75 mm and 1 / 500 for structural size angles, with a leg size of 75 mm or more. All the measured values for out-of-strangeness fall well within the tolerance. The mean value for in-plane out-of-straightness of 1 / 2090 is only one forth of the more stringent tolerance - for the structural size angles. Out-of-plane, the mean value of 1 / 3730 is only about one seventh of the tolerance.

5.3 Composite truss

5.3.1 Dimensions

Measurements of the concrete cover slab, width and thickness, given in Table 5.5, show that the slab was slightly thicker and wider than the specified values of 2350 mm and 65 mm, respectively.

Table 5.5 Concrete slab dimensions

Dimension	n	Mean, mm	Standard deviation, mm
b	15	2363	4.2
t_c	45	66	2.2

5.3.2 Composite truss properties

Based on the dimensions of the concrete given in Table 5.5, the dimensions of the steel given previously, and a tangent modulus of elasticity of the concrete at the time of the flexural test of 19 500 MPa, corresponding to a modular ratio of the concrete to steel of 10.4, as related to the modulus of elasticity of the bottom chord, the elastic neutral axis was computed to lie 736 mm above the lower surface of the bottom chord, i.e., in the flutes. The transformed moment of inertia, I_t, was 1182×10^6 mm^4. When this value is decreased by multiplying by 1 / 1.10, to allow for the open web system, and then further decreased to allow for the flexibility of the steel - concrete interface connection, as given by [2.4], the effective moment of inertia, I_e, was determined to be 991.9×10^6 mm^4. This latter value is only 0.84 of the transformed moment of inertia.

5.4 Weights

Weights of the truss at various stages of construction were measured using one calibrated load cell (the weight at each end of the truss was measured and then added to determine the total weight). The measured weights, and weights deduced by subtraction, are given in

Table 5.6. Where the date of measurement is not recorded, the weight reported has been deduced. The weight of the composite truss including all components was obtained 68 days after casting.

Table 5.6 Weight measurements and analysis

Component	Date of measurement, 1993	Weight, kN
Steel truss	June 22	6.33
Steel truss + deck + edge angles + shoring	June 28	10.51
Steel truss including all components except the concrete	July 19	11.01
Composite truss including all components	September 28	73.52
Concrete, at 68 days	-	62.51
Shoring + deck + edge angles	-	4.18
Strain gauge boxes + mesh + measuring devices	-	0.50

The weight of the concrete just after casting, but before setting, cannot be deduced from the measurements given in Table 5.6. From Mindess and Young (1981), it can be inferred that at a relative humidity of 50%, the ultimate weight loss for concrete paste is about 15%. From the mix design, the paste accounts for 17.2% of the total weight of the concrete. Davis and Troxel (1929), as summarized by Lea (1981), give a weight loss versus time curve, from which it can be inferred that approximately 87% of the weight loss has already occurred by 68 days. The conjecture is therefore made that the original weight of the concrete is $62.51 / [1 - (0.15 \times 0.172 \times 0.87)] = 63.9$ kN (as the weight loss ratio applies to the original weight of the concrete, not the weight at 68 days). As the weight loss is itself a small percentage of the total weight (about 2%), errors in calculating it have a relatively small effect. From the inferred weight of concrete at the time of casting and knowing the deflections that occurred when the concrete was cast, the effective moment of inertia of the steel truss can be deduced.

6 MATERIAL PROPERTIES AND BEHAVIOUR

6.1 Steel

All hot rolled steel sections were specified to conform to CSA Standard G40.21 - M92 Grade 300W (CSA 1992b). All members of a given size were specified to be from the same heat of steel. Mill test certificates were requested and supplied.

6.1.1 Ancillary tests

6.1.1.1 Tension coupon tests

In the tension coupon tests, the locations of the 26 coupons cut from the angles and chords are given in Figures 6.1a and 6.1b, respectively. The results of the tests are given in Table 6.1. The coupons were cut and milled in accordance with ASTM E8-91 (ASTM 1991) for sheet type specimens. Where possible, the coupons were cut from members from the steel truss, to ensure representative material was tested. The failure of the composite truss, discussed in Chapter 9, loaded the interior web members to the point where they could not be used for tension coupons. Therefore, the specimens for the three smallest sizes of angles, specifically the L 1 x 1 x 1/8, L 1¼ x 1¼ x 3/8 and L 1½ x 1½ x 1/4, were cut from material supplied for ancillary testing by the truss fabricator. An electrical resistance strain gauge was applied to each of two sides of the coupons to determine strains. Normal elongation gauges were used for all specimens, except that high elongation gauges were used for five of the coupons taken from the bottom chord. An extensometer, with a gauge length of 50.8 mm, was used to measure large strains.

Table 6.1 Tension coupon test results

Coupon	Static yield strength, F_{ys}, MPa	Static tensile strength, F_{us}, MPa	Modulus of elasticity, E, MPa	R^2	n
A1	322	445	204400	0.99989	11
A1b	330	434	205800	0.99994	10
A2	321	464	207600	0.99972	12
A2b	-	465	191900	0.99995	7
A3	333	490	206200	0.99988	11
A3b	330	488	204200	0.99981	11
A4	327	483	204600	0.99993	9
A4b	362	493	204200	0.99998	9

Table 6.1 Continued on page 47

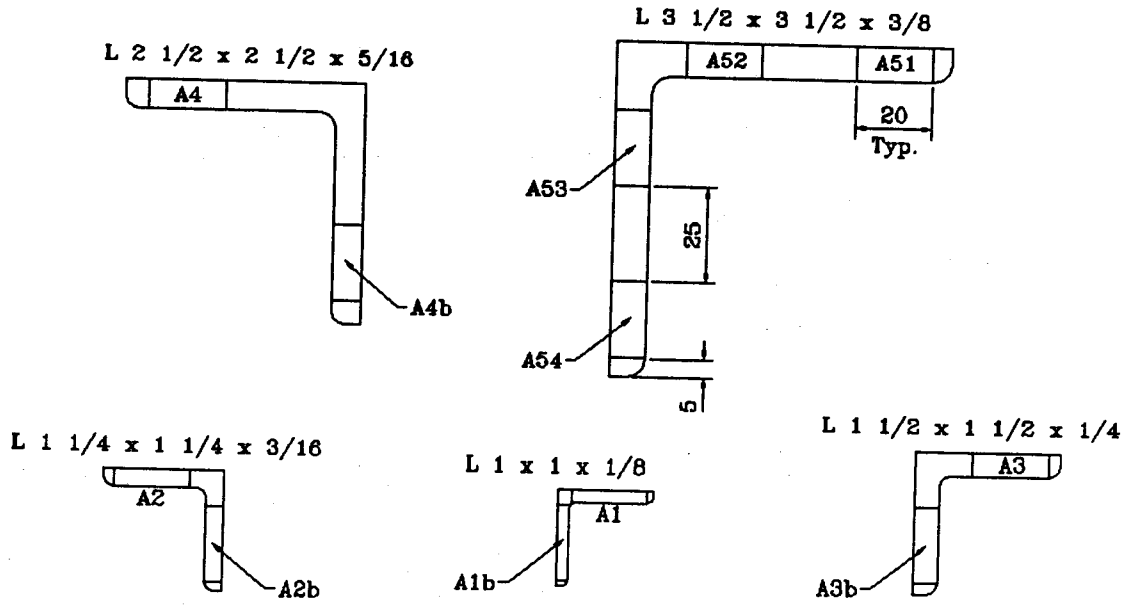

Fig. 6.1a Location of tension coupons of angles

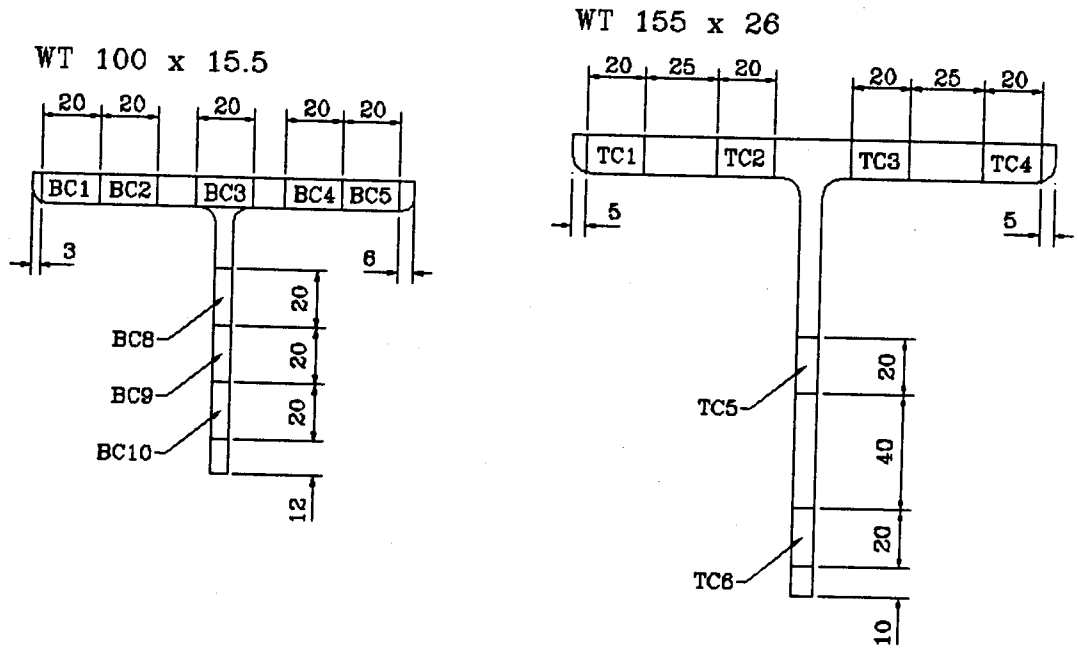

Fig. 6.1b Location of tension coupons of chords

Table 6.1 Tension coupon test results (continued)

Coupon	Static yield strength, F_{ys}, MPa	Static tensile strength, F_{us}, MPa	Modulus of elasticity, E, MPa	R^2	n
A51	372	514	214000	0.99993	12
A52	387	490	208600	0.99993	13
A53	382	504	207200	0.99996	11
A54	411	524	207700	0.99986	14
TC1	-	544	211100	0.99907	10
TC2	311	509	205700	0.99965	10
TC3	297	497	205200	0.99993	7
TC4	321	496	202200	0.99986	7
TC5	329	508	211200	0.99989	7
TC6	325	495	213900	0.99938	4
BC1	-	501	208200	0.99998	9
BC2	319	492	209500	0.99995	12
BC3	311	490	204600	0.99997	7
BC4	298	459	198700	0.99985	12
BC5	303	467	193400	0.99994	14
BC8	-	503	201200	0.99993	10
BC9	336	500	206900	0.99970	12
BC10	339	501	203000	0.99980	11

The coupons were tested in an MTS 810 machine, using a Fluke 2400 data acquisition system. A typical stress strain curve is shown in Figure 6.2a. Figure 6.2b shows the first portion of this stress-strain curve at a larger scale. The dips in these curve are strains at which the strain rate was reduced to zero. These data points were used to calculate the static yield and ultimate strengths. The modulus of elasticity was determined using a least square fit. The modulus of elasticity was generally found by using a four point moving mean as suggested by Kennedy and MacGregor (1984). In three cases, a linear regression analysis was used by systematically eliminating data points from the ends of the apparently linear region to achieve an R^2 value of 0.999 or greater.

In four of the tests, the static yield strength was not determined. For the tests on coupon A2b and TC1, the coupons were accidentally loaded in compression to a point exceeding the yield stress. For coupons BC1 and BC8, the yield plateau was very short or did not exist.

The mean cross sectional properties given for the seven different cross sections in Table 6.2 represent weighted averages based on the area of the cross section tributary to each particular coupon. The static yield strengths range from 5% to 29% greater than the

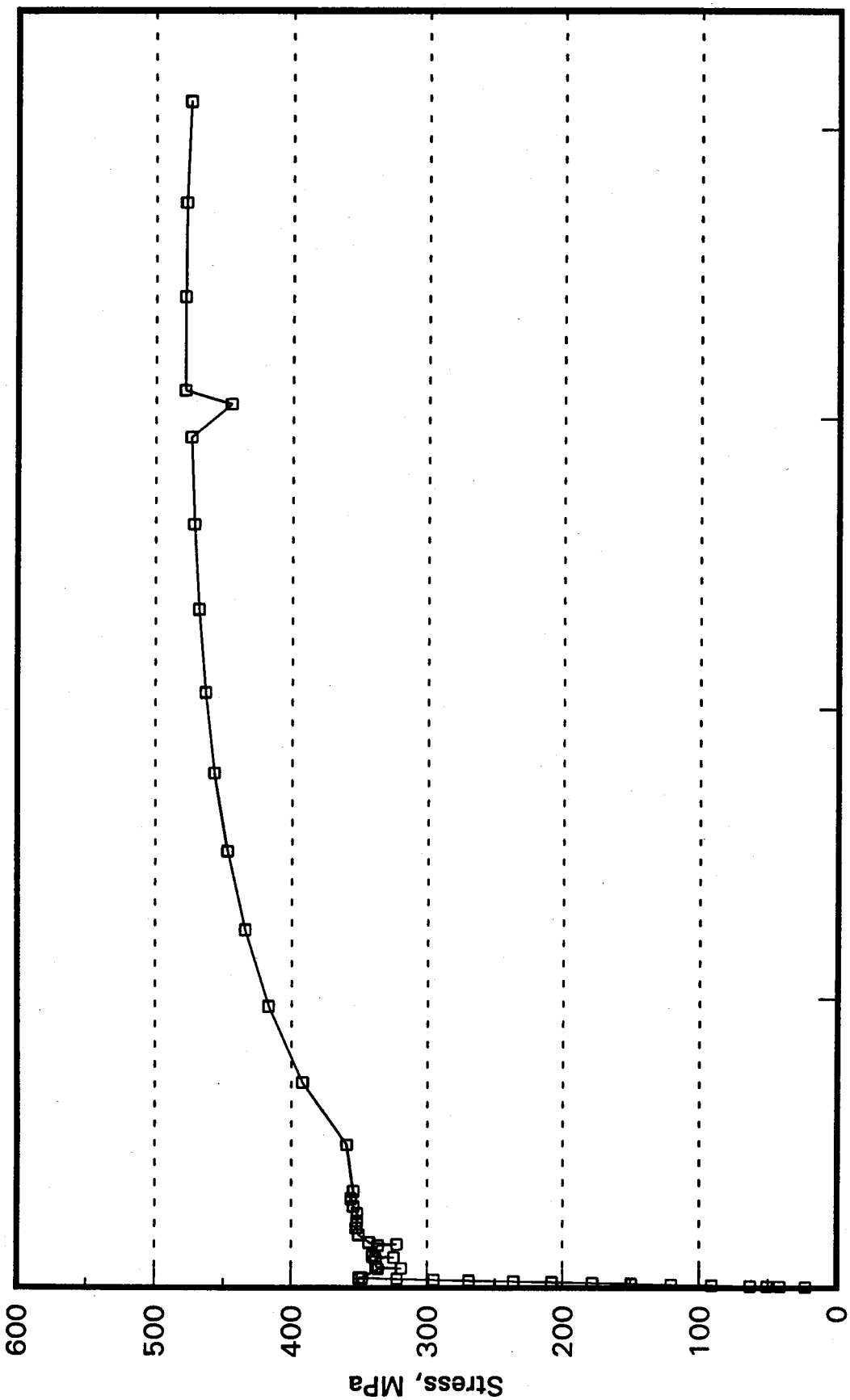

Fig. 6.2a Typical stress-strain curve for tension coupons (coupon A1)

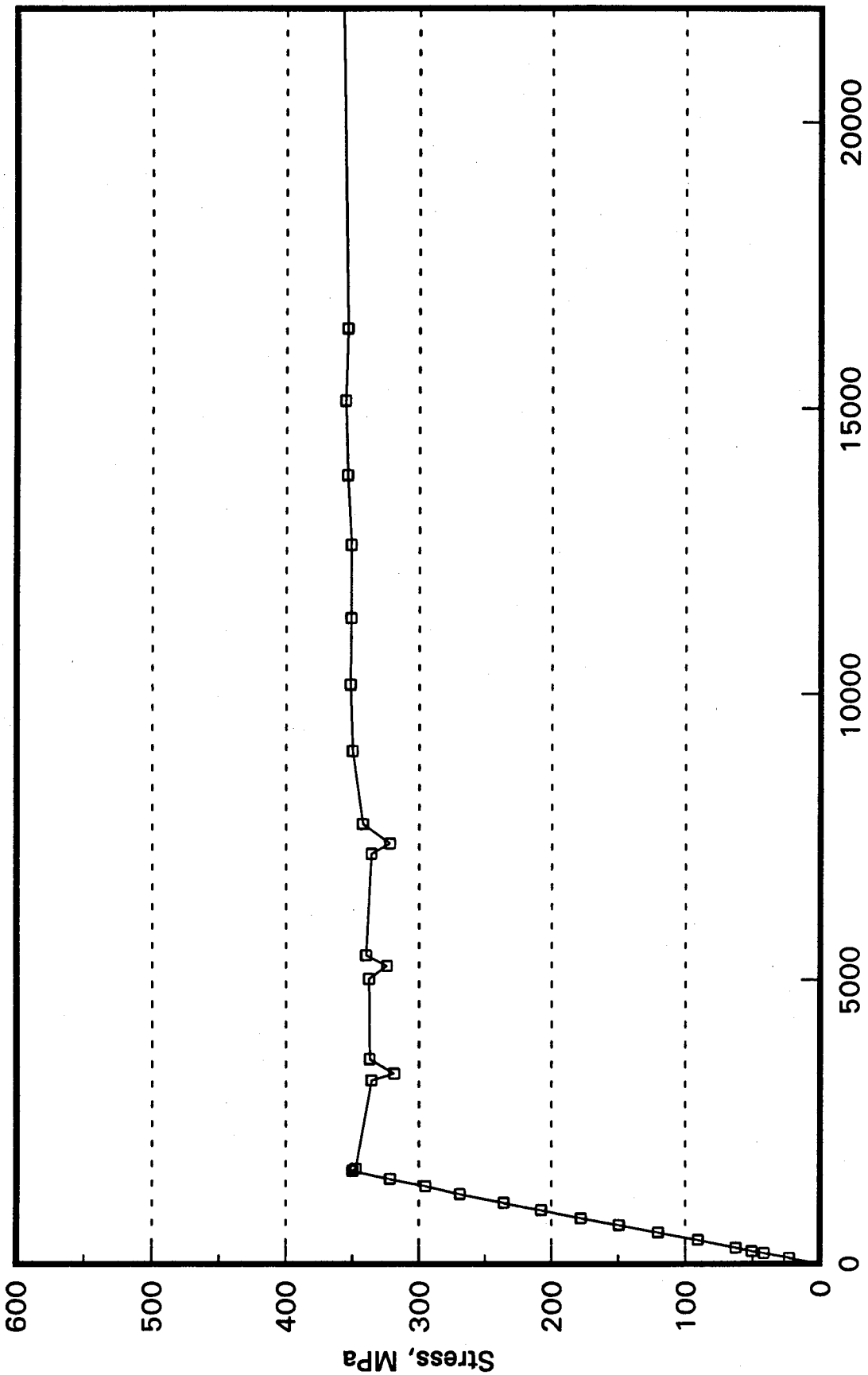

Fig. 6.2b Detail of yield plateau (coupon A1)

specified minimum values and, on the average, are about 11% greater. The modulus of elasticity, on the average, is about 2% greater than the nominal value of 200 000 MPa.

Table 6.2 Material properties for steel sections

Element	Static yield strength, F_{ys}, MPa	Static tensile strength, F_{us}, MPa	Modulus of elasticity, E, MPa	Test / specified ratios	
				Modulus of elasticity	Yield strength
Top chord	314	508	207600	1.038	1.048
Bottom chord	315	487	203100	1.015	1.050
Web 2	388	507	209300	1.046	1.293
Web 1, 4 & 6	334	488	204400	1.022	1.115
Wen 3 & 5	331	489	205200	1.026	1.104
Web 7	321	465	199800	0.999	1.070
Web 8	326	440	205100	1.025	1.086
			Mean	1.024	1.109
			Coefficient of variation	0.015	0.076

6.1.1.2 Residual strain tests

Residual strains were determined, according to technical memorandum number 6 of the Structural Stability Research Council (Galambos 1986), for the two WT chords and the web 2 sections. The pieces tested were cut from the truss after the flexural test. This eliminates the possibility of not having representative material. The pieces used for the chords were selected from the ends of the chords, which were not heavily loaded. The central portion of the web member was chosen to avoid areas that may have yielded locally near the connections. As well, none of the pieces selected had had flaking of the whitewash, which is indicative of yielding. Figure 6.3 shows the locations where the Pfender gauge points were installed on the cross sections. The gauge length was 100 mm. Having installed the gauge points, and measured the initial length, the specimens were cold sawn to a length of 140 mm and then cold sawn longitudinally into sections. By measuring the change in length on each side of a section, and averaging, no corrections for curvature of a section, that sometimes develops, are required. As the strains measured are relaxation strains, the residual stresses that were present before sectioning are obtained as the negative of the residual strain multiplied by the deduced modulus of elasticity for the cross section.

To the computed residual stresses, three linear corrections were made to ensure that static equilibrium was satisfied with the sum of the residual stresses over the area equal to zero and the sums of the moments over the area about the two principal axes equal to zero. Both the computed and corrected residual stresses are given in Table 6.3, but, only the corrected residual stresses, as a percentage of the measured yield stress, are plotted in Figure 6.4. The correction of the residual strains was generally small, with the exception of the top chord - especially about the x-axis. The axial forces and moments required to

L 3 1/2 x 3 1/2 x 3/8

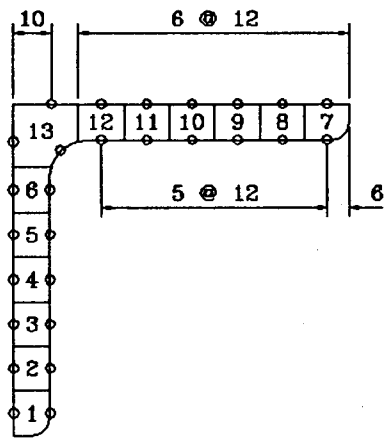

WT 100 x 15.5

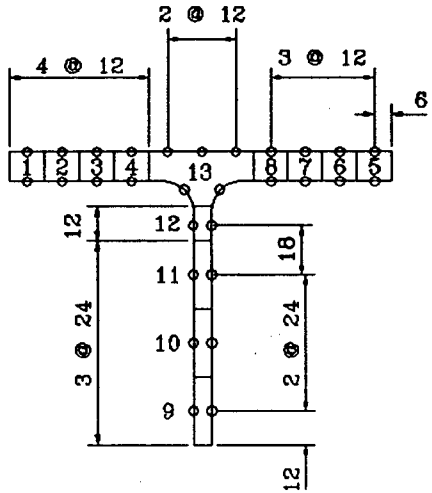

WT 155 x 26

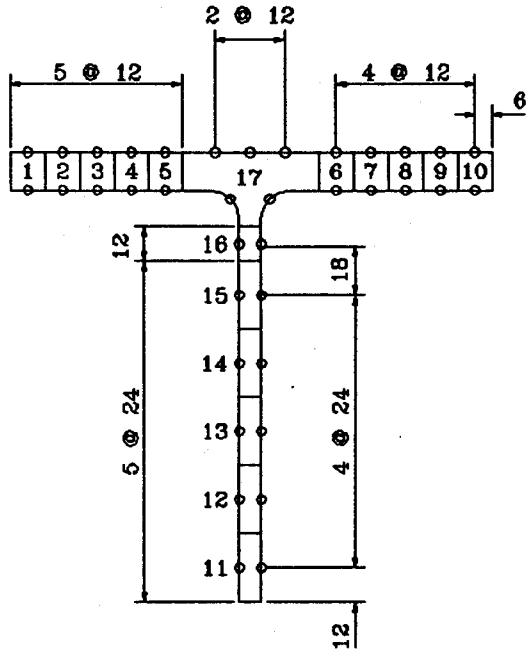

○ One set of Pfender gauge points

Note:
The scale of the angle and the chords is not the same.

Fig. 6.3 Residual strain section locations

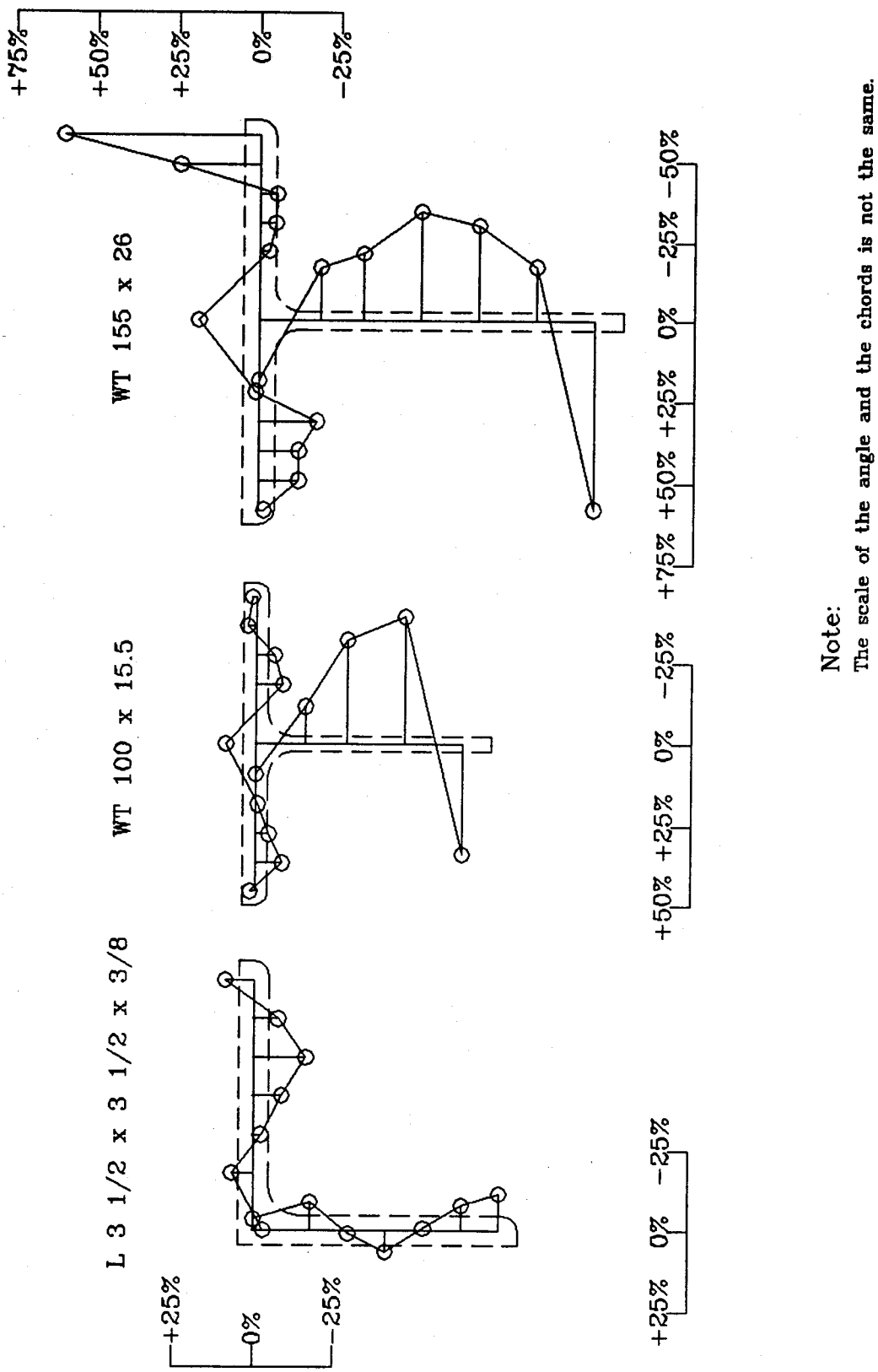

Note:
The scale of the angle and the chords is not the same.

Fig. 6.4 Corrected residual stresses

equilibrate the measured residual stresses, for each of the residual strain specimens, are listed in Table 6.4.

Table 6.3 Residual stresses, MPa

Section	Top chord		Bottom chord		Web 2	
number	Computed	Corrected	Computed	Corrected	Computed	Corrected
1	-5.2	45.6	5.1	14.7	-45.0	-23.5
2	-39.5	1.9	-26.4	-17.5	-30.3	-11.2
3	-39.5	-7.6	-13.2	-4.9	-2.1	14.6
4	-57.1	-34.7	-2.0	5.6	26.2	40.5
5	3.1	16.0	4.1	6.9	4.2	16.1
6	-9.3	-43.1	8.1	11.7	-34.5	-25.0
7	-15.6	-58.8	-18.3	-14.1	33.5	52.2
8	-16.6	-69.3	-26.4	-21.5	-30.3	-13.6
9	76.8	14.6	105.6	118.9	-63.8	-49.1
10	194.1	122.5	-123.9	-112.5	-34.5	-21.7
11	181.7	185.8	-101.5	-92.1	-9.4	1.4
12	-54.0	-52.4	-36.6	-28.6	25.1	34.0
13	-95.5	-96.4	28.8	35.6	-13.3	-6.0
14	-109.0	-112.4	-	-	-	-
15	-68.5	-74.4	-	-	-	-
16	-52.9	-60.7	-	-	-	-
17	58.1	48.0	-	-	-	-

Table 6.4 External force and moments for equilibrium of residual strain specimens

Element	P, kN	M_x, kN·m	M_y, kN·m
Top chord	24.8	2.474	0.940
Bottom chord	15.1	0.088	0.142
Web 2	21.2	0.053	0.097

The maximum measured compressive residual stress on the angle is about 64 MPa or 16% of the yield strength and occurs at about mid-width of one of the legs. The other leg has a similar residual stress pattern, but is reversed, with tension at the mid-width.

For the bottom chord, the maximum computed tensile residual stress is about 106 MPa, or about 34% of the yield strength. The residual stresses in the flange are approximately point symmetric about the web flange junction. This pattern of residual stresses is indicative of roller straightening (Lay 1982).

The top chord has a very similar residual stress pattern as the bottom chord, except the magnitudes tend to be larger in the top chord. The maximum computed compressive and tensile residual stresses in the top chord were 109 MPa and 194 MPa, respectively.

6.2 Concrete

The concrete specified for the slab was 20 MPa normal weight concrete with a slump of 80 mm, no air entrainment and made with type 10 cement. A batch of 3.5 m^3 was required. The mix design is shown in Table 6.5.

Table 6.5 Concrete mix design

Item	Mass, kg/m^3
Water, maximum	150
Cement, type 10	240
Fly ash	26
20 - 14 mm aggregate, saturated surface dry	683
14 - 5 mm aggregate, saturated surface dry	368
Sand, saturated surface dry	953
Water reducing agent	470 mL / 100 kg cementitious

Because the slump was too low on delivery, about 20 kg of water were added, before casting the slab. The resulting slump was 75 mm. The cylinders were cast in accordance with CSA test procedure A23.2 - 3C - M90 (CSA 1990). Polyethylene was placed over the cylinders to provide a suitable curing environment. The cylinders were cured in a heated building and were stripped after one day and placed in a curing tank.

6.2.1 Ancillary tests

The compression cylinders were tested, in sets of three at ages from four to 120 days, according to CSA A23.2 - 9C - M90 (CSA 1990) to determine the ultimate strength and the modulus of elasticity. Split cylinder tests were performed at 120 days according to CSA A23.2 - 13C - M90 (CSA 1990) to determine the tensile strength. Shrinkage control specimens were monitored during the period of the shrinkage test to determine the free shrinkage strain.

Results of the compression cylinder tests are given in Table 6.6,

Table 6.6 Concrete properties

Age, days	Ultimate strength, f'_c, MPa	Tangent modulus of elasticity, E_c^*, MPa	E_c, MPa	E_c^* / E_c
4	16.8	-	20470	-
7	18.9	-	21720	-
14	19.9	13910	22290	0.6238
28	23.1	15920	24010	0.6631
120	30.7	19520	27680	0.7053

No data acquisition system was available on the machine on which the first two sets of cylinders were tested and only the ultimate load was recorded. The test value of the modulus of elasticity, E_c^*, recorded is a tangent modulus found using a linear regression analysis. In performing the analysis, end data points were removed until the coefficient of determination, R^2, was at least 0.995. The ratio of the test to that given by CSA Standard A23.3 - M84 (CSA 1984), as

$$[6.1] \quad E_c = 5000\sqrt{f'_c},$$

is significantly less than 1.0. This has previously been attributed (MacGregor 1991) to the aggregates in the Edmonton region and suggests that the coefficient in [6.1] should be reduced to about 3300 for concrete made with these aggregates. A typical stress-strain diagram for a compression test is given in Figure 6.5.

The average tensile strength of 3.07 MPa obtained from two split cylinder tests at 120 days is 10.0% of the compressive strength at the same age.

The gauge length of the rod-dial gauges assemblies used to measure the overall change in length of the two shrinkage control specimens was about 900 mm. The actual gauge lengths were used to determine the shrinkage strains, as reported in Chapter 7.

6.3 Nelson studs

Two push-out test specimens were constructed to determine the shear capacity and load deflection response of the studs. In order to make the specimens symmetric, two WTs were welded together as shown in Figure 6.6. There were eight studs in each specimen, two per flute spaced 87 mm on center, with 22 mm of cover. In specimen 1, the studs were positioned 40 mm from the lower edge of the flute as shown. This placement is opposite to that recommended by Chien and Ritchie (1984), and in fact, the downward shear force in the test applied to the stud would tend to cause it to break out of the concrete. In specimen 2, the studs were centered in the flutes, as they were in the composite truss. A single layer of welded wire mesh, 152 x 152 - MW9.1 x MW9.1, was placed with 25 mm cover.

6.3.1 Push-out tests

The specimens were tested in the 6600 kN MTS machine, using stroke control, on October 21 and 22, 1993. In test 1, the instrumentation consisted of four dial gauges mounted on the WTs reacting against magnetic blocks. For the lower two gauges, the magnetic blocks were placed against the lower half of the flutes. The upper magnetic blocks were placed against the upper end angle, which extended below the flute. In retrospect, this positioning of the dial gauges measures only the interfacial slip and not the

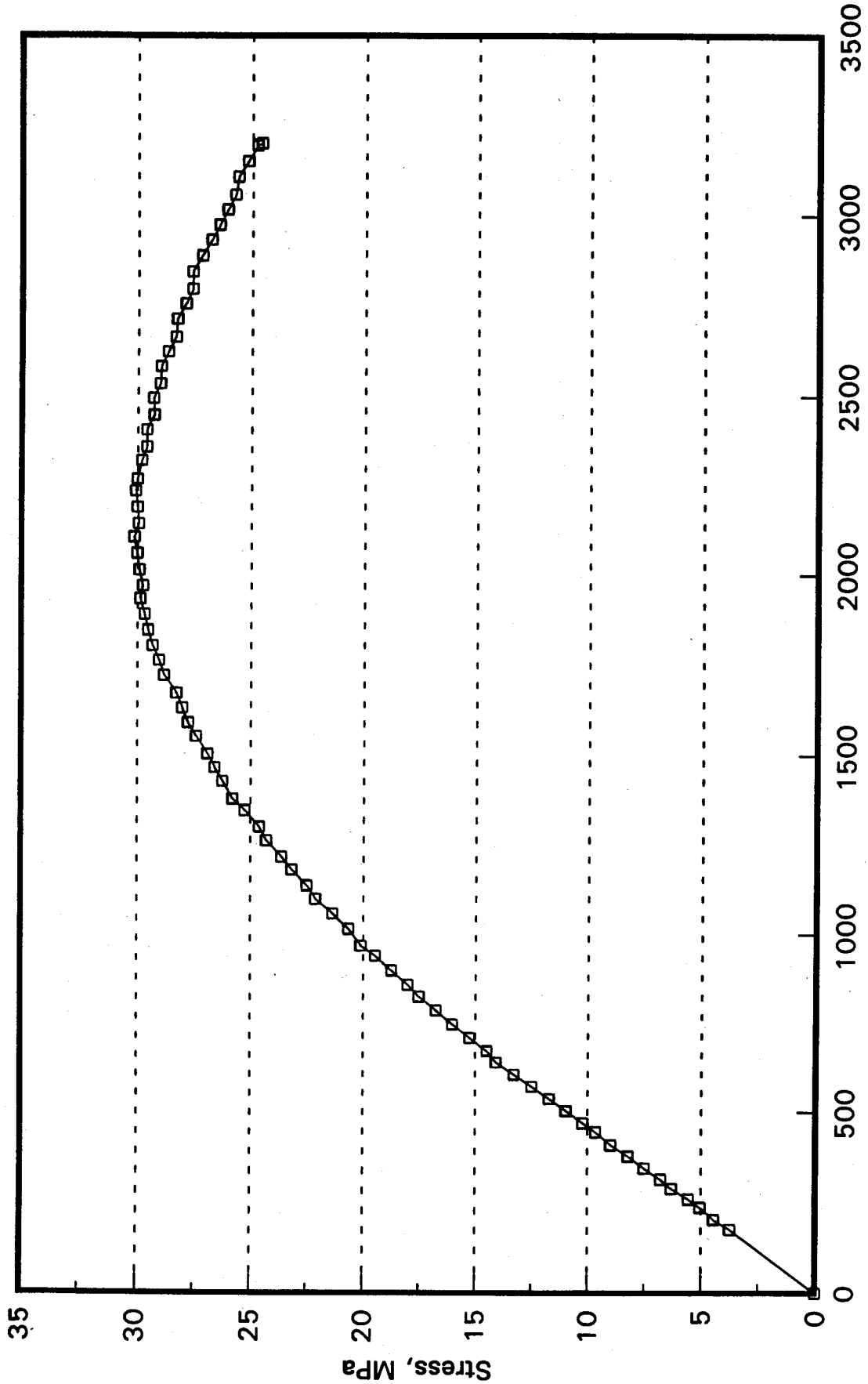

Fig. 6.5 Typical stress-strain curve for concrete cylinders at 120 days

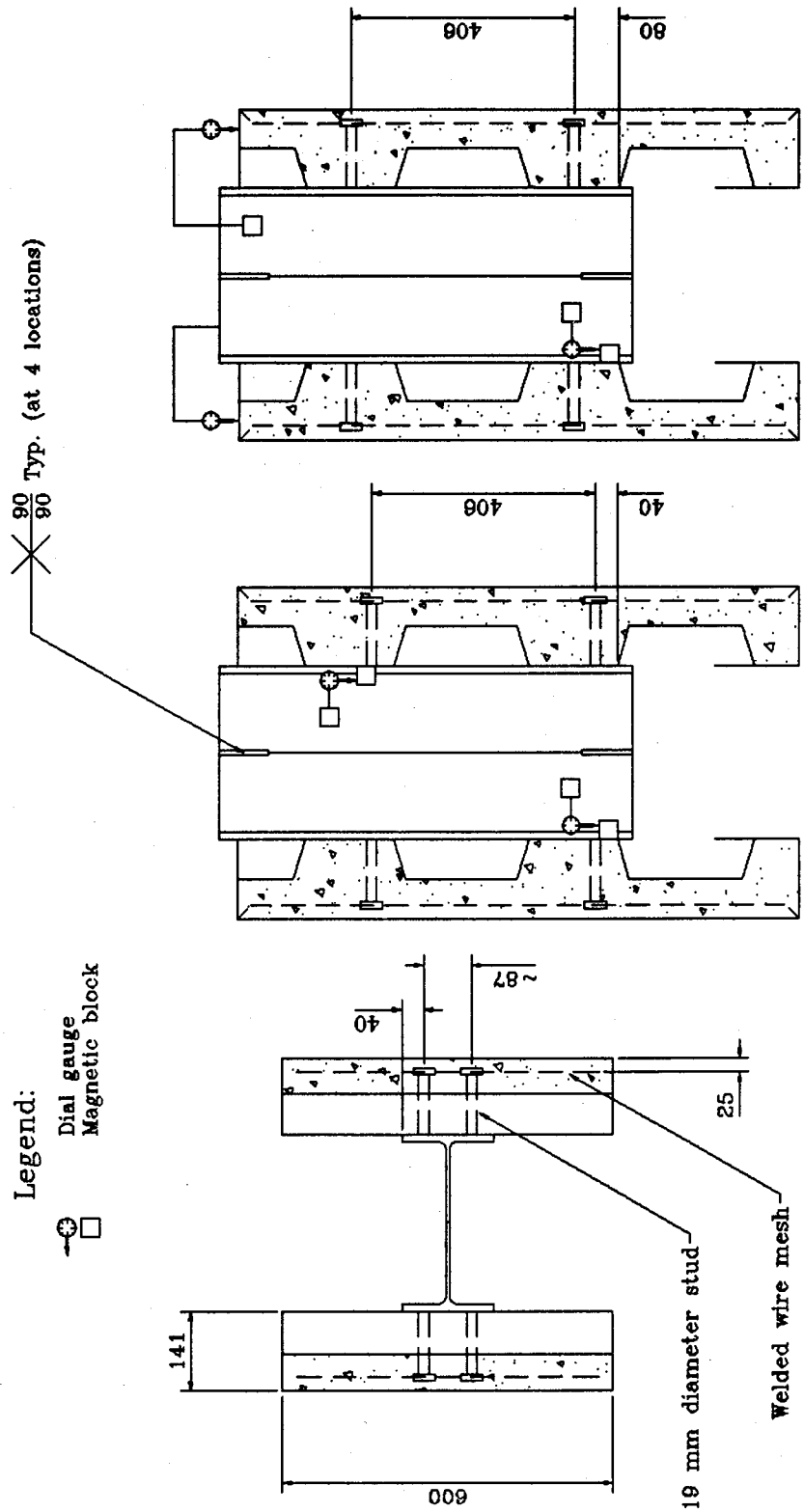

Fig. 6.6 Push-out test specimens

movement that occurs due to distortion of the studs. Therefore, in test 2, two of the dial gauges were positioned at the top of the specimen to measure the overall movement of the cover slab with respect to the WTs. All dial gauges had a sensitivity of 0.01 mm. Loads were taken to be those applied by the MTS machine. These loads and MTS head displacements were recorded electronically for specimen 2.

The upper dial gauges in test 1 malfunctioned when the end angle distorted. The interfacial slip shown in Figure 6.7 is the average of the two bottom dial gauge readings. The peak load curve is drawn through the maximum recorded for any load step, while the static load curve is that for a zero strain rate. The two points falling below the continuous curves may be due to minor leakage in the hydraulic system. This also occurred in the second test shown in Figure 6.8.

In test 2, one of the interfacial slip dial gauges stuck for a portion of the loading curve. The interfacial slip curve in Figure 6.8 is based on the single reading in this interval and the average of the two readings at lower and higher loads. Also shown in the figure is the relative movement of the steel section with respect to the mid-depth of the cover slab. This is called the concrete slip curve and represents the load-deflection response of the studs. Only the static load curves are shown in Figure 6.8.

6.3.2 Test results

The maximum static load obtained in test 1 was 411.2 kN (102.8 kN per pair of studs in a flute). In test 2, with the studs in a more favorable position, the maximum static load was 442.3 kN (110.6 kN per pair of studs). The static resistance of 110.6 kN per pair of studs, when compared to the unfactored design resistance as obtained from CSA Standard S16.1 of 109.6 kN per pair, gives a test to predicted ratio of 1.01.

The limited data of the two tests indicate that the static capacity for studs in the unfavorable position is 93% of that for studs placed at the center of the flutes. The lower strength is attributed to the fact that the stud, relatively near the edge of the flute, tends to push the concrete in front of it out of the flute. A bulge formed in the steel deck on the side of the flute near the studs. The bulges on the bottom flutes were appreciably larger than the bulges on the top flutes. These bulges were not visible in test 2. Figure 6.9 compares the interfacial slip for the two push-out tests. It is seen that test 1 is much more flexible than test 2, because of the displacement and deformation of the concrete in front of the stud.

During each test, the concrete separated from the deck. In test 1, a longitudinal crack formed on the surface of the slabs, more of less along the centerline of the specimens. In both tests, a transverse crack formed, on the sides of both the cover slabs, at the edge of the flute below the upper pairs of studs.

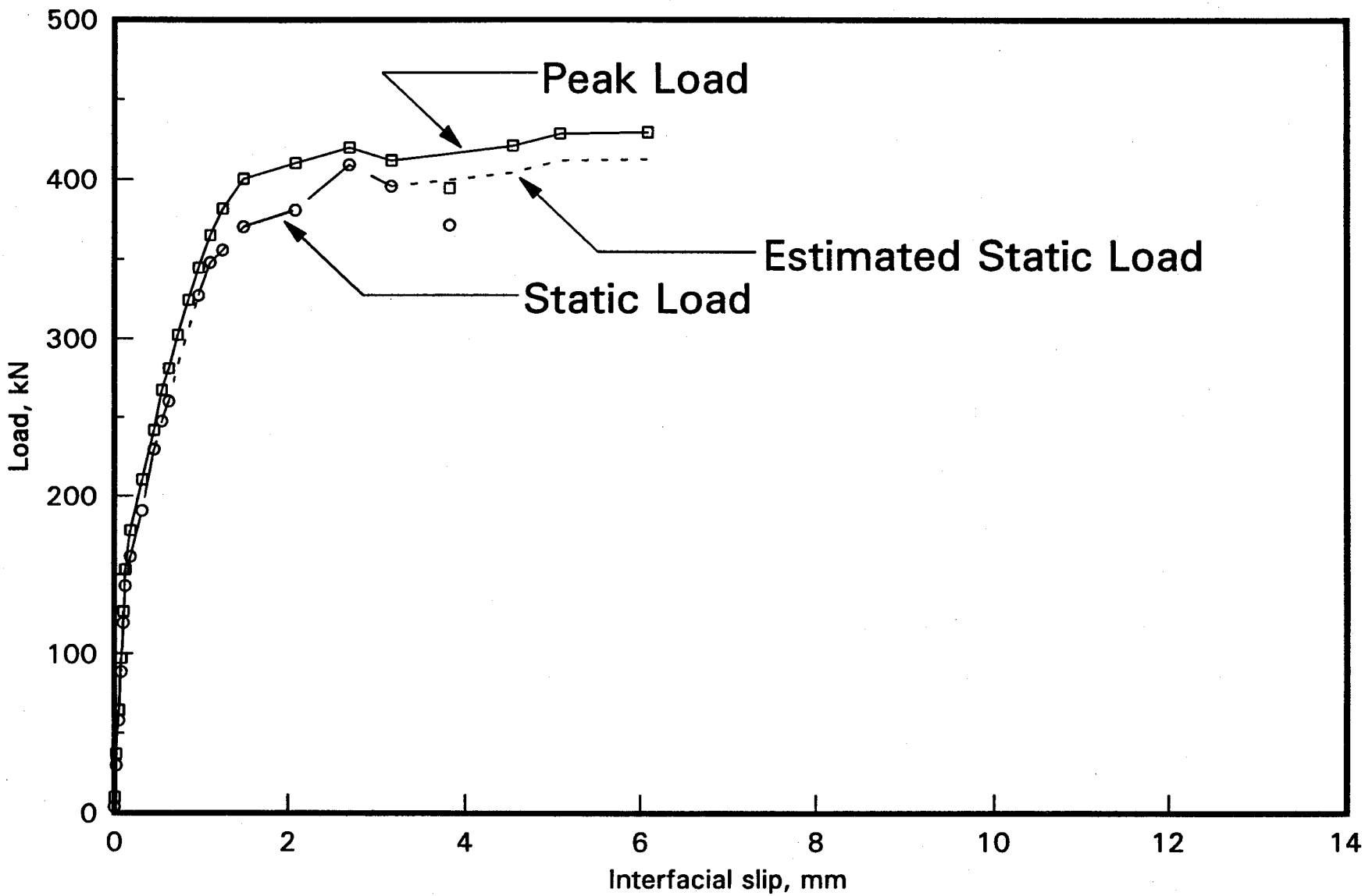

Fig. 6.7 Load-interfacial slip curve, push-out test 1

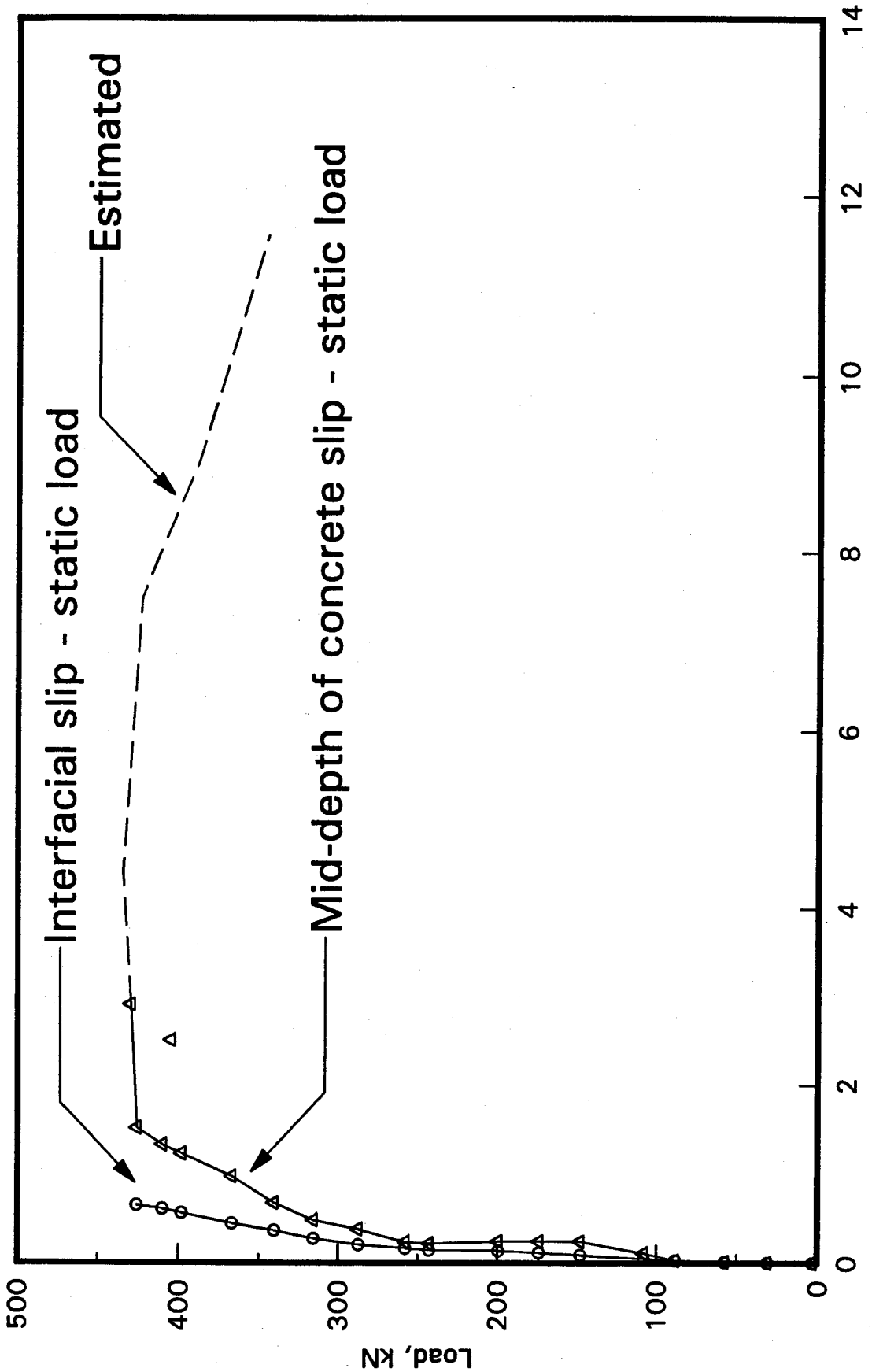

Fig. 6.8 Load-slip curve, push-out test 2

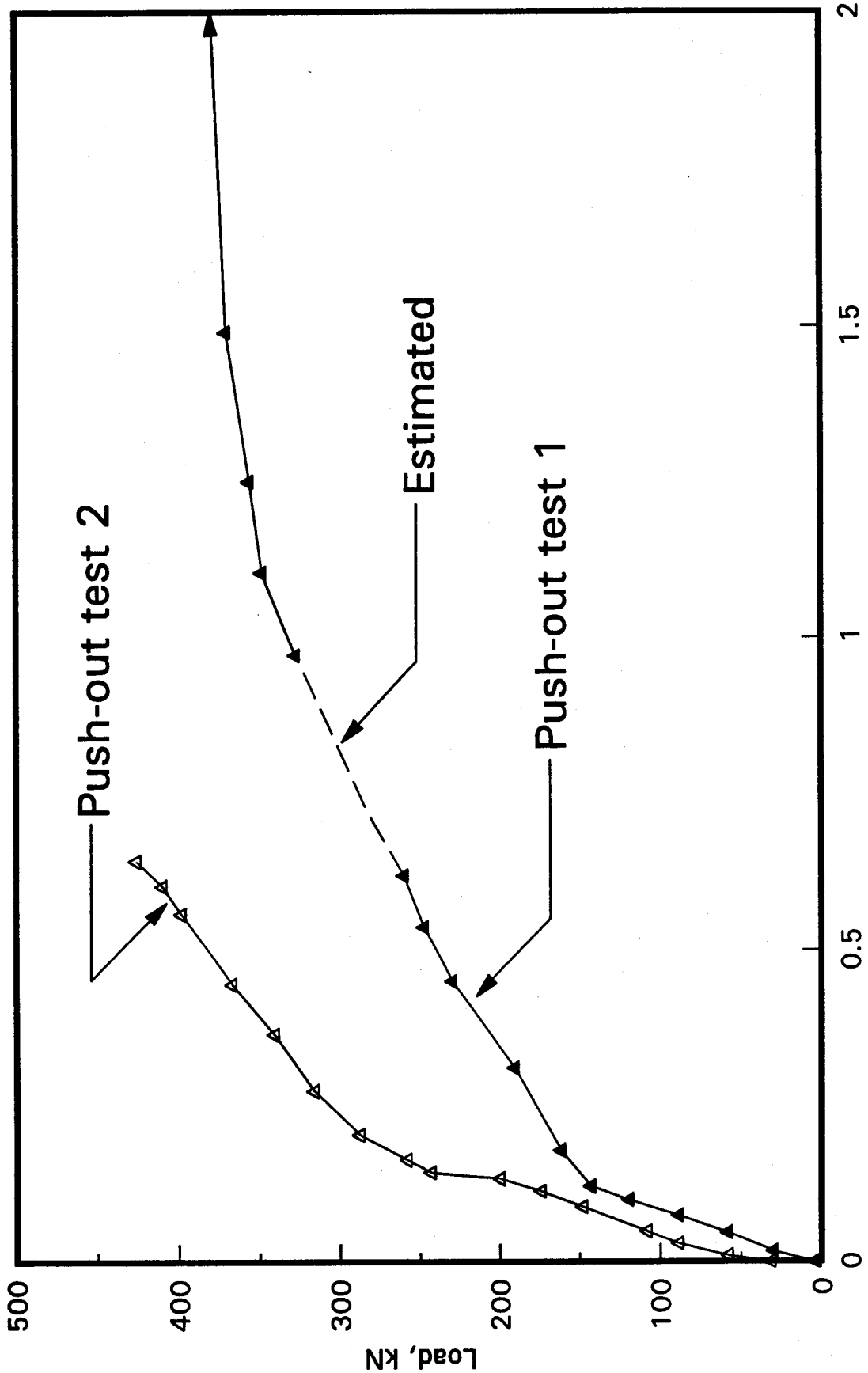

Fig. 6.9 Load-interfacial slip curves, push-out tests 1 and 2

In all cases, failure occurred in the concrete; in no case did the studs either shear off or pull away from the steel section. The variety of failure modes is summarized in Table 6.7 and shown in the photographs in Figures 6.10, 6.11 and 6.12. The photographs in Figure 6.10 were taken after removal of the loose concrete. For Figure 6.11, more of the concrete was removed using a small hammer and chisel. In Figure 6.12, all of the concrete was removed to reveal the studs.

Table 6.7 Concrete failure modes

Test	Slab	Flute	Mode
1	North	Top	Pull-out cone
		Bottom	Asymmetric cone-flute shear
	South	Top	None
		Bottom	None
2	North	Top	Pull-out cone
		Bottom	Symmetric cone-flute shear
	South	Top	None
		Bottom	Asymmetric cone-flute shear

In the three cases where the failure is indicated as "none", the concrete remained intact around the stud. Typical pull-out cone failures occurred both in test 1 and test 2 in the north top flutes. In this failure, a pull-out cone forms extending from the top of the stud towards the deck on all sides. As shown in the top flute in Figure 6.10a, the angle of the cone is about 30° measured from the bottom of the flute. The failure that occurred in test 2 north slab bottom flute is described as a symmetric cone-flute shear failure as seen in the bottom flute of Figure 6.10a. In this failure mode, the pull-out cone around the head of the studs extends downward approximately to the level of the top of the flute, where a shear plane forms. The failure mode described as an asymmetric cone-flute shear failure is intermediate between the pull-out cone failure mode and the symmetric cone-flute shear failure mode, with the pull-out cone extending down to the deck on one side and terminating at a shear failure surface on the top of the flute on the other. The photograph of the bottom flute in Figure 6.10b shows this failure mode. The failure modes with some component of flute shear were probably precipitated by the finite slab width of the push-out specimens and would be unlikely to occur in a composite truss, which would therefore have higher failure loads.

Figure 6.12 shows deformed studs after testing and removal of the concrete. Figure 6.12a, the bottom stud of the north slab in test 1, shows the only case where the studs in a flute were severely bent. In this case, the studs were in the less favorable position, close to the edge of the flute in the direction in which they were being pushed. Figure 6.12b and 6.12c show studs that have undergone a shear deformation, and were typical of all the remaining studs.

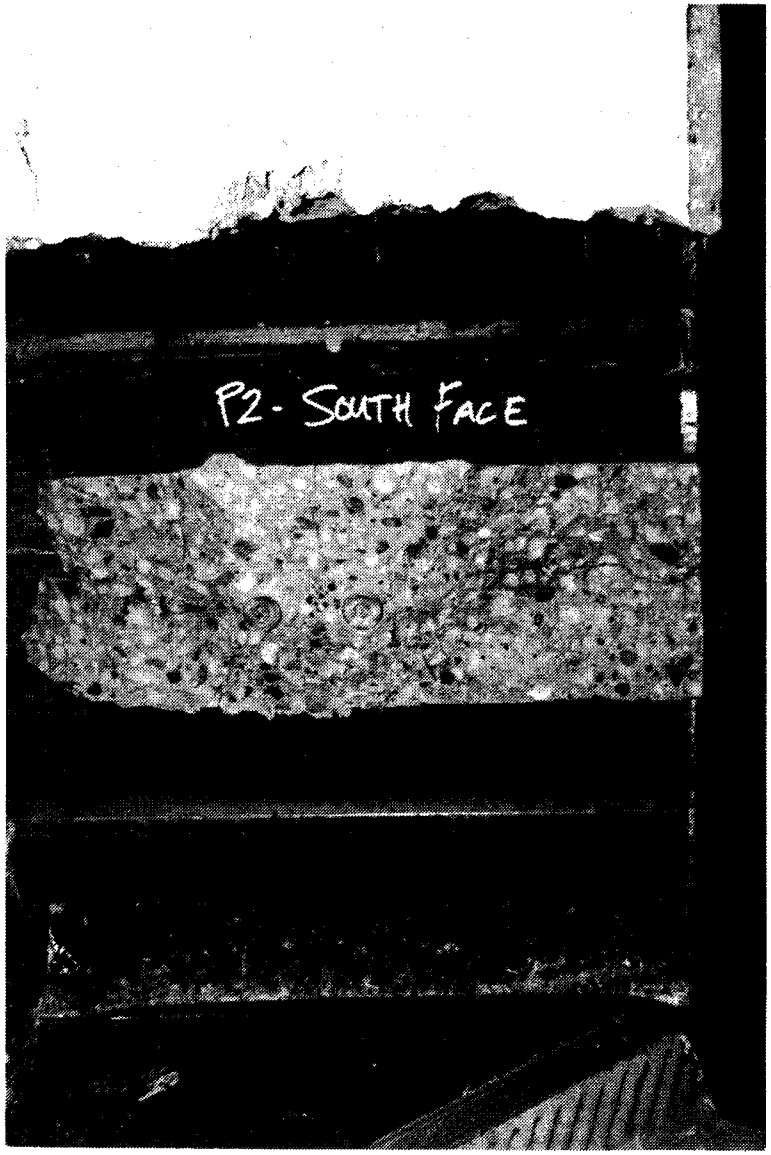

Fig. 6-10b Concrete failure types:
none and asymmetric flute shear

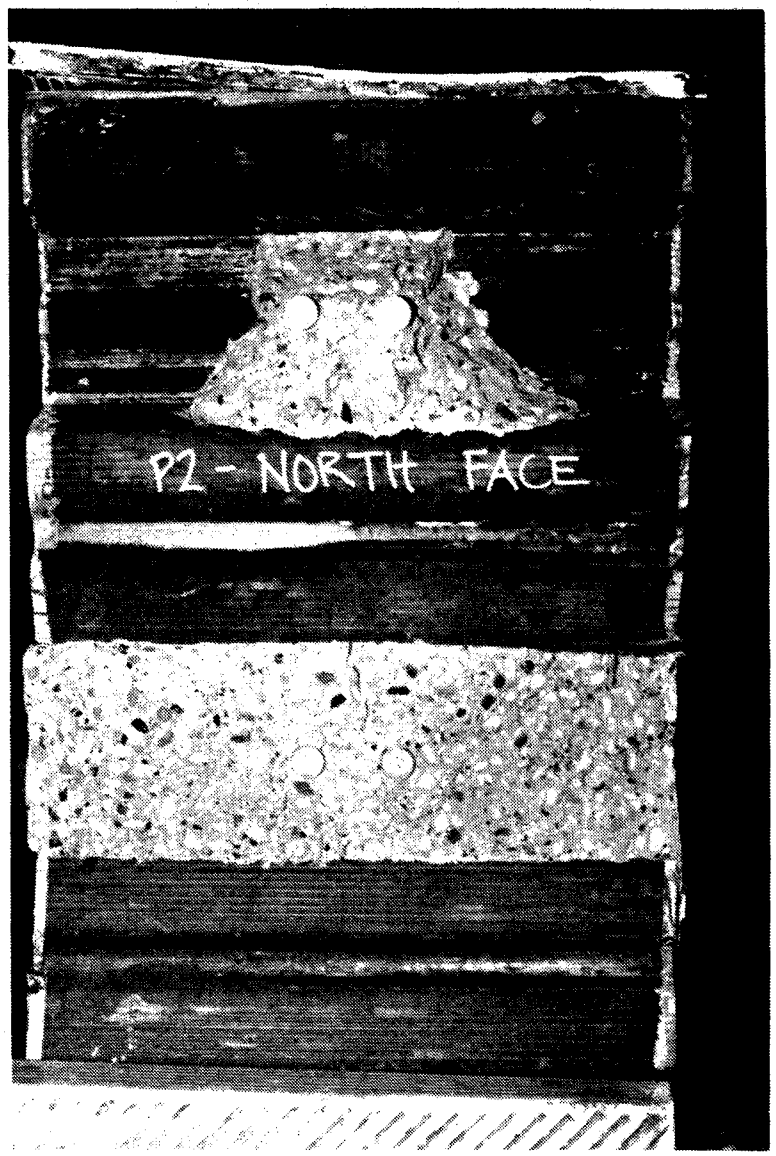

Fig. 6-10a Concrete failure types:
pull-out cone and symmetric flute shear

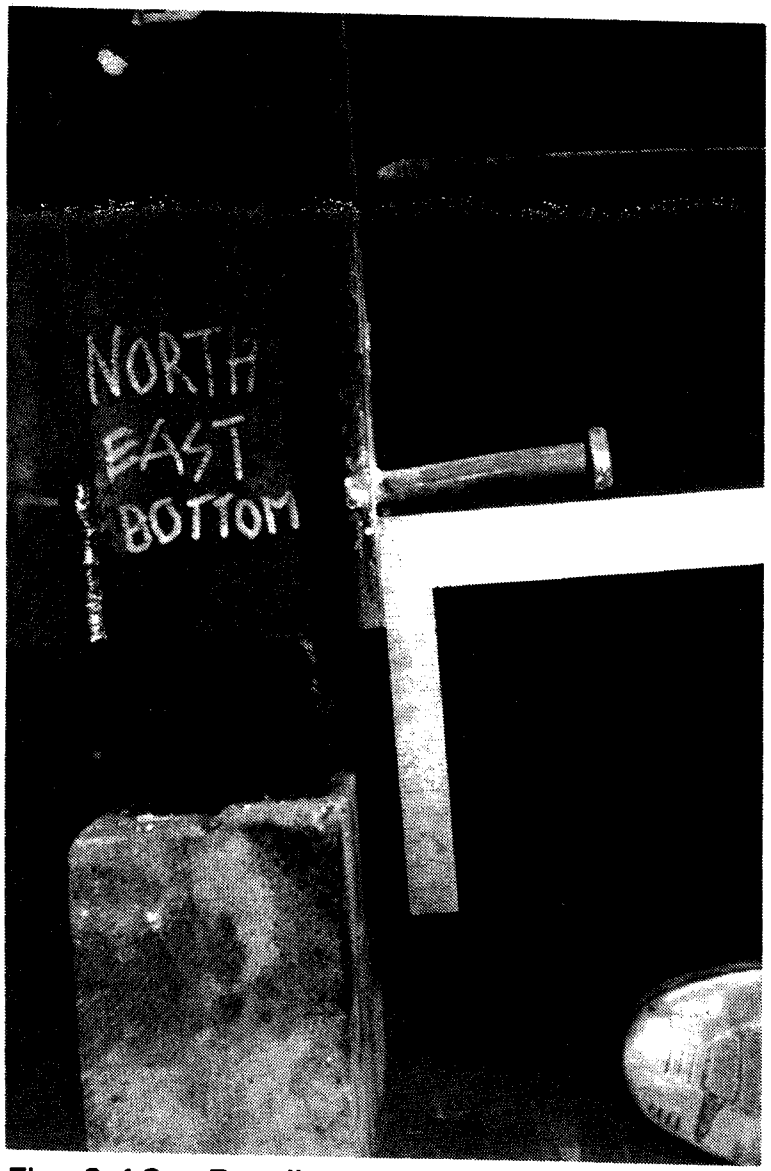

Fig. 6-12a Bending of stud
test 1 - northeast bottom

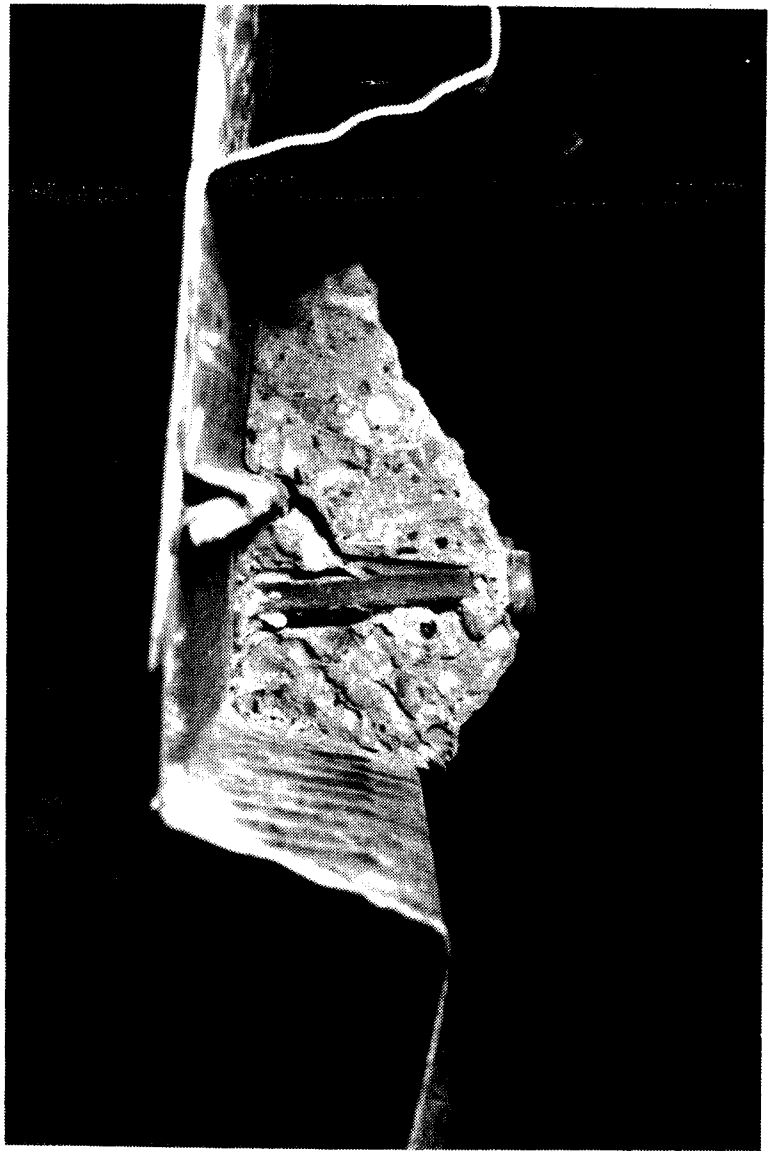

Fig. 6.11 Concrete failure detail

Fig. 6.12c Bending of stud
test 2 - northeast top

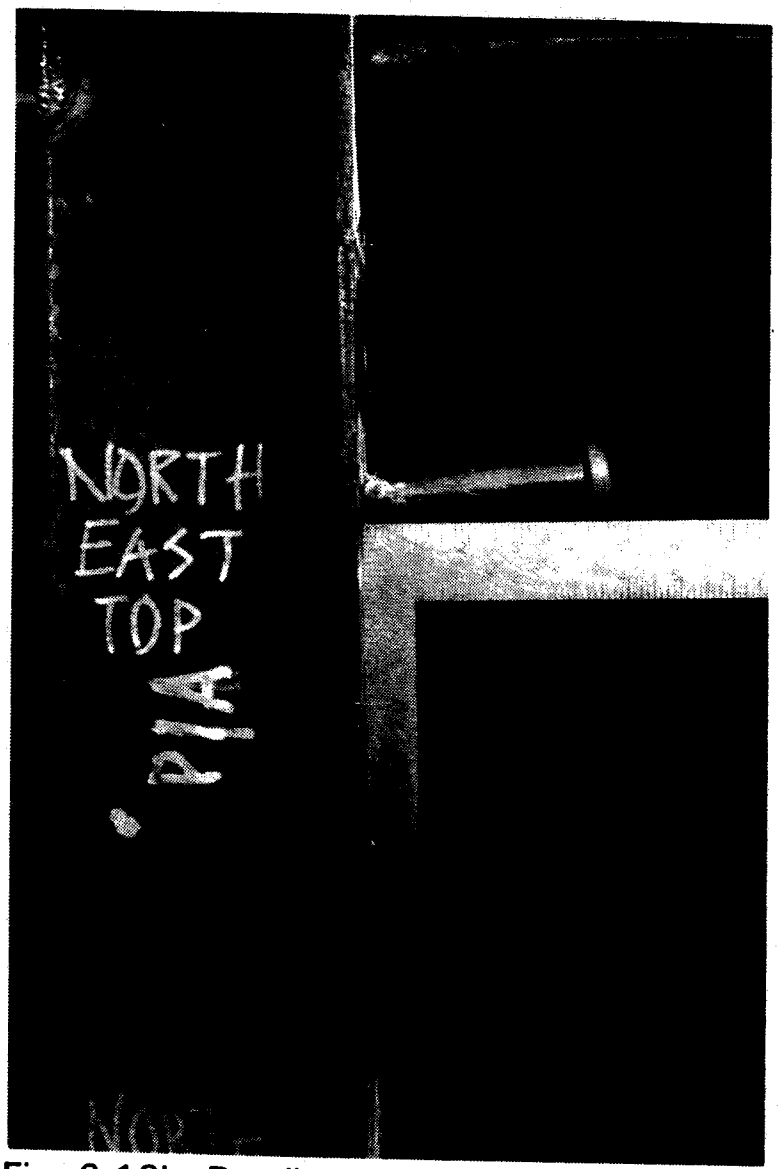

Fig. 6.12b Bending of stud
test 1 - northeast top

7 SHRINKAGE TEST RESULTS

The shrinkage measurements were taken over a period of 68 days from July 22 to September 28, 1993. The ambient temperature and relative humidity during this time are plotted in Figure 7.1. The first six relative humidity readings are invalid and are not plotted, as the hygrometer was not functioning properly. The hygrometer was replaced.

The zero readings for all measurements taken on the steel, consisting of the deflections of the truss and the local and overall strains of the top and bottom chords, were the readings taken shortly after casting the concrete. The initial readings for the measurements of the concrete, consisting of the local and overall strains of the slab and the overall strains of the shrinkage control specimens, were taken one day after casting.

7.1 Shrinkage control specimens

The overall shrinkage strain of the two shrinkage control specimens was determined by dividing the total shortening determined from the rod-dial gauge assemblies by the gauge length. The curvature of the specimens due to greater shrinkage of the exposed top surface, as compared to that of the sealed bottom and side surfaces, was not measured. The variation of shrinkage strain with time is given in Figure 7.2. A correction to the data was made, by adding a constant value to each measured free shrinkage strain, to force the curve to pass through the origin to account for the shrinkage that occurred between the time of casting and the time of the initial measurement on the day after casting. This curve is discussed in Section 8.1.1.2. (The uncorrected curve is shown in Figure 7.6.) The dial gauge on the north specimen did not function and was replaced on the thirteenth day. For this specimen, the shrinkage up to the thirteenth day was assumed to be equal to that of the south specimen. Subsequently, it is seen that the two curves are essentially identical. Covering of the specimens with the polyethylene sheet had little effect on the initial shrinkage behaviour of the control specimens. This suggests there was little increase in the relative humidity under the sheet, which would have tended to delay shrinkage. The shrinkage strains increased with time at a decreasing rate, but at 68 days were continuing to increase significantly. At this time, the free shrinkage strain had reached a value of 709 $\mu\varepsilon$.

7.2 Shrinkage deflection of truss

Figure 7.3 shows the deflection of the composite truss due to the shrinkage of the concrete. The change in behaviour at seven days coincided with the removal of the polyethylene sheet. Even at 68 days, the deflections were continuing to increase, although, at a decreasing rate. The overall shape of the curve and the fact that the deflections are still increasing at 68 days is probably influenced by the fact that the relative humidity tended to decrease from about 60% at day 10 to about 40% at day 68. Increased drying

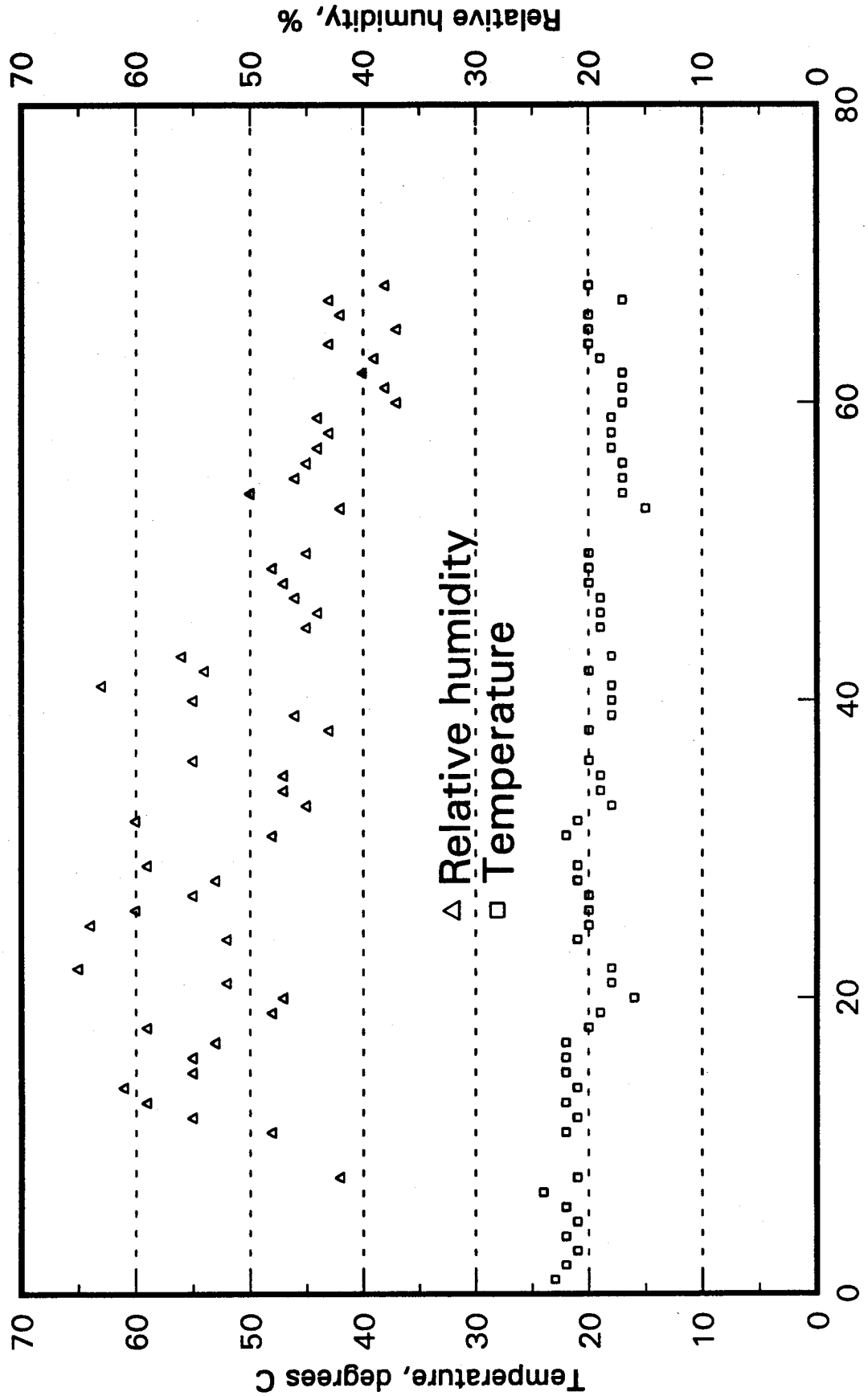

Fig. 7.1 Temperature and relative humidity

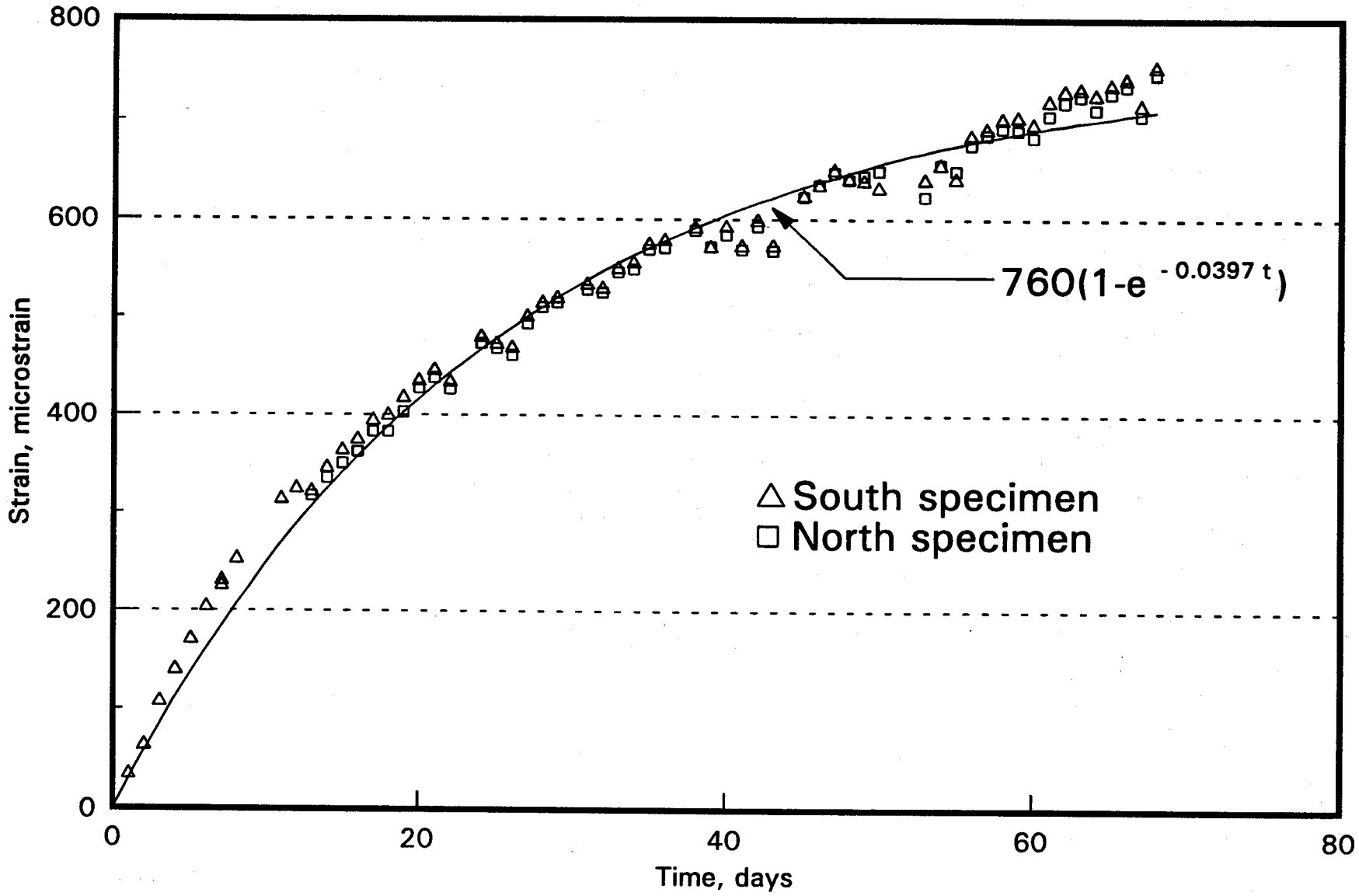

Fig 7.2 Unrestrained shrinkage strains

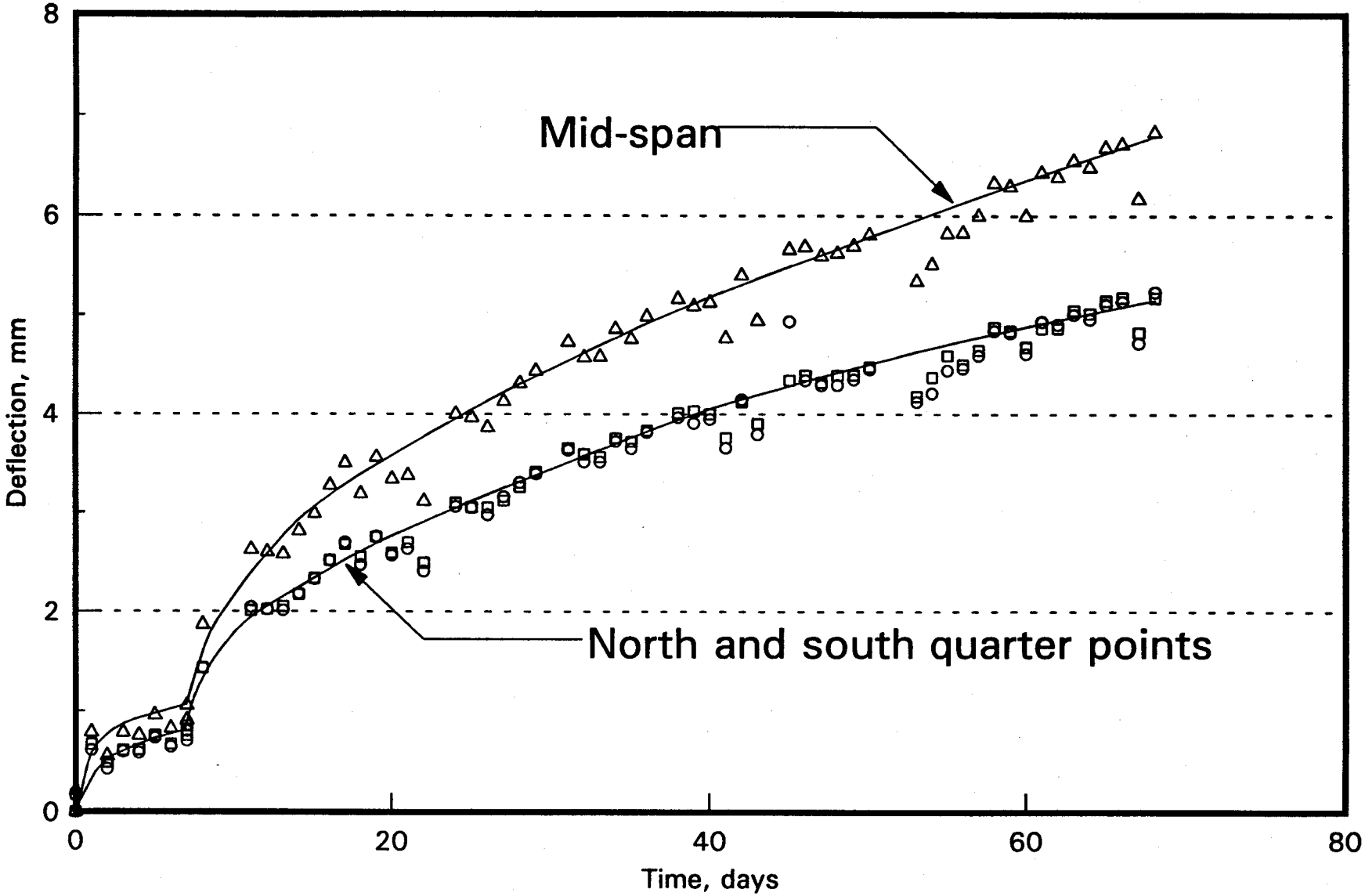

Fig. 7.3 Shrinkage deflection of truss

shrinkage would occur with the decreasing relative humidity. At 68 days, the shrinkage deflection was 6.8 mm. The scatter in the curves is considered to be due to variations in the shrinkage due to the variable relative humidity. As well, the temperature of the steel would fluctuate more rapidly than that of the considerably more massive concrete slab, leading to deflections of the truss.

7.3 Concrete shrinkage strains

7.3.1 Overall concrete shrinkage strains

Figure 7.4 shows the overall longitudinal and transverse shrinkage as determined using the rod-dial gauge assemblies supported above the concrete surface. Little strain occurred when the concrete was under the polyethylene sheet. Subsequently, the strains increased at a decreasing rate.

The two measurements of the overall longitudinal slab shrinkage strain agreed within 2.5%. At 68 days, the average overall shrinkage strain measured 34 mm above the slab was about 284 με. Correcting this strain to the surface of the slab, based on a radius of curvature of 2.394×10^6 mm, the average value calculated from the three measured deflections, gives an overall average strain at the concrete surface of 284 - 14 = 270 με, about 40% of the average free strains of the control specimens.

7.3.2 Local longitudinal concrete shrinkage strains

The variation of longitudinal strain across the width of the slab on each transverse line of Pfender points did not exhibit any pattern and was deemed to be random in nature. This indicates that the shrinkage strain across the width can be considered to be uniform. Therefore, the curves in Figure 7.5, showing the development of local shrinkage strains at five locations on the slab (locations 0.074 L and 0.926 L are mirror images of each other), were obtained by averaging the strains on each line, having used Chauvenet's criterion to reject outliers from the entire set of 21 local strains on each day. The data point plotted at about four days and -150 με, is a result of a large negative reading on one Pfender point. This reading is considered to be anomalous, despite not being rejected using Chauvenet's criterion.

All the local strains were considerably smaller than the free shrinkage strain at the corresponding time. However, the average local strain at each of the five locations is greater than the overall average obtained from the longitudinal rod-dial gauge assemblies, corrected to the surface. It was expected that the local strains would be marginally smaller than the overall strains, due to the fact that the restraint from shrinkage develops at a relatively small distance from the end of the truss (Brattland 1986). No shrinkage cracks

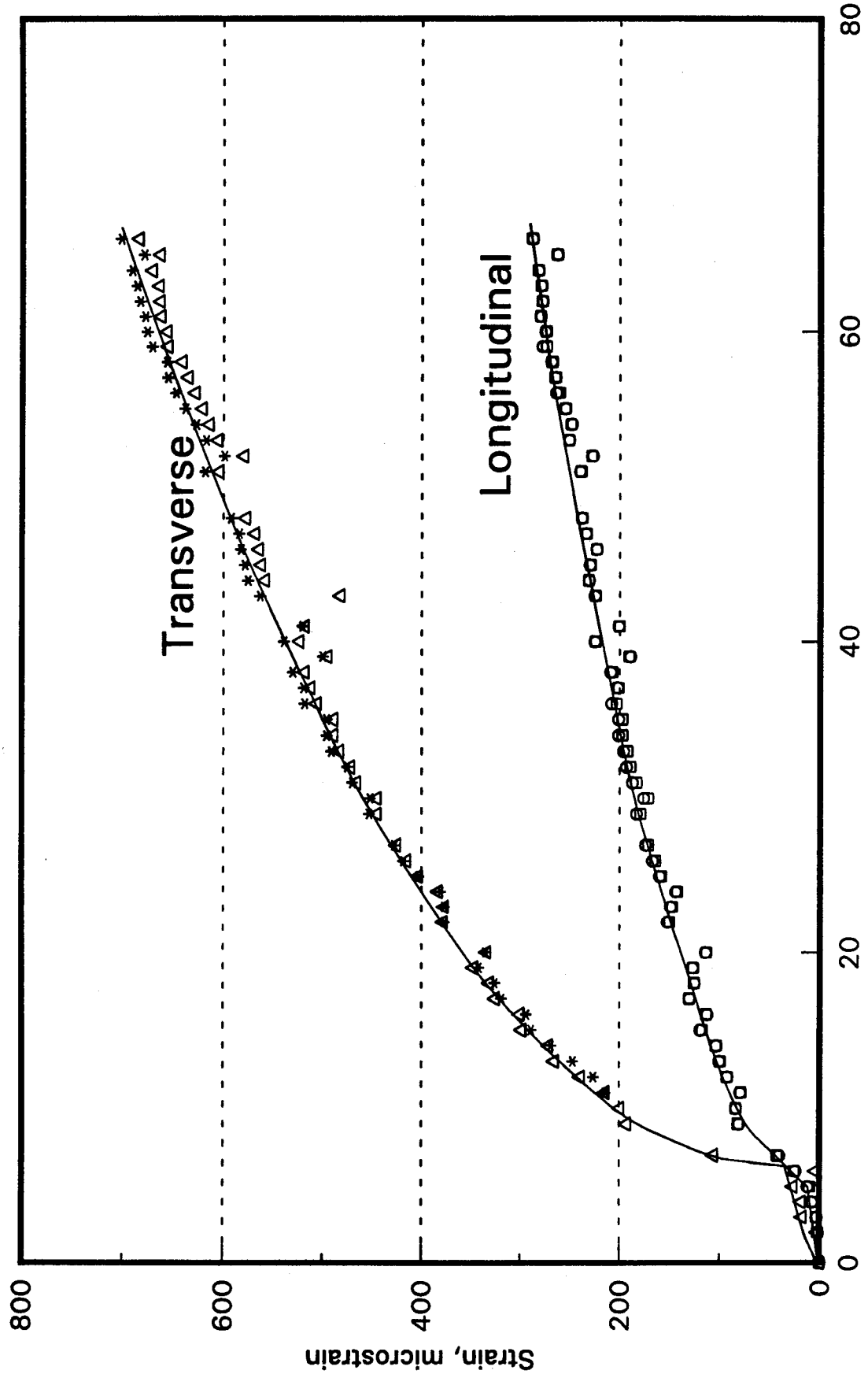

Fig. 7.4 Overall concrete shrinkage strains

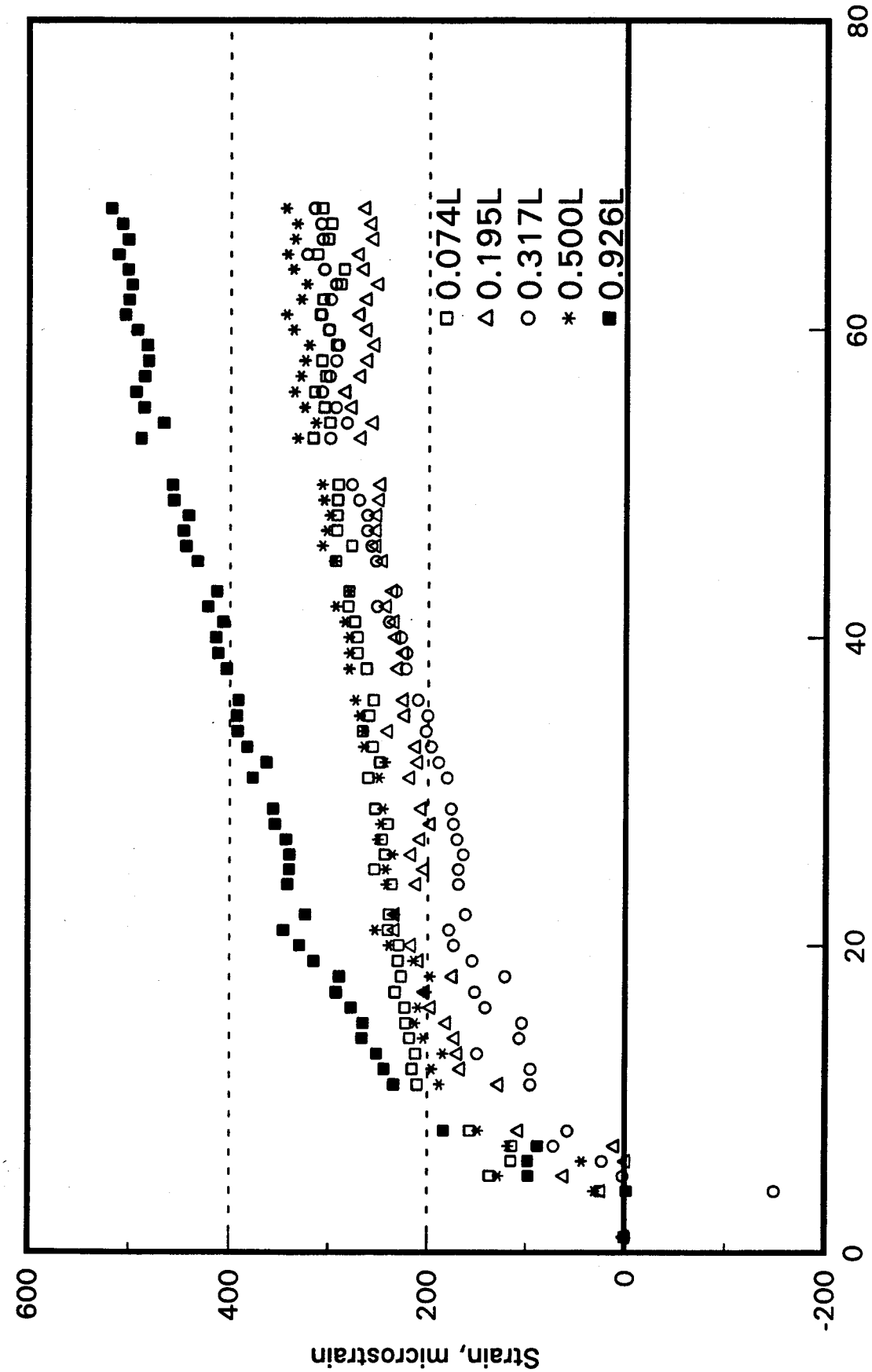

Fig. 7.5 Local concrete shrinkage strains

were observed throughout the duration of the shrinkage test, and, hence, are not deemed to be the cause of this inconsistency.

It was noted, however, that the Pfender point locations were not consistently placed with respect to the flutes of the steel deck. It is suggested that local strains measured on the thicker portion of the concrete slab (over a flute) are higher than the measured overall longitudinal strain, based on two assumptions:

1. a constant tension is applied over the region where the local strain is measured and
2. the concrete is not cracked.

In a general sense, the local longitudinal strain data support this hypothesis. The proximity of the change in thickness of the concrete (from a flute to a crest in the steel deck) to the Pfender gauge lengths may adversely affect the local strain readings.

Examination of the individual strain measurements reveals a wide variability. For example, at 68 days, the mean value of the 21 local strains is 338 με with a standard deviation of 126 με, resulting in a coefficient of variation of 0.37. Even eliminating the three relatively high strains measured at 0.926 L, does not change the coefficient of variation appreciably. The wide variation in the data results in Chauvenet's criterion rejecting very few data points. Even some data that, visually, seem not to belong to the data set, were not rejected. Whatever the reason for the variation, these local strain measurements are not considered to be reliable.

7.3.3 Comparison of concrete shrinkage strains

In Figure 7.6 are plotted the average unrestrained shrinkage strains of the control specimens, the average overall longitudinal slab strains, the average overall transverse slab strains and the average local longitudinal shrinkage strains. To be consistent, the free shrinkage strain was not corrected in this figure (as described in Section 7.1), because the rest of the data also had the initial readings taken the day after casting. The transverse shrinkage strains are only slightly less (about 3% at 68 days) than the unrestrained shrinkage strains indicating that little restraint to transverse shrinkage existed due to the mesh reinforcement and the steel deck. The overall longitudinal strain, corrected to the surface of the slab, is much less than the unrestrained shrinkage strain and indicates that the concrete is heavily restrained in the longitudinal direction. The average of the local longitudinal strain measurements in the longitudinal direction exceeds the overall longitudinal strain, although, the curves, in general, parallel one another.

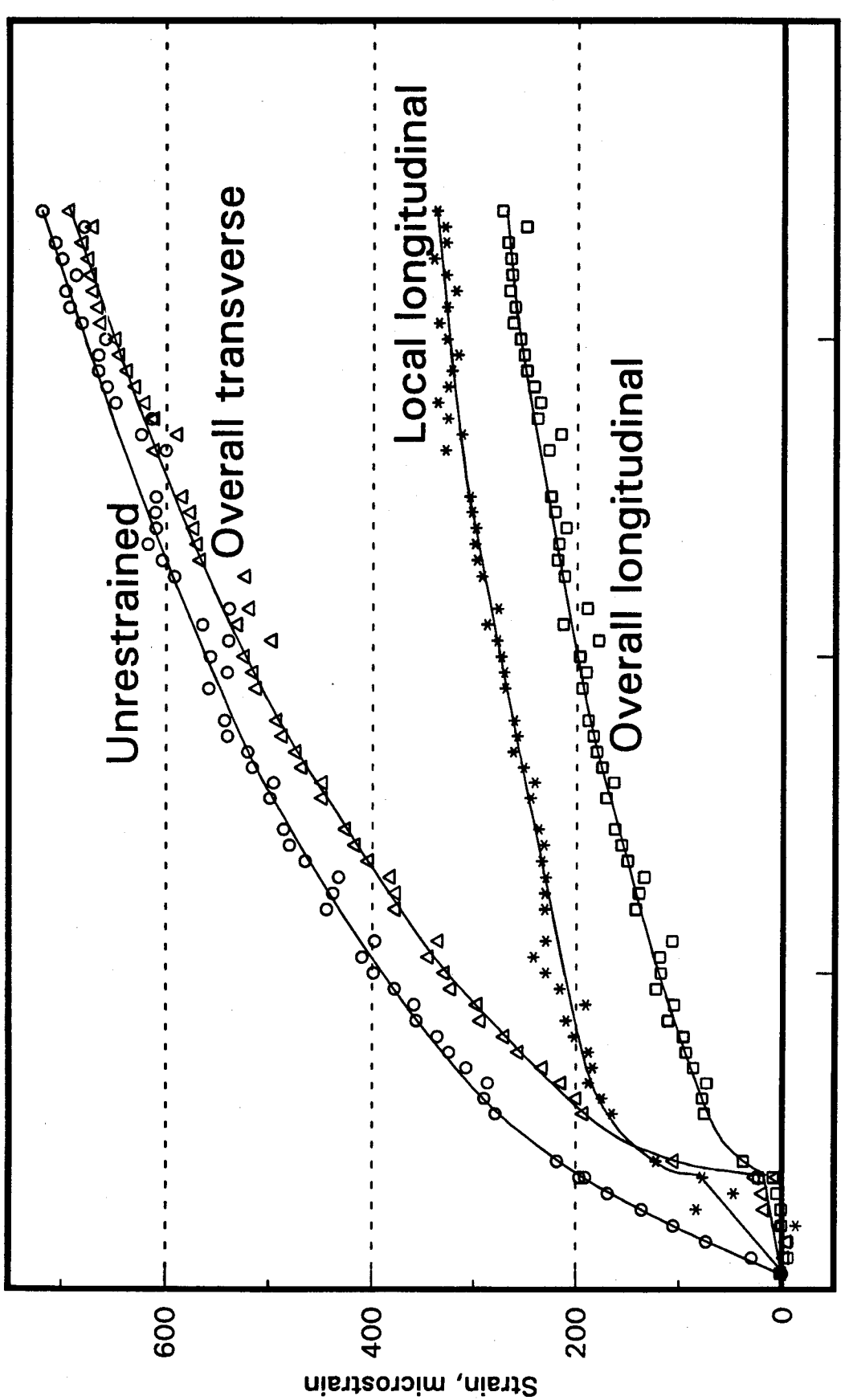

Fig. 7.6 Concrete shrinkage strains

7.4 Steel shrinkage strains

7.4.1 Overall steel shrinkage strains

The overall shrinkage strains, as measured by the three rod-dial gauge assemblies fastened to the top and bottom steel chords, versus time are plotted in Figure 7.7. The strain induced in the top chord is compressive, and in the bottom chord is tensile. For both chords, the strain increases with time at a decreasing rate.

Some local variations from the general trend are obvious. These appear to be related to a more rapid change in length due to temperature variations of the rods of the rod-dial gauge assemblies than the structural components to which they were fastened. Records show than on days 53, 54 and 67 that the main truck door of the lab was open when the outside temperature was in the order of 10°C. A relative shortening of the rod would result in an apparent positive strain in the structural components, which was the case. Neglecting this fluctuation, the overall bottom chord strain at 68 days was about 77 με. When this is corrected to the bottom surface of the bottom chord, based on a curvature corresponding to the mid-span deflection of 6.8 mm, a correction of 8 με is obtained, giving an induced strain at the level of the bottom surface of the bottom chord due to the concrete shrinkage of 69 με. A similar correction, but of 35 με magnitude, applied to the strain obtained from the rod-dial gauge assembly for the top chord, results in a strain of 190 με at the top surface of the top chord, based on an apparent strain of 155 με, of the rod-dial gauge assembly level.

7.4.2 Local steel shrinkage strains

In Figures 7.8 and 7.9 are plotted the strains induced in the steel top and bottom chords due to the shrinkage of the concrete as measured by electrical resistance strain gauges located near the mid-span of the truss. As a result of very erratic readings for the first week of the shrinkage test, the Budd Strain Indicator was replaced. As well, there exists a sudden jump of the strain readings at about 36 days, which is reversed at about 53 days. Two sets of strain gauge readings were taken at 36 days, which were significantly different. It is the contention of the author that this variation in the data is due to the instability of the Budd Strain Indicator system used to read the strain gauges, which, during a single reading, showed relatively small variation in strains. However, when duplicate readings were taken, the second and third readings were typically much different from the original reading. Readings were taken until a stable reading was encountered, sometimes up to the fourth iteration. No other explanation is offered for the variability of the strain gauge readings. Also, there are diurnal variations presumed to be due to temperature fluctuations in the lab. These data are not utilized.

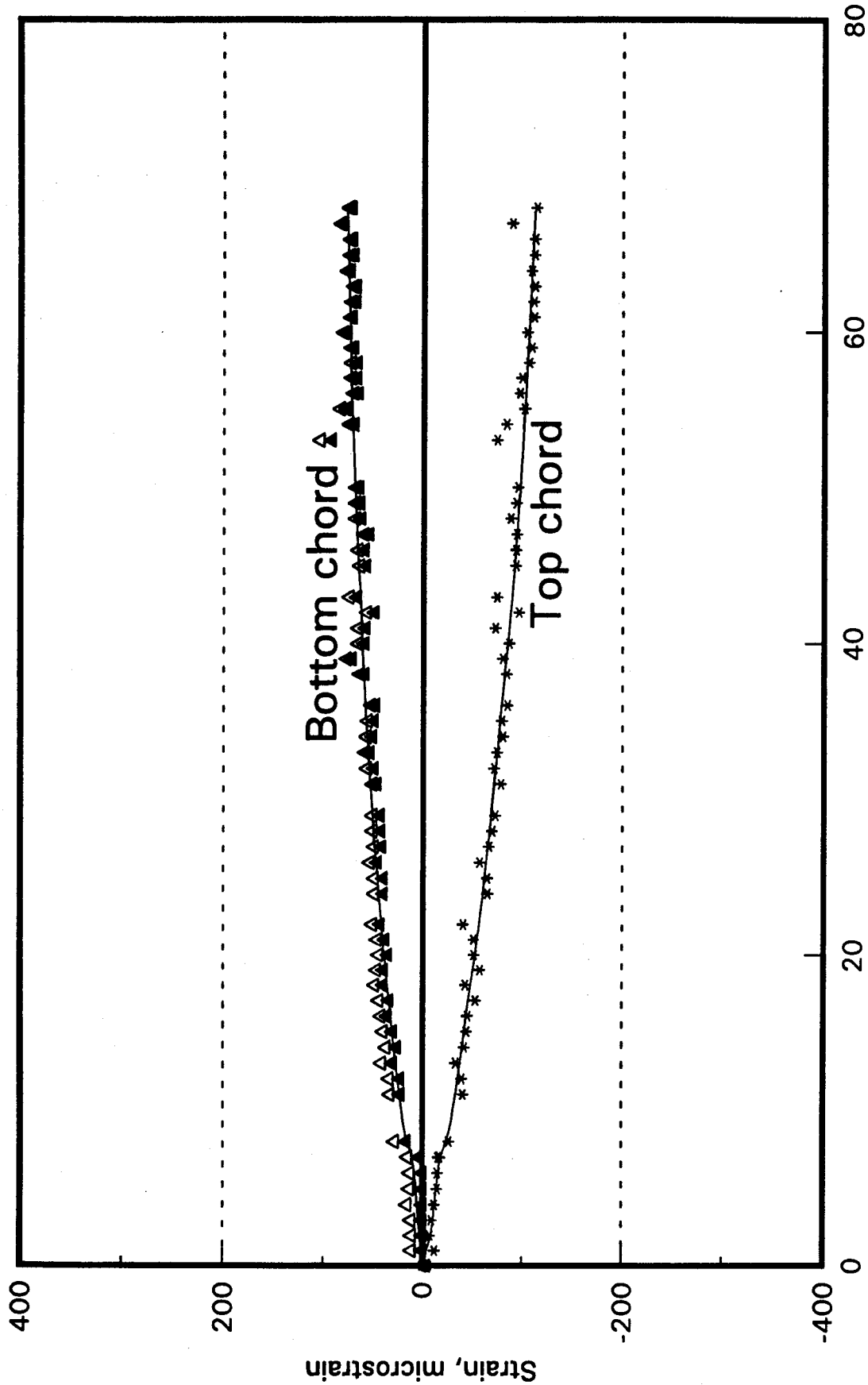

Fig. 7.7 Overall steel shrinkage strains

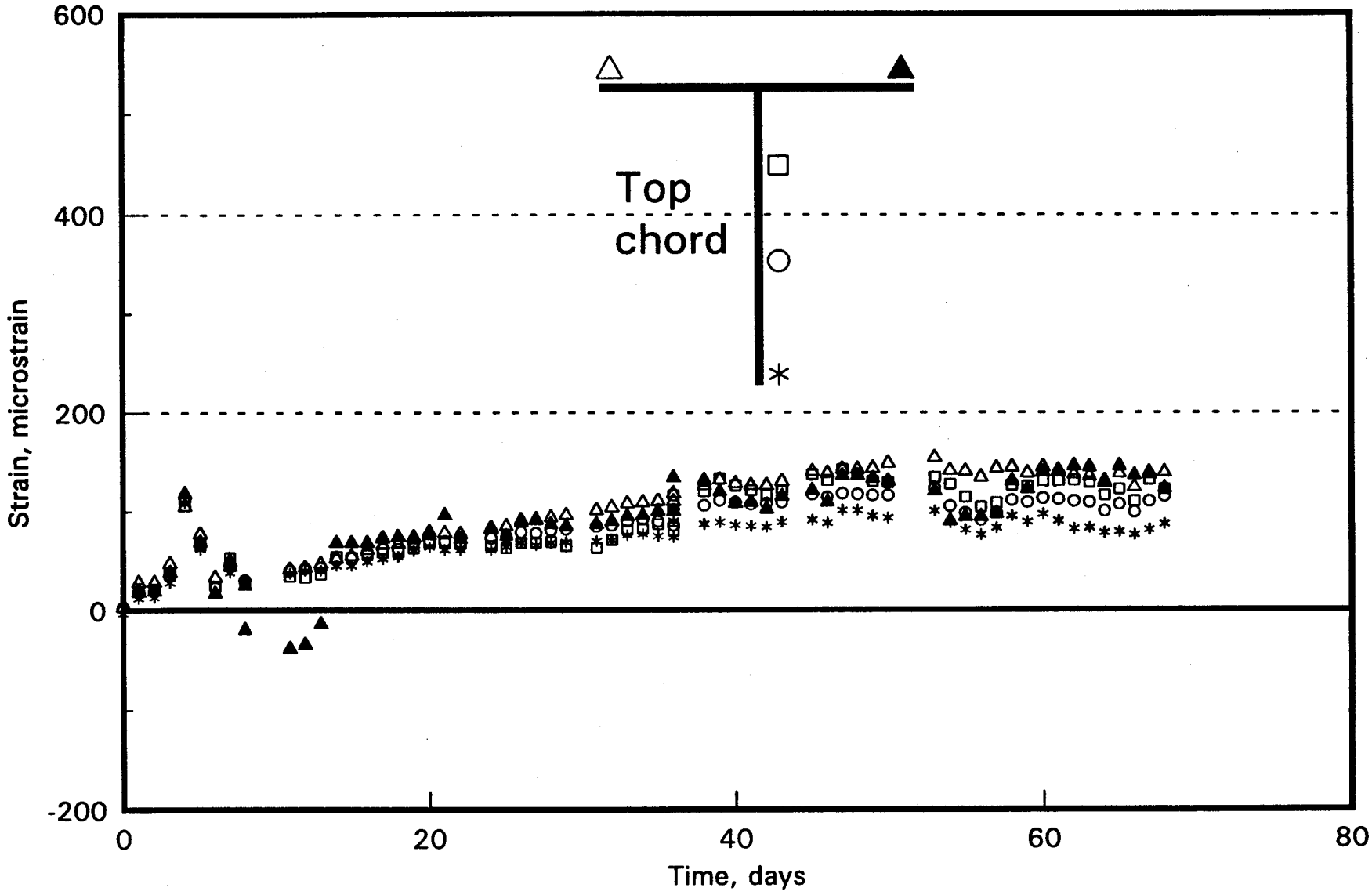

Fig. 7.8 Local steel shrinkage strains, top chord

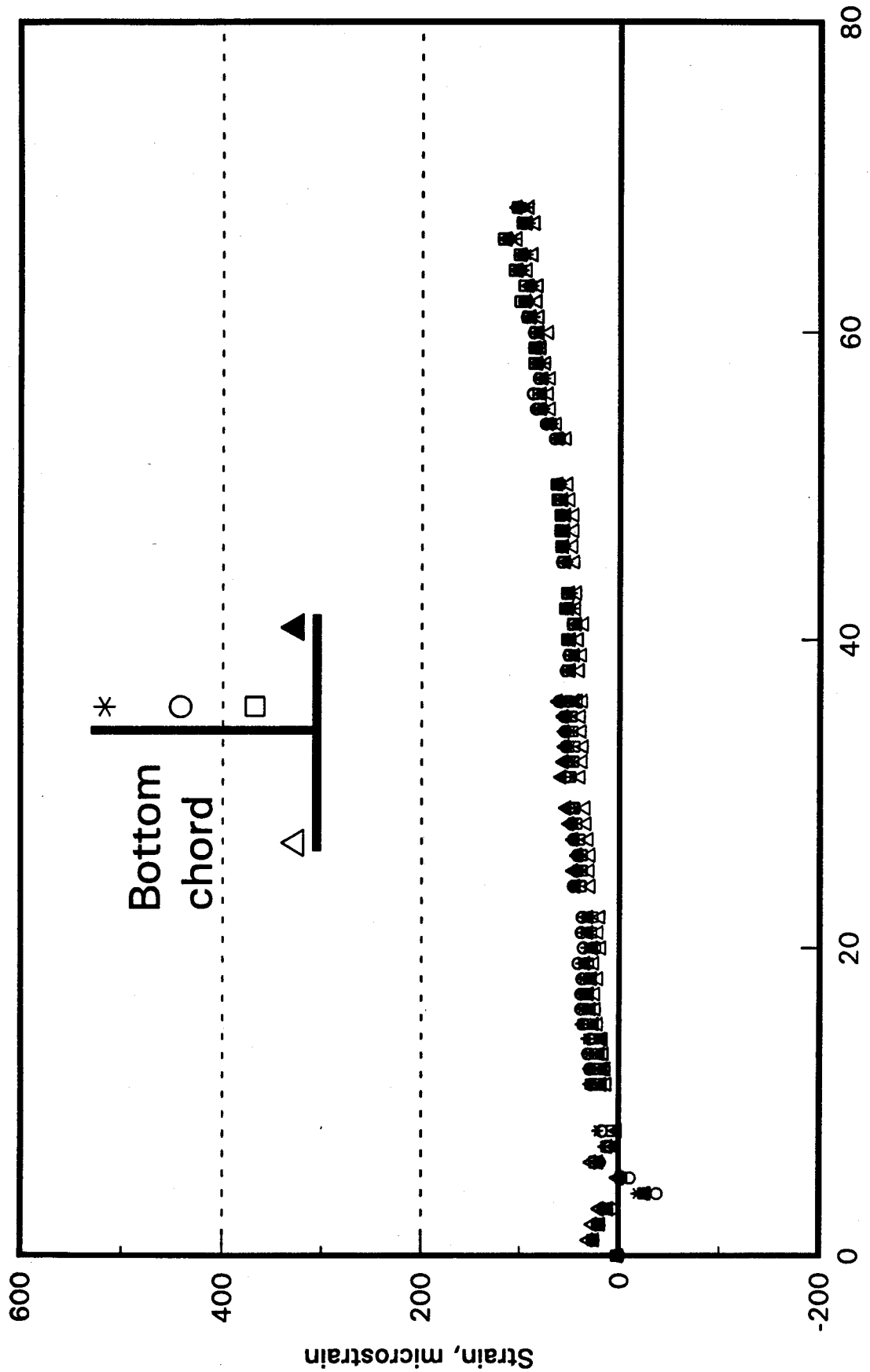

Fig. 7.9 Local steel shrinkage strains, bottom chord

8 ANALYSIS OF SHRINKAGE TEST RESULTS

8.1 Shrinkage deflections

CSA Standard S16.1 - 94 refers to the equilibrium method and the unrestrained shrinkage method for determining deflections due to concrete shrinkage. The equilibrium method (Brattland 1986) was modified by Kennedy and Brattland (1992), and is further modified here. The unrestrained shrinkage method was developed by Montgomery et al. (1983).

8.1.1 Equilibrium method

This is based on Kennedy and Brattland (1992). Consider the free body diagram of one half of the truss shown in Figure 8.1 in which the concrete is subject to a tensile force, T_S, when restrained in shrinking by the steel truss to which it is attached. For equilibrium, summing forces in the horizontal direction and summing moments about the line of action of the force in the steel top chord, we have

[8.1] $C_{tc} = T_s + T_{bc}$

[8.2] $a \cdot T_s = b \cdot T_{bc}$.

From the shrinkage strain distribution of the truss depth shown in Figure 8.2

[8.3] $\varepsilon_r = \varepsilon_f - \varepsilon_s$

[8.4] $\dfrac{\varepsilon_r + \varepsilon_{bc}}{\varepsilon_{tc} + \varepsilon_{bc}} = \dfrac{a+b}{b}$.

Furthermore

[8.5] $T_s = \varepsilon_s E_c' A_c$

[8.6] $C_{tc} = \varepsilon_{tc} E_{tc} A_{tc}$

[8.7] $T_{bc} = \varepsilon_{bc} E_{bc} A_{bc}$.

Kennedy and Brattland (1992) define E'_C in [8.5] as the effective modulus of elasticity of concrete in tension. (For reasons given subsequently, this modulus is later redefined as the apparent modulus of elasticity.) This modulus may bear no relation to that measured in compression cylinder tests at 28 days.

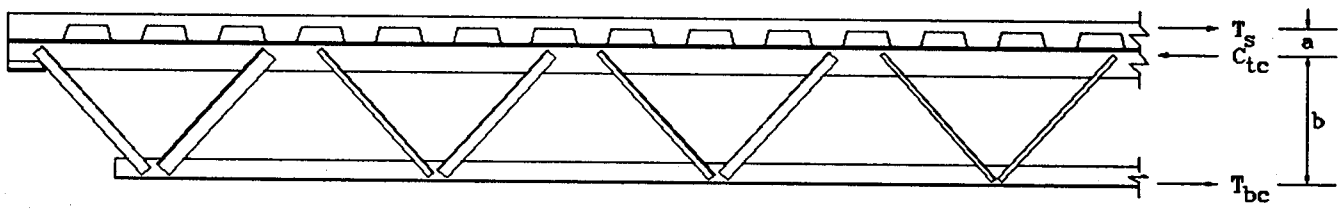

Fig. 8.1 Free body diagram of shrinkage induced forces

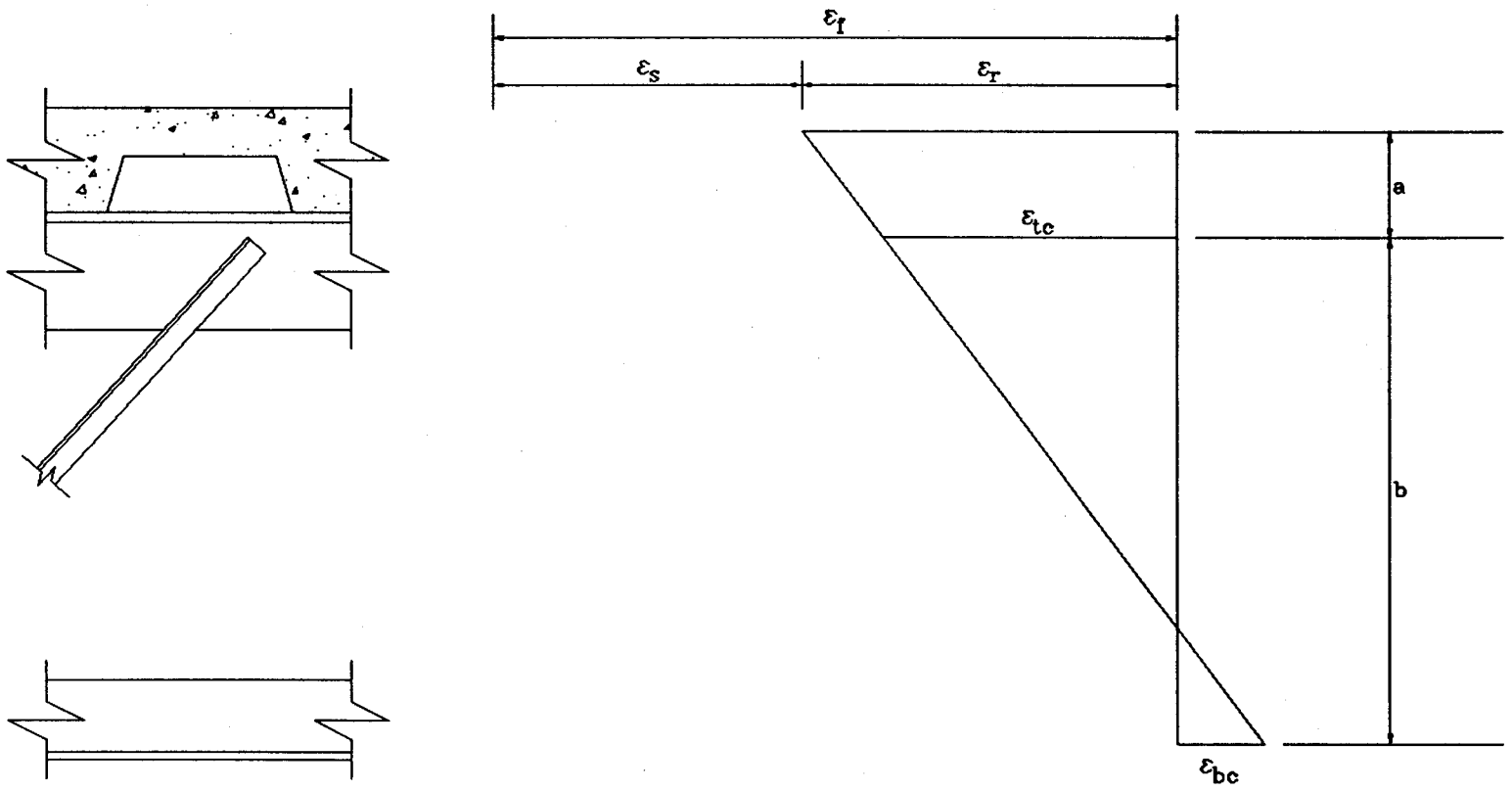

Fig. 8.2 Shrinkage strain distribution over the truss depth

From the definition of curvature,

$$[8.8] \quad \frac{1}{\rho} = \frac{\varepsilon_{bc} + \varepsilon_r}{a+b} = \frac{\varepsilon_{bc} + \varepsilon_{tc}}{b} .$$

When the curvature is assumed to be constant over the length of the truss

$$[8.9] \quad \Delta_{sh} = \frac{L^2}{8\rho} .$$

In fact, the curvature increases from zero at the ends to the value given by [8.8], however Kennedy and Brattland (1992) show that, because the shrinkage forces develop within a short distance from the ends of the truss, that the error introduced by using [8.9] is less than 2% even under extreme circumstances.

Kennedy and Brattland (1992) then develop three equations relating the strains at the three levels and note that, for equilibrium, when the strain distribution is assumed to be linear, that a unique relationship exists among the three strains ε_r ,ε_{tc} and ε_{bc}.

Rearranging [8.4] gives

$$[8.4a] \quad \varepsilon_r = \frac{a+b}{b}\varepsilon_{tc} + \frac{a}{b}\varepsilon_{bc} .$$

Combining [8.1], [8.2], [8.6] and [8.7] results in

$$[8.10] \quad \varepsilon_{tc} = \frac{a+b}{a}\frac{E_{bc}A_{bc}}{E_{tc}A_{tc}}\varepsilon_{bc} ,$$

and from [8.1], [8.3], [8.5], [8.6] and [8.7]

$$[8.11] \quad \varepsilon_{tc}E_{tc}A_{tc} = (\varepsilon_f - \varepsilon_r)E_c'A_c + \varepsilon_{bc}E_{bc}A_{bc} .$$

Equations [8.4a] and [8.10] provide a relationship among the three strains. Assuming a relative value of the restrained shrinkage strain, ε_r, of 1.000, based on the measured values of the axial stiffness, EA, of the top and bottom chords, the ratios of ε_r:ε_{tc}:ε_{bc} are established to be 1.000:0.786:0.231. These ratios and [8.11], in conjunction with the known axial stiffnesses of the steel chords, may be used to calculate the restrained shrinkage strain in the concrete (and, hence, the induced shrinkage strains in the chords), if

the axial stiffness of the slab ($A_cE'_c$) and the free shrinkage are known. Hence, the shrinkage deflection is then found from [8.8] and [8.9]. Conversely, if the strain distribution has been determined, the shrinkage deflection can be calculated and the effective modulus of elasticity of the concrete in tension, E'_c, can be deduced.

8.1.1.1 Shrinkage deflection based on measured strains

In Figures 8.3a to 8.3f are plotted, against the depth of the truss, the strains in the longitudinal direction obtained from the rod-dial gauge assemblies at the three levels, the average of the local concrete strains at the level of the concrete surface and the strains at the centroidal axis level of the top and bottom steel chords obtained from the electrical resistance strain gauges mounted on them, for six different times during the shrinkage test. Assuming that the strain distribution through the depth of the truss is linear, Kennedy and Brattland (1992) showed that a unique set of the ratios of the restrained shrinkage strain and the strains in the top and bottom chords were necessary for a given truss geometry, to satisfy equilibrium conditions. As discussed previously in Section 8.1.1, for this truss, the ratios of the strains ε_r:ε_{tc}:ε_{bc} is 1.000:0.786:0.231. This restraint of the relative strains fixes the point of zero strain at 174 mm above the bottom surface of the bottom chord. Using this constraint, linear regression analyses were carried out on the strain data for the six different times to determine the best fit lines, which are plotted in Figures 8.3a to 8.3f. The coefficients of determination varied between 0.8517 and 0.9312 and generally increased with time.

Using the regressed strain distributions of 8.3a to 8.3f and assuming that the corresponding curvature applies through the entire span of the truss, the deflection of the truss was calculated from [8.8] and [8.9]. These calculated deflections are compared with the measured deflections at the corresponding time in Table 8.1. The calculated deflections agree well with the measured values, with a mean value of the ratio of the calculated deflection to the measured deflection of 1.029 and a coefficient of variation of 0.025.

Table 8.1 Regression analysis deflection calculations

	Deflection, mm		
Day	Measured, Δ_m	Calculated, Δ_c	Δ_m / Δ_c
20	3.68	3.54	1.041
31	4.62	4.54	1.017
40	5.24	5.26	0.996
50	5.83	5.77	1.011
60	6.39	6.15	1.040
68	6.79	6.35	1.069
		Mean	1.029
		Coefficient of variation	0.025

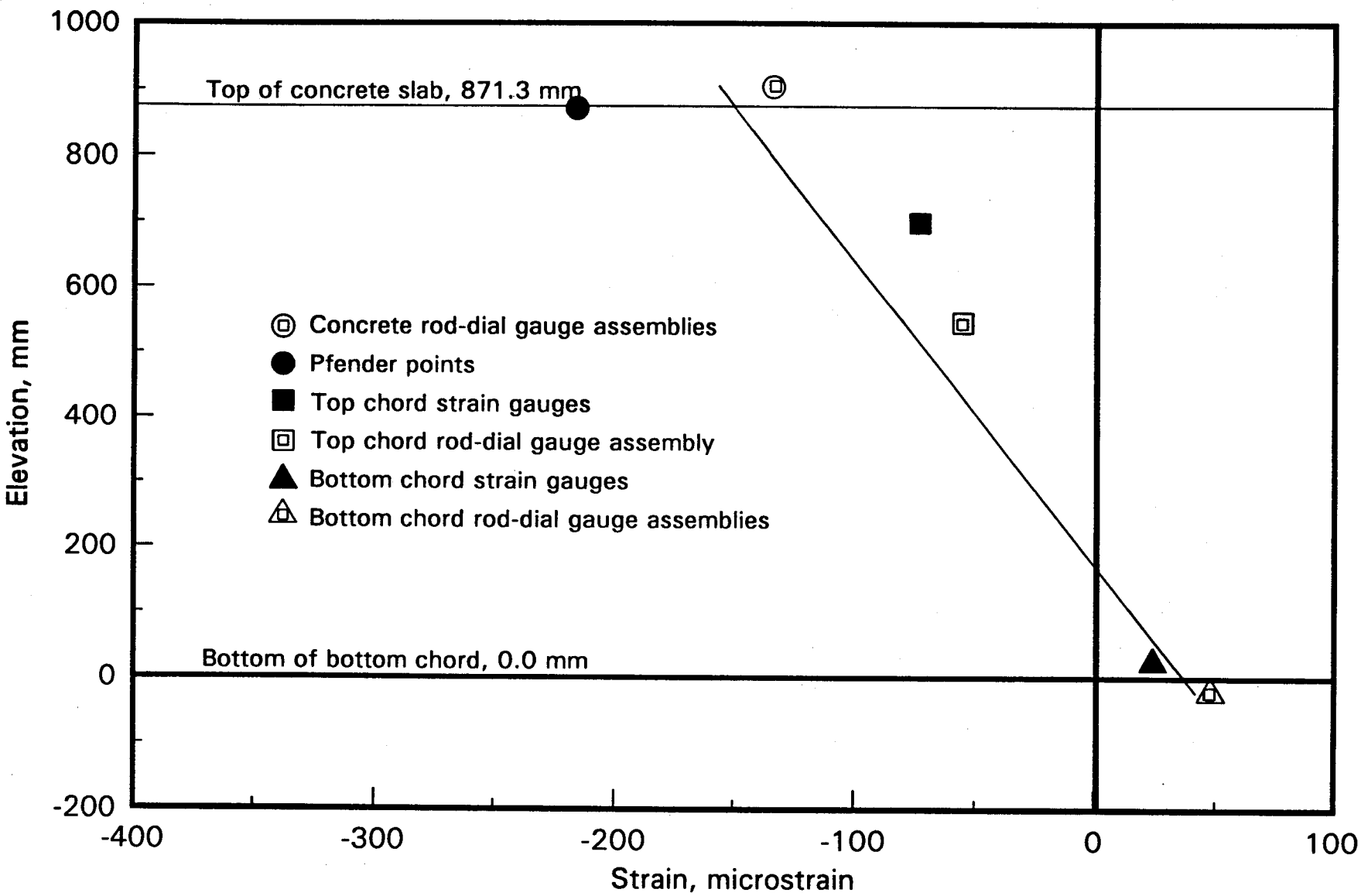

Fig. 8.3a Shinkage strain distribution at 20 days

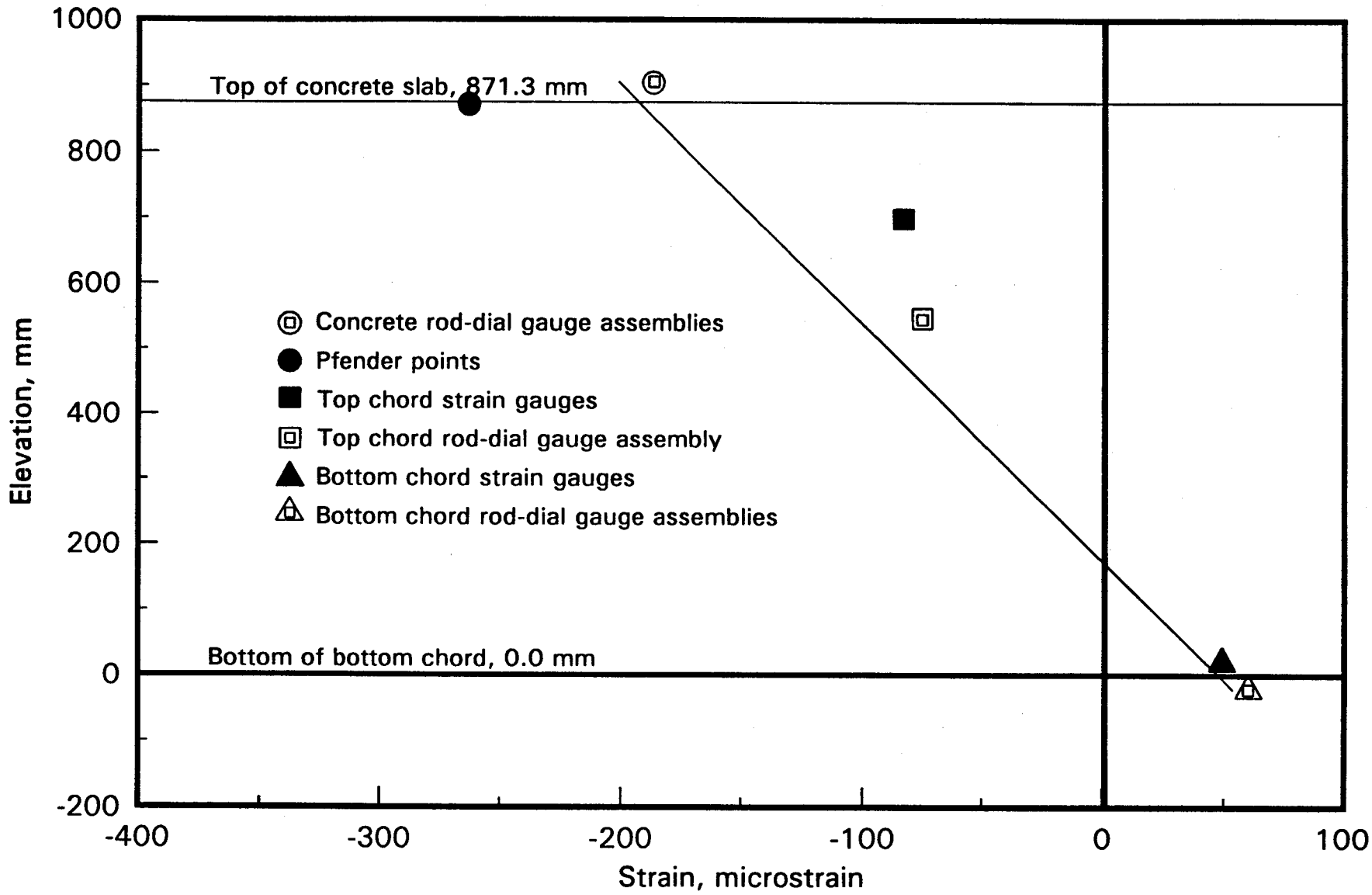

Fig. 8.3b Shrinkage strain distribution at 31 days

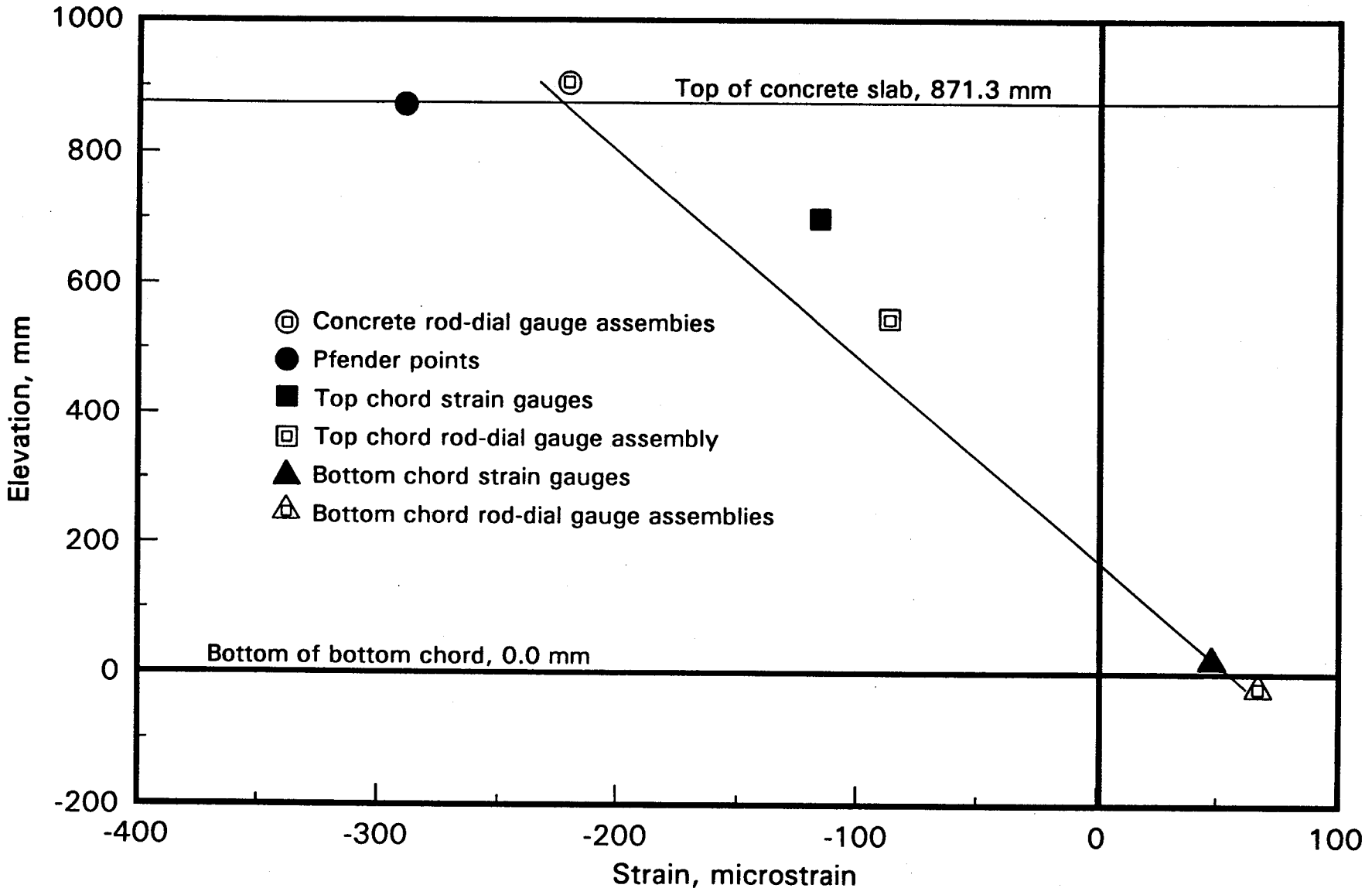

Fig. 8.3c Shrinkage strain distribution at 40 days

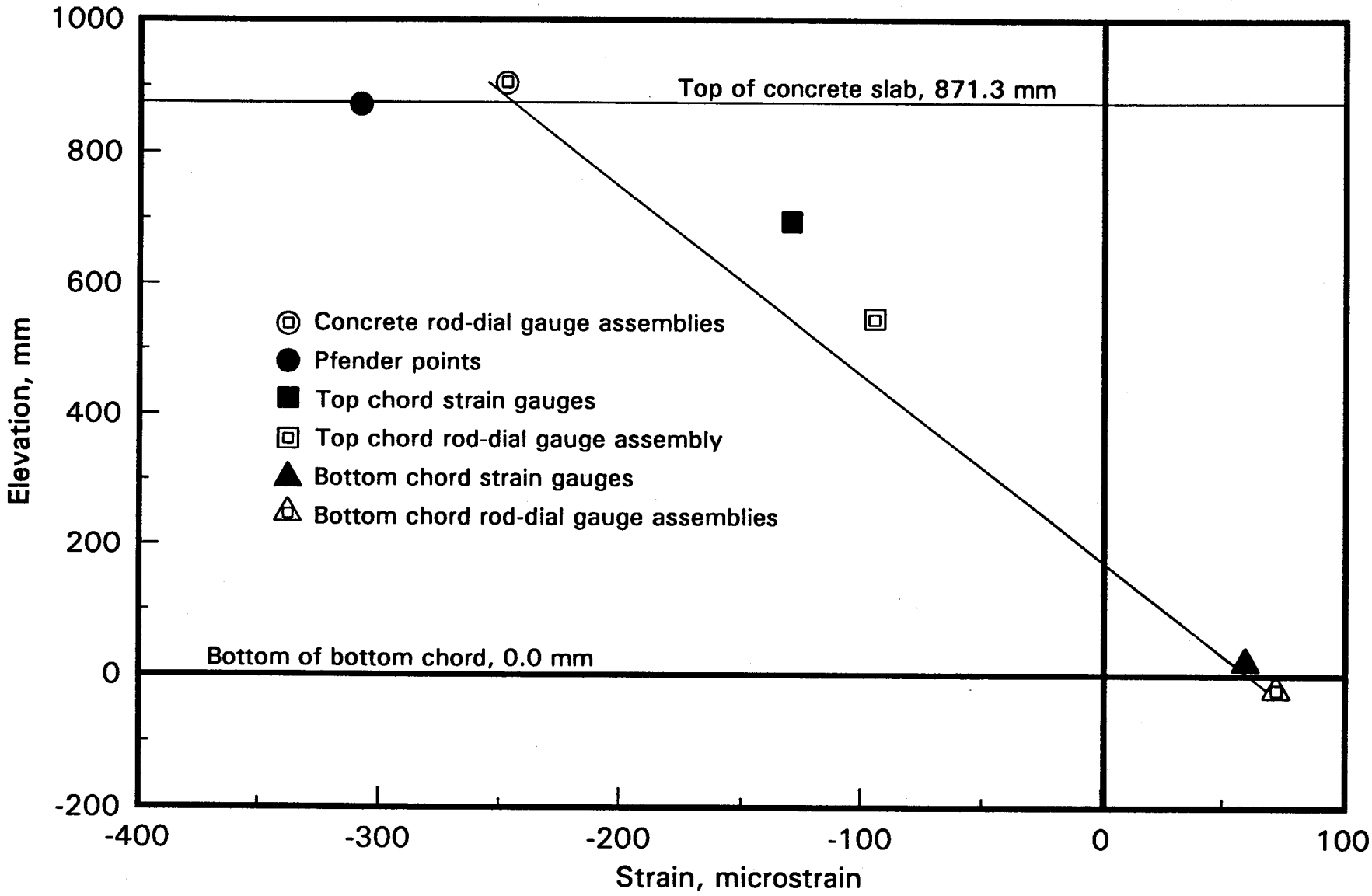

Fig. 8.3d Shrinkage strain distribution at 50 days

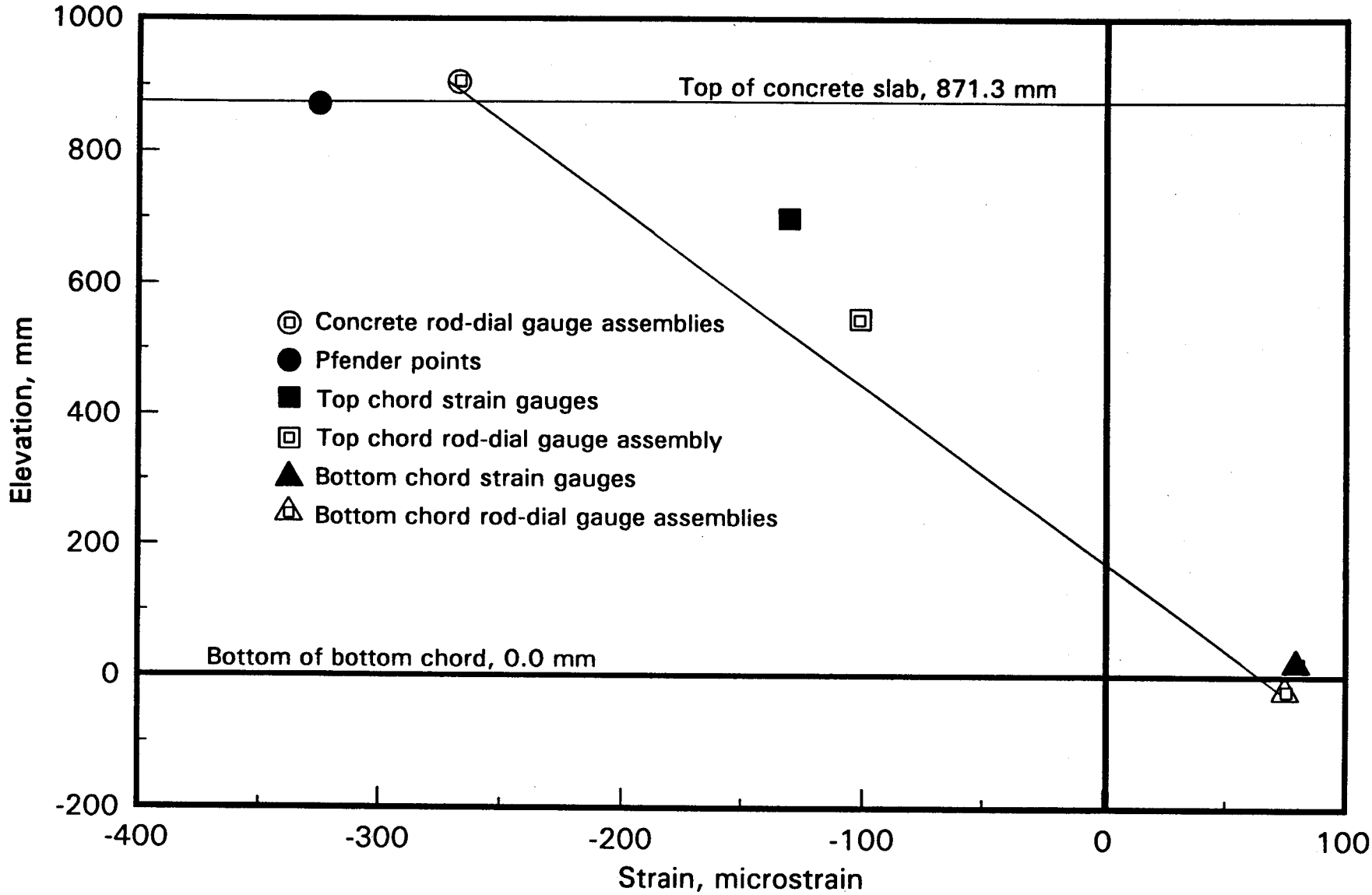

Fig. 8.3e Shrinkage strain distribution at 60 days

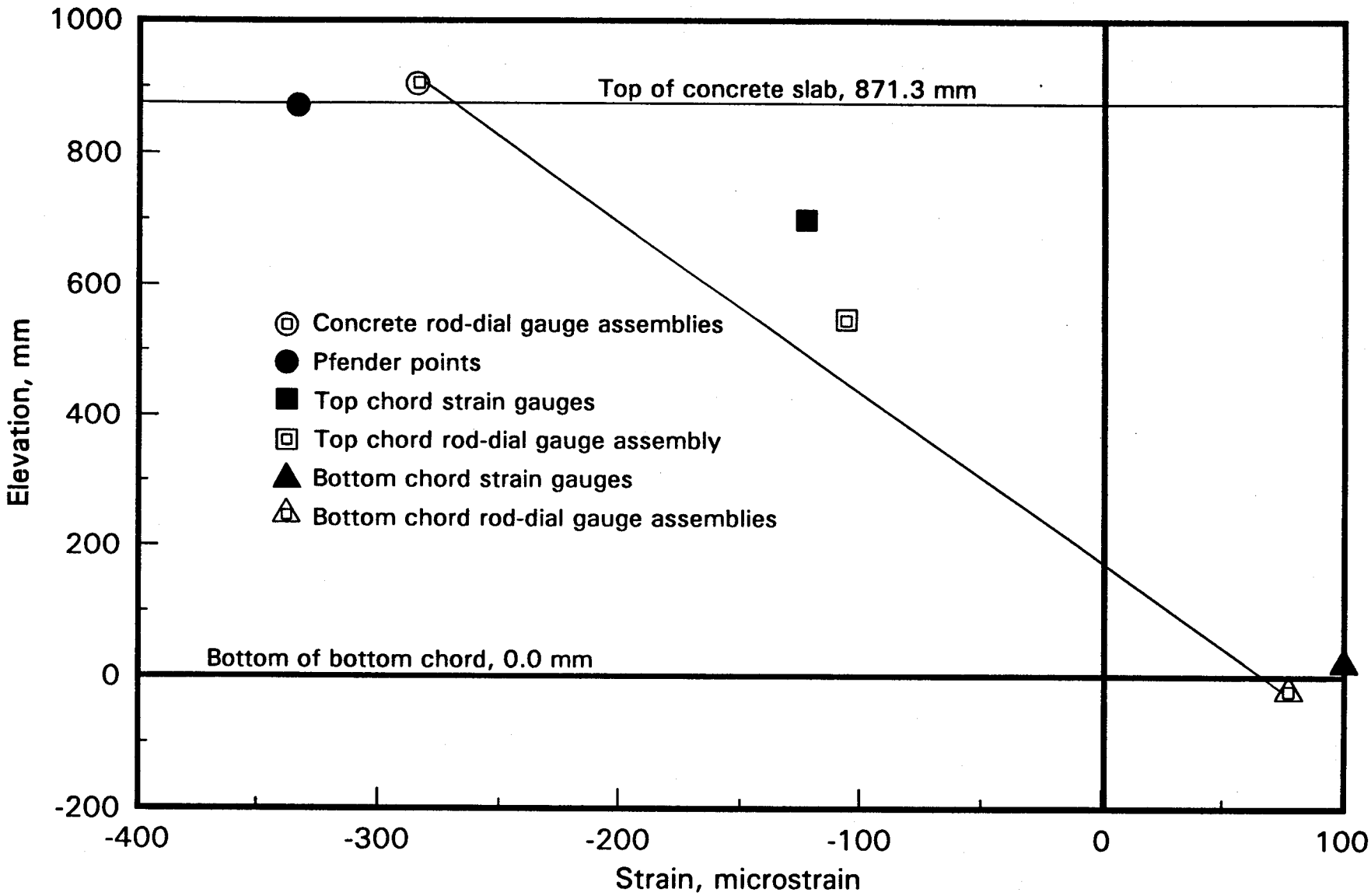

Fig. 8.3f Shrinkage strain distribution at 68 days

8.1.1.2 Shaker's general method

Shaker (1991) proposed a general equilibrium method, based on the work of Kennedy and Brattland (1992), to calculate the deflection of a composite beam or truss. The method estimates the free shrinkage strain, ε_f, using empirical equations derived by him, and then follows an iterative process.

The free shrinkage strain may be expressed as

[8.12] $$\varepsilon_f = \alpha\left(1 - e^{-\beta t}\right),$$

where, from Figure 7.2, the values of α and β, based on a least squares fit of the data, have been determined to be 760 and 0.0397, resulting in a free shrinkage strain, ε_f, at 68 days of 709 $\mu\varepsilon$. The corresponding values of α and β for Shaker's two concrete mixes were 855 and 0.0245 for f'_c = 30.5 MPa, and 748 and 0.0323 for f'_c = 38.7 MPa, resulting in free shrinkage strains, ε_f, at 68 days of 693 $\mu\varepsilon$ and 665 $\mu\varepsilon$.

Shaker also derived an empirical relationship between the effective modulus, E'_c, and the concrete tensile stress, σ_s, induced by restraint to concrete shrinkage including creep effects, at 180 days. Using his time dependent equations for the modulus of elasticity , the relationship between the tensile stress and the effective modulus at 68 days was derived and is shown in Figure 8.4. Also shown in the figure is the relationship given by CSA Standard S16.1 - 94, which represents extreme conditions.

The iterative process is as follows:

1. Determine or estimate the free shrinkage strain, ε_f.

2. Estimate E'_c, and hence, calculate the restrained shrinkage strain, ε_r, from

[8.13] $$\varepsilon_r = \varepsilon_f \left\{ \frac{1}{1 + \dfrac{\Lambda E_{tc} A_{tc} - \Phi E_{bc} A_{bc}}{A_c E'_c}} \right\},$$

which is derivable from the equations previously cited.

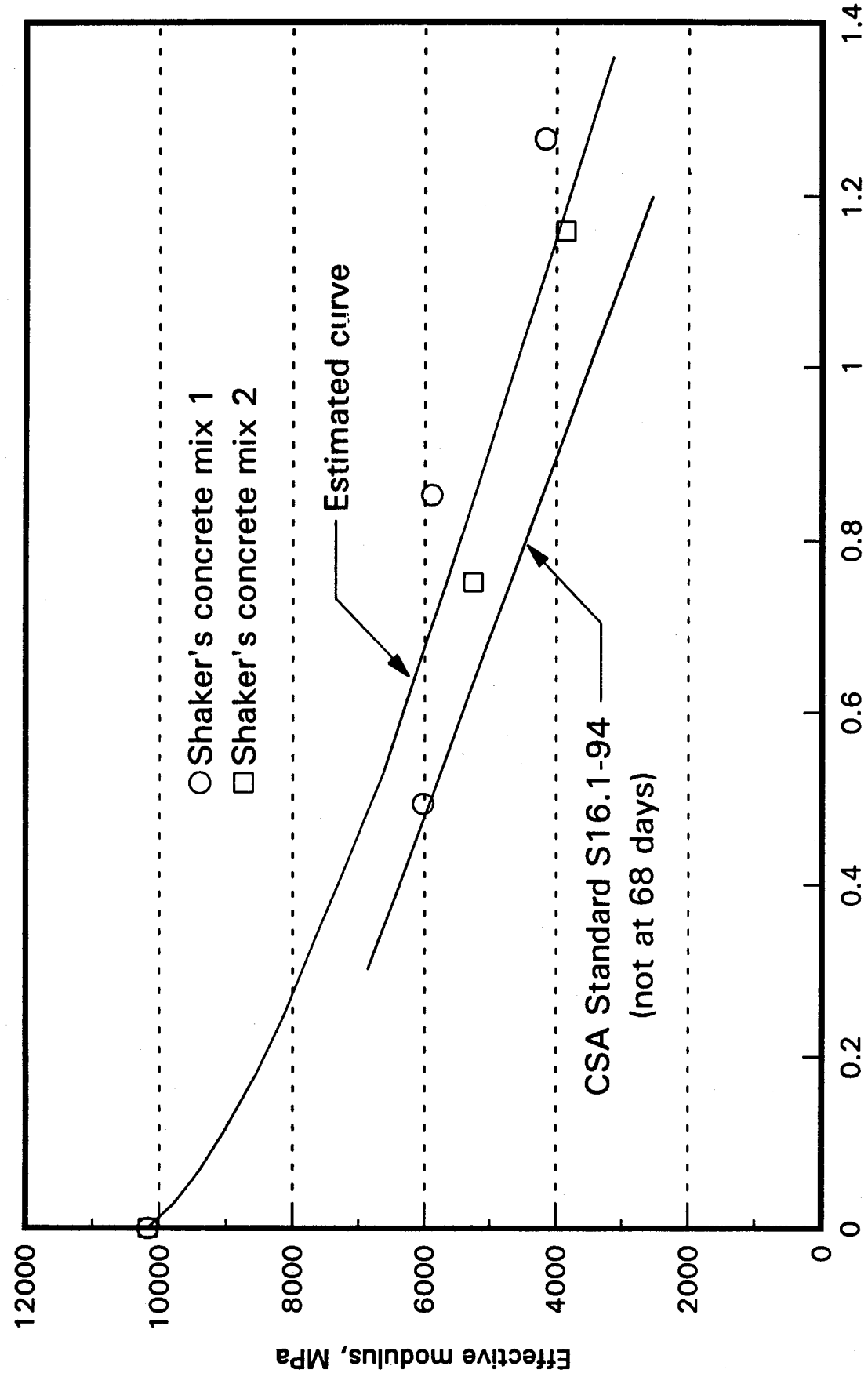

Fig. 8.4 Effective modulus of concrete versus the tensile stress at 68 days

The parameters Φ and Λ are defined in [8.14] and [8.15], respectively as

[8.14] $$\Phi \equiv \frac{b}{\left[(a+b)(1+\Omega)-b\right]}$$

[8.15] $$\Lambda \equiv \Phi\Omega ,$$

where Ω is defined as

[8.16] $$\Omega \equiv \left\{\frac{(a+b)E_{bc}A_{bc}}{aE_{tc}A_{tc}}\right\} .$$

The parameters Φ and Λ, which are constant for any given composite truss configuration, are, in fact, the ratio of the steel top and bottom chord strains respectively, to the restrained shrinkage strain, i.e., $\varepsilon_r:\varepsilon_{tc}:\varepsilon_{bc} = 1.000:\Phi:\Lambda$.

3. Rearranging [8.3] gives

[8.3a] $$\varepsilon_s = \varepsilon_f - \varepsilon_r .$$

Hence, the tensile strain in the concrete can be calculated.

4. Rearrange [8.5] and define σ_S as

[8.5a] $$\sigma_s \equiv \frac{T_s}{A_c} = \varepsilon_s E_c' .$$

From which the tensile stress in the concrete can be calculated.

5. Iterations are performed until the values of E'_C and σ_S are compatible with the relationship given in Figure 8.4.

6. Because the ratios of the strains through the depth of the truss are known to be $\varepsilon_r:\varepsilon_{tc}:\varepsilon_{bc} = 1.000:\Phi:\Lambda$, the other strains can be calculated from the calculated value of the restrained shrinkage strain, ε_r. Using [8.8] and [8.9], the shrinkage deflection of the truss can then be calculated.

Using this iterative process, an effective modulus of elasticity, E'_C, of 3980 MPa was calculated and a corresponding tensile stress in the concrete, σ_S, of 1.16 MPa, based on

the relationship derived from Shaker. The deflection of the composite truss at 68 days is calculated to be 10.4 mm. This deflection, 1.5 times the measured deflection, results from the fact that the value of E'_c is considerably greater than that determined for this shrinkage test, as discussed subsequently.

8.2 Modulus of elasticity of concrete in tension

The value of the modulus of elasticity of concrete in tension, now called the apparent modulus, can be computed from the equations given in Section 8.1.1, either based on the measured deflections or the strain distributions determined by the regression analysis, as follows:

1. The curvature , assumed to be constant over the entire span, is related to the mid-span and quarter point deflections by

[8.17] $$\frac{1}{\rho} = \frac{8\Delta_m}{L^2}$$

and

[8.18] $$\frac{1}{\rho} = \frac{32\Delta_q}{3L^2},$$

where Δ_m is the deflection at mid-span and Δ_q is the deflection at a quarter point. Recall the curvature-strain relationship

[8.8] $$\frac{1}{\rho} = \frac{\varepsilon_{bc} + \varepsilon_r}{a+b} = \frac{\varepsilon_{bc} + \varepsilon_{tc}}{b}.$$

2. Equilibrium requires that

[8.4a] $$\varepsilon_r = \frac{a+b}{b}\varepsilon_{tc} + \frac{a}{b}\varepsilon_{bc}$$

[8.10] $$\varepsilon_{tc} = \frac{a+b}{a}\frac{E_{bc}A_{bc}}{E_{tc}A_{tc}}\varepsilon_{bc},$$

as discussed previously. Therefore, knowing the curvature, $1/\rho$, the three strains, ε_r, ε_{tc} and ε_{bc}, can be calculated using [8.8], [8.4a] and [8.10]. These strains are also obtainable from the regression analysis performed on the measured trains through the depth of the truss.

3. At any time, the free shrinkage strain, ε_f, is obtained from

[8.12] $$\varepsilon_f = \alpha\left(1-e^{-\beta t}\right) .$$

Hence, the tensile strain in the concrete is obtained from

[8.3a] $$\varepsilon_s = \varepsilon_f - \varepsilon_r .$$

4. Combining [8.1], [8.5], [8.6] and [8.7] and define E_a as

[8.19] $$E_a \equiv E_c' = \frac{\varepsilon_{tc}E_{tc}A_{tc} - \varepsilon_{bc}E_{bc}A_{bc}}{\varepsilon_s A_c} .$$

The results of such calculations are given in Table 8.2 and in Figure 8.5.

Table 8.2 Calculated values of apparent modulus of elasticity, E_a, MPa

Day	Mid-span deflection	Quarter point deflections	Regression analysis
20	1531	1505	1440
31	1465	1436	1428
40	1486	1480	1495
50	1546	1550	1520
60	1649	1659	1551
68	1740	1744	1563

The values computed from the deflections at the mid-span and the quarter points are essentially the same and are considered to be more accurate than those obtained by the regression analyses, because of the relative ease in measuring deflections as compared to strains.

These values of the apparent modulus of elasticity for periods up to 68 days from casting are considerably smaller than those obtained by Shaker in controlled prismatic shrinkage tests. This is attributed to two factors that increase the flexibility of the composite truss: the interfacial slip at the concrete-steel interface and the flexibility of the open web system. The apparent values of the modulus of elasticity are based on a linear strain distribution,

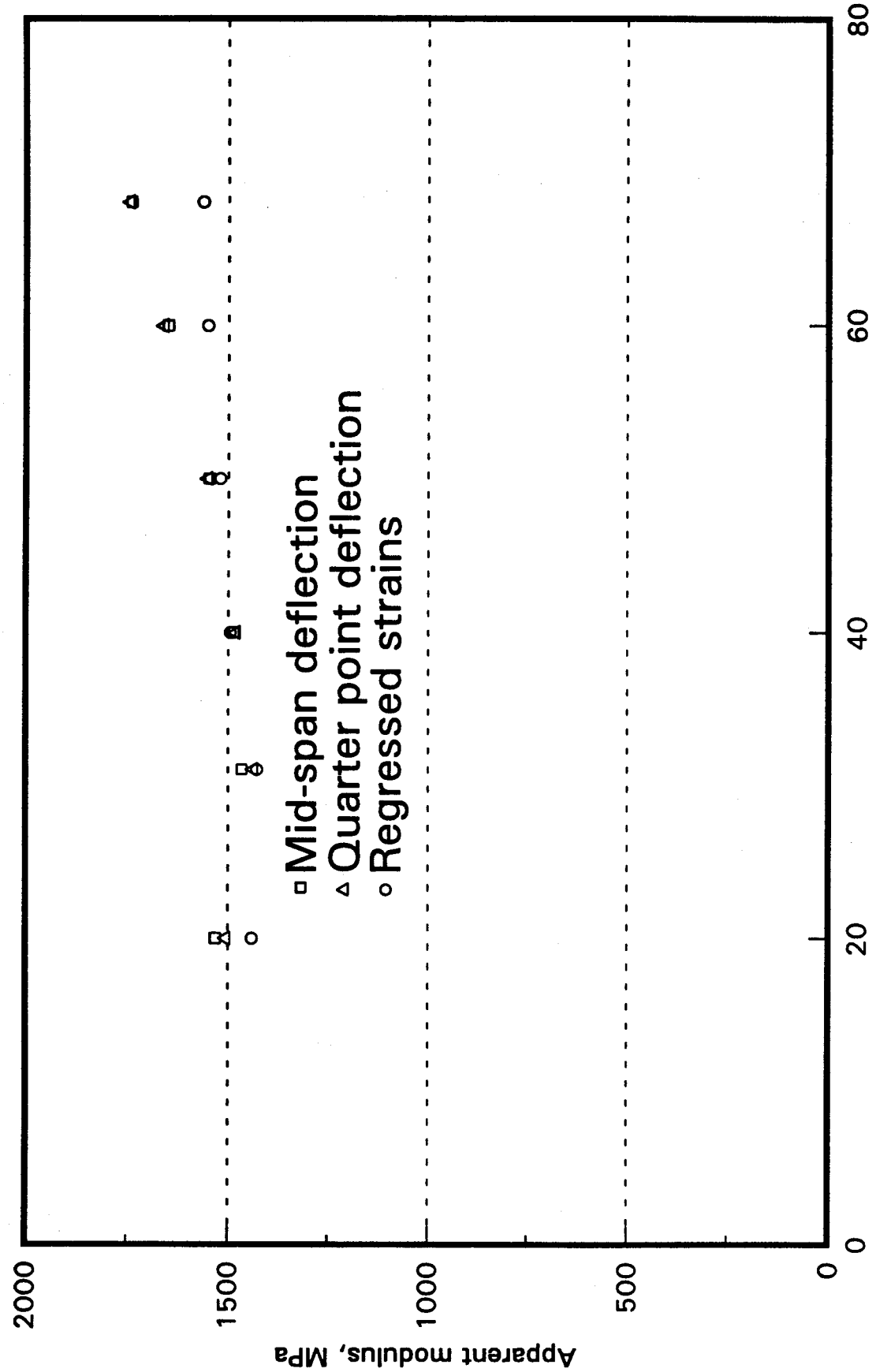

Fig. 8.5 Apparent modulus of concrete in tension

and therefore no interfacial slip, and also attribute all of the deflection to flexural action, without considering shear deflections of the open web system.

A relationship between the apparent modulus of elasticity and the effective modulus of elasticity can be established by equating the transformed moment of inertia, based on the apparent modulus, to the effective moment of inertia, based on the effective modulus . This, by definition, would take into consideration the interfacial slip and the deflection of the web system. Therefore we have

$$[8.20] \quad I_{tE_a} = I_{eE'_c} \equiv \frac{I_s + 0.85(I_{tE'_c} - I_s)}{1.10} ,$$

from which

$$[8.20a] \quad I_{tE'_c} = \frac{1.10 I_{tE_a} - 0.15 I_s}{0.85} \cong 1.294 I_{tE_a} - 0.176 I_s .$$

Starting with a value of the apparent modulus of elasticity, E_a, of 1740 MPa, as determined from the mid-span deflection at 68 days, the transformed moment of inertia, based on this modulus, I_{tEa}, is calculated to be 737.8 x 10^6 mm^4. Using [8.20a] results in a transformed moment of inertia, based on the effective modulus of elasticity, $I_{tE'c}$, of 853.7 x 10^6 mm^4. This requires that the effective modulus of elasticity be 3605 MPa. This value is in reasonable agreement with that of about 3980 MPa determined for Shaker's (1991) concrete mixes at a stress level of about 1.2 MPa. The correspondence between these two values confirms that the apparent modulus is relatively small compared to the effective modulus (due to interfacial slip and web deformations of the truss).

Calculated shrinkage deflections, based on the effective modulus of elasticity, as was done in Section 8.1.1.2, are seen to be greater than those calculated on the basis of the apparent modulus. This follows from the fact that stiffer concrete develops a greater force when restrained, and the composite truss is calculated to deflect more under the action of the larger shrinkage forces.

These arguments lead to the conclusion that accurate assessments of shrinkage deflections of composite trusses should be based on the apparent moduli of elasticity. When using Branson's method (Section 8.1.2) in

$$[2.1] \quad \Delta_s = \frac{\varepsilon_f A_c L^2 y}{8 n_t I_{et}} ,$$

the values of the modular ratio, n_t, the distance from the centroid of the slab to the elastic neutral axis, y, and the moment of inertia, I_{et}, should all be based on the apparent modulus of elasticity. Thus compensation for the interfacial slip and shear deflection, both of which are difficult to assess, is made by modifying the effective modulus of elasticity. When shrinkage deflections are based on the effective, and therefore larger modulus of elasticity, and associated values of n_t and y, an overestimate of the shrinkage deflections will be obtained. This is the method given in S16.1-94, because, a priori, the apparent modulus of elasticity is not known.

9 FLEXURAL TEST RESULTS

The composite truss was tested to failure over a period of two days, beginning on November 18 and finishing on November 19, 1993. In the following discussion and figures, the test load is the average load applied to the specimen at each of the four jack locations.

9.1 Deflections and overall behaviour

In Figure 9.1, the average of the four jack loads is plotted against the mid-span truss deflection. As the two reactions were also measured, one quarter of their sum should give an equivalent jack load. Examination of the data recorded, however, showed that the jack loads displayed considerably less variability than the reactions. In particular, at one load step, an unexpected increase in the south reaction occurred. On the other hand, the jack loads were remarkably consistent, generally exhibiting a coefficient of variation of 0.01, or even less. Therefore, the average jack loads were considered to be the most reliable loads.

On many occasions, loads were recorded immediately upon closing the valves and then just prior to opening the valves to apply another increment of load. This interval, during which measurements were taken and the test conditions checked, varied from five to 45 minutes. As the data show, the load decreased during these intervals, from the upper to the lower points, for which different symbols are used in Figure 9.1. In the inelastic region, three reasons for this decrease in load are postulated:

1. As yielding occurs, due to movement of dislocations, which is not instantaneous (Lay 1982), the load would decrease upon reducing the strain rate to zero (closing the valves) and the deflections would increase slightly as the movement of the dislocations gradually ceases (assuming that the hydraulic oil in the loading system is a slightly compressible fluid and therefore allowing for a slightly larger deflection to be realized due to the corresponding decrease in pressure).
2. Creep of the concrete (over a relatively small time interval) may also account for some of the decrease in load, which should be accompanied by little change in deflection.
3. As well, leakage in the loading system would cause the load to decrease, during which some elastic rebound would be expected to occur.

Some evidence of leakage is that when the truss was left loaded overnight the load decreased from 100 kN per jack to 91 kN per jack, and was accompanied by a slight decrease in deflections. Therefore, the decrease in the load during the time when the measurements were taken may contain a small component due to leakage in the system. It is conservative to disregard this (and the creep of the concrete) and consider the lower data points to represent data obtained at zero strain rate. A smooth curve has therefore been drawn through these points.

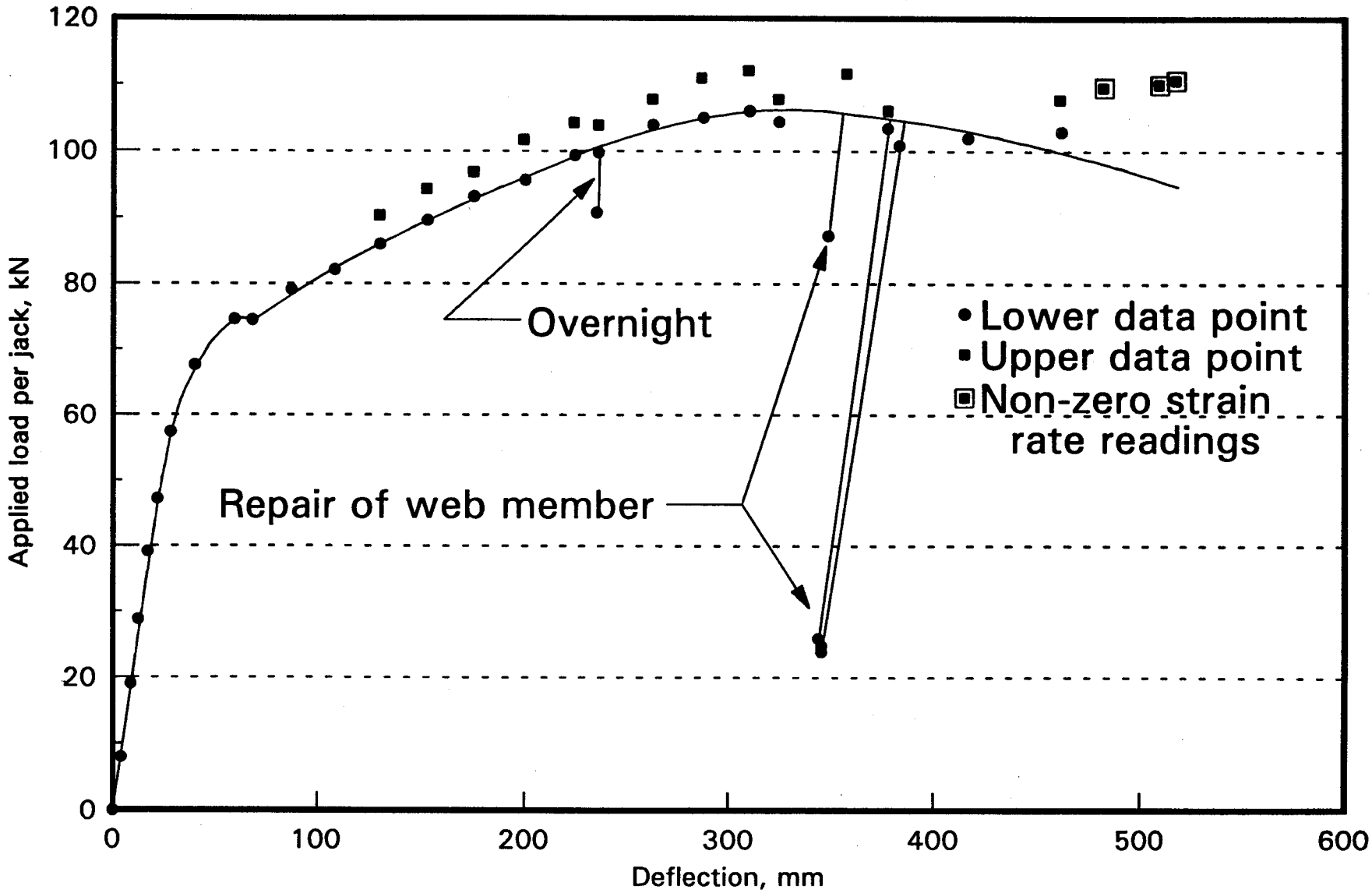

Fig. 9.1 Load-deflection response at mid-span

Three anomalies exist in the curve as constructed. The first, labeled "overnight", shows the decrease in load as the truss was left loaded overnight. The second, labeled "repair of web member", consists of two drops in the load below the curve. At the load reached before the first of these drops, it was noticed that the truss had deflected onto a block positioned to prevent the truss from falling too far, should it collapse. The first drop occurred when the load was decreased to remove the block. Unfortunately, the block supplied a sufficient upward reaction to buckle web member 7, selected to meet slenderness limits, as under symmetric loading it was a zero force member. On reloading, the buckle in this web member increased. Therefore, the load was reduced to about 25 kN per jack, while repairs to the web member were made. The third anomaly relates to the last three upper data points, which would appear to show an increasing load. The points were, however, obtained as load was being applied, and therefore, do not reflect zero strain rate conditions.

In examining the load deflection response, it should be taken into account that the dead load of the truss of 71.6 kN (causing a mid-span moment of 103 kN·m) is equivalent to a load per jack of 17.9 kN, because the loading configuration used emulates a uniform load reasonably well.

The truss behaved in a linear elastic manner up to an applied load of about 47 kN per jack, when increasing non-linear behaviour, attributed to the presence of residual stresses in the bottom chord, occurred. Cracking noises were heard, starting at a load of about 40 kN per jack, and became successively louder as the load increased. At an applied load of about 75 kN per jack, the load deflection curve exhibits a short yield plateau. At the end of this plateau, considerable flaking of the whitewash on the flange and stem of the bottom chord, extending over the central three panels, was observed. With subsequent loading, the load-deflection curve rises with a gradually decreasing slope until a maximum load of about 107 kN per jack is reached at a mid-span deflection of 340 mm. More cracking noises were heard during this loading and especially when the load reached 100 kN per jack, when the longitudinal cracking in the slab was first observed, as discussed subsequently. Beyond the maximum, the load gradually decreased until the last reading at a mid-span deflection of 520 mm, or 1 / 22 of the span, was taken. The truss, therefore, exhibited great flexibility.

Failure occurred unexpectedly when the whole truss, with reactions and loads providing only a state of neutral equilibrium, suddenly moved to the south. This resulted because one or more of the loading jacks was not vertical. This in turn was caused when the jack was adjusted to align the considerably extended piston rod and cylinder body. (In the extended position, the rod and piston seals provide little lateral restraint and the piston rods tend to "jack-knife", with respect to the cylinder body.)

Figure 9.2 shows the truss after the maximum load was reached, still carrying a load of 103 kN per jack, at a mid-span deflection of 460 mm. Note that the bottom chord tends to consist of a series of straight line segments between panel points where significant bending

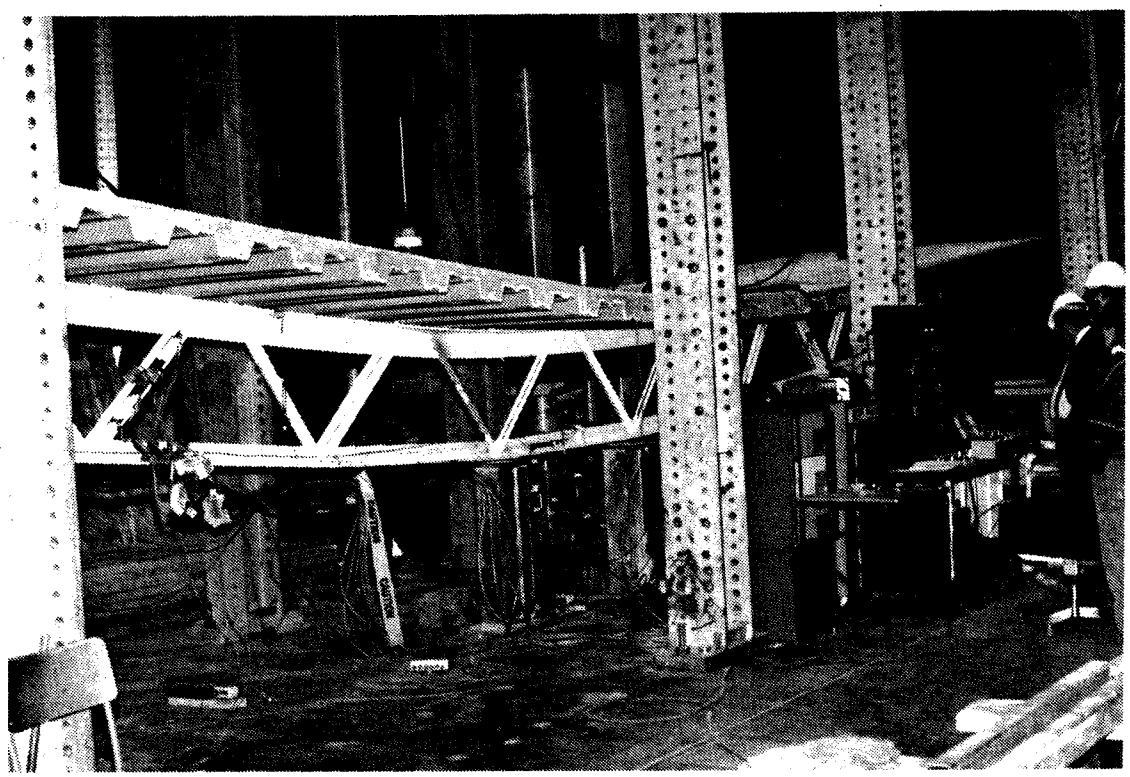

Fig. 9.2 Truss after maximum load was reached

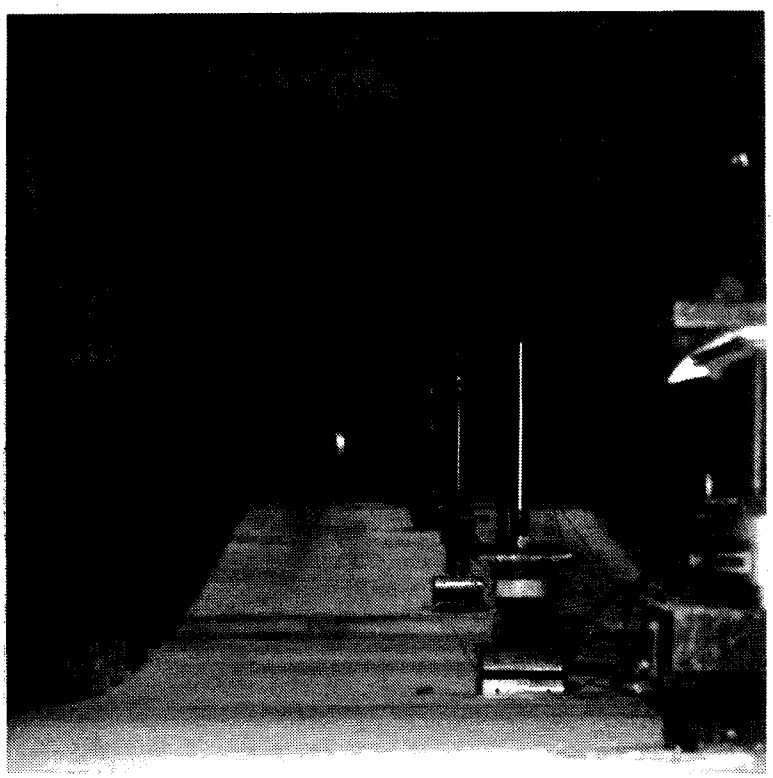

Fig. 9.3 Deflected shape of concrete slab near maximum load

of the chord has taken place. (This effect is exemplified in Figure 9.11, discussed subsequently.) Also note that the top chord was bent significantly, with most of the curvature concentrated near the mid-span of the truss. The small central web member 7, that was repaired, can be distinguished by its gray colour, compared to the other white ones. Just above its upper end, the bright vertical line, is the piston rod extension of one of the jacks.

Figure 9.3 shows the top surface of the concrete slab when the truss had deflected a considerable amount. Three of the loading jacks are discernible. The bright vertical lines, especially that of the jack in the foreground, show the piston rod extension of the jacks.

The lower panel point shown in Figure 9.4, where web members 11 and 12 are joined to the bottom chord, marks the south end of the three central panels where the bottom chord is most heavily strained. Flaking of the whitewash on the stem of the left hand portion of the bottom chord WT (which is only faintly visible on the photographic reproduction) is clear evidence of significant axial straining. The flaking between the web members shows that local yielding was occurring, as was typical for the bottom chord panel points. Corresponding to the three central bottom chord panels, the two central panels of the top chord, between the interior jacks, underwent the most severe curvature as is seen in Figure 9.2 and 9.3.

Figure 9.5 shows a portion of the longitudinal cracks that formed over the six central panels at a load of 100 kN per jack and a mid-span deflection of 235 mm. With further loading, longitudinal cracks formed along two lines, approximately over the top of each stud in the stud pairs. This cracking initially was between the north and south exterior loading jacks. When the mid-span deflection was about 310 mm, at a sustained load of 106 kN, longitudinal cracks developed from the north exterior loading jack to the north reaction. At this time, a transverse crack also formed about 310 mm from the north end of the truss. It extended vertically downward on the slab edge to the upper corner of the end of the flute. As shown in Figure 9.6, this caused a change in slope of the slab surface at this location.

Three other observations, indicative of distress in the concrete occurred at or shortly after the maximum load was reached. This distress is considered to be the mode of failure. Figure 9.7 shows the concrete separating from the deck, one panel point from the north end. A diagonal crack that formed on the edge of the cover slab is shown, as well. A total of 14 cracks were visible on the edges of the concrete cover slab. Only two of these were on the south half of the truss, and these were within 1500 mm of mid-span. Figure 9.8 shows a bulge in the side of the flute towards mid-span of the truss, near the second panel point from the north end, and also lifting of the deck from the top chord at the next flute. These bulges occurred on 11 of the 14 flutes on the north half of the truss but none on the south half of the truss.

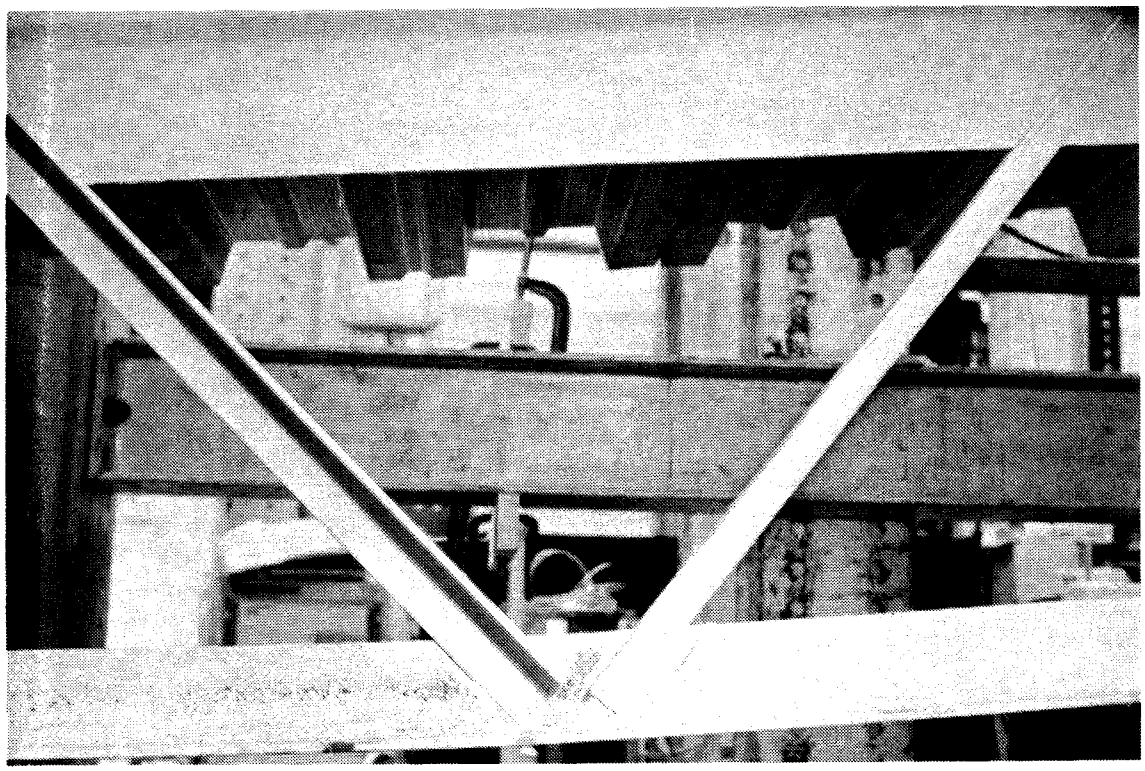

Fig. 9.4 Lower panel point, web 11 and 12, at completion of test

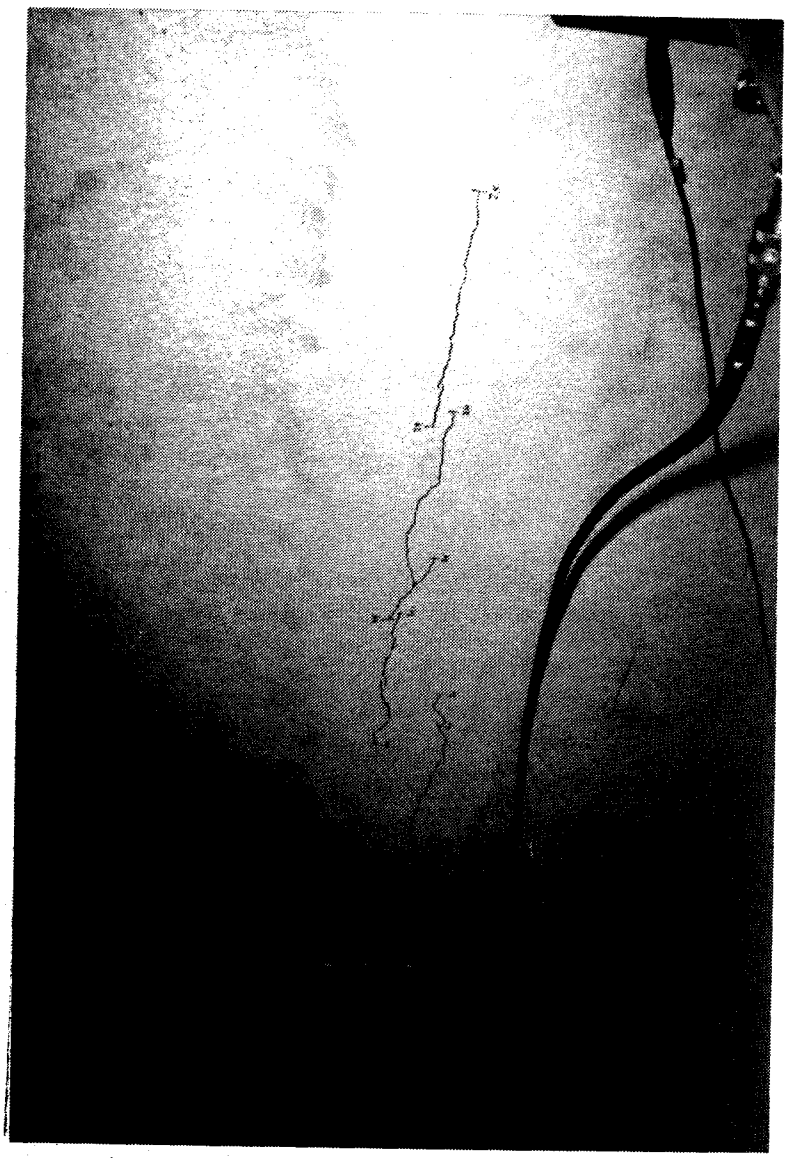

Fig. 9.5 Longitudinal cracks in slab at a mid-span deflection of 235 mm

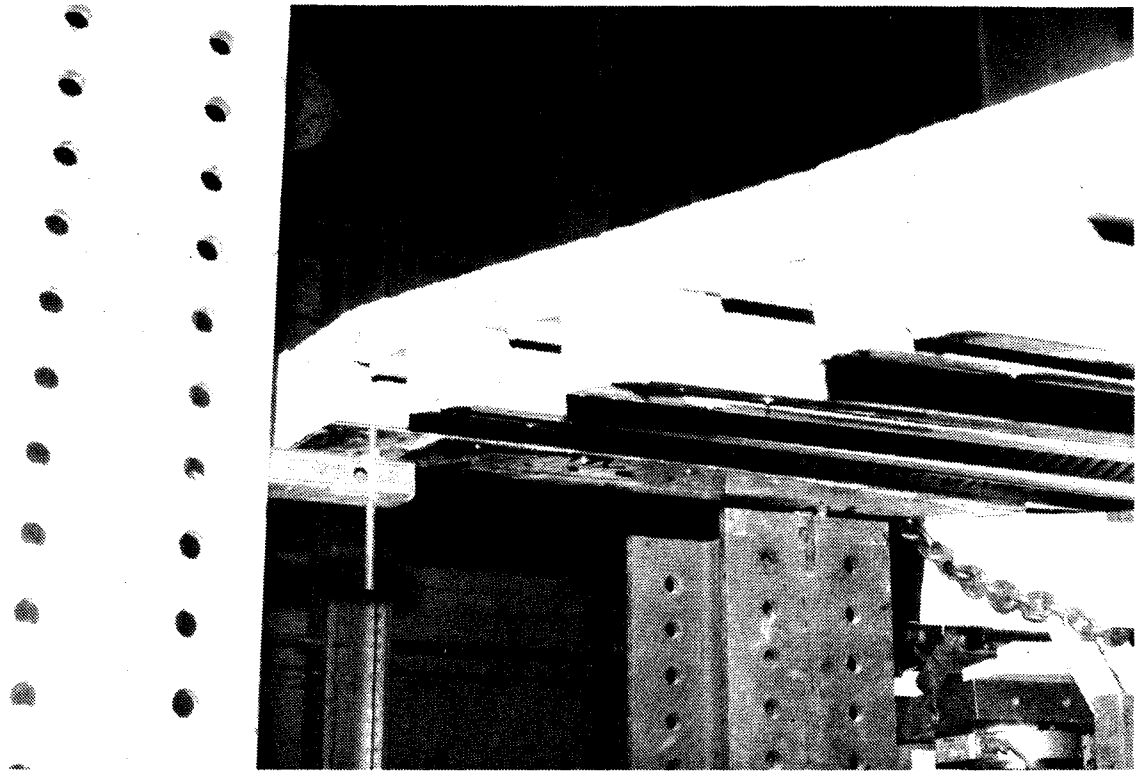

Fig. 9.6 Change in slope of slab at north end due to transverse crack

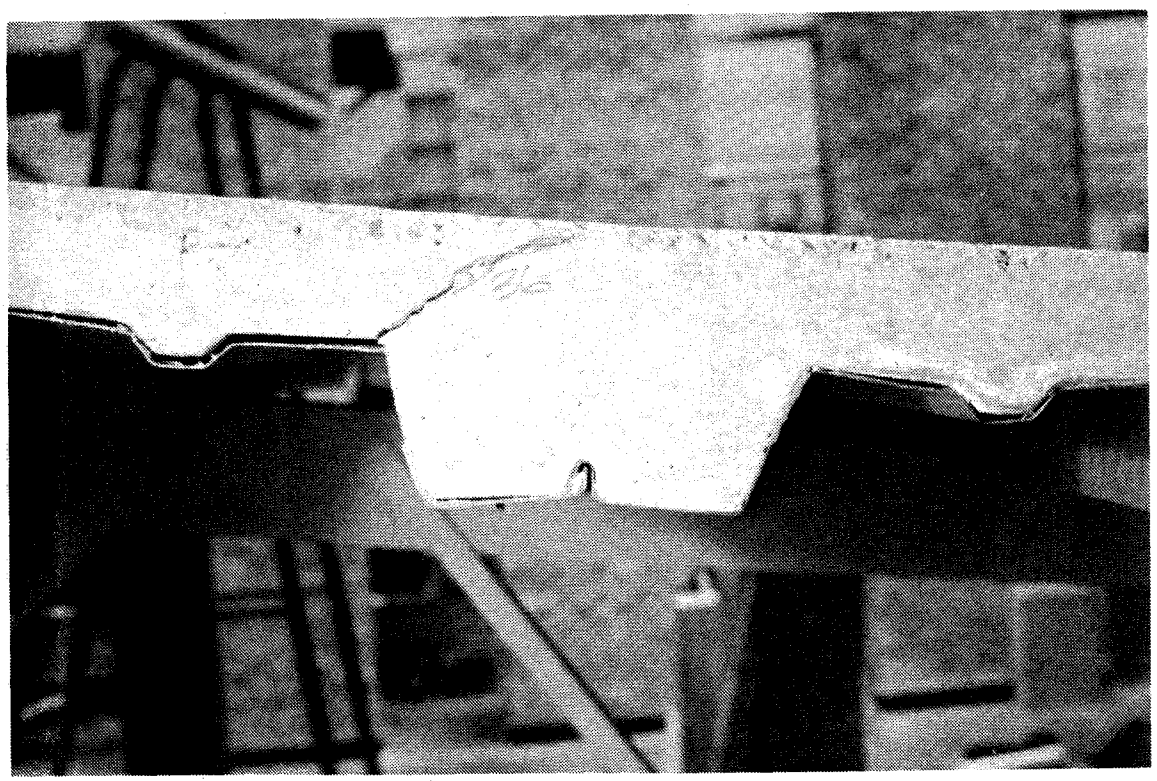

Fig. 9.7 Separation of concrete from steel deck

Fig. 9.8 Bulge in side of flute

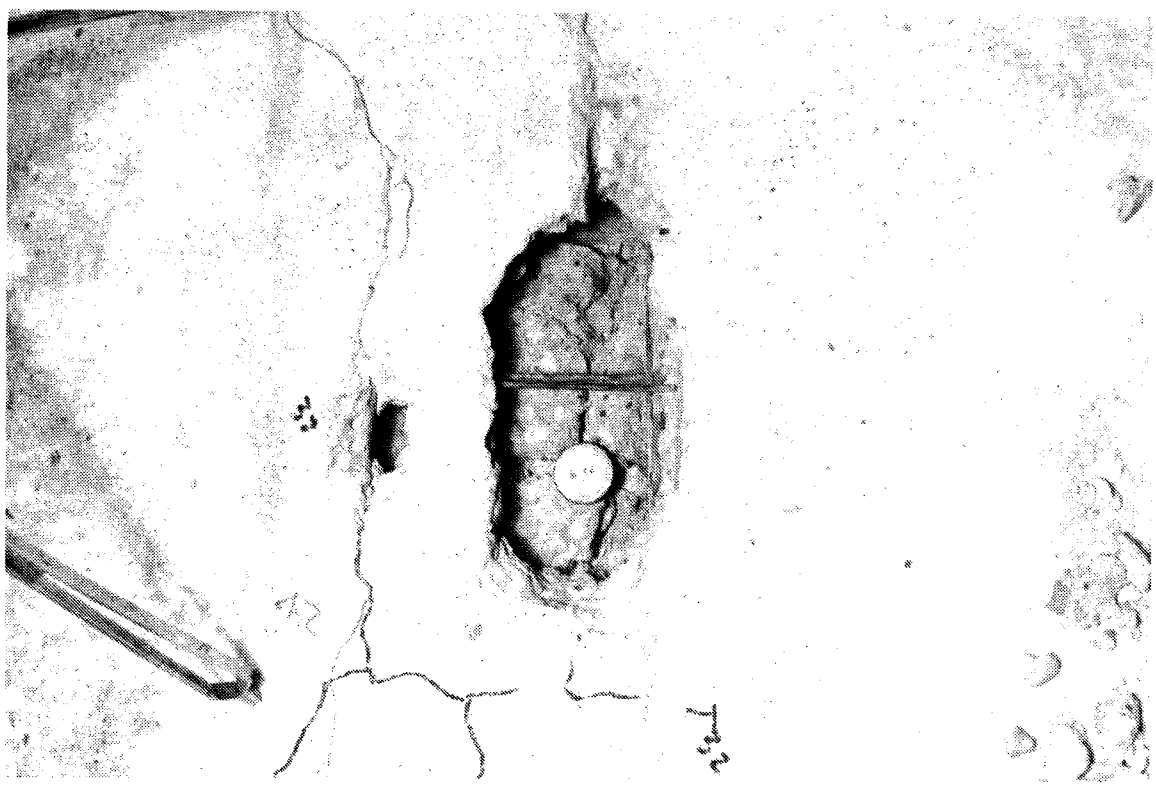

Fig. 9.9 Cavity at top of studs

Following the test, a small chipping hammer was used to remove concrete over the top of some studs at the north end. When chipping reached the level of the top of the studs, a cavity was encountered. In the cavity shown in Figure 9.9, one's fingers could be passed in the cavity from the large hole, in the middle, to the small hole, on the left. The cavity appeared to be the top of a pull-out cone failure of the concrete. On removal of the remainder of the concrete around the studs, as shown in Figure 9.10, it was evident that the studs had not failed, but that there was relative movement of the deck and concrete towards the end of the truss. This relative movement is estimated from the figure to be 20 mm to 25 mm. The deck wrinkled on the mid-span side of the studs. This behaviour is consistent with the bulges in the flutes, as discussed previously.

Failure is, therefore, attributed to the development of pull-out cones, over the top of the studs at the north end. This failure was accelerated by the transverse crack near the north end, as discussed previously. It is postulated that the transverse crack formed due to a moment induced in the cover slab at the end of the first (wide) flute counteracting, in part, the couple formed by the non-collinear compressive force in the cover slab and the shear in the first pair of studs.

Figure 9.11 shows the curvature of the top and bottom steel chords after failure occurred and the loads were removed. The top chord is seen to have significant curvature, and the bottom chord is seen to consist of a series of straight lines between panel points, at which concentrated curvatures occur. Also visible in the figure, are the web members, some of which have been buckled (including web member 7, which was repaired during the test). All of the web members that buckled, were buckled during failure of the truss, when the truss moved suddenly south. At this time, the knife edge at the south end jumped out of the reaction assembly, and the truss dropped approximately 200 mm onto support pedestals placed under the steel truss to provide support in case of sudden failure, thus loading the central web members in compression. These members were not designed to carry large compressive forces, and hence, buckled. The buckling of the web members was a result of the truss failure, not a cause of it.

The deflection of the truss at the north and south quarter points is plotted in Figure 9.12. The points indicated by solid and open circles represent the loads where the truss stabilized at the end of a set of readings (as in Figure 9.1 for the mid-span deflection). For the most part, the two load-deflections curves are identical. At the beginning of the second day of testing, a slight difference in the deflections was noticed. A much larger difference occurred after web member 7 had been buckled inadvertently. Smooth curves have been drawn through the lower data points, as was done in Figure 9.1. The load deflection curve, in all respects, is similar to that of Figure 9.1, but, obviously, displays a smaller deflection.

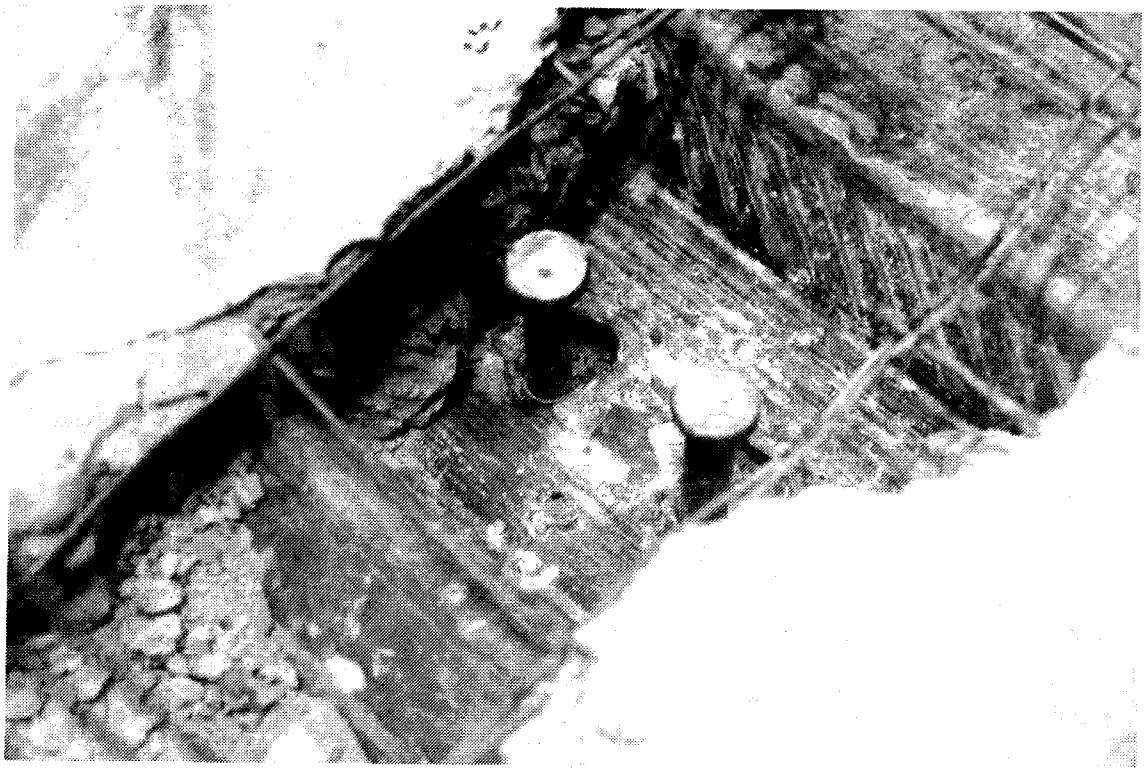

Fig. 9.10 Studs at end of test with concrete removed

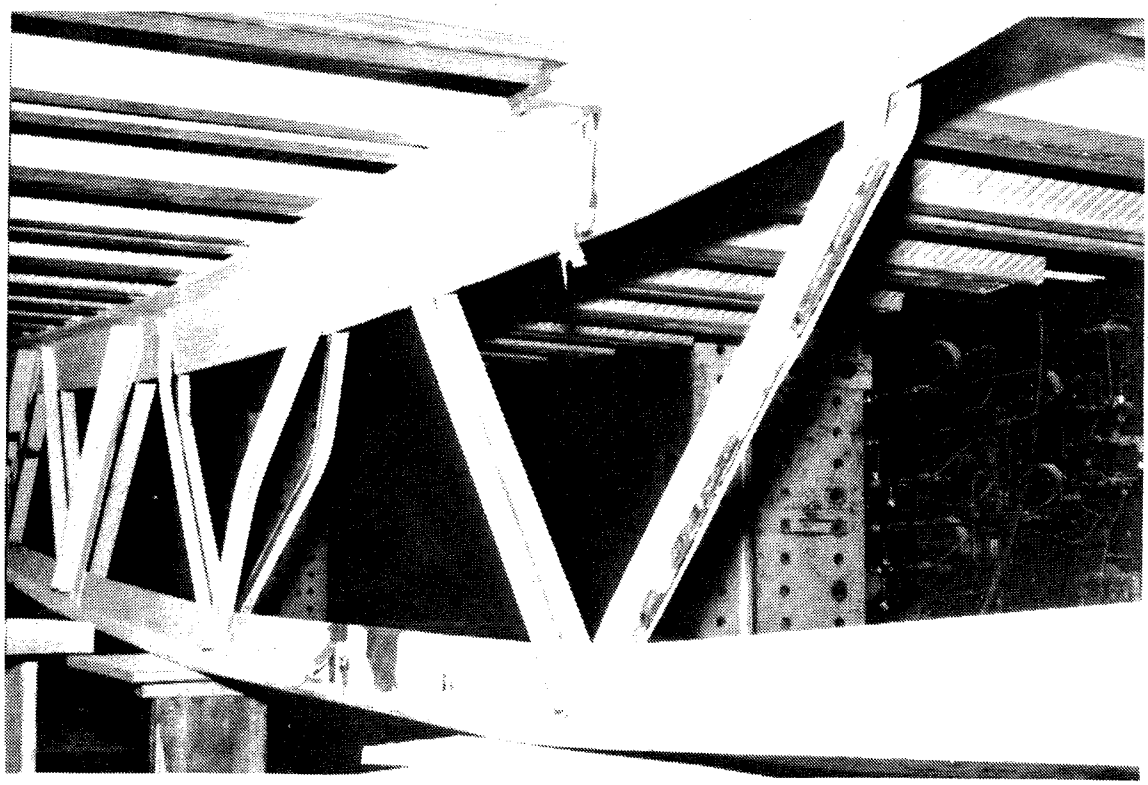

Fig. 9.11 Bottom chord after truss failure (no load)

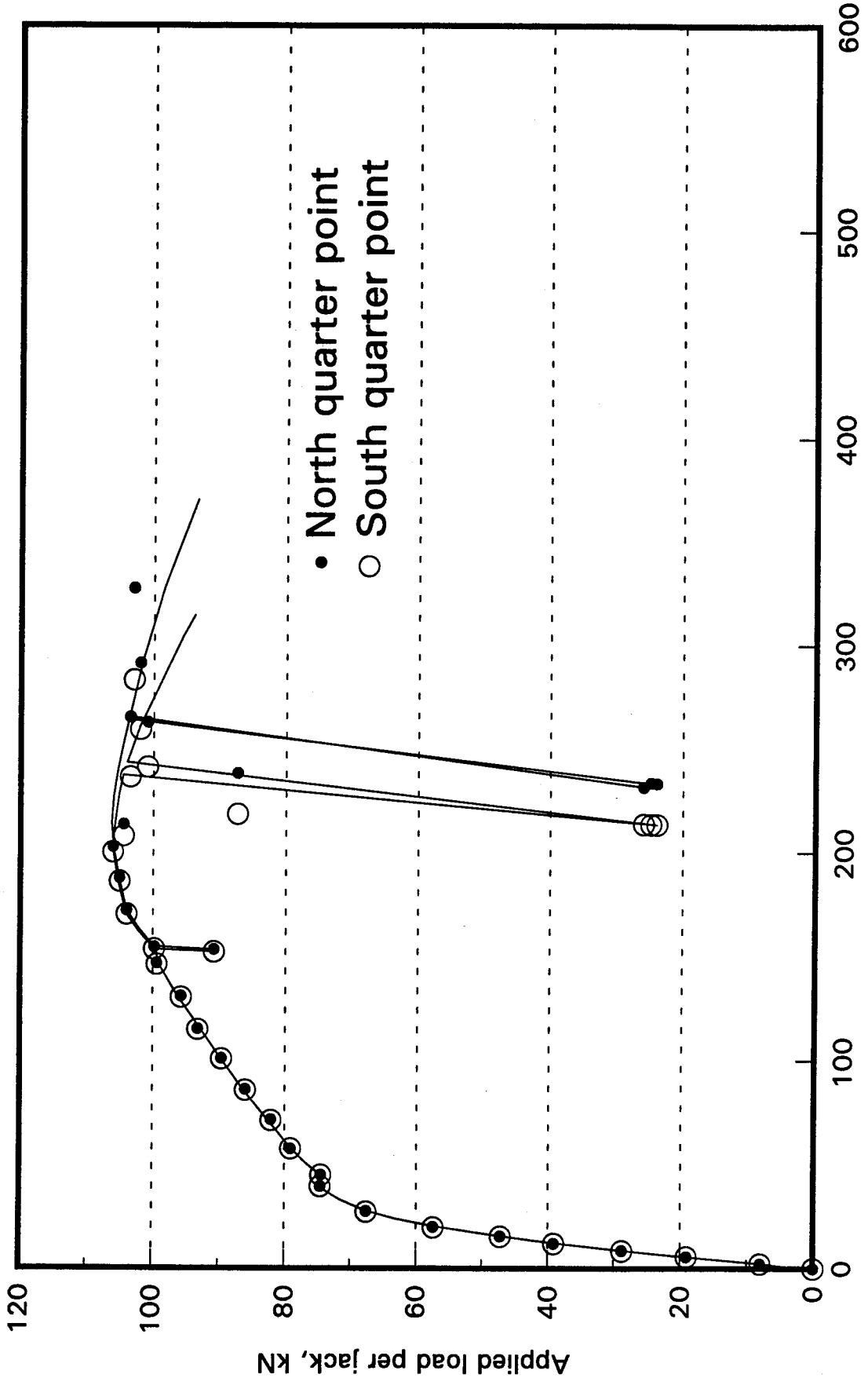

Fig. 9.12 Load-deflection response at quarter points

9.2 Bottom chord strains

In Figure 9.13 are shown the strains of the bottom chord, considered to represent the zero strain rate load, plotted against the jack load. Data related to unloading are not shown. The strains plotted are those calculated at the centroid of the bottom chord, from a linear regression analysis of the strain gauge data at each load step. The two changes in length measured by the LVDTs were converted to strains by dividing the changes in length by the gauge length. The strains plotted are the average of the two LVDT strain readings. A significant difference exists between the strain gauge strains and the LVDT strains, for example, the maximum strains differ by a factor of about 1.25.

The bottom chord first behaves in a linear manner, with respect to the applied load per jack. Above a load of about 70 kN per jack, the mean strains increase substantially, finally reaching strains in excess of 30 000 με. At a load of about 75 kN per jack, there is a marked increase in the bottom chord strains, as determined from the LVDTs, which is attributed to yielding of the bottom chord. The curves of Figure 9.13 (and indeed Figure 9.16 for the top chord and Figure 9.18 for the concrete strains that follow) reflect this overall behaviour. Rapid straining occurs following yielding of the bottom chord and the load decreases from its maximum value when the shear connectors at the north end failed.

Figure 9.14 shows the variation of strains, as determined from five strain gauges, through the depth of the bottom chord for the first five load steps for which the truss appeared to behave in a linearly elastic manner. The strains at 23 mm and 93 mm above the bottom surface have been interchanged because of an apparent misconnection. The linearly regressed lines shown for the five loads indicate that the chord is subjected to both axial load and moment. The scale has been enlarged greatly, for clarity.

In Figure 9.15, the strain distribution through the depth of the bottom chord is plotted for eight load steps, with the lowest load being that for which the behaviour was essentially linearly elastic. The strains appear to vary linearly through the depth, and in fact, a linear regression analysis at the maximum load plotted of 105 kN per jack, results in a coefficient of determination of 0.99. As noted in Section 9.1, however, the bottom chord straightened out after yielding at the panel points under the action of the tensile force. This paradox is discussed in Section 10.3, subsequently.

9.3 Top chord strains

Figure 9.16 shows the regressed tensile strain at the level of the centroid of the top chord, in the region of constant moment, as determined by a linear regression analysis of the four strain gauge readings, plotted against the applied jack load. (Note that the strain scale for this figure is 20 times that for Figure 9.13.) The strains plotted are only for the lower data points obtained when the load had essentially stabilized. As for the bottom chord strains

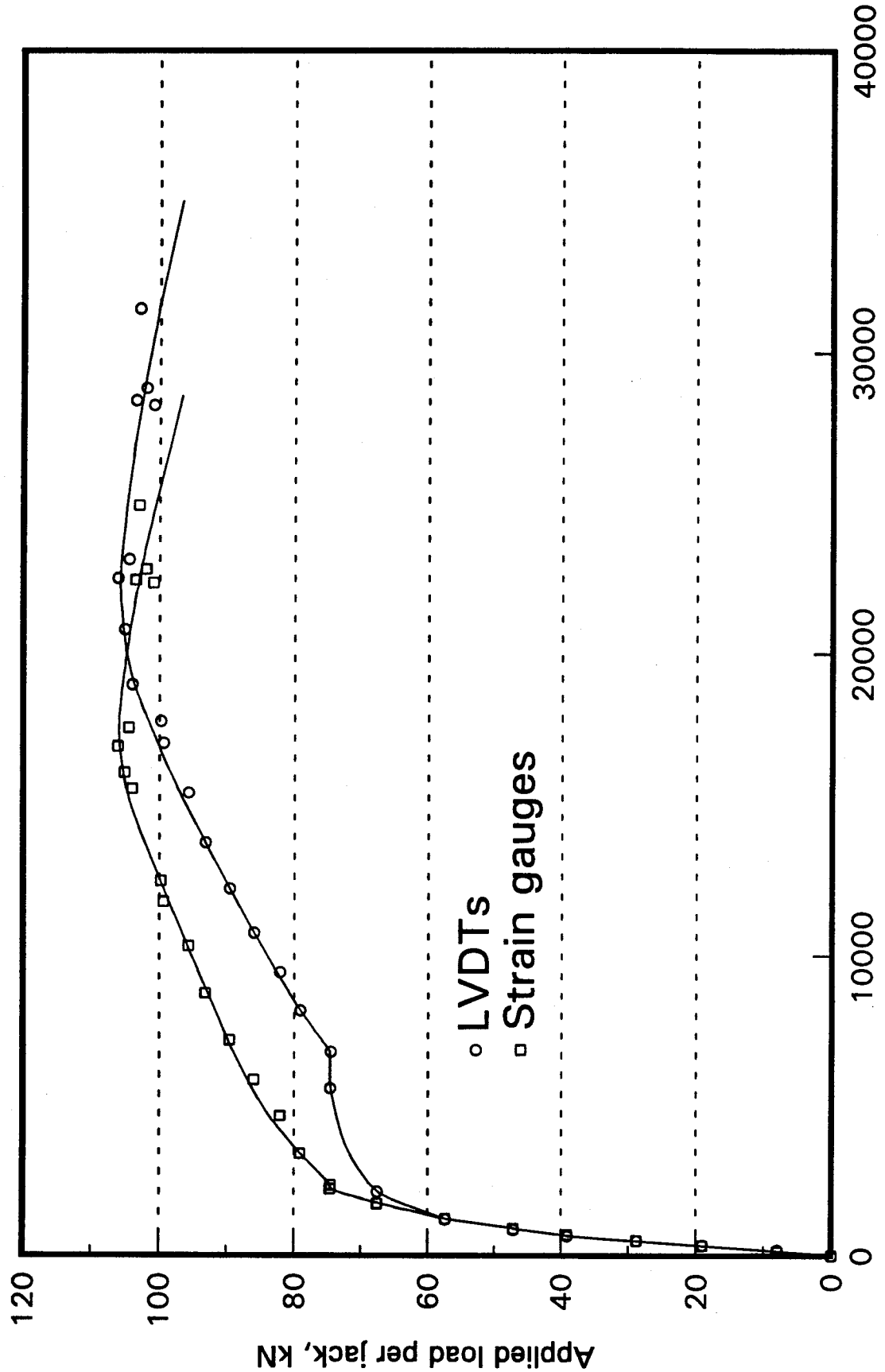

Fig. 9.13 Bottom chord strains

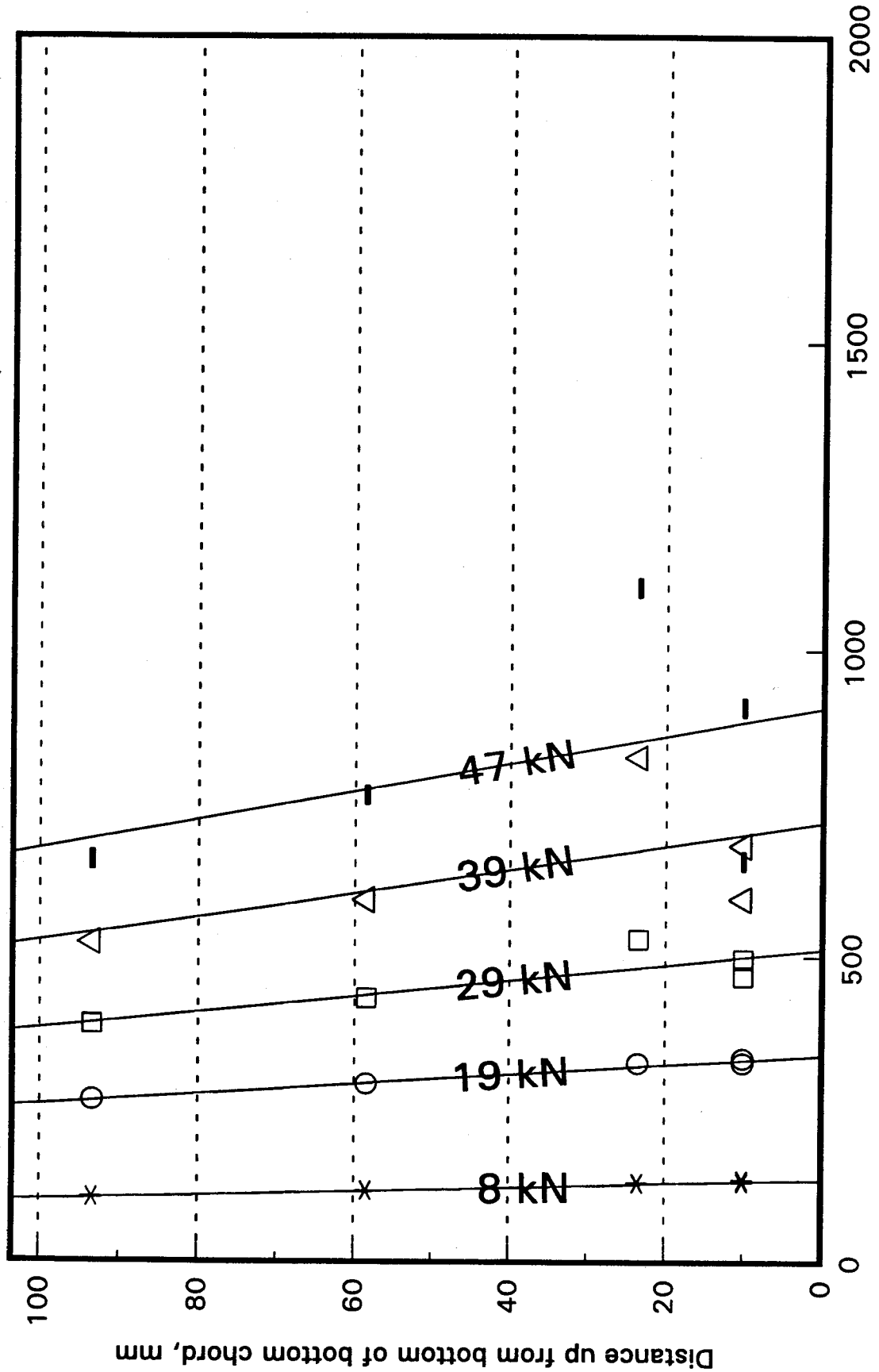

Fig. 9.14 Bottom chord strain variation through the depth

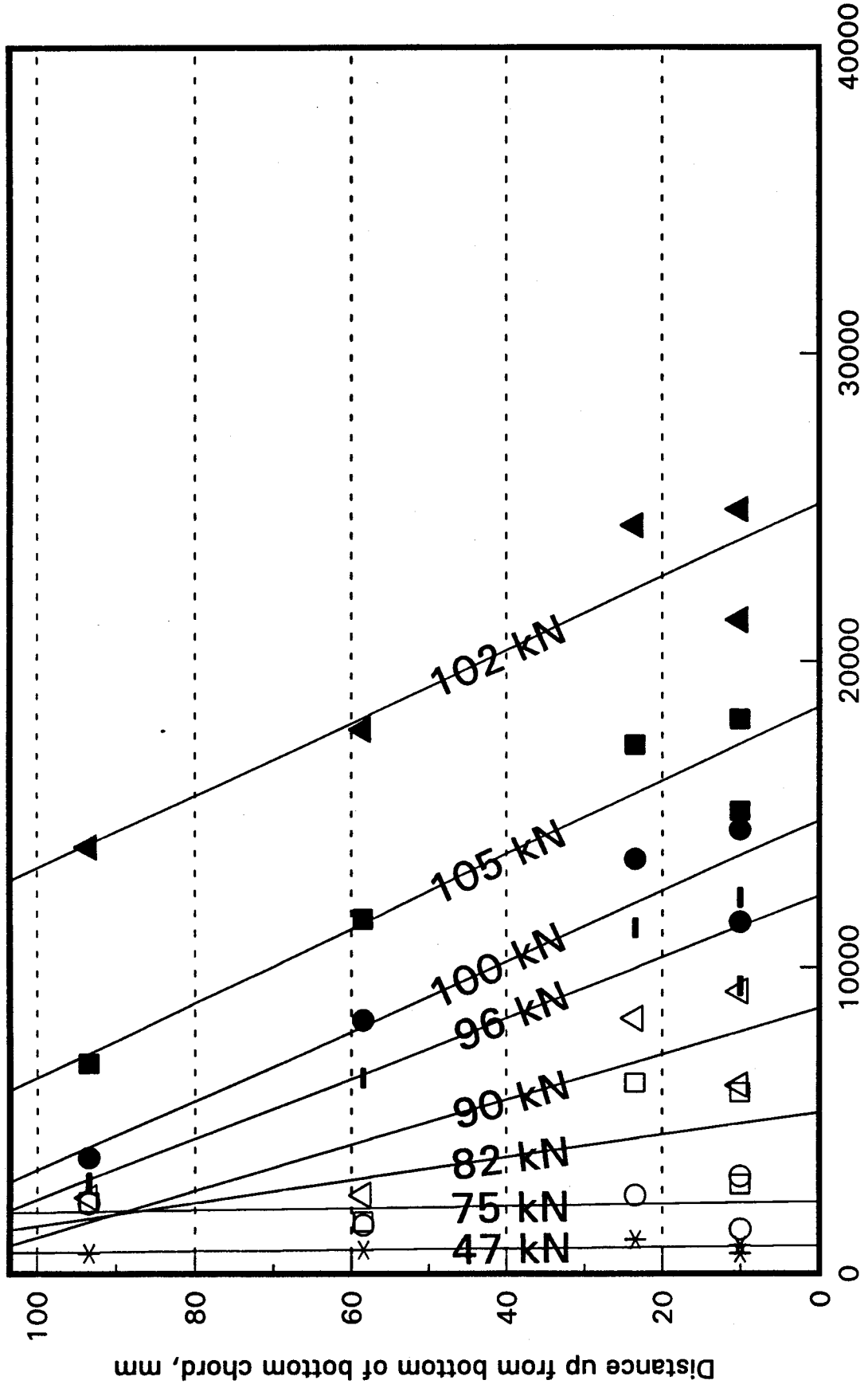

Fig. 9.15 Bottom chord strain variation through the depth

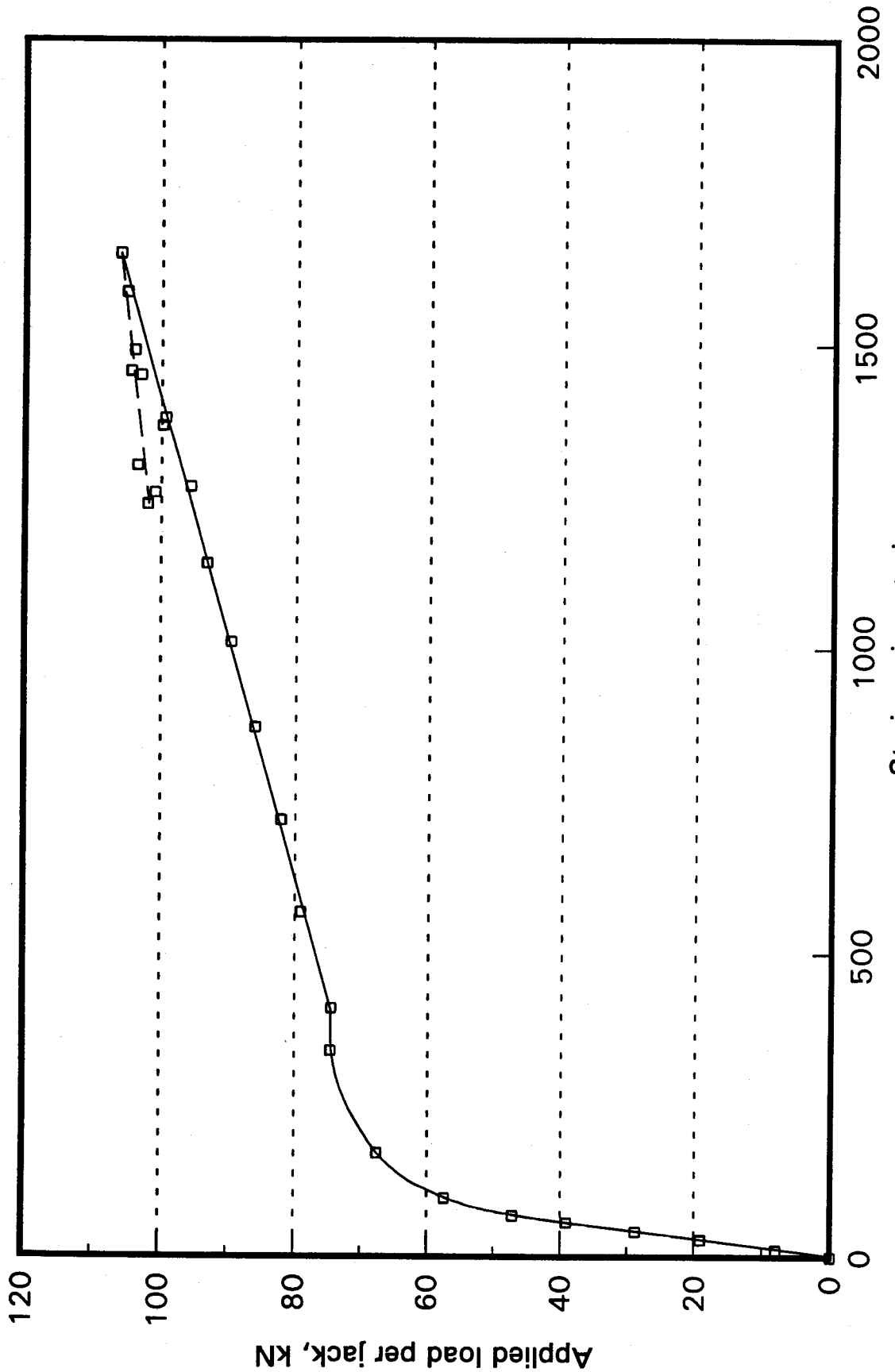

Fig. 9.16 Top chord strains

given in Figure 9.13, data related to unloading are not shown. A smooth curve has been drawn through the data. The solid line represents the loading portion of the curve up to a maximum recorded load of 106 kN, while the dashed curve corresponds to the post peak load, during which the regressed strain in the top chord actually reduced.

The behaviour of the top chord, as depicted by the regressed strain is dominated by the overall behaviour of the truss. Initially the top chord behaves in a linear manner with respect to the applied load per jack, but this soon gives way to rapidly increasing strains because of yielding in the bottom chord. All coefficients of determination for the regression analyses performed to obtain Figure 9.16 exceeded 0.94.

Figure 9.17 gives the strain distribution through the depth of the top chord for eight different loads. The strains plotted are those due to the applied loads only and do not include the compressive strains that were induced when the steel truss carried its self weight and that of the concrete slab. The straight lines, determined by regression analysis, show that the top chord is severely bent in addition to carrying significant axial tension.

9.4 Concrete strains

9.4.1 Mid-span strains

Plotted in Figure 9.18 is the average of the five strains, measured on the surface of the slab using the Pfender gauge, at the mid-span of the truss versus the applied load. (Note that the strain scale for this figure is 20 times that for Figure 9.13.) In general, the strains vary in a manner similar to the deflection of the truss, which is essentially dependent upon the straining of the bottom chord. In other words, the strains in the concrete are directly related to the strains in the bottom chord.

Also plotted in Figure 9.18 is the average concrete strain obtained from two Pfender gauge points mounted on either side of the truss at mid-depth of the cover slab. The strain at mid-depth, naturally only a portion of that at the surface of the slab, has the same general trend. The data obtained for the mid-depth strains for loads greater than 96 kN per jack appeared to be unreliable and have not been plotted.

9.4.2 Variation of strains across the slab width

In Figures 9.19a to 9.19e are plotted the strains across the width of the slab, as determined from Pfender gauge points mounted on the slab surface for eight different loads. The Pfender gauges were located at five sections along the length of the slab and at up to five locations at each section. The strains plotted for a load of 102 kN per jack were obtained on the decreasing part of the load-deflection response curve.

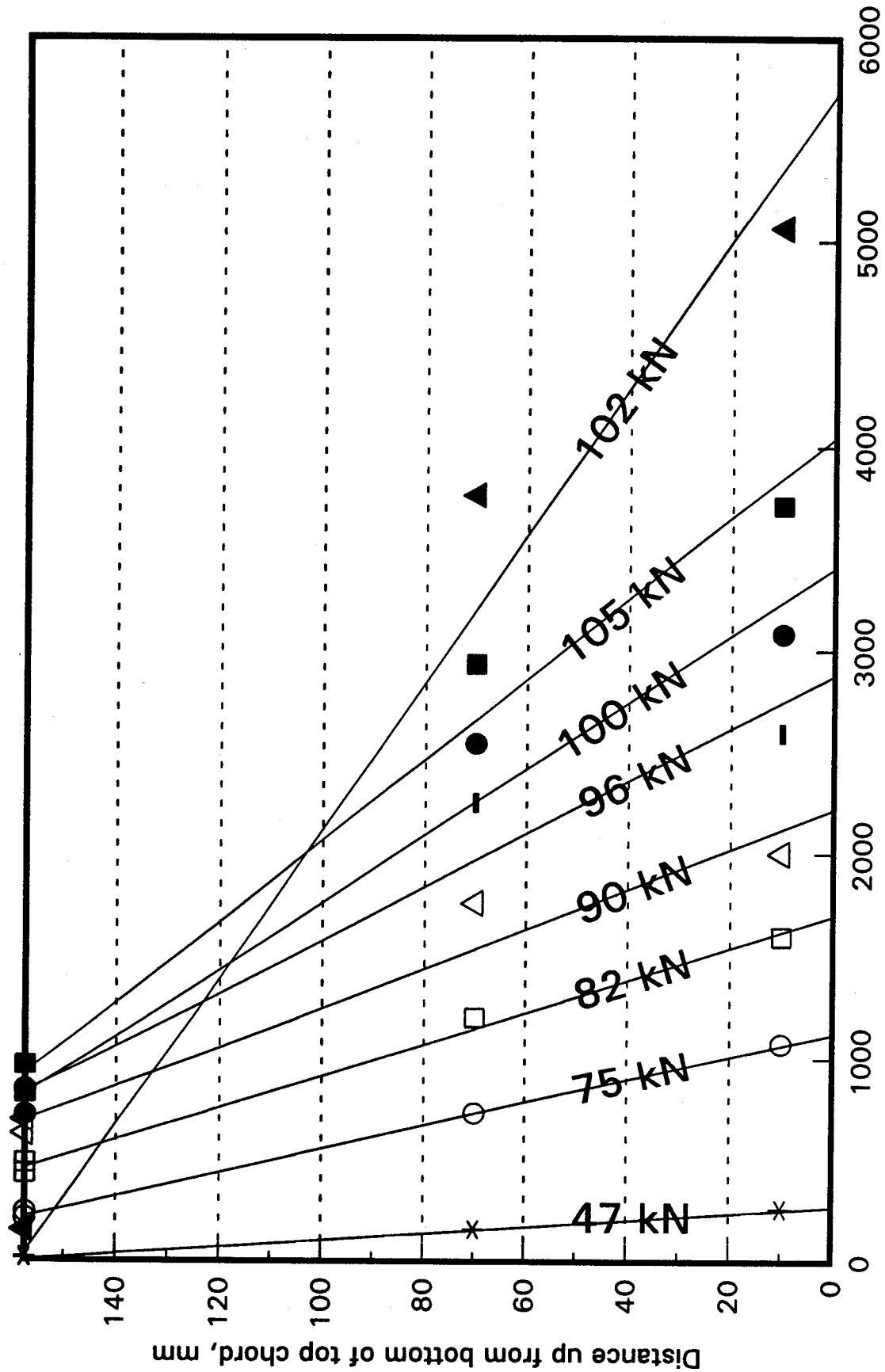

Fig. 9.17 Top chord strain variation through the depth

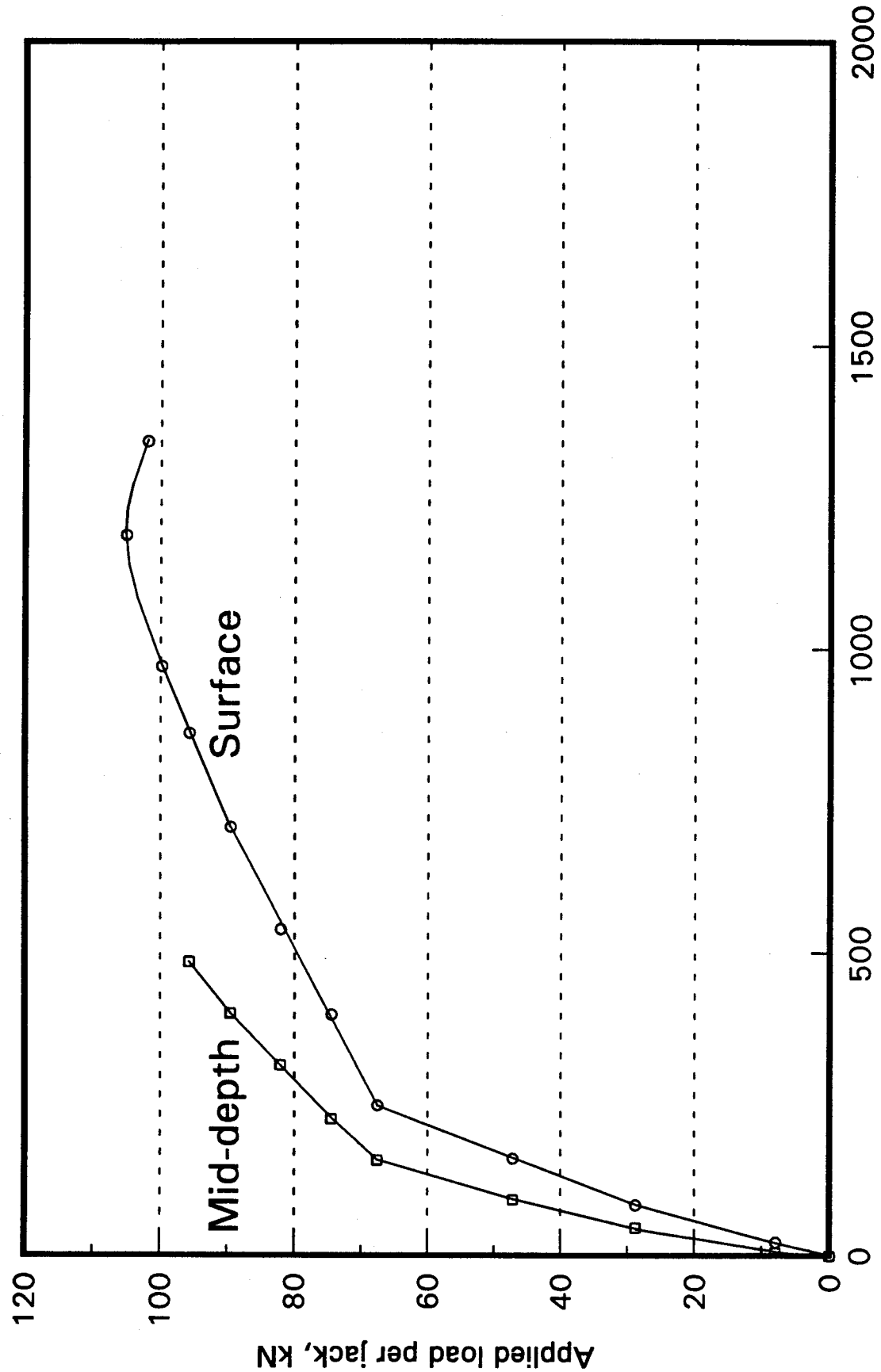

Fig. 9.18 Concrete strains at mid-span

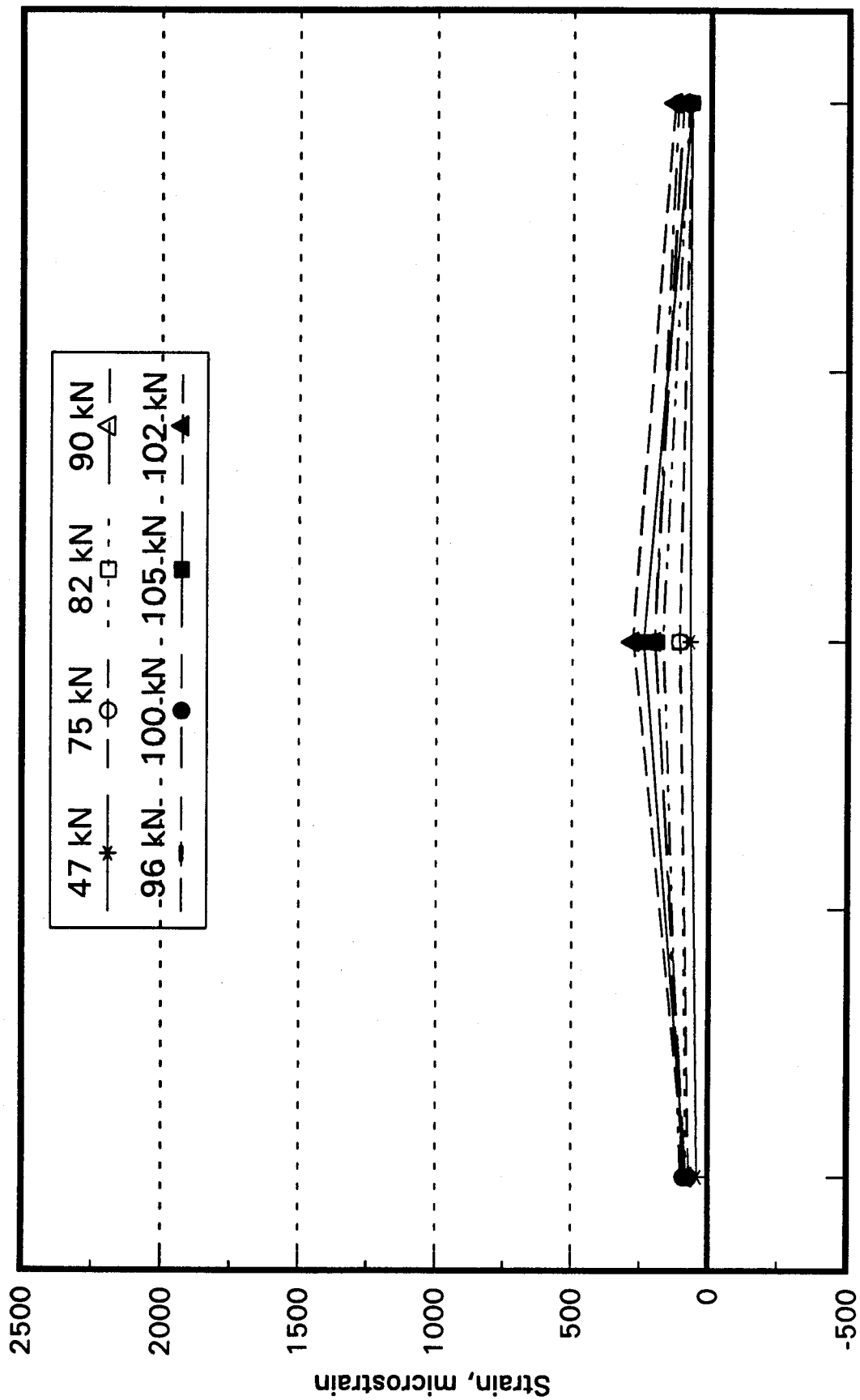

Fig. 9.19a Concrete strains at 0.926 L

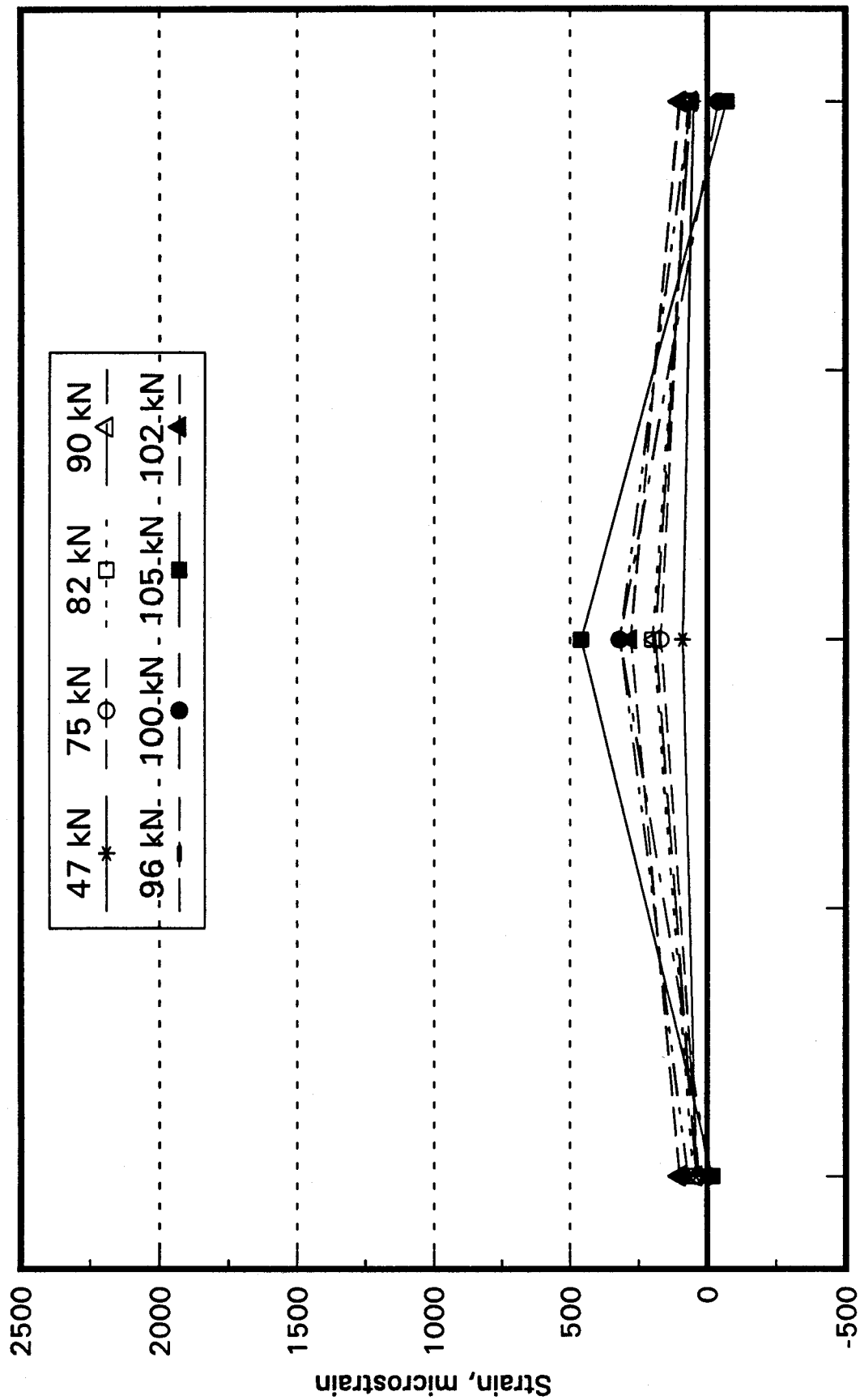

Fig. 9.19b Concrete strains at 0.074 L

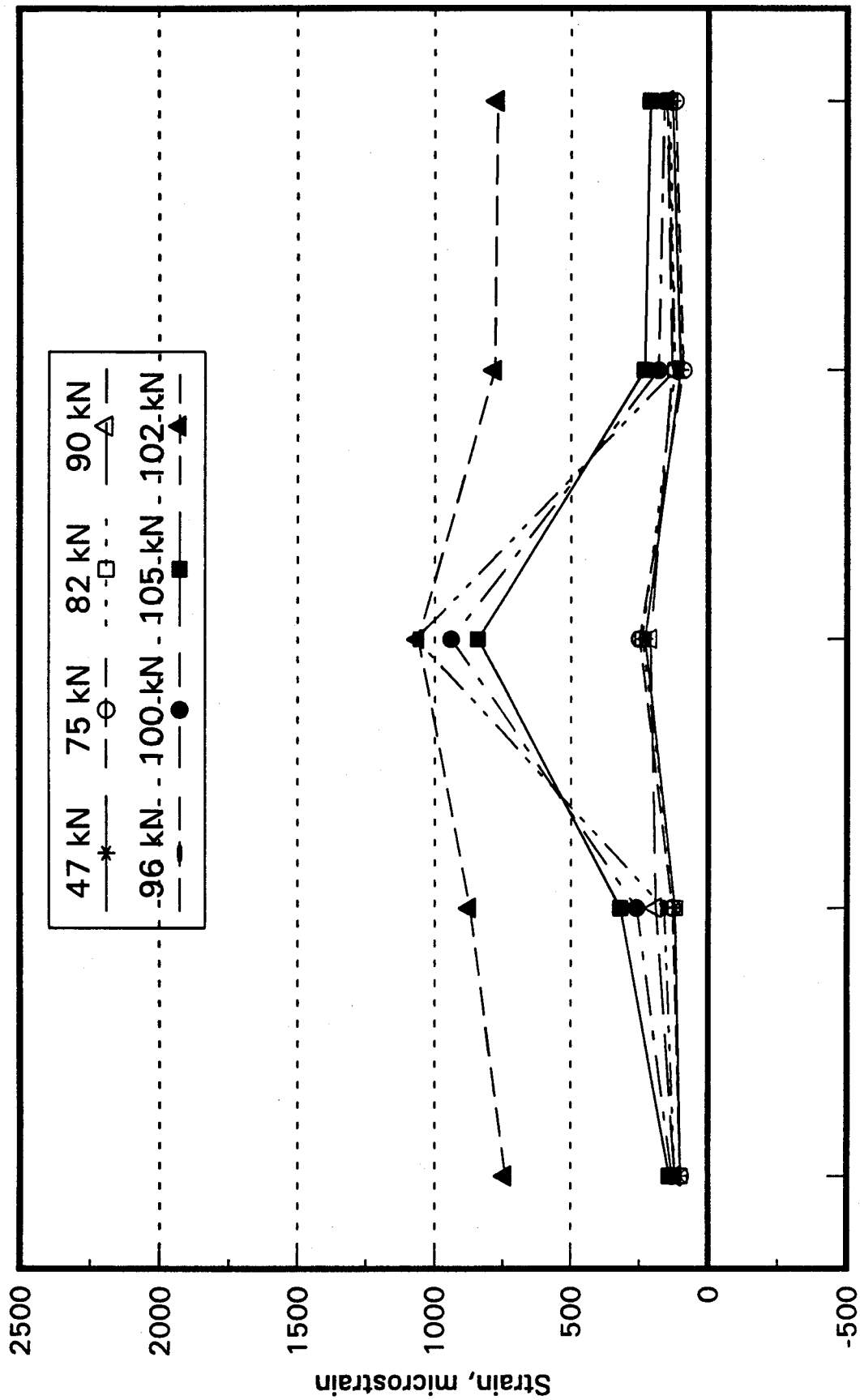

Fig. 9.19c Concrete strains at 0.195 L

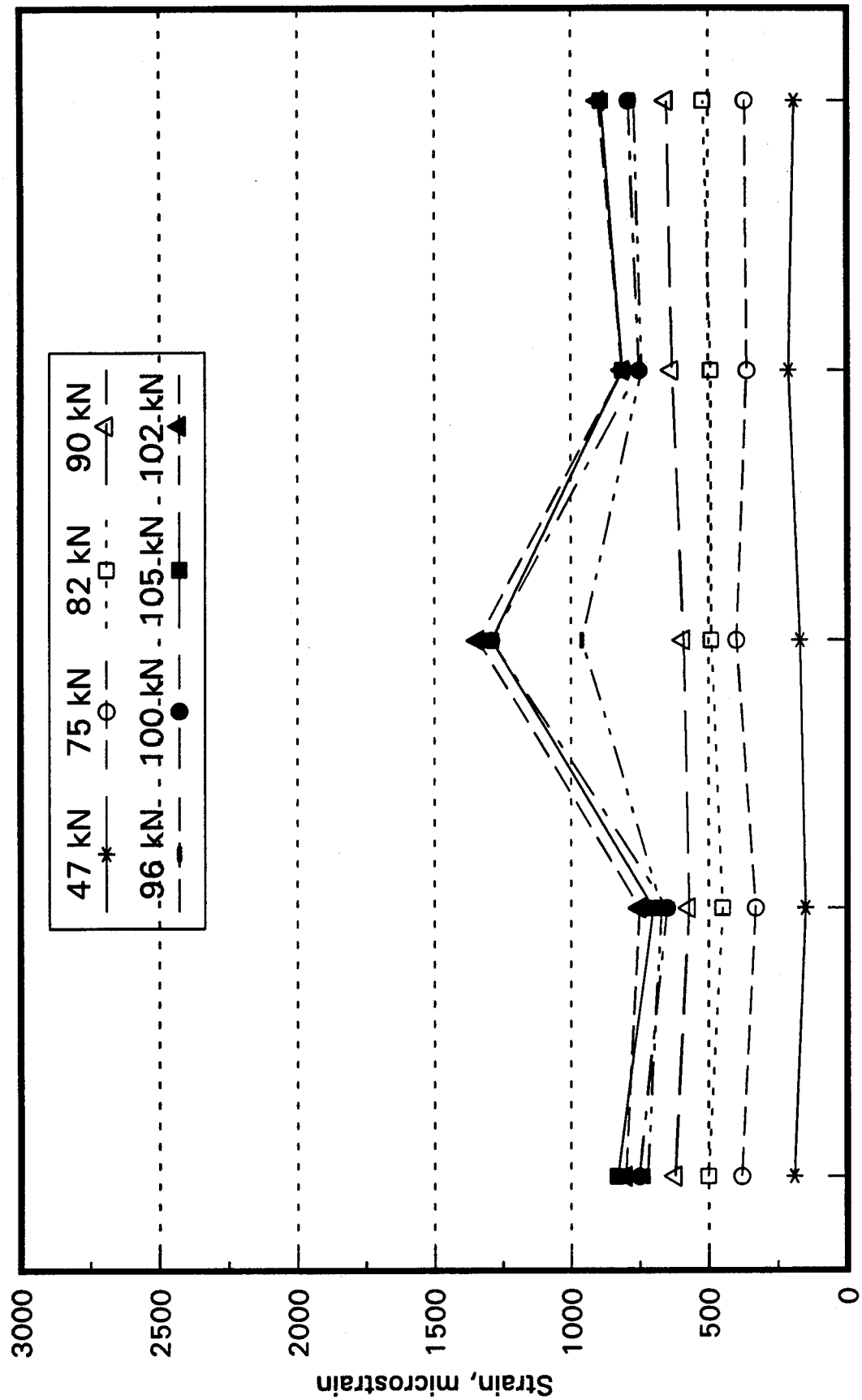

Fig. 9.19d Concrete strains at 0.317 L

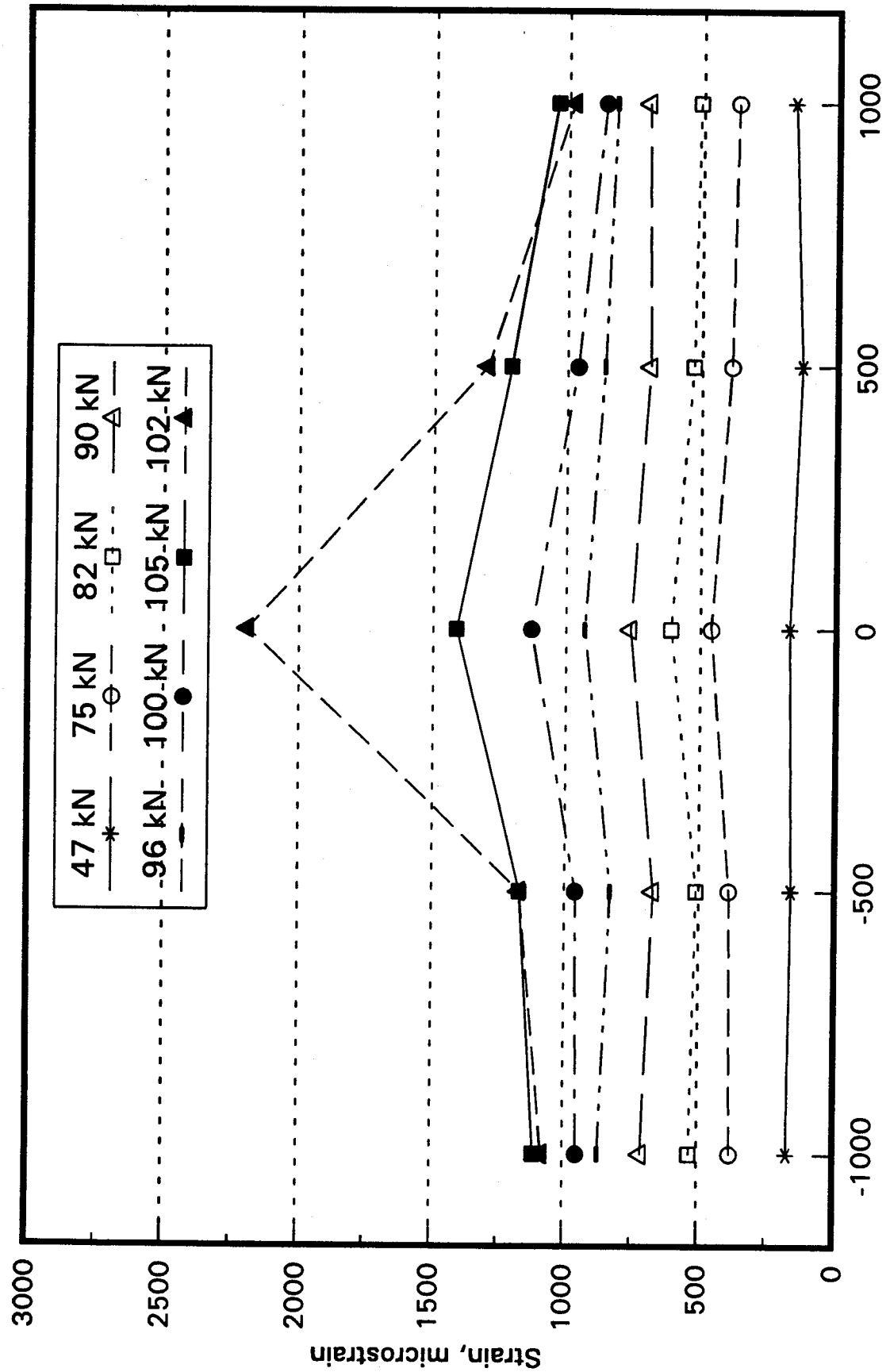

Fig. 9.19e Concrete strains at mid-span

The strains in Figure 9.19a at 0.926 L and in Figure 9.19b, equidistant from the mid-span at 0.074 L, are quite similar and exhibit significant shear lag that tends to increase with load. In Figure 9.19b, for strains near the north end of the truss, the shear lag is most pronounced at the maximum plotted load of 105 kN. It then reduces for the post-peak load of 102 kN. This reduction is attributed to the loss of shear transfer by the end shear connectors and is not exhibited at the south end (0.926 L) where shear connection failure did not occur.

In Figure 9.19c, for concrete strains at 0.195 L, the shear lag is relatively small at low loads. At a load of 96 kN, the shear lag appears to have increased in a pronounced manner. This could be due to more shear transfer by the shear connectors further from the north end because of reduction in shear transfer in the end connectors. Beyond the maximum load, a more uniform strain distribution, i.e., less shear lag, is apparently re-established. The reason for this is not apparent.

In Figure 9.19d, for strains at 0.317 L, shear lag is essentially non-existent for loads up to 90 kN. It would be expected that the shear lag would reduce from that exhibited near the ends toward the mid-span. At a load of 96 kN, higher strains are evident at the centerline than elsewhere, indicative of shear transfer from the connectors progressing towards mid-span as end connectors progressively fail. The shear lag increases even after the maximum load is reached.

At mid-span, as shown in Figure 9.19e, shear lag is essentially non-existent up to a load of 96 kN per jack. In fact, at this load, the ratio of the centerline strain to the average strain is 1.08. Beyond this load, the shear lag increases, following the same trend as was evident at the sections 0.195 L and 0.317 L, from the end. At the post-peak load of 102 kN, the shear lag is very pronounced and is somewhat unexpected.

9.5 Separation of compression angle web members

In Figure 9.20a is plotted the separation of the two pairs of L 3½ x 3½ x 3/8 constituting each of web members 2 and 15. For clarity, only the data obtained with increasing load are shown. Note that the scale is large. The separation of the two angles, with about one half attributable to each of the pair, reaches a maximum value of about 0.8 mm at a load of about 100 kN per jack and is essentially linear. The small separation indicates that bending of the angles out of the plane of the truss is relatively minor.

Figure 9.20b gives the same information for web members 4 and 13, each composed of a pair of L 2½ x 2½ x 5/16. Again, the behaviour is linear, with a maximum separation of about 0.8 mm at a load of about 100 kN per jack. The stress level in all four web members at a given load on the truss is approximately the same, because the angles were selected to carry their respective loads.

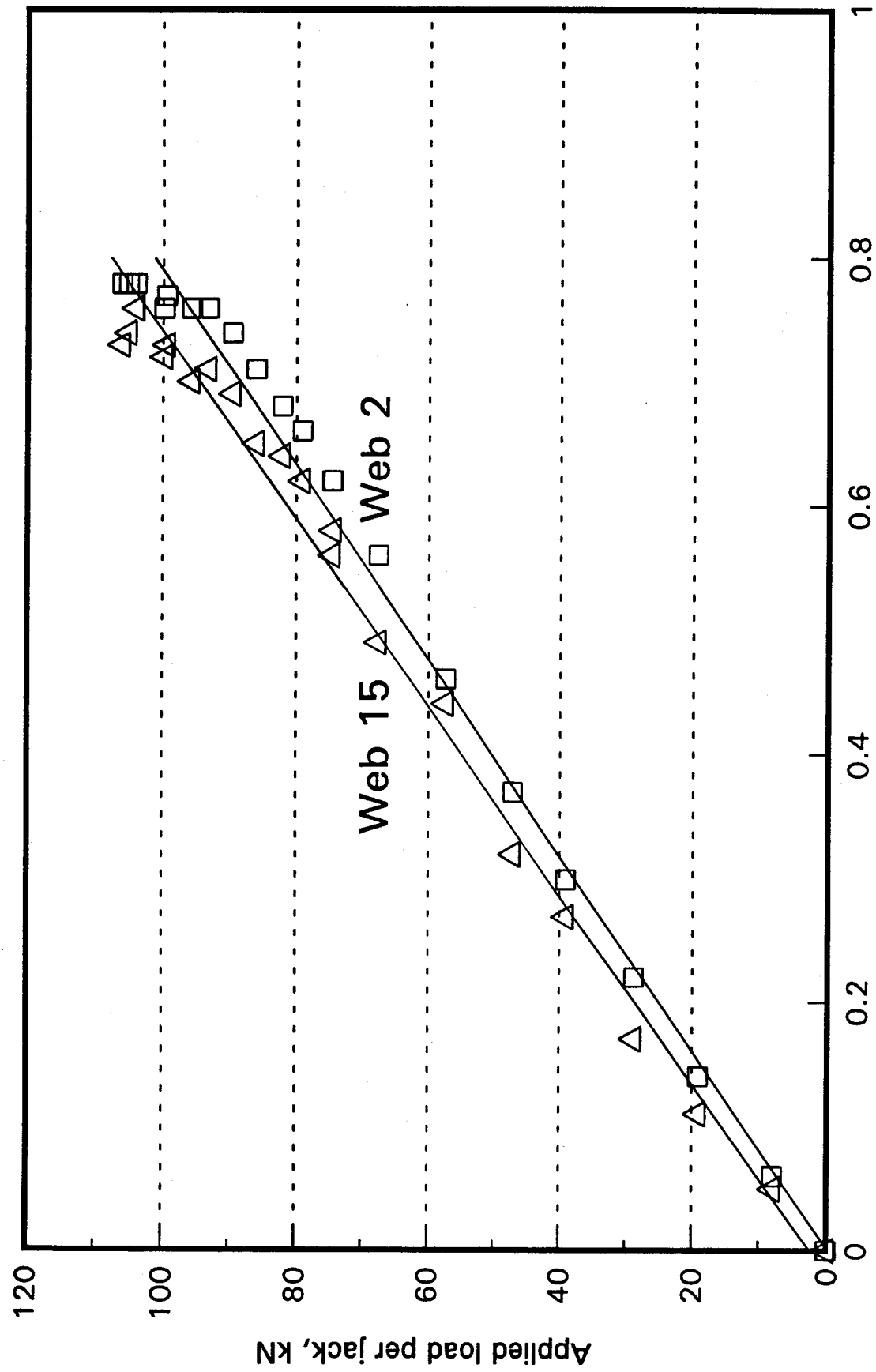

Fig. 9.20a Separation of web members 2 and 15

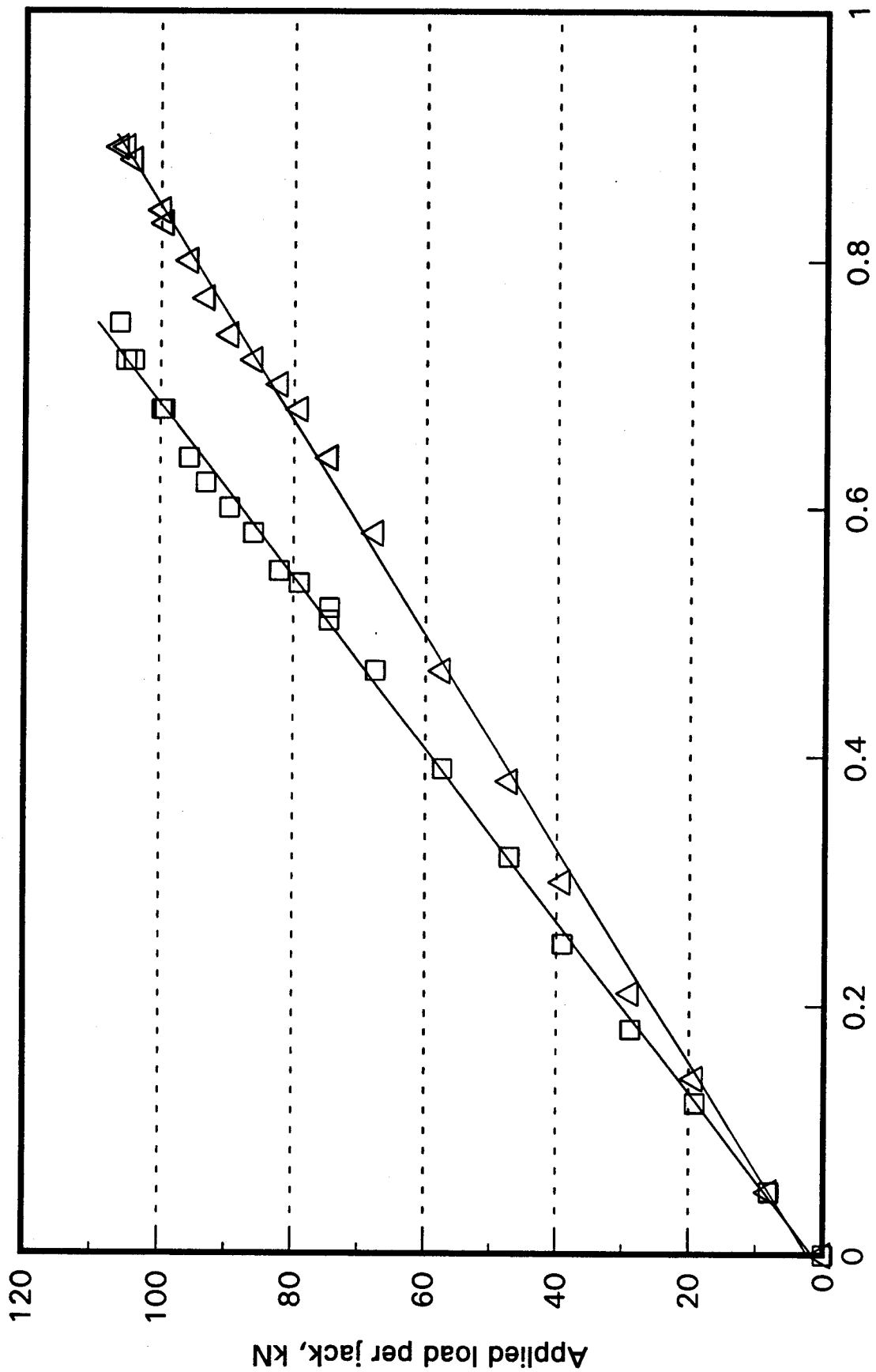

Fig. 9.20b Separation of web members 4 and 13

9.6 Interfacial slip between concrete and steel

Figures 9.21a and 9.21b show the interfacial slip at the north and south ends of the truss and at the north and south quarter points, respectively, plotted against the applied load per jack. Smooth curves have been drawn through the ascending load points. At a load of about 105 kN per jack, the interfacial slip at both the north end and north quarter point increased substantially. The interfacial slip is indicative of failure in the shear connection between the concrete slab and the steel top chord. In Section 9.1, the relative movement, at the studs near the north end, was estimated to be 20 mm to 25 mm.

The peculiar shape of the load-slip curve at the south quarter point for loads greater than 70 kN per jack can only be attributed to some local anomaly. Comparing the slip at the south quarter point to that at the south end, at a load of 100 kN, it is considered impossible that the apparent quarter point slip of 0.8 mm could exceed the south end slip of 0.4 mm.

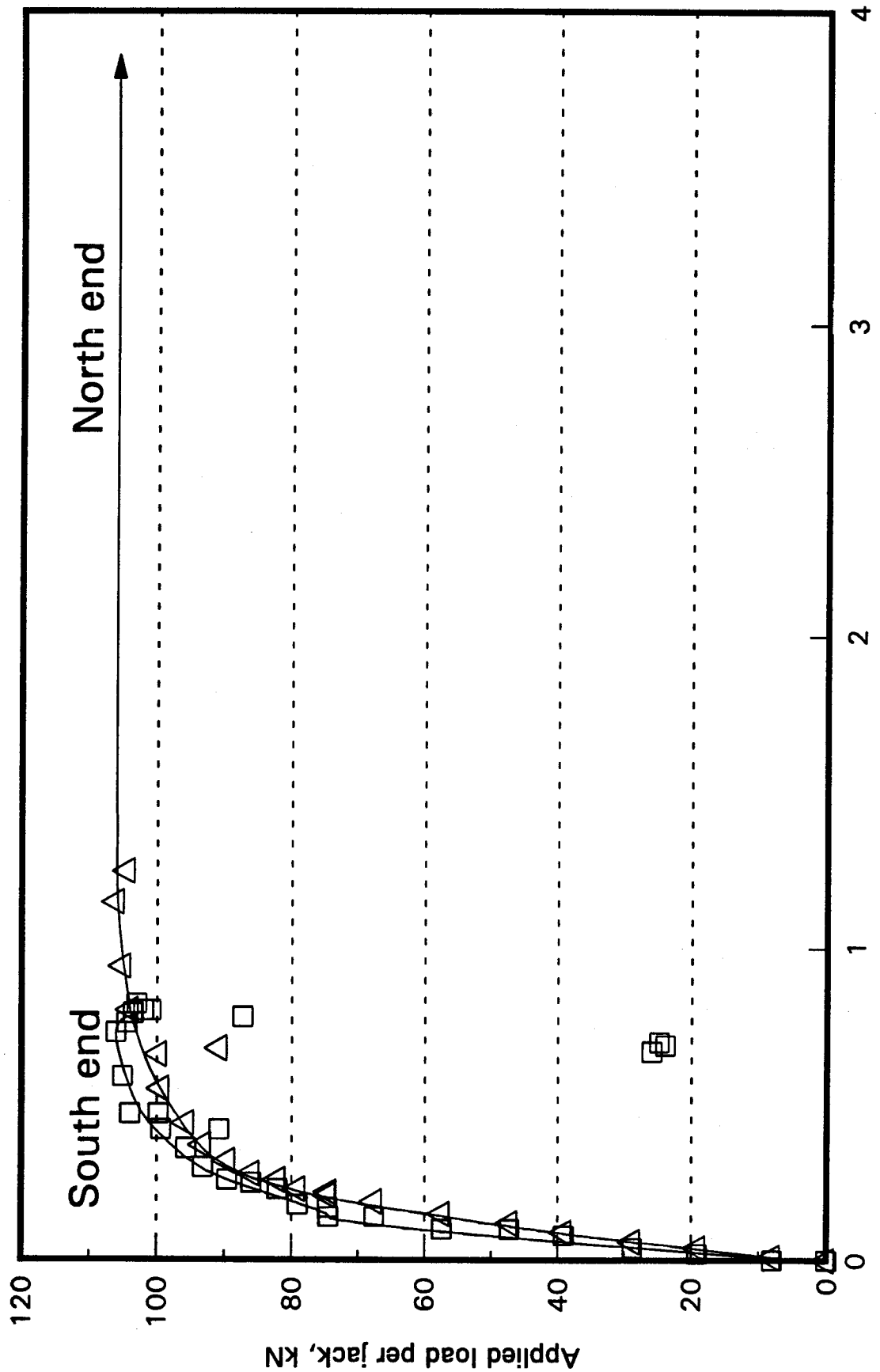

Fig. 9.21a Interfacial slip at ends of slab

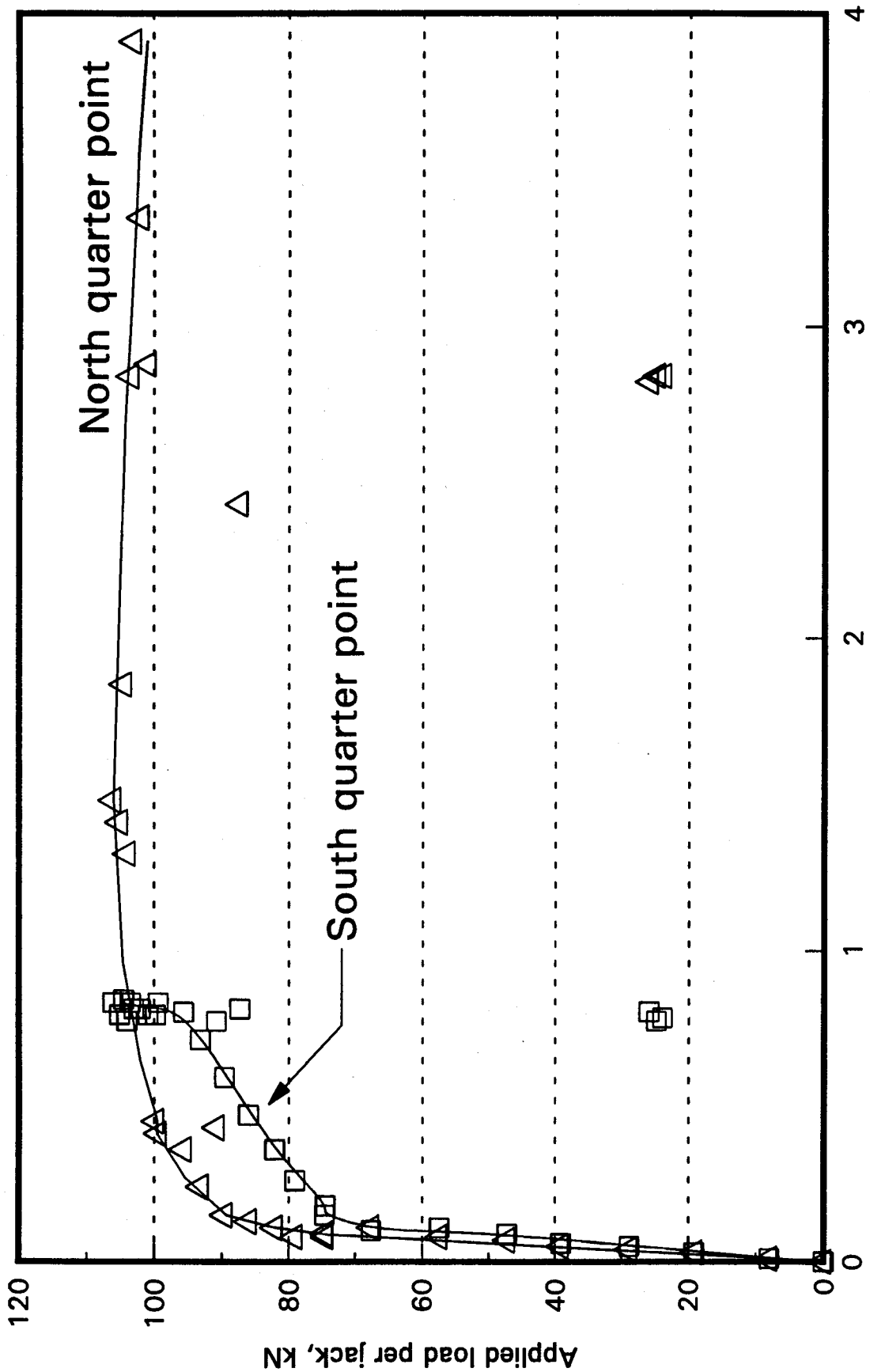

Fig. 9.21b Interfacial slip at quarter points

10 ANALYSIS OF FLEXURAL TEST RESULTS

10.1 Effective moments of inertia

10.1.1 Steel truss

It is common practice to calculate the effective moment of inertia of an open web steel joist or light steel truss simply as the moment of inertia of the chords divided by a factor to account for the shear deflection arising from the deformation of the web members. For this steel truss, the moment of inertia of the chords about their centroidal axis was 573.0×10^6 mm^4, and dividing by the commonly used factor of 1.10, gives an effective moment of inertia of 520.9×10^6 mm^4. Assuming that the dead load of the composite truss is uniformly distributed, the mid-span deflection due to the dead weight of 71.6 kN is calculated to be 13.4 mm, based on the effective moment of inertia. The truss had a measured deflection, due to the weight of 63.9 kN of the concrete alone, of 12.9 mm. Scaling this number for the extra weight of steel, gives a deflection, due to the total dead weight, gives a deflection of 14.4 mm, 8% greater than the calculated value.

10.1.2 Composite truss

To calculate the deflection of composite flexural members, the effects of creep and shrinkage of the concrete should be taken into account. Moreover, the increased flexibility due to partial shear connection and interfacial slip should also be considered. As well, of course, the increased deflection due to the vertical (transverse) shear, which causes deformation of the web members, must be considered for trusses and open-web steel joists.

Because the truss was tested quickly, and because the measured deflections were those subsequent to the determination of shrinkage effects, no allowance has been made for the effects of creep and shrinkage. Furthermore, the concrete stresses, even at maximum load, are relatively small. It is therefore reasonable to determine the transformed moment of inertia, I_t, based on a tangent modulus of elasticity of the concrete determined from a standard cylinder test at the time of testing of the composite truss.

In Table 6.6, the tangent modulus of elasticity at 120 days is given as 19 500 MPa, resulting in a transformed moment if inertia of 1182×10^6 mm^4, as given in Section 5.3.2. Using [2.4] which accounts for interfacial slip and incorporating a factor of 1.10 to account for the shear deformation of the web members and recognizing that full shear connection exists, the effective moment of inertia was calculated to be 991.9×10^6 mm^4, also given in Section 5.3.2.

The effective moment of inertia can also be determined from the slope of the linear elastic region of the load-deflection response curve given in Figure 9.1. For the loading

configuration used, as discussed in Section 10.2, with four equal concentrated loads, the mid-span moment is given closely by 5750P N·mm, where P is expressed in Newtons. Using the moment-area method, the corresponding mid-span deflection is $71.01\ M / I_e$. From Figure 9.1, by drawing a best fit line through the first five points on the curve and using the relationship between load, P, and moment, M, given previously, the mid-span deflection is computed to be 71.3×10^{-9} M mm, where M is expressed in N·mm. Equating the two expressions for mid-span deflection, gives an effective moment of inertia, I_e, of 996.5×10^6 mm^4. This is about 1.005 times the calculated value of 991.9×10^6 mm^4.

It is therefore concluded, on the basis of this single test, that [2.4] is valid for computing the effective moment of inertia of composite trusses, when the factor of 1.10 is used to account for the flexibility of the open web system. This is in contrast to the experimental work of Brattland and Kennedy (1992), who recommended that the coefficient of 0.85 of [2.4] be reduced to 0.77. Using this reduced factor, the moment of inertia is calculated to be 947.2×10^6 mm^4. The effective moment of inertia is 1.052 times this calculated moment of inertia.

10.2 Moment-deflection response

A non-dimensionalized moment-deflection curve is plotted in Figure 10.1, based on the smooth curve for the load-deflection response of Figure 9.1. The moments are non-dimensionalized by dividing by the yield moment of the truss, calculated from the measured cross-sectional and material properties of the steel bottom chord and concrete slab, assuming that the steel top chord does not contribute to the flexural strength. The yield moment, assuming the bottom chord is fully yielded, was calculated to be 524.5 kN·m. This yield moment corresponds to the unfactored moment resistance given in CSA Standard S16.1, but is based on the measured cross-sectional and material properties, as indicated in Figure 10.1. It therefore serves to determine test to predicted ratios. The moments plotted include the dead load moment of the truss (computed for a weight of the steel, concrete, deck and mesh of 71.6 kN) of 103 kN·m. As this moment was carried solely by the bare steel truss, the initial slope of the moment-deflection curve is not as steep. The initial portion of the applied moment curve, for which linear elastic behaviour was obtained, has been extrapolated backward to give the zero point for plotting deflections. Starting at this zero point, then, gives a response which considers all of the moment (that due to dead and applied loads) to be applied to the composite truss.

The deflections were normalized by dividing by the mid-span deflection, corresponding to the yield moment, calculated by assuming that the behaviour is linearly elastic up to this moment and using the measured moment of inertia of the composite truss as determined in Section 10.1.2. This deflection, for the loading configuration used, shown in Figure 10.2, was 37.5 mm.

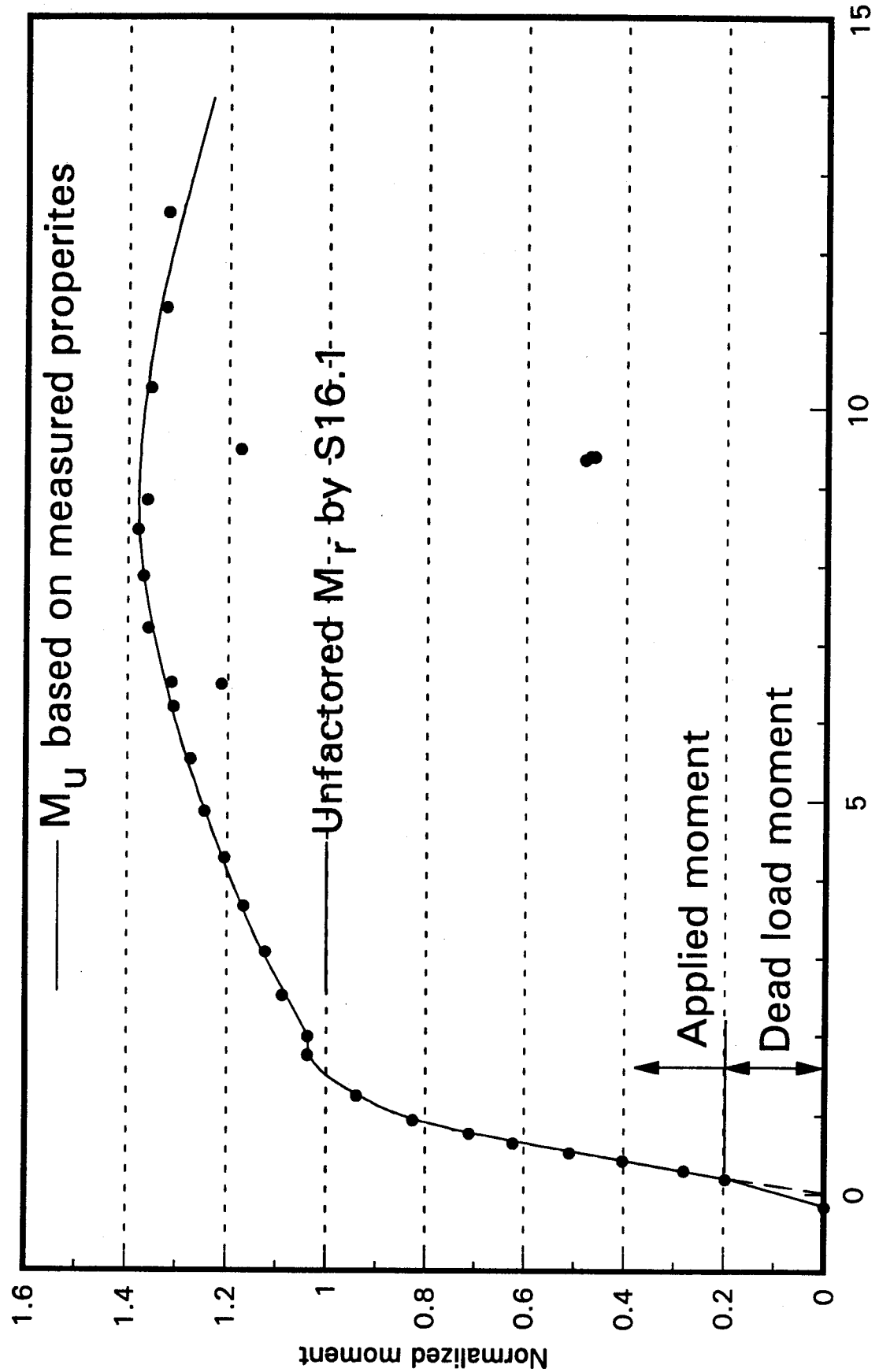

Fig 10.1 Normalized moment-deflection response

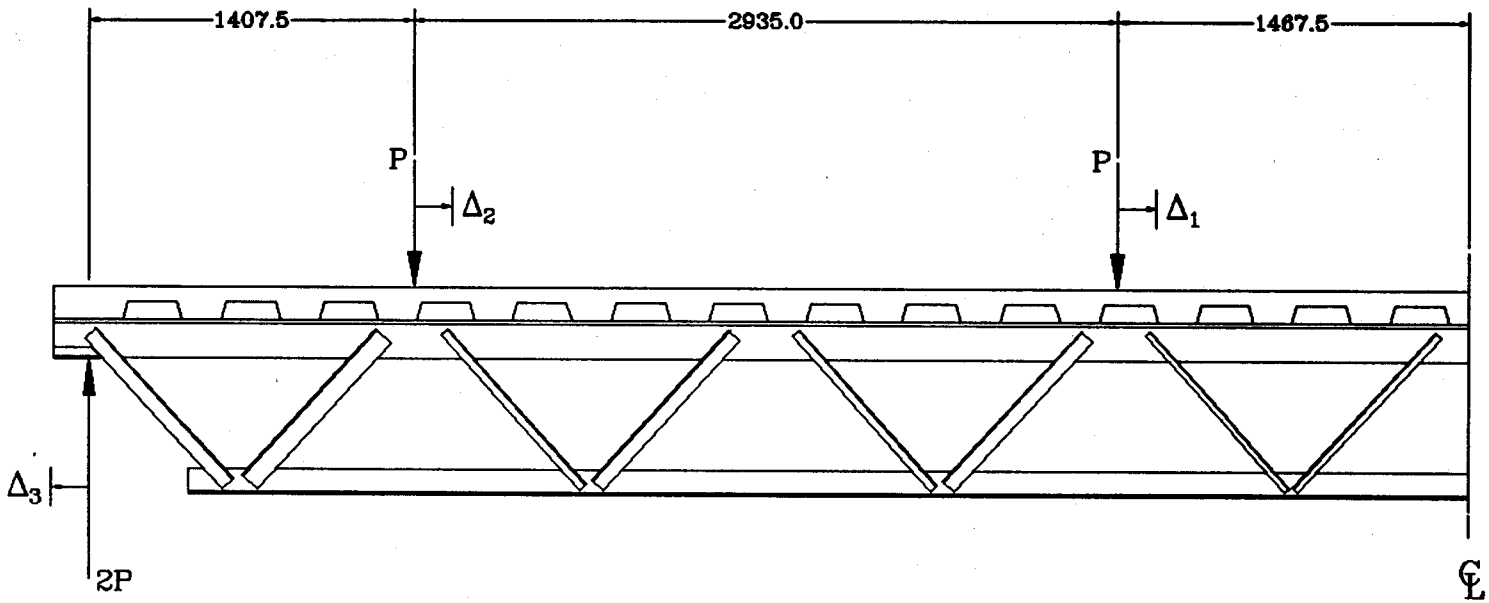

Fig. 10.2 Loading configuration with potential movement of loads and reactions

Figure 10.2 also shows the potential movement of the loads and reactions as the truss deflects. From the diagram, the maximum moment in the constant moment region is computed to be

[10.1] $M = (5750 + \Delta_1 + \Delta_2 + 2\Delta_3)P$.

In Figure 10.3 are plotted the movements of the loads and reactions, Δ_1, Δ_2 and Δ_3 versus the normalized mid-span deflection. For the first two of these curves, a zero correction was needed. The inward deflections, Δ_1 and Δ_2, of the interior and exterior loading points respectively, are seen to vary linearly with the mid-span deflection. This inward deflection is due to the shortening of the top fibres of the truss. The movement of the reaction, Δ_3, is curvilinear, as shown in the figure, first moving outward as the fibres below the neutral axis elongate and then moving inward at relatively large deflections as the chord distance (from one reaction to the other) shortens relative to the arc length.

The moments plotted in Figure 10.1 take into account the movement of the reactions and load points. Because the reactions and load points are not far from the neutral axis of the truss, these corrections were found to be much less significant than for a standard beam test, when the reactions and load points are one half the beam depth from the neutral axis. The increase in moment at the maximum moment, due to this correction, was only about 0.6%.

From Figure 10.1, is seen that the truss behaved in a linear elastic manner for the first five applied loads, up to a normalized moment of about 0.62. Beyond this, inelastic action is discernible. At a normalized moment of 1.03, a short yield plateau exists, indicating that the bottom chord had fully yielded at this load as discussed subsequently. With further loading, the moment increases substantially (even though the bottom chord is extending at the yield load) because the top chord strains significantly in tension, as discussed in Section 9.3. A maximum normalized moment of 1.38 was obtained at a normalized deflection of 8.8 when pull-out cone failures occurred over the shear connectors at the north end of the truss.

Based on a weighted mean ultimate tensile strength of 487 MPa of the bottom chord, the ratio of the ultimate moment to the yield moment is calculated to be 1.54. Therefore, the maximum normalized moment corresponds to 0.90 of the ultimate moment. Beyond the maximum moment, the truss continued to behave in a ductile manner, with the moment decreasing slowly to an estimated value of the normalized moment of 1.25 at a normalized deflection of 14.0. This ductile behaviour is attributed to the ability of the studs to carry only slightly decreasing shear after failure and due to the redistribution of shear from the end studs, where failure occurred, to those further from the end. The redistribution of the shear connection force required the truss to behave non-compositely near the north end, where the applied bending moment would have been relatively small.

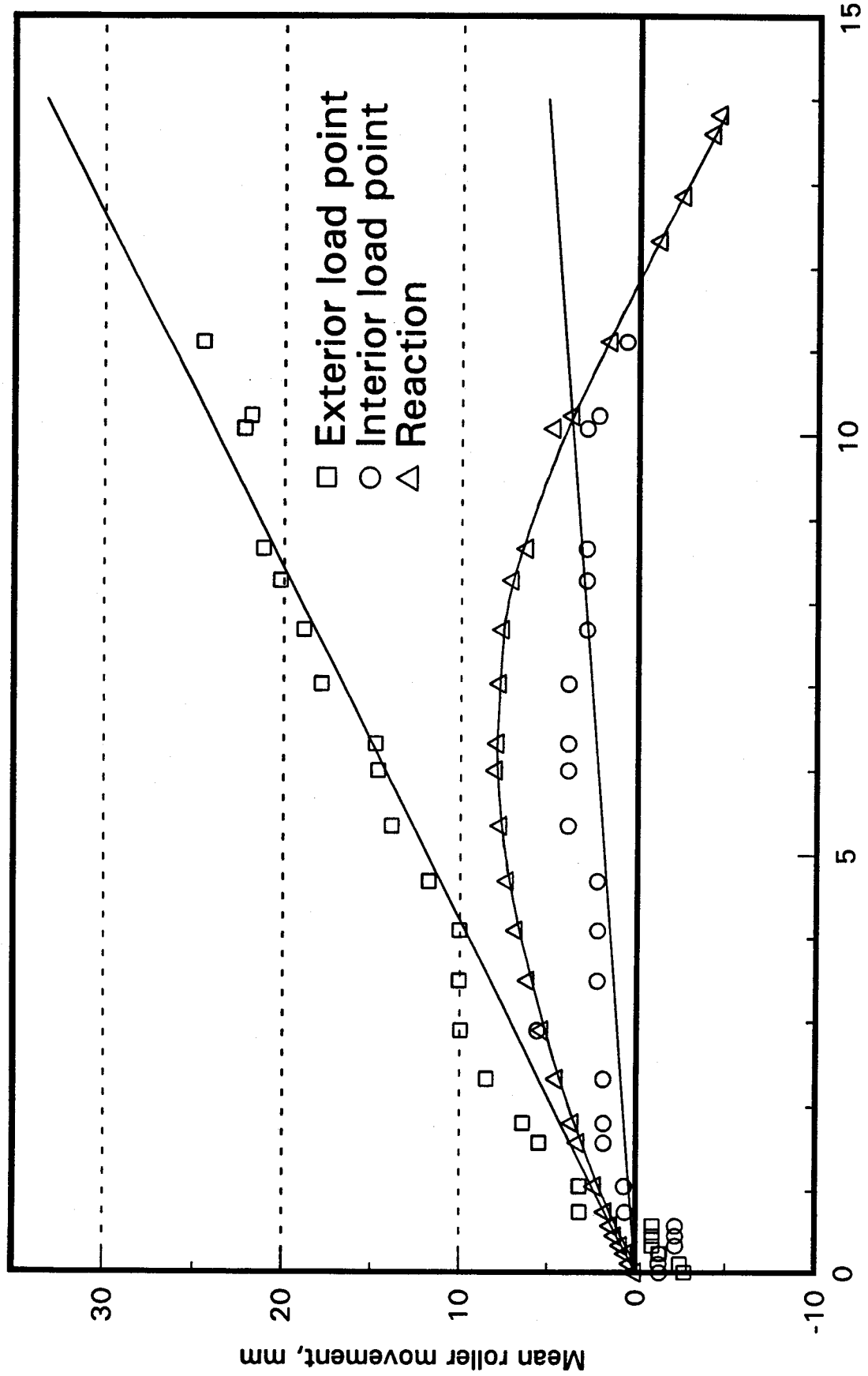

Fig 10.3 Mean roller movement of load points and reactions

In Figure 10.4 are plotted normalized deflections of the truss as deduced from the mid-span and quarter point deflection measurements, for the selected total moments of 327 kN·m and 712 kN·m, corresponding to normalized moments of 0.62 and 1.36, respectively. The deflections have been normalized so that the two curves have the same ordinate of 1.00 at mid-span. The diagram shows, as was expected, that the curvatures for the higher load, recorded just before the maximum load was reached, are very much concentrated in the central three panels. The solid line, for the lower moment, represents the theoretical deflected shape for elastic behaviour under a uniformly distributed load. It fits the measured data well. The dashed line is an estimated curve based on the measured deflections at a total moment of 712 kN·m.

The composite truss exhibited good strength and ductility. A maximum total moment of 1.38 times the yield moment, based on measured properties, was reached. This indicates that the bottom chord was strained sufficiently to result in top chord strains extending into the inelastic region. Bottom chord strains up to 35 300 με were recorded. The moment attained was 0.90 of the ultimate moment of 808 kN·m, based on fracture of the bottom chord and neglecting any contribution of the top chord. Had the shear connection between the steel top chord and the concrete not failed, it is anticipated that the truss would have reached a somewhat larger moment, corresponding to fracture of the bottom chord, with some contribution from the top chord, as both were exhibiting considerable ductility and no sign of distress was apparent.

Deflections at the maximum moment of about 8.8 times the yield deflection demonstrate the ductility of the truss. At a moment to yield moment ratio of 1.00, the normalized deflection is about 1.4. Because the effects of interfacial slip and shear deflections due to the straining of the web members have been taken into account, the reason the deflection at yield exceeds that predicted (1.00 assuming linear behaviour to the yield moment) is considered to be due to the presence of residual stresses in the bottom chord.

The overall behaviour of the truss was very ductile. The truss reached a maximum normalized deflection of 14.0 when the state of neutral equilibrium was upset, and the truss moved suddenly to the south, as discussed in Section 9.1. Had this not occurred, it is anticipated that mid-span deflection attained could have been significantly larger, because the loss in moment capacity due to shear pull-out cone failure was quite gradual.

10.3 Bottom chord behaviour

In Section 9.2, it was noted that the strains in the bottom chord, measured by the strain gauges and the LVDTs, differed significantly. In order to determine the better reading, an analysis of deflections was performed, by drawing two deformed trusses to scale (using the measured strains) at a load of 105 kN per jack and comparing the resulting deflection with the corresponding measured deflection of 288 mm. The two deflected trusses were drawn, with the strains in the central three panels of the bottom chord of 15 170 με and

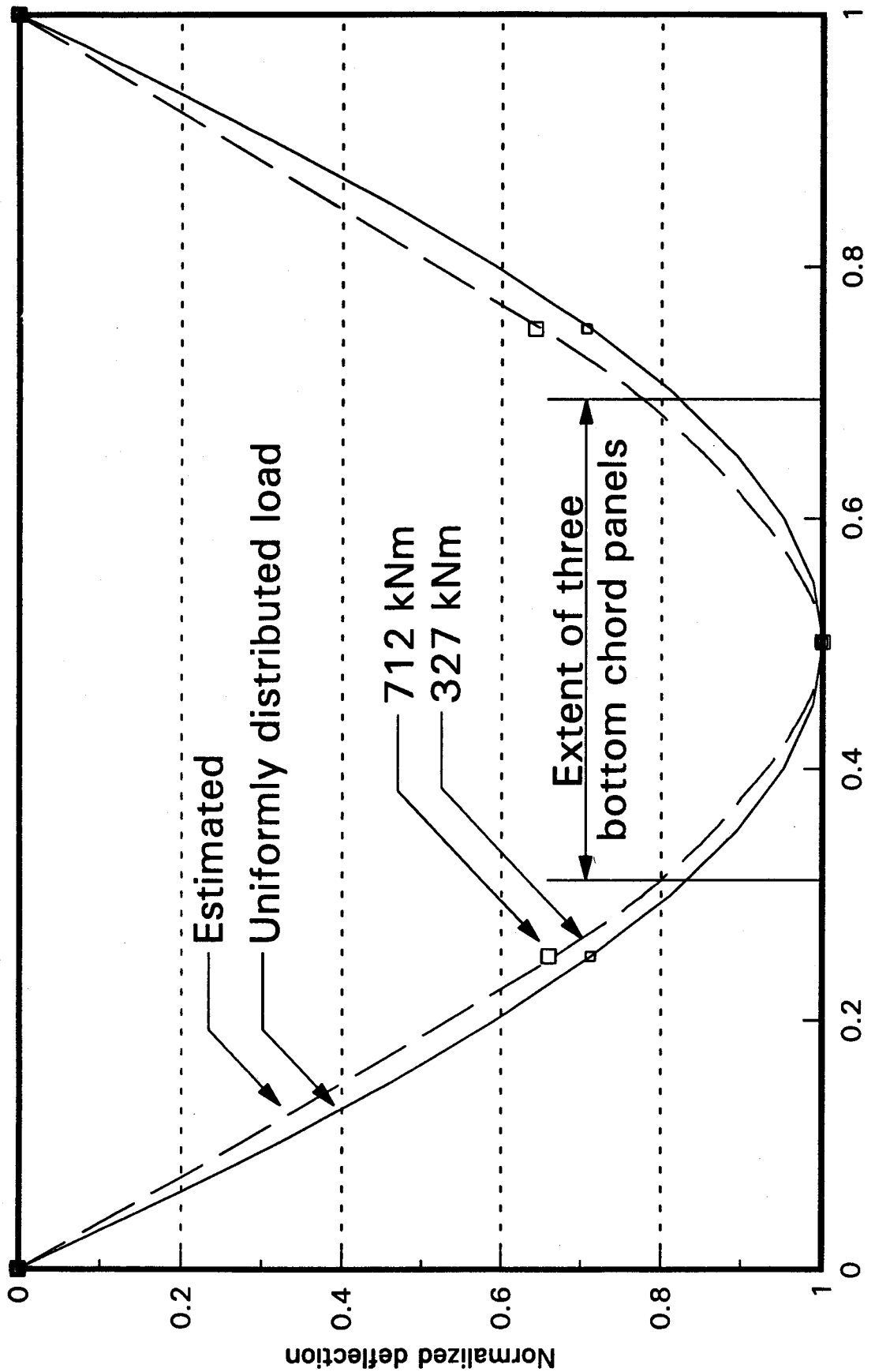

Fig 10.4 Non-dimensionalized deflected shape

20 800 με, corresponding to the strain gauge and LVDT readings respectively. The measured concrete strains were used to determine deformations of the top chord. Elastic deflections of all of the remaining members were taken into account. The resulting deflections were 233 mm and 293 mm for the strain gauge readings and the LVDT readings, respectively. Hence, the LVDT strain readings are deemed to be the better measure of the strain in the bottom chord, for strains corresponding to loads of 68 kN per jack and greater. For lesser loads, it is considered appropriate to use either the strain gauge readings of the LVDT readings, as there was little difference between the two.

For small strains, that is, for linearly elastic behaviour, it would be expected that the ratio of the axial load to moment would be constant. From Figure 9.14, the mean ratio of the regressed strain at the centroid of the cross-section divided by the slope of the strain diagram for the five load steps was found to be 311×10^6 with a coefficient of variation of 0.036. Thus, for these load steps, the axial load and moment increased proportionally, indicating that the behaviour was linearly elastic.

For the same five load steps, the force, and hence strain in the bottom chord was calculated and compared to the weighted measured value as follows. For small deflections, when shear span corrections are negligible, the total moment, as given by [10.1], is 5750P, where P is the applied load per jack. Equating this external moment to the internal couple gives

[10.2] $5750 \cdot P = T_{bc} \cdot d_1 + T_{tc} \cdot d_2$.

The force T_{tc} was computed from the regressed strain in the top chord using the appropriate modulus of elasticity and area. The force in the bottom chord was then computed from [10.2]. The mean strain was determined from the force in the bottom chord.

Table 10.1 compares the test or measured weighted average strain to that calculated from [10.2]. The weighted average strain was based on the portion of the area considered to be tributary to each of the five strain gauges. The table shows excellent agreement between the measured and calculated strains with a mean ratio of 1.023 and a coefficient of variation of 0.019 for the five low loads.

Table 10.1 Comparison of measured (test) strain to calculated strains for bottom chord

Applied load, kN	ε_{test}, με	ε_{calc}, με	$\varepsilon_{test} / \varepsilon_{calc}$
8.0	128	128	0.998
19.1	319	306	1.042
28.8	471	463	1.018
39.1	635	628	1.012
47.2	793	759	1.044
		Mean	1.023
		Coefficient of variation	0.019

At high loads, Figure 9.15 strongly suggests that the strain distribution in the bottom chord is linear (but not uniform). The regression analyses performed on these data have coefficients of determination generally greater than 0.90. However, the contrary evidence is deemed to even stronger. As shown in Figures 9.2 and 9.12 and as noted in the test log book, the bottom chord had straight segments between panel points (within the tolerances of visual acuity). If the bottom chord was indeed straight, the strain distribution through the depth must be uniform. At the peak load, the strain distribution implied by the strain gauges would have resulted in a deflection between panel points of about 40 mm, which would have been clearly perceptible. It is also noted that this curvature is greater than that for the truss a whole, which also defies logic. Apart from the strains at a load of 47 kN per jack, all strains shown in Figure 9.15, for load steps prior to the attainment of the maximum load (i.e., excluding 102 kN per jack), represent strains on the yield plateau. It is postulated that the difference in strains from one strain gauge to another is simply due to the phenomenon of discontinuous yielding (Lay 1982). Any portion of the gauge length may be at the yield strain or at the strain hardening strain, with a measured value anywhere between the two.

10.4 Strain distribution through the truss depth

Figures 10.5a, 10.5b and 10.5c show the strain variation through the depth of the truss at or near the mid-span for jack loads of 90 kN, 100 kN and 105 kN, respectively. In each figure, a best fit straight line has been drawn through the strains recorded for the top chord (regressed strain gauge readings) and the bottom chord (mean LVDT readings) and parallel to this line, the best fit straight line through the concrete cover slab has also been drawn. These are shown as solid lines. The jog between the two lines at the concrete steel interface is an indication of the interfacial slip at this level. Also drawn on each figure as a dashed line is the best fit straight line assuming that no interfacial slip has occurred. This line is only an approximation to the true behaviour, but nevertheless, fits the strain data reasonably well. From the straight line approximation, the curvature for the central portion of the truss, as represented by this behaviour, could be determined.

In Figure 10.6 are drawn strain distributions through the depth of the truss for eight different loads, assuming that no interfacial slip occurs. The figure shows that the neutral

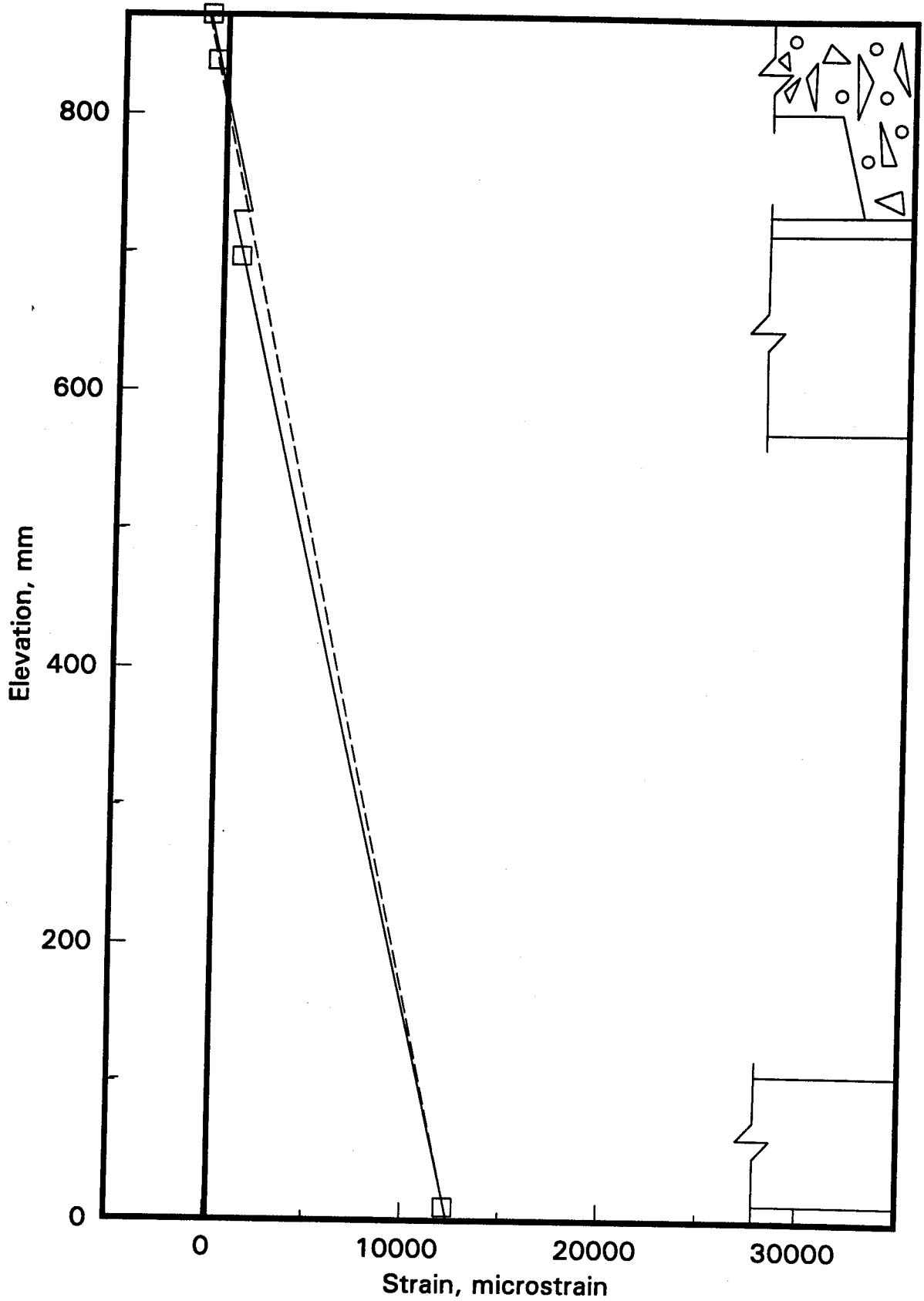

Fig. 10.5a Flexural strain distribution at 90 kN

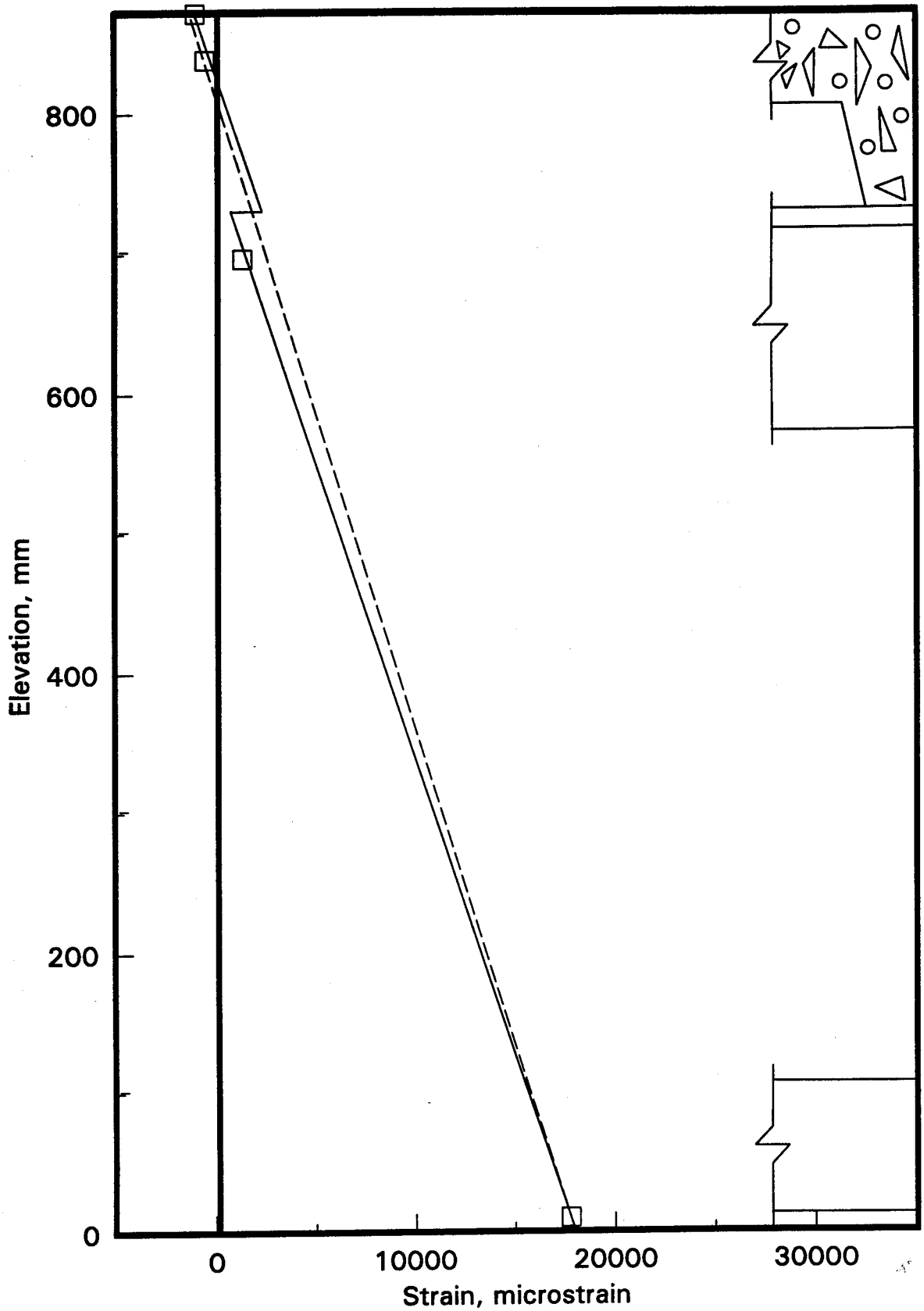

Fig. 10.5b Flexural strain distribution at 100 kN

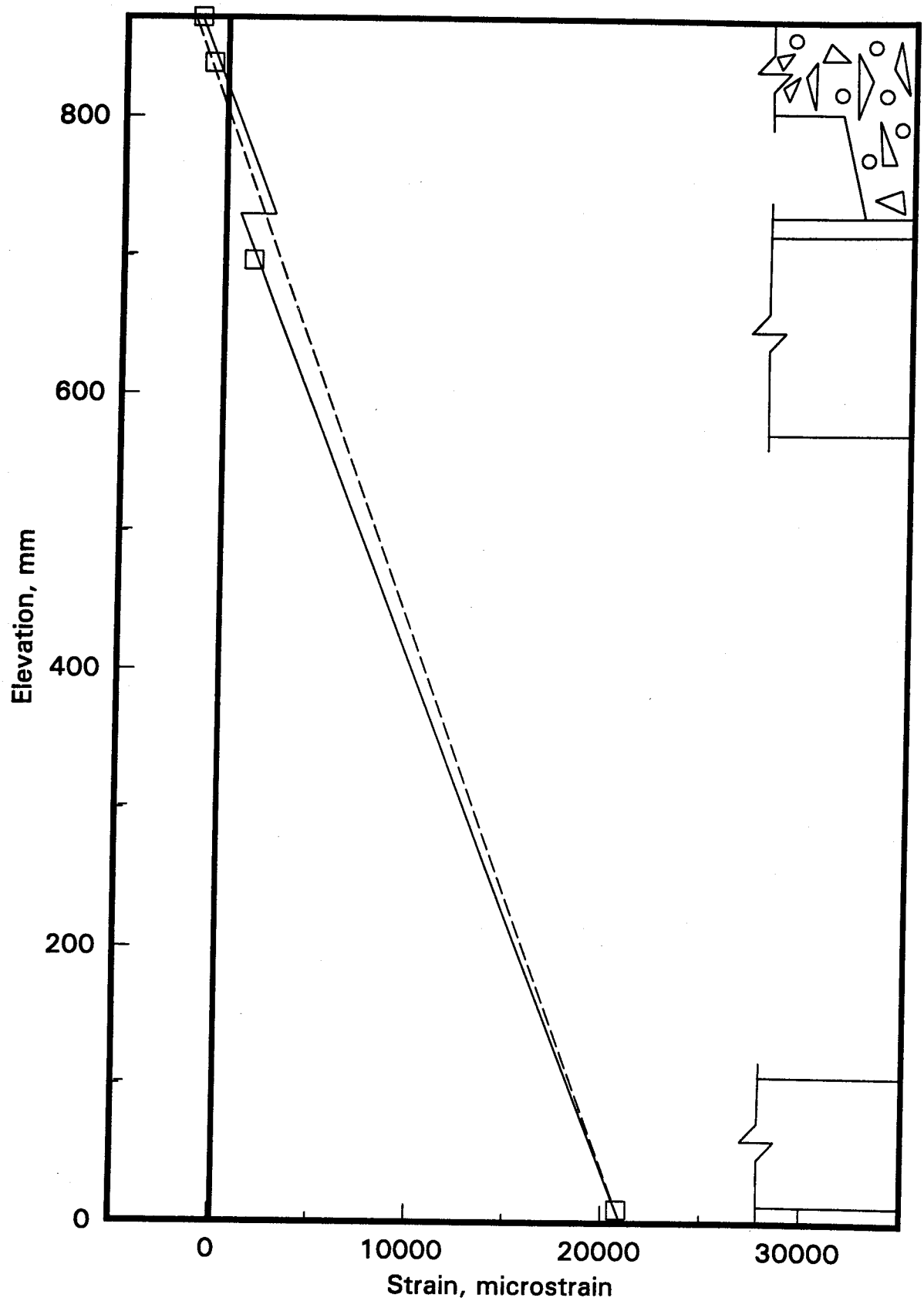

Fig. 10.5c Flexural strain distribution at 105 kN

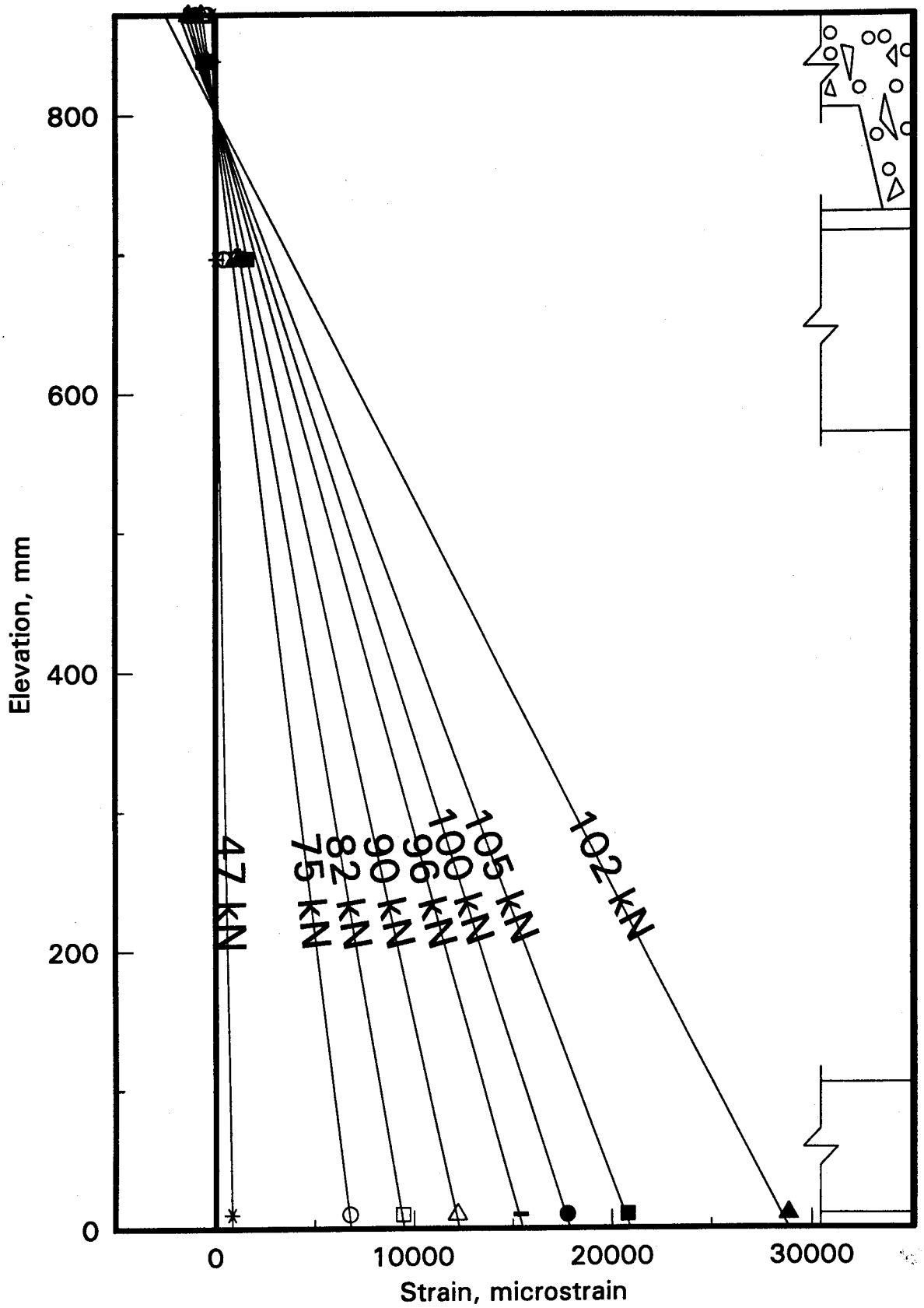

Fig. 10.6 Flexural strain distribution

axis rises, marginally, as the load increases. This results from the increased straining of the bottom chord and for all loads, except the first, the bottom chord was yielded. The minimum coefficient of determination for the eight regression analyses was 0.986.

10.5 Strain-force-moment relationships

From the strain distributions given in Figures 9.13 and 9.17, it is estimated that, at maximum load, the strain in the bottom chord and top chord were, respectively, 22 475 + 381 = 22 855 με and 1650 - 225 = 1425 με. These values take into account the initial strains induced in the steel chords by the dead weight of the composite truss. It should also be noted that the top chord is partially yielded, and hence

[10.3] $T_{tc} \neq \varepsilon_{tc} E_{tc} A_{tc}$.

Having taken the above into account, the corresponding forces, using the typical stress-strain curve (Figure 6.2a) for the bottom chord, prorated for the difference in yield strengths, and the measured material properties of the top chord from Table 6.2, are 692 kN and 718 kN, respectively, giving rise to a total moment of 686 kN·m, or a normalized moment of 1.31 as compared to a test ratio of 1.38. The ratio of the normalized test moment to the normalized moment based on the strain measurement in the chords at maximum load is 1.05. This discrepancy is considered to be due to the problem of converting strains to forces, even when the strain instrumentation was carefully applied and when the stress-strain characteristics of the materials have been measured (Brattland 1986).

The flexural strength of the composite beam is increased above the yield moment by two factors: the strain hardening of the bottom chord and the tensile force in the top chord. The yield force in the bottom chord, using measured properties, is calculated to be 620 kN. Strain hardening then, must account for an additional force of 692 - 620 = 72 kN in the bottom chord. This force multiplied by its moment arm to the compressive force in the concrete results in a moment of 60 kN·m, or 0.11 times the yield moment. The contribution of the force in the top chord to the moment resistance is 111 kN·m, or 0.21 times the yield moment.

10.6 Analysis of failure mode

The shear studs were designed to carry a shear that corresponded to the force in the bottom chord when it reached 90% of its factored specified maximum tensile strength of 620 MPa acting on its nominal area of 2000 mm^2, that is, 1004 kN. The resistance of the shear stud connectors was 1433 kN, based on a failure load of 110.6 kN per pair of studs as found in push-out test 2, with studs at the centerline of the flute, together with an

estimated (unfactored) failure load of a single stud of 81.8 kN, based on the shear cone area.

As discussed in Section 10.2, the maximum moment attained in the test was only 0.90 times the predicted ultimate moment, based on measured material and geometric properties. The calculated force of the bottom chord, based on measured properties, is 692 kN. The question arises why the shear connectors failed when they had been designed to carry a shear of 1433 kN, which is much greater than 692 kN.

Because the concrete must equilibrate the horizontal tensile forces in both the top and bottom chords, the shear connectors must resist a force that is much greater than the force of the bottom chord (which is itself larger than the yield force). In fact, the shear studs resist a force of 718 kN and 692 kN , in the top and bottom chords respectively, or a total force of 1410 kN. The test to predicted ratio for the resistance of the shear connectors is therefore 1410 / 1433 = 0.98. The test to predicted ratio for the shear connection force is 1410 / 620 = 2.27. This reveals an inadequacy in S16.1 - M89, discussed subsequently.

Failure by overloading the shear connectors is inevitable for the truss as designed, provided that the web members do not fail prematurely. Each component of the composite truss was designed to resist forces concomitant with the bottom chord reaching 90% of its factored specified, neglecting the contribution of the top chord to the flexural strength. The contribution of the top chord to the horizontal shear will, by necessity, overload the shear connectors before any other component fails.

Canadian Standard S16.1 - M89 requires the shear connection force be designed to resist the yield force in the bottom chord. Because the forces in the top chord were large, S16.1 is seen to be unconservative if the top chord is allowed to strain appreciably. The strain hardening of the bottom chord contributed an extra 72 / 620 = 0.12 times the yield force in the bottom chord and the force induced in the top chord contributed an extra 718 / 620 = 1.16 times the yield force in the bottom chord to the force in the shear connectors. It is recommended that S16.1 should account for the contribution of the top chord to the shear connection force.

Because the contribution of the top chord is very much larger than the strain hardening contribution, it is obvious that the most effective way to reduce the design shear (without significantly affecting the design moment resistance of the composite section) would be to reduce the force induced in the top chord, which is directly related to its area. Consequently, the designer can influence beneficially the shear connection behaviour of the composite truss at its ultimate moment by selecting a top chord with minimum area. This is discussed subsequently, in Section 10.7.

10.7 Top chord behaviour

One of the unique design features of the composite truss tested was that the centroidal axes of the web members were aligned to meet at mid-depth of the cover slab. The web members were therefore about 250 mm apart at panel points on the top chord. The alternating compressive and tensile forces in the web members, in a Warren truss configuration, would thus induce bending moments in the top chord. Very limited local yielding of the top chord occurred and no gross signs of distress in the top chord were noted due to the use of this triangulation system.

Figure 9.17 shows that the top chord was subjected to significant bending strains, in addition to axial tensile strains under the action of the applied loads. At the higher loads, about five-sixths of the depth of the cross-section was yielded in tension. As discussed previously, the top chord contributes significantly to the longitudinal shear on the connectors and, limited by the small lever arm to the compressive force in the concrete, to the flexural strength of the truss.

To reduce the force developed in the top chord, and therefore the load carried by the shear connectors, the top chord should be made as small as possible, consistent with its function in the composite truss to act as the connector between shear connectors and the web members, and in the steel truss, as the top chord, when unshored construction is used. In the latter case, positioning of the web members to minimize joint eccentricities in the top chord of the steel truss would result in a smaller top chord, as it was this condition that governed the design of the top chord, for this particular truss. This, therefore suggests that the preferred triangulation system, for the web members would be to minimize the joint eccentricities for the steel truss, although the behaviour and ultimate strength with such a triangulation system has not been confirmed. It is noted that, with a smaller top chord, the end shear, acting on the stem of the top chord WT would be more critical requiring, in all probability, significantly greater reinforcement. Furthermore, the advantage of steep diagonals, with lines of action intersecting at the mid-depth of the cover slab, is lost.

10.8 Web member behaviour

Planar regression analyses were performed based on the work by Woldegiorgis and Kennedy (1994). These analyses of web members 2, 4, 13 and 15 proved to be unreliable in that the axial forces computed in each web member showed a wide variation at each load step, with the maximum calculated load divided by the minimum in a single web member ranged from 1.28 to 2.17 with a mean value of 1.53. For example, the calculated forces in web member 4 at an applied load of 47 kN per jack, were: 16.1 kN, 17.9 kN, 19.9 kN and 21.7 kN. This variation in the axial force for a given member at a given load step cannot be explained. Furthermore, the coefficient of determination varied from 0.253 to 0.990 with a mean value of 0.820 for the 80 planar regression analyses performed.

11 SUMMARY, CONCLUSIONS AND RECOMMENDATIONS

11.1 Summary

1. A full-scale composite truss, designed and constructed for shrinkage and flexural tests, had the following features:

   a. the steel truss consisted of WT chords and double angle web members,

   b. the triangulation system minimized joint eccentricities for the composite truss by aligning the centroidal axis of the web members to intersect at the mid-depth of the cover slab and the centroidal axis of the bottom chord WT,

   c. the flexural capacity was based on the ultimate tensile strength rather than the yield strength of the bottom chord,

   d. components of the composite truss were designed to resist the loads that would develop when the bottom chord reached 90% of its factored ultimate strength:

      i. tension diagonals were designed for axial forces only,

      ii. compression diagonals were designed for axial forces with an out-of-plane (of the truss) eccentricity equal to one third the centroidal distance of the angle concerned. The resulting moment was resolved about the principal axes of the angle. The angle was then designed as a biaxially loaded column. Due to the triangulation system used, no in-plane moments were considered,

      iii. the welded connections of the web members were designed to transfer the axial load that would develop in the angle plus the maximum in-plane moment that could coexist (which was determined by using the axial load and setting the S16.1 interaction value to 1.0),

      iv. the shear connectors were designed to resist a somewhat larger force than the maximum force expected to develop in the bottom chord, due to the premature failures of the shear connectors in similar tests conducted previously by Brattland and Kennedy (1986), and

      v. the end bearing detail was designed to resist both shear and bearing forces resulting from the vertical loads applied to the truss.

2. The measured geometric properties of the steel sections, the concrete slab and the composite truss were used for all analyses of the test data.

3. Material properties were determined from ancillary tests on steel tension coupons, residual strain specimens, push-out specimens, concrete cylinders and concrete prisms.

4. The effect of concrete shrinkage on the composite truss was monitored for 68 days, and included measurements of truss deflections, concrete strains, steel strains, temperature and relative humidity. The free shrinkage strains of two 100 x 100 x 1000 mm plain concrete control specimens were also monitored during the shrinkage test.

5. Measured values of strains and deflections were compared to values calculated by the equilibrium method to verify its validity.

6. The composite truss was loaded in flexure to failure using four concentrated loads. Forces and roller movements at load and reaction points, truss deflections, concrete strains, steel strains, interfacial slip and web member separations were measured at intervals during the test.

7. The flexural test data were analyzed to obtain the moment-deflection response and to study the behaviour of the individual components of the composite truss.

8. The effective moments of inertia of the steel and composite truss were determined from load and deflection measurements.

11.2 Conclusions and recommendations

1. For the steel sections, the mean modulus of elasticity was about 2% greater than specified, whereas the mean yield strength was about 11% greater than specified.

2. The failure load of a pair of shear studs placed at the center of the flute, as measured by a push-out test, was 1% greater than the unfactored value given in CSA Standard S16.1 - M89. Placement of the studs in an unfavorable position in the deck flute only reduced the failure load by about 7%.

3. Both temperature and relative humidity showed a general decreasing trend with time over the shrinkage test period.

4. Shrinkage induced deflections (at the mid-span and quarter points) and strains (free shrinkage strain, concrete slab strains and steel chord strains) generally increased at a decreasing rate over the test period of 68 days.

5. At 68 days, the free shrinkage strain was 709 με and the mid-span deflection of the composite truss was 6.8 mm. Both of these quantities were still increasing at this time. At 28 days, about 72% of the 68 day free shrinkage strain and about 78% of the 68 day mid-span deflection had occurred. The deflection was limited for the seven days in which the slab was covered with the polyethylene sheet. An expression relating the free shrinkage and time was determined.

6. Transverse strains in the concrete were close to the measured free shrinkage strains, indicating that the deck offers little restraint to concrete shrinkage. For a number of composite trusses in parallel in a real structure, more restraint in the transverse direction may be realized than for the single truss as tested (with free edges). In the longitudinal direction, however, the steel truss offers much restraint, and the measured strains in this direction are only about 40% of the free shrinkage strain at 68 days.

7. Concrete strain distributions along the length of the truss show that restraint due to shrinkage of the slab developed within a short distance from each end.

8. At mid-span, the strains induced due to shrinkage of the concrete varied approximately linearly through the depth of the truss.

9. Measured shrinkage deflections agreed well with values calculated from the measured strains in the composite truss members, based on the equilibrium method (Brattland and Kennedy 1986). The equilibrium method, used for the calculation of shrinkage deflections, has been modified slightly here, to facilitate easier use. This method is based on the equilibrium of the shrinkage induced forces at mid-span, a linear strain distribution through the depth of the truss assumed to induce a constant curvature over the entire length of the specimen, the free shrinkage strain of the concrete, the stress-strain characteristics of concrete in tension over the period that the shrinkage test occurs and the stress-strain characteristics of the steel.

10. Using Shaker's general method, which is based on the equilibrium method, The calculated deflection exceeded the measured deflection at 68 days by a factor of about 1.5.

11. The modulus of elasticity of concrete in tension was deduced from measured deflections using the equilibrium method and is referred to as the apparent modulus. The apparent modulus was considerably smaller than the effective modulus of elasticity of concrete in tension as reported by Shaker (1991). This is because the apparent modulus includes the effects of interfacial slip and the open web system, whereas, the effective modulus determined by Shaker, from the deformation of concrete prisms, does not. A correction procedure proposed to account for this effect which gives reasonable agreement between the measured and calculated values of deflection. This, therefore, confirms the equilibrium method as a method to calculate shrinkage deflections.

12. The method suggested to calculate shrinkage deflections in CSA Standard S16.1 - 94 will overestimate the deflection of a composite truss, because the effective modulus of elasticity of concrete in tension is greater than the apparent modulus, due to flexibility in the truss web members and the concrete-steel interface. If this method was modified, by using the apparent modulus instead of the effective modulus, a better estimate of the shrinkage deflection would be obtained. However, the apparent modulus may be difficult to estimate, because it is dependent upon many factors, such as: relative truss chord and web member stiffness, concrete properties, curing conditions and loading conditions.

13. Flexurally induced compressive strains across the width of the concrete cover slab were typically uniform, only displaying significant shear lag as the load increased and the concrete was showing signs of distress.

14. Separation of the gauged web members was minimal, reaching a maximum value of about 0.8 mm attributable to each of the angles in the pair (about L / 1000). Bending of the angle out of the plane of the truss was therefore relatively minor.

15. Interfacial slip measurements were generally less than 1 mm. At higher loads, however, values of about 30 mm, indicative of shear connection failure, were recorded at the north end. The corresponding value recorded at the north quarter points was about 4 mm.

16. For the determination of deflections, the effective moment of inertia, I_e, calculated in Clause 17.3.1(a) of CSA Standard S16.1 - M89 (which accounts for reductions in stiffness due to partial shear connection and interfacial slip) should be divided by a factor of 1.10 to account for flexibility in the open web system of a truss.

17. At low loads, calculated and measured strains in the bottom chord agreed well, and the axial load and moment in the bottom chord increased proportionally with the applied load, indicating linear behaviour. At higher loads, despite some evidence to the contrary, it is considered that the bottom chord was uniformly strained, because it was observed to have straightened out as it yielded. The top chord, however, did not straighten, as it was attached to the concrete cover slab.

18. Initially, the truss behaved in a linear manner. The maximum moment was 1.38 times the yield moment calculated by S16.1 - M89 procedures using measured material and geometric properties. This maximum moment corresponds to 90% of the ultimate moment, calculated using measured properties and by assuming that only the bottom chord contributes to the flexural strength.

19. At a moment to yield moment ratio of 1.00, the deflection was about 1.4 times the deflection at the yield moment calculated by assuming linear behaviour to that level. This is attributed to residual stresses in the bottom chord. At the maximum moment the mid-span deflection was 8.8 times the deflection at the yield moment (about 325 mm).

20. A maximum deflection of 14.0 times the deflection at the yield moment (about 525 mm), corresponding to 1 / 22 of the span, was recorded. It is anticipated that a much higher value would have been obtained if the reaction assembly, in a state of neutral equilibrium, had not lurched sideways. Although the shear connection between the concrete and steel was showing signs of distress at the north end of the truss, it was exhibiting considerable ductility. These large deflections indicate that the composite truss system, as designed, was ductile. The maximum recorded bottom chord strain was about 23 times the yield strain (in excess of 35 000 $\mu\varepsilon$) and well into the strain hardening region. This strain corresponds to about 127% of the yield stress and about 82% of the ultimate tensile strength of the bottom chord.

21. The upset of the state of neutral equilibrium limited the maximum recorded deflection. Despite this, the maximum moment had already been reached, therefore failure of the composite truss occurred as a result of pull-out failures of the shear studs on the north half of the truss.

22. At low loads, the deflected shape of the truss corresponded well to the theoretical deflected shape of an elastic beam under uniform load. However, at higher loads the curvature was very much concentrated in the central three panels, due to the inelastic deformation of the bottom chord.

23. A linear variation of bending strains through the truss depth, neglecting any discontinuity at the steel-concrete interface due to interfacial slip, fits the data reasonably well, but a better fit is achieved taking the discontinuity at the steel-concrete interface into account.

24. Appreciable tensile strains were induced in the top chord. At the maximum load, the top chord was partially yielded, and carried a force of 718 kN. The force in the bottom chord was calculated to be 692 kN, which is 72 kN greater than the yield force of 620 kN, due to strain hardening. These values give a moment of 686 kN·m, or 1.31 times the yield moment. The maximum test moment was 1.38 times the yield moment. The difference between these values is considered to be a result of the difficulty in accurately converting strains to forces, even when the properties have been carefully measured. The flexural capacity was increased by 0.21 times the calculated yield moment due to the contribution of the top chord and by another 0.11 times the calculated yield moment from the contribution of the additional force in the bottom chord due to strain hardening. (This results in $1.00 + 0.21 + 0.11 \sim 1.31$ times the yield moment, as given above.)

25. The total shear acting on the shear stud connectors was the sum of the forces in the top and bottom steel chords, not only the yield force in the bottom chord, as implied by S16.1 - M89. Due to this, the studs, at failure, were carrying a force of 1410 kN, not 620 kN. The value of 1410 kN is 2.27 times the calculated yield force of the bottom chord ($A_s F_y = 620$ kN), but corresponds very well with the calculated resistance of the shear studs of 1433 kN. The load in the shear connectors was increased by 1.16 times the calculated yield force of the bottom chord because of the contribution of the top chord and by another 0.12 times the calculated yield force in the bottom chord because of the additional force in the bottom chord due to strain hardening (This results in $1.00 + 1.16 + 0.12 \sim 2.27$ times the calculated yield force in the bottom chord, as given above.) It is recommended that S16.1 be modified to account for the contribution of the top chord to the shear connection force.

26. It is inevitable that the failure of composite trusses designed in accordance with S16.1 - M89 with the slight modifications in the design philosophy used herein, will occur in the shear connection between the concrete and steel.

27. The current design procedures suggested in CSA Standard S16.1 - M89 for the determination of the shear stud connectors resistance would appear adequate, based on this test, with a calculated force in the shear connectors of 1410 kN and an unfactored design resistance of 1424 kN.

28. No gross signs of distress were noted in the top chord, hence, the triangulation system used is considered to be satisfactory, in that respect. However, the large area of the top chord, required by the triangulation system used, produced excessive loads in the shear studs. It is anticipated that minimizing the area of the top chord would facilitate better behaviour of the shear connection between the concrete and steel, and hence may improve overall truss behaviour. It is therefore recommended that the joint eccentricities be minimized in the steel truss, at least with trusses with WT chords. Experimental tests are required to ensure the ultimate performance of this triangulation system is satisfactory.

29. To guard against premature failure of less ductile components, it would appear sufficient to have these components designed for a force that ensures that the bottom chord, with a yield strength greater than the minimum specified, does in fact yield first. One approach, when the yield strength of the bottom chord governs, would be to design for the mean yield strength plus a number of standard deviations as determined from a statistical analysis. Kennedy and Baker (1984) give, for rolled sections, a mean value of the yield strength of 1.06 times the specified minimum and a coefficient of variation of 0.051. The yield strength, three standard deviations above the mean, would be 1.22 times the specified minimum value. For a truss where the ultimate strength of the bottom chord governs (trusses using 700Q steels or having bolted connections with $0.85A_nF_u$ less than A_gF_u), a similar approach, based on the statistical variation of the ultimate tensile strength, could be used.

30. Strain analyses based on the work of Woldegiorgis and Kennedy (1994) proved that the strain data were unreliable.

31. It is recommended, in experimental testing of composite trusses, that the local concrete strains be measured at locations consistent with respect to the transverse flutes. It may be beneficial to measure strain both above the flutes and above the crests in the deck.

11.3 Areas of further research

Areas needing further research have been identified as:

1. Further testing of long span composite trusses with full shear connection, designed based on the bottom chord reaching a stress greater than the minimum specified yield level based on some statistical approach, should be done. The shear connector resistance must include the contribution from the top chord if the strains in the top chord are expected to be appreciable.

2. Additional experimental studies to measure shrinkage deflections of a wide variety of composite flexural members would confirm procedures for estimating shrinkage deflections.

3. The proposed correction of the apparent modulus of elasticity of concrete in tension to an effective modulus should be verified.

4. The feasibility of using the apparent modulus of elasticity of concrete in tension (with the equilibrium method) for shrinkage deflection calculations should be investigated. Specifically, the relationship between the apparent modulus and the factors that it depends on should be established. A modification of the method proposed by Lawther and Gilbert (1992) using the properties of concrete in tension instead of compression, should be correlated with the effective modulus of elasticity of concrete in tension (Shaker 1991), or to the use of an apparent modulus, as presented here.

5. An analytical study may be required to investigate the behaviour of the two triangulation systems with respect to ultimate load behaviour of the shear studs for trusses with both HSS and WT chords. If the analytical work verifies the above recommendation that the joint eccentricities be minimized for the steel truss instead of the composite truss, as was the case in this test, experimental work should then be carried out to confirm the analytical findings and determine if this triangulation system adversely affects the ultimate behaviour.

6. Further analysis of the web member strain data may result in an improved model of behaviour over that proposed by Woldegiorgis and Kennedy (1994).

REFERENCES

American Concrete Institute (ACI), 1982. Designing for the effects of creep, shrinkage and temperature in concrete structures. SP76, Committee 209, American Concrete Institute, Detroit, Michigan.

American Standards for Testing and Material (ASTM), 1992. Standard test methods for tension testing of metallic materials (Metric). ASTM E 8M - 92. Philadelphia, Pennsylvania.

Bjorhovde, R., 1981. Full-scale test of a composite truss. Structural Engineer Report 97. Department of Civil Engineering, The University of Alberta, Edmonton, Alberta, 40 p.

Blodgett, O. W., 1966. Design of welded structures. The James F. Lincoln Arc Welding Foundation, Cleveland, Ohio.

Bradford, M. A. and Gilbert, R. I., 1991. Time-dependent behaviour of simply-supported steel-concrete composite beams. Magazine of Concrete Research, 43(157), pp. 265 - 274.

Bradford, M. A. and Gilbert, R. I., 1992. Composite beams with partial interaction under sustained loads. Journal of Structural Engineering, 118(7), pp. 1871 - 1883.

Branson, D. E., 1964. Time-dependent effects in composite concrete beams. Proceedings, Journal of the American Concrete Institute, Vol. 61, February, pp. 213 - 229.

Brattland, A. and Kennedy, D. J. L., 1986. Shrinkage and flexural tests of two full-scale composite trusses. Structural Engineer Report 143. Department of Civil Engineering, The University of Alberta, Edmonton, Alberta, 40 p.

Brattland, A. and Kennedy, D. J. L., 1992. Flexural tests of two full-scale composite trusses. Canadian Journal of Civil Engineering, Vol. 19, No. 2, pp. 279 - 295.

Canadian Standards Association (CSA), 1984. Design of concrete structures for buildings, National Standard of Canada CAN3 - A23.3 - M84, Canadian Standards Association, Rexdale, Ontario.

Canadian Standards Association (CSA), 1989. Limit states design of steel structures. National Standard of Canada CAN / CSA - S16.1 - M89, Canadian Standards Association, Rexdale, Ontario.

Canadian Standards Association (CSA), 1990. Methods of test for concrete, National Standard of Canada CAN3 - A23.2 - M90, Canadian Standards Association, Rexdale, Ontario.

Canadian Standards Association (CSA), 1992a. General requirements for rolled or welded structural quality steel. National Standard of Canada CAN / CSA - G40.20 - M92, Canadian Standards Association, Rexdale, Ontario.

Canadian Standards Association (CSA), 1992b. Structural quality steels. National Standard of Canada CAN / CSA - G40.21 - M92, Canadian Standards Association, Rexdale, Ontario.

Canadian Standards Association (CSA), 1994. Limit states design of steel structures. National Standard of Canada CAN / CSA - S16.1 - 94, Canadian Standards Association, Rexdale, Ontario.

Chien, E. Y. L. and Ritchie, J. K., 1984. Design and construction of composite floor systems. Canadian Institute of Steel Construction, Willowdale, Ontario, 323 p.

Chien, E. Y. L. and Ritchie, J. K., 1993. Composite floor systems - a mature design option. Journal of Constructional Steel Research, Vol. 25, No. 1 - 2, pp. 107 - 139.

Cran, J. A., 1972. Design and testing composite open web steel joists. Technical Bulletin 11, Stelco, January, 28 p.

Dezi, L. and Tarantino, A. M., 1993. Creep in composite continuous beams II: parametric study. Journal of Structural Engineering, 119(7), July, pp. 2112 - 2133.

Galambos, T. V. (Editor), 1988. Structural Stability Research Council. Guide to stability design criteria for metal structures, Fourth edition. John Wiley & Sons, New York, New York, 786 p.

Gilbert, R. I., 1989. Time-dependent analysis of composite steel-concrete sections. Journal of Structural Engineering, 115(11), November, pp. 2687 - 2705.

Grant, J. A., Fisher, J. W. and Slutter, R. G., 1977. Composite beams with formed steel deck. Engineering Journal, American Institute of Steel Construction, Vol. 14, First Quarter, pp. 24 - 43

Jayas, B. S., and Hosain, M. U., 1988. Behaviour of headed studs in composite beams: push-out tests. Canadian Journal of Civil Engineering, 15(2), pp. 240 - 253.

Jayas, B. S., and Hosain, M. U., 1989. Behaviour of headed studs in composite beams: full-size tests. Canadian Journal of Civil Engineering, 16(5), pp. 712 - 724.

Kennedy, D. J. L. and Baker, K. A., 1984. Resistance factors for steel highway bridges, Canadian Journal of Civil Engineering, Vol. 11, June, pp. 324 - 334.

Kennedy, D. J. L. and Brattland, A., 1992. Shrinkage tests of two full-scale composite trusses. Canadian Journal of Civil Engineering, Vol. 19, No. 2, pp. 296 - 309.

Kennedy, J. B. and Neville, A. M., 1986. Basic statistical methods for engineers and scientists, Third edition, Harper and Row, Publishers, New York.

Kennedy, S. J. and MacGregor, J. G. 1984. End connection effects on the strength of concrete filled HSS beam columns. Structural Engineering Report 115, Department of Civil Engineering, The University of Alberta, Edmonton, Alberta, 251 p.

Lawther, R. and Gilbert, R. I., 1990. Rate-of-creep analysis of composite steel-concrete cross sections. Structural Engineer, 68(11), June, 1990, pp. 208 - 213.

Lawther, R. and Gilbert, R. I., 1992. Deflection analysis of composite structures using the rate-of-creep method. Structural Engineer, 70(12), June, 1990, pp. 220 - 223.

Lay, M. G., 1982. Structural steel fundamentals - an engineering and metallurgical primer. Vermont South, Victoria, Australian Road Research Board.

Lea, F. M., 1970. The chemistry of cement and concrete. Arnold, London.

MacGregor, J. G. 1991. Civ E 672 (concrete behaviour and design) lecture notes. University of Alberta.

Mindess, S. and Young, J. F., 1981. Concrete. Prentice Hall Inc., New Jersey.

Montgomery, C. J., Kulak, G. L., and Shwartsburd, G., 1983. Deflection of a composite floor system, Canadian Journal of Civil Engineering, Vol. 10, No. 2, June, pp. 192 - 204.

National Building Code of Canada, 1990. National building code of Canada. Clause 4.1.4. National Research Council of Canada, Ottawa, Ontario.

Press, W. H., Teukolsky, S. A., Vetterling, W. T. and Flannery, B. P., 1992. Numerical recipes in FORTRAN, Second edition. Cambridge University Press, 963 p.

Shaker, A. F. and Kennedy, D. J. L., 1991. The effective modulus of elasticity of concrete in tension. Structural Engineering Report 172, Department of Civil Engineering, The University of Alberta, Edmonton, Alberta, 160 p.

Temple, M. C. and Sakla, S. S. S., 1994. Balanced and unbalanced welds for angle compression members. Canadian Journal of Civil Engineering, Vol. 21, No. 3, June, pp. 393 - 403.

Woldegiorgis, B. F. and Kennedy, D. J. L., 1994. Some behavioural aspects of composite trusses. Structural Engineering Report 195, Department of Civil Engineering, The University of Alberta, Edmonton, Alberta, 111 p.

Recent Structural Engineering Reports

Department of Civil Engineering

University of Alberta

179. *Finite Element Analysis of Distributed Discrete Concrete Cracking* by Budan Yao and D.W. Murray, May 1992.

180. *Finite Element Analysis of Composite Ice Resisting Walls* by R.A. Link and A.E. Elwi, June 1992.

181. *Numerical Analysis of Buried Pipelines* by Zhilong Zhou and David W. Murray, January 1993.

182. *Shear Connected Cavity Walls Under Vertical Loads* by A. Goyal, M.A. Hatzinikolas and J. Warwaruk, January 1993.

183. *Frame Methods for Analysis of Two-Way Slabs* by M. Mulenga and S.H. Simmonds, January 1993.

184. *Evaluation of Design Procedures for Torsion in Reinforced and Prestressed Concrete* by Mashour G. Ghoneim and J.G. MacGregor, February 1993.

185. *Distortional Buckling of Steel Beams* by Hesham S. Essa and D.J. Laurie Kennedy, April 1993.

186. *Effect of Size on Flexural Behaviour of High Strength Concrete Beams* by N. Alca and J.G. MacGregor, May 1993.

187. *Shear Lag in Bolted Single and Double Angle Tension Members* by Yue Wu and Geoffrey L. Kulak, June 1993.

188. *A Shear-Friction Truss Model for Reinforced Concrete Beams Subjected to Shear* by S.A. Chen and J.G. MacGregor, June 1993.

189. *An Investigation of Hoist-Induced Dynamic Loads* by Douglas A. Barrett and Terry M. Hrudey, July 1993.

190. *Analysis and Design of Fabricated Steel Structures for Fatigue: A Primer for Civil Engineers* by Geoffrey L. Kulak and Ian F.C. Smith, July 1993.

191. *Cyclic Behavior of Steel Gusset Plate Connections* by Jeffrey S. Rabinovitch and J.J. Roger Cheng, August 1993.

192. *Bending Strength of Longitudinally Stiffened Steel Cylinders* by Qishi Chen, Alla E. Elwi and Geoffrey L. Kulak, August 1993.

193. *Web Behaviour in Wood Composite Box Beams* by E. Thomas Lewicke, J.J. Roger Cheng and Lars Bach, August 1993.

194. *Experimental Investigation of the Compressive Behavior of Gusset Plate Connections* by Michael C.H. Yam and J.J. Roger Cheng, September 1993.

195. *Some Behavioural Aspects of Composite Trusses* by Berhanu Woldegiorgis and D.J. Laurie Kennedy, January 1994.

196. *Flexural Behavior of High Strength Concrete Columns* by Hisham H.H. Ibrahim and James G. MacGregor, March 1994.

197. *Prediction of Wrinkling Behavior of Girth-Welded Line Pipe* by L.T. Souza, A.E. Elwi, and D.W. Murray, April 1994.

198. *Assessment of Concrete Strength in Existing Structures* by F. Michael Bartlett and J.G. MacGregor, May 1994.

199. *The Flexural Creep Behavior of OSB Panels Under Various Climatic Conditions* by Naiwen Zhao, J.J. Roger Cheng, and Lars Bach, June 1994.

200. *High Performance Concrete Under High Sustained Compressive Stresses* by S. Iravani and J.G. MacGregor, June 1994.

201. *Strength and Installation Characteristics of Tension – Control Bolts* by Scott T. Undershute and Geoffrey L. Kulak, August 1994.

202. *Deformational Behavior of Line Pipe* by Mohareb, M., Elwi, A.E., Kulak, G.L., and Murray, D.W., September 1994.

203. *Behavior of Girth-Welded Line Pipe*, by Yoosef-Ghodsi, N., Kulak, G.L., and Murray, D.W., September 1994.

204. *Numerical Investigation of Eccentrically Loaded Tied High Strength Concrete Columns* by Jueren Xie, Alaa E. Elwi, and J.G. MacGregor, October 1994.

205. *Shear Strengthening of Concrete Girders Using Carbon Fibre Reinforced Plastic Sheets* by Efrosini H. Drimoussis and J.J. Roger Cheng, October 1994.

206. *Shrinkage and Flexural Tests of a Full-Scale Composite Truss* by Michael B. Maurer and D.J. Laurie Kennedy, December 1994.